Diss. ETH No. 21107

Affinity-based Structural Studies of microRNA Precursors

A dissertation submitted to the
ETH ZURICH

for the degree of
Doctor of Sciences

presented by
M. REBHAN
Eidg. dipl. Apotheker
born 21. Januar 1976
citizen of Boswil/AG - Schweiz

accepted on the recommendation of
Prof. Dr. J. Hall, examiner
Prof. Dr. G. Schneider, co-examiner

2013

Für meine Familie

Contents

Summary

MicroRNAs (miRNAs) are a recently discovered class of short ($\sim$22 nt) non-coding RNA molecules that regulate gene expression. Upon binding to the 3'-untranslated region (UTR) of target messenger RNA (mRNA) they repress translation of the mRNA or induce their degradation and, accordingly, play important roles in health and many human diseases including cancer, (cardio)-metabolic disorders, and viral infections. The precursors of miRNAs——pri- and pre-miRNAs—have a characteristic secondary structure comprising a double stranded RNA stem and a single-stranded loop region, in total called "hairpin". Recent investigations of pri- and pre-miRNAs with conserved terminal loop regions suggest a crucial role of these loop regions during the biogenesis of the mature miRNAs.

Ten years after the discovery of miRNAs, there are more than 2'200 human miRNAs identified (as of 20.11.2012) and there are more than 5'000 miRNA-disease associations from over 2'700 scientific publications. From these, miR-122 is of particular interest because of its role in hepatitis C viral replication and antagonists of its function are currently being tested in clinical trials.

Therefore direct targeting of non-coding (ncRNA) with antisense oligoribonucleotides (ASOs) has promise as a valuable alternative to the "classical" protein based drug discovery. However, rational design or identification of small-molecule drugs that selectively and safely interact with nucleic acids has to date been unsuccessful. My work begins with the hypothesis that the distinct secondary structure of pre-miRNAs might offer enhanced binding affinity and selectivity for very short complementary ASOs due to pre-organization. Short oligonucleotides would represent a major advance in targeting RNAs.

Surface plasmon resonance spectroscopy (SPR) is an optical technique for the detection and quantification of molecular interactions without the need of labeling and in real-time. Since its first usage with organic monolayers about 30 years ago, SPR has become the method of choice for the characterization of macromolecular interactions involving peptides, proteins and nucleic acids.

As a part of a program in our lab to probe the accessibility of miRNA precursors (pre-miRNA) and particularly the conserved terminal loop regions of pre-miRNAs I developed an SPR-based binding assay for the identification of binding sites of pre-miRNAs for complementary oligoribonucleotides. I synthesized libraries of short (7–14 nt) fully complementary ASOs against stem-loop structured RNA oligoribonucleotides and tested them by SPR for their binding affinity to the hairpin captured to the surface of an SPR chip. With these systematic screens ("walkarounds") I unambiguously identified the single stranded terminal loop region as preferred binding sites. Further investigations of these loop-binding oligoribonucleotides, named "LooptomiRs", revealed an uniform preference for the 3'-end of the loop region. The results are presented in chapter 2.

Co-workers in our group developed protocols for the chemical modification of single nucleotides with the intention to selectively modify binding properties and enhance affinity for

their nucleic acid targets. In collaboration with them I tested a large set of modified "Loop-tomiRs" against the hairpin of pre-miR-122 for their ability to enhance the binding affinity towards structured target RNA molecules. The testing of this library revealed a ≈ 20–30 fold increase in binding affinity of certain molecules which is presented in chapter 4. These molecules are currently under investigation in our laboratory in cellular assays.

RNase H is an enzyme (ribonuclease) which belongs to the most ancient protein folds identified. It is ubiquitously found in prokaryotes, eukaryotes and in viruses and cleaves RNA molecules in RNA/DNA duplexes. This property is exploited for the target degradation of RNA molecules by introducing complementary ASOs. In collaboration with Dr. med. F. Paun, a master student in pharmaceutical sciences who worked under my supervision, I established an enzymatic assay for the detection and identification (chapter 3) of RNase H-mediated cleavage products, which is presented in chapter 5.

Finally, I developed a novel method for the SPR-based measurement of extremely low dissociation rates, k_{d}, in the range of 10^{-6} / $10^{-7}\,\mathrm{s}^{-1}$. This method, which we termed INSTED, was successfully tested with the determination of the dissociation rate of biotin-streptavdin and is presented in chapter 6.

Zusammenfassung

MikroRNAs (miRNAs) sind kurze ($\sim$ 22 nt), nicht für Proteine kodierende RNA Moleküle, welche die Genexpression regulieren. Durch Bindung an die sogenannte "3'-untranslated region" (UTR, eine Sequenz ausserhalb des Proteincodes) von messenger RNA (mRNA) unterdrücken sie entweder die Translation der mRNA oder leiten deren Abbau ein. Dadurch spielen sie eine wichtige Rolle sowohl im gesunden Organismus (z.B. bei der Zellproliferation oder Apoptose), als auch bei vielen Krankheiten, wie z.B. Krebs, Stoffwechselstörungen und auch viralen Infektionen. Die miRNA Vorläufer (pri- und pre-miRNAs) formen sich zu einer charakteristischen Sekundärstruktur, welche aus einem doppelsträngigen RNA Strang und einer einzelsträngigen Schleife besteht und "hairpin" (z.dt. "Haarnadel") genannt wird. Neuere Untersuchungen dieser Vorläufer, welche eine konservierte Primärsequenz der Schleife aufweisen, deuten darauf hin, daß diese Schleife eine wichtige Aufgabe während der Biogenese von reifen miRNAs einnimmt.

In den letzten 10 Jahren seit der Entdeckung der miRNA wurden über 2'200 menschliche miRNAs beschrieben (Stand 20.11.2012) und über 5'000 Beziehungen zwischen miRNAs und Krankheiten festgestellt. Wegen ihrer Schlüsselrolle bei der Replikation des Hepatitis C Virus (HCV) ist die mikroRNA-122 von besonderem Interesse und Inhibitoren dieser mikroRNA sind bereits in klinischen Studien.

Aus diesen Gründen erscheint der Angriff auf nichtkodierende RNA (ncRNA) mit komplementären Oligonukleotiden eine durchwegs valable Alternative zu den "klassischen" Methoden der Medikamentenentwicklung, welche auf Proteinen basiert, zu sein. Dies insbesondere, weil es bisher nicht möglich war, kleine Moleküle zu entwickeln, welche selektiv und ohne Schäden für die Gesundheit, mit Nukleinsäuren interagieren und diese so in ihrer Funktion beeinträchtigen. Meine Arbeit setzt an dieser Stelle an: Gestützt auf die Hypothese, dass die ausgeprägte Sekundärstruktur der pre-miRNA eine erhöhte Affinität gegenüber sehr kurzen komplementären Oligonukleotiden hat, begab ich mich auf die Suche nach solchen. Die erfolgreiche Inhibierung von pre-miRNAs mit sehr kurzen Oligonukleotiden brächte einen entscheidenden Fortschritt in der Entwicklung von neuen Medikamenten.

Oberflächenplasmonenresonanzspektroskopie (SPR) ist eine optische Messmethode zur Bestimmung und Quantifizierung von Molekülinteraktionen, welche in Echtzeit und ohne die Notwendigkeit einer Markierung durchgeführt werden kann. Seit ihrer Entwicklung vor etwa 30 Jahren wurde sie zu einer Standardmethode zur Charakterisierung der Bindung zwischen Makromolekülen, einschliesslich Proteinen, Peptiden und Nukleinsäuren.

Als Teil eines Programms zur Identifikation möglicher Bindungsstellen von miRNA Vorläufern (pre-miRNAs) im Allgemeinen und konservierter Schleifen im Speziellen habe ich einen auf SPR basierenden "assay" entwickelt, mit welchem die Bindungsstärke von kurzen Oligonukleotiden an diese Vorläufer gemessen werden kann. Dazu wurden Bibliotheken von kurzen (etwa 7–14 Nukleotide) komplementären Oligonukleotiden synthetisiert, welche gegen die Sekundärstruktur der pri-/pre-miRNA gerichtet sind. Diese Oligonukleotide wurden systematisch gegen die Vorläufer getestet, was eindeutig eine bevorzugte Bindungsstelle in

der einzelsträngigen Schleifenregion ergab. Weitere Untersuchungen dieser sogenannten "LooptomiRs" ergaben, daß das 3'-Ende der Schleife bevorzugt gebunden wird. Die Ergebnisse dieser Untersuchung werden in Kapitel 2 dargelegt.

Mitarbeiter unserer Arbeitsgruppe haben Protokolle zur Modifizierung von Nukleotiden entwickelt, mit dem Ziel, die Bindungsstärke von kurzen Oligonukleotiden an ihre Ziel-RNA zu erhöhen. Eine Bibliothek der zuvor entdeckten Oligonukleotide mit einzelnen solcher modifizierten Nukleotiden wurde gegen die pre-miRNA-122 getestet. Dabei wurden Oligonukleotide entdeckt, welche eine um bis zu 30-fach erhöhte Affinität aufwiesen. Kapitel 4 beschreibt diese Ergebnisse.

RNase H ist eine Ribonuklease welche zu den ältesten Proteinen gezählt wird und in Prokaryoten, Eukaryoten und Viren exprimiert wird. Sie schneidet RNA, welche sich in RNA/DNA Duplexen befinden. Durch diese Eigenschaft kann man den Abbau von RNA durch eingebrachte komplementäre DNA induzieren. In Zusammenarbeit mit Dr. F. Paun, einem Masterstudenten, habe ich einen Enzymassay zur Identifikation von Abbauprodukten von RNase H implementiert, welcher erfolgreich mit DNA "LooptomiRs" getestet wurde. Die Ergebnisse werden in Kapitel 5 vorgestellt.

Die Quantifizierung von sehr kleinen Dissotiationsgeschwindigkeiten in der Grössenordnung von 10^{-6} / $10^{-7}\,s^{-1}$ mittels SPR ist nur beschränkt möglich. Kapitel 6 zeigt die Ergebnisse einer von mir neu entwickelten Methode zur Bestimmung von sehr kleinen Dissotiationsgeschwindigkeiten, welche erfolgreich am Beispiel der Dissotiation des Biotin/Streptavidin-Komplexes angewendet wurde.

1. Introduction

1.1. The drugability of RNA

F OR a long time, RNA has been regarded as a machinery exclusively devoted to de-
coding genomic information into protein. With the discovery of ribozymes, small
nuclear RNA (snRNA)—and especially—microRNA (miRNA) this paradigm required
an extension: In the past 20 years, the important role of noncoding RNA (ncRNA) has be-
come more and more obvious. Recent findings revealed that about 40 % of all transcribed
bases remain uniquely in the nucleus (33 % as long non-coding RNA) [1] and that there is
a large portion of transcripts of the **antisense** DNA strand, which is regarded as source of
unique regulatory RNA [2]. Modulation of gene expression by ncRNA is a crucial regulatory
mechanism and RNA can be directly linked to diseases e.g. in the case of altered miRNA
expression [3] or other mechanisms which include RNA-mediated impairments by genetic
changes (reviewed in [4, 5]).

Direct targeting of ncRNA may become a valuable alternative to the "classical" protein based
drug discovery. However, rational design or identification of small-molecule drugs that selec-
tively and safely interact with nucleic acids [6] is challenging. Relatively unselective nucleic
acid binding drugs are however in use, for example DNA-interacting cytotoxic chemothera-
peutics [7] and aminoglycoside [8, 9] or macrolide [10] antibiotics which bind to bacterial
ribosomal RNAs. Recent studies have shown that streptomycin (an aminoglycoside an-
tibiotic) not only binds to bacterial ribosomal RNA but also directly interacts with a human
pre-microRNA (pre-miRNA-21 [11]).

First investigations with antisense-based oligonucleotides targeting mRNA were already re-
ported in the late 1970's by Zamecnik and Stephenson [12]. Meanwhile the targeting of
RNAs with complementary oligoribonucleotides has become a validated approach [13–16]:
currently (status September 2011) there are over 100 clinical trials with antisense-based
oligoribonucleotides [17] in the USA. However, there are still demanding challenges to the
technology such as poor pharmacokinetics (at least with first-generation oligoribonucleo-
tides), issues of tissue-specificity (e.g. accessibility to the brain, heart or muscles) or high
manufacturing costs [18]. The search for generally applicable nucleic acid based therapeu-
tics has just begun. . . .

1.2. MicroRNA

MicroRNAs (miRNAs) are a recently discovered class of short (≈ 22 nt in length), non-coding
RNAs that regulate gene expression in eukaryotic cells via binding to mRNA. Upon binding
to complementary bases in the 3'-UTR of a mRNA they either inhibit translation or initiate
mRNA degradation [19, 20].They have important roles in health and disease and it is esti-
mated that miRNAs regulate up to 60 % of protein-coding genes in mammals [21]. Currently

there are more than 2200 human miRNAs identified (www.mirbase.org, state 20.11.2012) and there are more than 5000 miRNA-disease associations from over 2700 publications (entries retrieved from the human microRNA disease database on January 2013) such as cancer [22–24], (cardio)metabolic disorders [25], schizophrenia [26], HCV-infection [27] and many more (reviewed in [28–30]).

Although the question has been extensively investigated in the past 12 years, the biogenesis of mature miRNAs is a process which is still only partially understood. Recent findings such as the regulation of the drosha-mediated cleavage of pre-miR-18a by hnRNP A1 (cf. sections 1.3.1, 2.1.1.3 and [31]) suggest that yet undiscovered cofactors influence pri-/pre-miRNA processing. In the following sections I outline the most important steps during miRNA biogenesis.

1.2.1. Discovery of microRNA

In 1993 Lee, Feinbaum, and Ambros described the negative regulation of lin-14—a protein which acts as a developmental timer—by lin-4 in the nematode *C. elegans* and reported that this negative regulation was driven by an antisense RNA-RNA interaction with repeated sequence elements in the 3' untranslated region (UTR) [32]. They described two transcripts of the lin-4 gene with lengths of 22 and 61 nt—corresponding to the mature miRNA and its precursor hairpin, respectively.

The true impact of these findings was reinforced in 2000 as a second microRNA was discovered which was shown to have widespread abundance: let-7 [33–35]. At this time, lin-4 and let-7 were called small temporal RNAs (stRNAs). One year later, the laboratories of Bartel, Tuschl, and Ambros reported many more of these small RNAs in *C. elegans* [36–38] in the same issue of Science and concordantly renamed the small temporal RNA microRNA (miRNA).

Meanwhile there are almost 50'000 scientific articles containing the concept "microRNA" (on Scifinder, as of March, 4th 2013). and the number of new miRNA-related publications per year is growing exponentially.

1.2.2. microRNA biogenesis

Summary MiRNAs are generated from endogenous transcripts by RNA polymerase II. The primary stem-loop structures—pri-miRNAs—are processed in the nucleus by an RNase III-type enzyme called Drosha to yield the ∼60–70 nt long precursor miRNA (pre-miRNA). After export from the nucleus by Exportin-5, the pre-miRNAs are substrate of another RNaseIII-type enzyme—Dicer—which cuts off the terminal loop region resulting in the final mature miRNA which further regulates gene expression by targeting mRNA. The targeted mRNA can be disturbed in its function by either translational inhibition or cleavage.

In the following sections I give a short overview over the most important steps in miRNA biogenesis and function in health and disease.
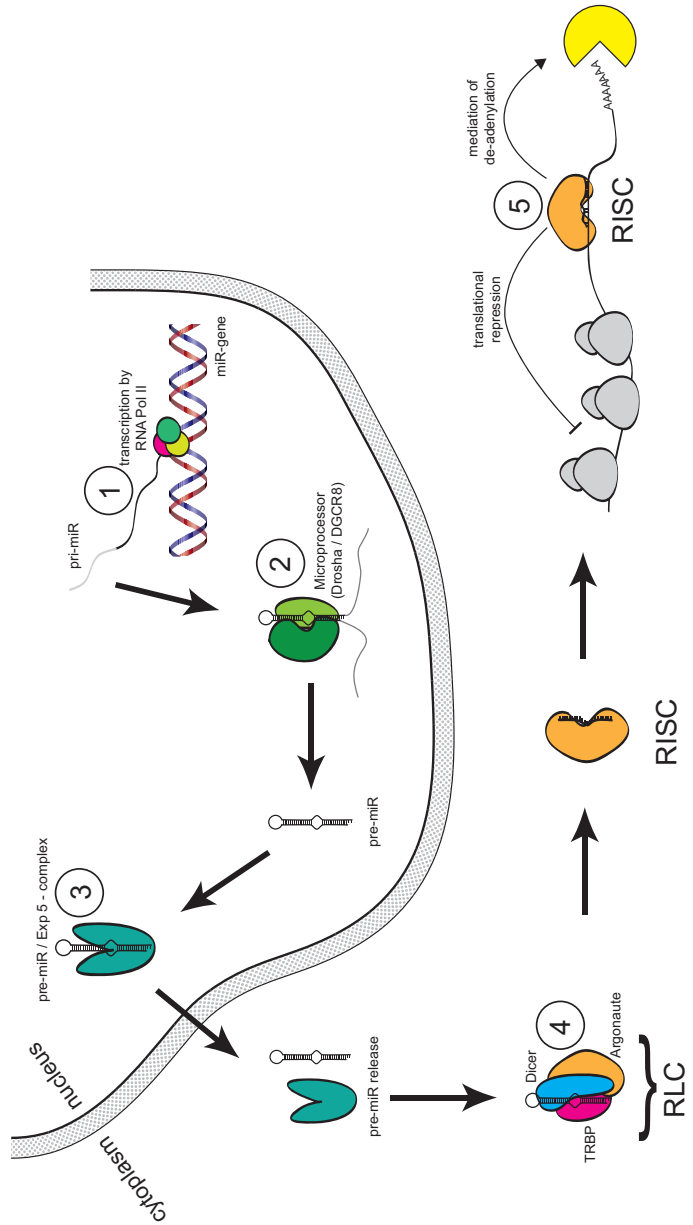
Figure 1.1. – Scheme of miRNA biosynthesis. After the transcription (1) of the miRNA gene, the pri-miRNA is cleaved by the microprocessor to yield the pre-miRNA (2). Export from the nucleus to the cytoplasm is mediated by Exportin-5 (3). The pre-miRNA is cleaved by Dicer (4) and handed over to Ago 2. The RISC-mediated inhibition of function of the target mRNA results in either translational repression or cleavage of the mRNA after deadenylation (5). Fig. adapted from [39, 40].

1.2.2.1. Transcription

Most mammalian miRNAs are transcribed by RNA polymerase II as independent transcription units [41] (cf. (1) in fig. 1.1, p. 15), other gene loci of miRNA were found to be in intronic or exonic regions of either coding or non-coding genes [40, 42–44]. They can be expressed polycistronically, where several miRNAs are clustered in close proximity to other miRNAs, or monocistronically [45]. The cluster members transcribed from polycistronic transcription units (TU) show a high level of conservation [46].

Although the promotors for transcription of intronic miRNAs are usually shared with their host genes [47], about one third of the intronic miRNAs were found to be transcribed with their own promotors [48]. Splicing is not a precondition prior to the processing by Drosha, as it has been shown that a disabled splicing of the host gene still led to effective maturation of pri-miRNAs [49].

Most miRNA genes are transcribed by RNA Polymerase II (Pol II) [41, 50], with a small fraction being transcribed by RNA Polymerase III [51]. After transcription by Pol II they are modified by a 3'-poly-(A) tail and a 5'-guanosine cap. These primary transcripts—called pri-miRNA—are usually several kilobases long and bear the typical hairpin structure of the pre-miRNA including the characteristic bulges.

Although the majority of mature miRNAs is derived from a Drosha-/Dicer-mediated biogenesis, there are alternative mechanisms which can produce miRNAs from other sources such as mirtrons [52], tRNA [53] or snoRNAs [54].

1.2.2.2. The microprocessor

In the nucleus, the pri-miRNA is further cleaved by an RNase III family enzyme called Drosha [55] (cf. (2) in fig. 1.1, p. 15). Drosha forms together with the *Di George syndrome critical region gene8* (DGCR8) a complex—the so called microprocessor—with a size of ∼650 kDa [56, 57]. DGCR8 is required for processing of pri-miRNA by Drosha [56, 57], as Drosha cannot cleave the pri-miRNA without DGCR8 [58].

A typical Drosha substrate is a hairpin with a ∼33 nt long stem that contains the characteristic bulges of mature miRNA duplexes [59]. Although early studies reported a crucial role of the loop region [59] (cf. section 1.3.2, p. 19) recent studies showed that the loop is not required for processing [60]. DGCR8 assists the processing by binding to the ssRNA segments and directs Drosha to cleave the substrate ∼ 11 bp away from the junction of the ssRNA flanks / dsRNA stem [59, 60]. As mentioned in section 1.3.2 there are additional co-factors of pri-miRNA cleavage such as hnRNP A1 which is required for the Drosha-mediated processing of mir-18a.

The released product is the precursor miRNA—pre-miRNA—which is subsequently exported to the cytoplasm by Exportin-5.

1.2.2.3. Exportin-5

The nuclear export protein Exportin-5 (Exp-5) is a member of the nuclear transport receptor family and acts in a RanGTP-dependent way [61, 62]. It recognizes the >14 bp long pre-

miRNA stem along with a short 3'-overhang [63] (cf. ③ in fig. 1.1, p. 15). After binding of the pre-miRNA and the GTP-bound cofactor RAN, the complex passes from the nucleus into the cytoplasm. There the release of the cargo is triggered by a RanGTPase-mediated hydrolysis of GTP to GDP [62]. The released pre-miRNA is then further cleaved by the RNase III endonuclease Dicer to yield the mature miRNA.

1.2.2.4. Dicer cleavage

Human Dicer is a 219 kDa multi-domain protein with a helicase/ATPase domain, a platform domain, a PAZ domain, the two catalytic domains RNase IIIa/b, a dsRBD and several regions of unknown function [64]. Dicer cleaves the substrate (pre-miRNA) in a Mg^{2+}-dependent fashion near the loop releasing the $\sim$22 nt long mature miRNA duplex [65–67] (cf. ④ in fig. 1.1, p. 15). Thus, the "open" end of the pre-miRNA was created by Drosha and the end which is generated by the cleavage of the loop-region is determined by Dicer.

Dicer associates with dsRNA-binding proteins such as TRBP [68] and PACT [69] which are not necessary for cleavage ([70]; we successfully applied in our laboratory a biochemical assay without any cofactors), but which facilitates the formation of the RNA-induced silencing complex—RISC [71]. The complex of Dicer, TRBP, PACT, and Ago-2 together is the RISC loading complex or RLC [72–74].

Dicer cleavage experiments performed with an artificial perfectly complementary dsRNA substrate that was provided with a loop exhibited an increased affinity, whereas the removal of the loop region from the pre-miRNA led to a slowed processing [75]. Another investigation of Feng et al. showed that the size of the loop is influencing the cleavage efficiency: hairpins with loops $\geq$ 10 nt were cleaved more efficiently [70]. This indicates once more that the targeting of the loop-region might be a promising alternative to alter or even inhibit Dicer-mediated cleavage of pre-miRNA.

1.2.2.5. RISC

After cleavage of the pre-miRNA to the mature miRNA, the resulting $\sim$22 nt dsRNA complex is loaded onto an AGO protein to form the RISC [76]. RISC is a multiprotein complex which comprises (besides Ago and the miRNA) protein cofactors that are used for the binding of the poly-(A) tail of the target mRNA (poly-(A) binding protein—PABP), as adaptors (GW182, which interacts with PABP) or for the cleavage of the poly-(A) tail (CCR4-NOT and PAN2-PAN3) [39, 77]. After incorporation of the dsRNA, Ago unwinds the duplex in an ATP-dependent way [78]. Thereby the strand with the lower thermodynamically stable 5'-end— the "guide" (also known as "sense" or miRNA strand)—is maintained and the other—the "passenger" (also known as "antisense" or miRNA* strand)—is degraded [79, 80]. In the RISC, Ago directs the miRNA to its target mRNA [81] which leads to either transcriptional repression [39] or mRNA degradation by deadenylation [82] (cf. ⑤ in fig. 1.1, p. 15).

1.3. Mechanisms of Antisense oligoribonucleotides: ASOs, AMOs, antimirs, LooptomiRs & co.

The targeting of RNA by antisense oligoribonucleotides (ASOs) is governed by Watson-Crick base pairing [83]. This interaction includes not only the specific hydrogen bonds between the bases of the single nucleotides, but also hydrophobic interactions and a coaxial stacking of the bases. ASOs are typically rather short oligonucleotides (8-50 nt) which alter the function of the target RNA upon binding. Therefore the term ASO refers to a more general mechanism of action.

There are two mechanisms in which antisense oligoribonucleotides can act (reviewed in [84, 85]):

1. Noncleavage-based mechanisms

2. Cleavage-based mechanism

Noncleavage-based mechanisms involve a binding to the target RNA and subsequent inhibition of its function. There are many stages at which ASOs can act: modification of translation [86, 87], splicing [88–90], or polyadenylation [91]. Further they can act as RNA (ant-)agonists [92, 93] or by disruption of the target RNA structure [94].

Cleavage-based mechanisms include the RNase H-induced cleavage of target RNAs [95–97] by using 'gapmer' oligonucleotides which comprise a central core of DNA flanked by modified nucleotides for enhanced nuclease stability (cf. section 1.3.3). Of equal importance today is the RNAi mechanism which uses Argonaute 2 (Ago 2) as the endogenous nucleases [98–100].

Our group focuses on the inhibition/alteration of miRNA biogenesis/maturation employing both noncleavage-based and cleavage-based mechanisms (cf. chapter 5) using AMOs / antimirs and LooptomiRs (short antisense oligoribonucleotides targeting hairpin RNA loops).

1.3.1. Targeting miRNA

Depending on the design, anti-microRNA antisense oligoribonucleotides (AMOs or antimiRs) inhibit miRNA function by only sterical blocking or subsequent degradation [101]. However, studies with 2'-MOE/DNA gapmers revealed only poor activity as AMOs, making the design of "steric blockers" the method of choice [102].

AMOs usually cover the whole length of the target miRNA. They can be shorter, but it is essential that they cover the 5'-end (the so called "seed-region", which is used for the recognition of their mRNA targets) in order to function [101]. Davis et al. showed that the acitivity of an AMO was raised if it was complementary from the second base on (the start of the "seed-region") [102].

A special form of an AMO was described by Krützfeldt et al. in 2005. By the introduction of a 3'-cholesterol group and flanking phosphorothioate (PS) linkages of the backbone this so called "antagomir" exhibited an improved cellular uptake with enhanced nuclease stability

and was shown to be an active miRNA silencer *in vivo* (mice) of pre-miR-122 and pre-miR-16 [103] (cf. section 1.3.3). Of note, the "antagomir" did not show any activity, if the PS linkages were placed between every nucleotide, maybe due to the lowered affinity. These findings validated the notion that the 2'-OMe/PS-chimera was stable enough against nucleases to be given intravenously. Other groups which were using the same "antagomir" design found similar results [104, 105].

1.3.2. The importance of secondary structures

With the example of hnRNP A1 and pri-miR-18a Michlewski and coworkers showed that the loop-region plays a key role for the processing of pre-miR-18a by Drosha [31]. This is in contrast to the work of other groups that report only a minor role of the terminal loops for processing [60] consistent with the poor phylogenetic conservation of these loops for most pre-miRNAs [106]. However, Michlewski et al. revealed that pri-/pre-miR-18a has a highly conserved terminal loop region and that about 14 % of all pri-miRNAs have phylogenetically conserved terminal loops. They predicted these as "landing pads" for protein factors that influence miRNA processing [31]. They reported for the first time a successful inhibition of the Drosha processing of five pri-miRNAs using loop-targeting ASOs (LooptomiRs[i]).

Michlewski et al. showed that only pri-miR-18a processing was affected by hnRNP A1 and that the other members of the same cluster were not [31]. Interestingly, Lünse et al. identified an aptamer that inhibited the biogenesis of all cluster members of pri-miR-17–19b-1 upon binding to the terminal ("apical") loop of pri-miR-18a [107].

In contrast to the findings by Han et al. [60], Zhang and Zeng [108] emphasized the importance of the loop region for the processing by Drosha and Dicer: mutants of pre-miR-16, pre-miR-30, and pre-miR-31 with modified and unmodified loops were less effective substrates of drosha processing of pri- as well as dicer processing of pre-miRNAs by loop-modifications [108].

Consequently, the design of LooptomiR oligoribonucleotides seems to be a promising therapeutic approach, especially for miRNAs with conserved terminal loop regions.

In work pre-dating the discovery of miRNAs, Lima et al. investigated the influence of the secondary structure of a hairpin on the binding affinity of ASOs. Using an enzymatic cleavage assay they determined that the secondary structure of part of the h-ras mRNA formed a hairpin. They then determined the binding affinities of 6 decamers targeting different positions of the hairpin based on a gel shift assay (cf. section 2.1.1.1, p. 31) [109, 110].

Kierzek investigated the hybridization of binding of different RNA hairpin structures to isoenergetic microarray probes with penta- and hexamers. She reported a strong binding of short hairpins to the microarray probes preferentially with bulges, internal loops and dangling ends, though no K_D values were given [111].

1.3.3. 2'-Modifications of RNA: the second generation of ASOs

Since the first report of anti-mRNA ASOs in 1978 [12], which were conducted with unmodified DNA molecules, much progress has been achieved concerning their medicinal chem-

---

[i]LooptomiRs: Loop Targeting Oligonucleotide anti miRNAs

istry. Unmodified DNA antisense oligoribonucleotides undergo rapid degradation in (human) serum and cells by endogenous endo- and exonucleases [112] and they have a rather poor uptake into cells. This rapid degradation is one of the major hurdles in antisense technology. To overcome this and other problems, such as insufficient binding affinity, chemical modifications were developed that endowed ASOs with increased nuclease resistance, increased binding affinity, better cellular uptake, and reduced potential of triggering an immune response [85, 101, 102, 113].

The most common variants of nucleic acids used for AMOs include two kinds of modifications [101, 113, 114], which are shown in fig. 1.2, p. 21:

1. Backbone modifications: These modifications include phosphorothioate (PS) linkages instead of phosphodiester (PO) linkages. Additionally, there are two non-ribose backbone modifications:

    - peptide nucleic acids (PNA), and

    - phosphorodiamidate morpholino oligonucleotides (PMO, "morpholinos").

2. Sugar modifications: These modifications include groups at the 2'-position of ribose. There are mainly 4 modifications:

    - 2'-OMe RNA: These nucleotides have a methylated hydroxyl group at the 2'-position.

    - 2'-MOE RNA: These nucleotides have a 2'-O-methoxyethyl group.

    - 2'-F RNA: These nucleotides have a fluorine at the 2'-position of deoxyribose

    - Locked nucleic acids (LNA): These nucleotides have a methylene bridge that tethers the 2'-O to the 4'-C.

One of the first modifications introduced was the 2'-OMe modified RNA [115], which is—compared to unmodified RNA and DNA—resistant against degradation by cellular nucleases [116]. This modification does not only provide an enhanced nuclease stability, but also raises the binding affinity substantially [117]. Finally, this is—as opposed to all other 2'-modifications—a naturally occurring 2'-modification (found in mammalian rRNAs and tRNAs) and thus is not toxic [118].

The phosphorothioate linkage replaces one of the non-bridging oxygens of the phosphate by a sulfur atom which reduces the capability of cleavage by many nucleases. It can be placed either throughout the whole sequence or at selected positions but reduces the binding affinity by an estimated 0.5–0.7 °C/modification [102, 114, 119].

Although the susceptibility of 2'-OMe RNA to nuclease cleavage is drastically reduced, pure 2'-OMe RNA oligoribonucleotides without PS linkages are degraded in serum rather quickly [120]. Therefore they are typically combined with flanking PS linkages for *in vivo* use [103]. When the more stable 2'-MOE modification with full PS linkages was used, the affinity was high enough for the fully 2'-MOE-PS modified oligoribonucleotide to act as an AMO. This was shown by Esau et al. for miR-143 in cultured adipocytes [121] as well as for miR-122 *in vivo* [122].

Locked nucleic acids, first synthesized by Obika et al. and Koshkin et al. [123, 124] hold the sugar conformation in a C3'-*endo* position yielding an extraordinary high binding affinity

A

DNA

RNA

LNA

2'-F

2'-OMe

2'-MOE

B

PNA

Phosphorothioate RNA

PMO

Figure 1.2. – Structures of nucleic acid modifications used for ASOs/AMOs. A) Sugar modifications. B) Backbone modifications: left: Phosphorothioate backbone modification, right: non-ribose backbones.
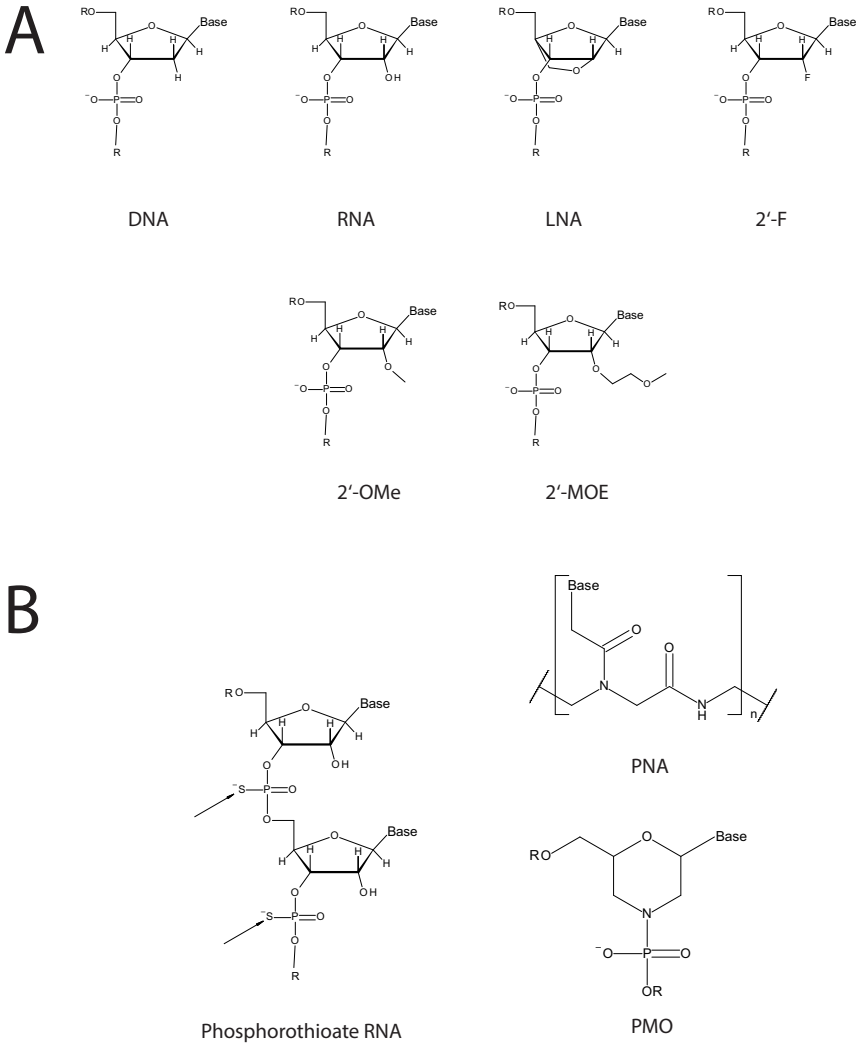
for RNA, as well as providing good nuclease stability [125]. The increase in binding affinity corresponds to higher melting temperatures of +1 − +8 °C/modification against DNA and +2 − +10 °C/modification against RNA [126].

Davis et al. performed an in-depth-analysis of differently combined AMOs using DNA, 2'-OMe, 2'-MOE, 2'-F, and LNA against miR-21 [102]. They showed that the melting temperature for a 2'-MOE-LNA-PS was 37 °C higher than its isosequential DNA-PO sequence (49 °C vs. 86 °C). Of note, although having by far the highest melting temperature, the 2'-MOE-LNA-PS AMO had not the highest activity and was outperformed by several other AMOs including a uniform 2'-MOE-PO and 2'-MOE-PS variant. Lennox et al. reported a reduced potency of an AMO if a certain affinity value was exceeded. They allocated this phenomenon to self-dimerization effects for very strong binders such as LNA modified AMOs [101]. Additionally, Davis et al. tested so called "gapmers" with a central DNA core and flanking nucleotides with 2'-modifications for RNase H induction [102]. Interestingly, these "gapmers" showed only a poor performance as AMOs indicating that the cleavage-based mechanism was not preferred (*vide supra*). Finally, they showed that truncation of an AMO by 1 base from its 3'-end (corresponding to the 5'-terminus of the target miRNA, thus starting with the seed-region), yielded an increased potency.

Taken together, one can state that a potent AMO has to have a blend of high affinity (up to a certain threshold) and increased nuclease stability, which is best reached with 2'-MOE modified nucleotides and flanking PS linkages. The most probable mechanism of action seems to be a steric-blocking mechanism.

1.4. SPR

The older methods for studying the interactions of DNA and/or RNA molecules (e.g. gel shift) are only qualitative or semiquantitative and the molecules often have to be labeled, which can interfere with the measurements. Furthermore, they do not allow measurements of kinetic rate constants, k_a and k_d, in real-time. With surface plasmon resonance spectroscopy (SPR) it is possible to monitor many different interactions of proteins, nucleotides, small molecules and even whole membrane-incorporated receptors such as GPCR's or cells. With labelfree and under real-time conditions one can determine many different parameters from thermodynamics (K_A, K_D, ΔH, ΔS), kinetics (k_a, k_d and $t_{1/2}$), competition/ Inhibition (IC_{50}, K_i), and specificity (yes/no-decisions).

Many SPR investigations have been performed on nucleic acid interactions and some examples are given in the next section.

1.4.1. SPR-based measurements of nucleic acid interactions

First measurements of DNA-DNA interactions with SPR date back to 1993 [127]. In 1997, Jensen et al. investigated the stability of pentadecamer PNA complexes with RNA and DNA complements and the impact of mismatches in the middle of the sequence. They showed a good correlation between the calculated K_D values of the measured PNA/RNA and PNA/DNA duplexes compared to melting point measurements: the most stable com-

plexes (highest Tm values) exhibited the lowest dissociation and the highest association rates [128].

An investigation of RNA-RNA interactions using SPR was carried out by the group of J.-J. Toulmé in 2000 [129]. Based on the findings of Gregorian and Crothers [130] who showed that the loop-closing base pair is crucial for the stability of the kissing complex in RNA I:RNA II complex of E. coli, Ducongé et al. analysed the binding towards a 59-nt long RNA element of HIV-1 virus called trans-activating-responsive region (TAR). TAR which is a transcription enhancing RNA hairpin necessary for viral replication, binds Tat—a HIV-1 viral trans-activator protein—in the upper part on a 3-nt bulge. Tat itself recruits cyclin T1, and cyclin-dependent kinase 9 (CDK9), both of which are host cellular factors that prevent the shut-down of the transcription of the retroviral genome. Using in-vitro selection Ducongé et al. identified some high-affinity anti-TAR aptamers in the form of hairpins, all characterized by a conserved loop-closing GA-pair. They revealed that this closing GA-pair is a crucial component for the stability of "kissing complex" formed by the loops of two hairpins. The stability of the complex concerning the closing base pair decreases in the order AG $>$ GG $>$ GU $>$ AA $>$ GC $>$ UA $>>$ CA, CU yielding a 50-fold difference in binding affinity.

As the TAR-TAR*-complex was determined to be a model system for RNA loop-loop interactions [131], Nair et al. investigated using SPR the stabilizing effect of a 2-thiouridine (s^2U) modification and whether it can be generalized to other loop-loop interactions [132] (the s^2U modification stabilizes RNA duplexes by stabilizing the 3'-*endo* sugar conformation (similar to LNA) of the nucleoside [133,134]). Nair et al. showed that a s^2U modified anti-TAR hairpin had an 8 times higher affinity to the fully complementary hairpin (bound to the chip surface) than the unmodified hairpin (1.58 nM vs. 12.5 nM), thanks to a doubled rate of association and a four times lower dissociation rate.

Finally, another SPR study on the TAR RNA motif was done by Darfeuille et al. in 2001 [135]. They investigated the binding of a N3'$\rightarrow$P5' modified variant of the most stable SELEX-based RNA aptamer finding similar affinities for the modified and unmodified molecules (4.1 nM (amidate) vs. 4.8 nM (amidite)).

Various SPR studies for the investigation of binding affinities of RNA hairpins against aptamers, single oligonucleotides or small molecules have followed these works [136–143].

There are—to my best knowledge—only two systematic screenings investigating the affinity of different oligoribonucleotides (either length or chemistry) against the loop of a hairpin with surface plasmon resonance.

The first was done by Di Primo et al. in 2007: based on an initial investigation [139] they modified the found 6 nt-loop of an aptamer with a set of 64 (= 2^6) LNA/2'-OMe sequences corresponding to all possible combinations of such residues. Subsequent testing against the 6-nt loop of the TAR element of HIV-1 (a binding called "kissing loops") revealed three combinations which displayed an affinity for TAR below 1 nM. These 3 combinations had either one or two LNA units located on the 3'-end of the aptamer loop [144].

The second account was done by Mandir et al. in 2009 [145]: Using DNA arrays with in situ oligonucleotide synthesis they determined accessible sites of three pre-miRNAs (pre-miR-155, pre-let-7a-3, pre-let-7c) with SPR. These tiling arrays with 6, 8, and 12mer oligonucleotide features revealed preferred binding sites of single-stranded loop regions or bulges (compared with lowest-energy structures as given by MFold). The array has the advan-

tage of screening large amounts of oligonucleotides in a high throughput screening mode, although no quantitative data was provided.

1.4.2. Short historical overview

Although the phenomenon of evanescent waves generated by the resonance of light with surface plasmons was discovered more than 100 years ago by R.W. Wood [146], the first use of Surface Plasmon Resonance with organic monolayers was described only in the late 1970's [147]. Facilitated by their high molecular weights, first applications of SPR were reported in the mid 1980's for the monitoring of antigen/antibody interactions [148, 149]. After reports of real-time binding events in the late 1980's [150, 151] the first commercially available SPR machine equipped with an appropriate microfluidic device, optical detection unit and kits for optimal surface chemistry treatment were developed by Pharmacia Biosensor AB (renamed Biacore AB Corporation in 1996 and acquired by GE Healthcare in 2006) and launched in 1990 [152] (http://www.biacore.com/lifesciences/history/index.html). To this day, GE Healthcare's Biacore machines dominate the SPR market with close to 90 % of all SPR related publications performed with a Biacore instrument (87 % in 2005, 89 % in 2007) [153, 154]. In 2009 there were more than 1500 papers that used SPR-based measurements and the number per year is constantly increasing [155]. In our laboratory, we are using a SPR 2 machine recently developed by SierraSensors Inc., Hamburg, Germany (www.sierrasensors.de). This machine uses a novel technique called Hydrodynamic Isolation™ for sample delivery and uses two sensor spots in one flow cell.

Because of the capability of monitoring binding-events in real-time and the lack of necessity for labeling, SPR has gradually become the method of choice for the detection and quantification of protein-protein, protein-peptide, Protein-DNA/RNA, and DNA/RNA-DNA/RNA interactions [156]. The variety of applications is practically endless: Pharmaceutical (fragment-based) lead discovery [157, 158], food analysis [159, 160], detection of pathogens and infectious agents [161, 162], patient serum/blood analysis [163, 164], etc.. Besides this the SPR technique allows not only the determination of equilibrium dissociation constants, K_D, but as well an accurate measurement of the kinetic rate constants, k_a and k_d. This enables one to discriminate between different modes of binding behavior and to choose amongst the best binders those who have not only the best binding affinity, but as well the most favorable kinetics, e.g. the ones with the lowest dissociation rate constant.

1.4.3. Principles of SPR measurements

Total internal reflection is a phenomenon that occurs at the boundary of two non-absorbing media (e.g. water-air or buffer-glass). When a light wave, which propagates through one medium, hits the boundary of an adjacent medium of different refractive index under a angle, which is larger than a particular critical angle (Θ), the light wave is not refracted, but fully reflected. Collective vibrations of free electrons in (thin) metal layers yielding an electron gas (or plasma), which surrounds the atomic lattice sites, are called plasmons. Surface plasmons are evanescent waves, which propagate parallel to the surface on the boundary of the metal film. When the aforementioned interface between the two non-absorbing media is coated with a thin metal film (typically a gold-coating in SPR), these electromagnetic waves

can be excited by a photon of the reflected light beam. The excitation of surface plasmons by light is the so-called surface plasmon resonance (SPR) [165] (cf. fig. 1.3/A).
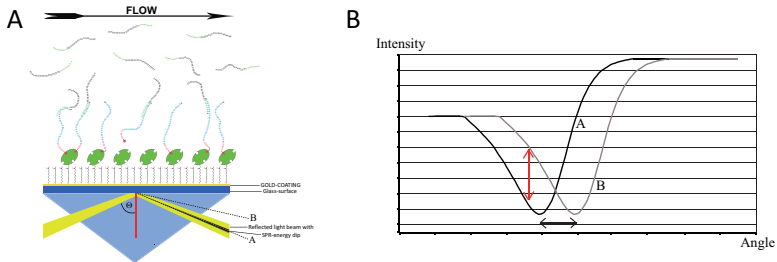
Figure 1.3. – Principle of SPR. A) The light beam which is reflected by the glass surface with total reflection generates an excitation of surface plasmons which results in an energy dip (black region in light beam). The angle of incidence—Θ—is larger than the critical angle for total reflection. B) Upon binding of a molecule to the chip surface, the refractive index on the chip surface changes which leads to a shift of the angle of the energy dip (A→B, cf. ↔ and A/B on the left). In our SPR setup, the change in light intensity due to that shift (cf. vertical red double arrow) is converted into the SPR signal.

This phenomenon can be used to determine the adsorption of material onto a thin gold or silver surface, because the oscillations are very sensitive to any change of the boundary of the metal and dielectric medium (=superstrate, e.g. air or liquid). The resulting change in the refractive index of the superstrate leads to a shift of the sharp intensity drop of the projected light beam interacting with the surface plasmon, which is produced by the energy transfer due to the resonance [156] (cf. fig. 1.3/B).

When one biomolecule binds to another which is immobilized on a sensor chip's gold surface, this leads to a change of refractive index. When a light beam is projected via a prism onto the surface of a sensor chip, the changed refractive index leads to a shift of the position of the reflected light minimum on the detector, which is proportional to the mass change of/on the metal surface (cf. fig. 1.3/A). The resulting change in light intensity (cf. red vertical double arrow in fig. 1.3/B) is converted into the SPR-signal.

There are five different phases in a Biacore experiment:

1. A pre-injection phase. (cf. ① in fig. 1.4) In this phase constant buffer flow conditions the chip surface carrying the immobilized ligand.

2. The analyte injection and association phase (cf. ② in fig. 1.4). The monitored change in angle (due to change in refractive index) is converted into the SPR signal which is increasing. The dominating association is the basis for the calculation of the k_a values.

3. In the equilibrium phase of the injection (cf. ③ in fig. 1.4), the association and the dissociation of the analyte to/from the ligand occur at equal rates. No change in Response is observed. The signal intensity during the equilibrium at different concentrations can be used for the determination of K_D in a scatchard plot.

4. The dissociation phase (cf. ④ in fig. 1.4). When the analyte solution is replaced by buffer, only the dissociation is observed. This phase is used for the calculation of k_d.

5. A regeneration phase (not shown). Remaining analytes are removed by injection of a suitable regeneration solution (cf. section 2.1.3, p. 35) to yield the same surface as prior to the injection of the analyte.
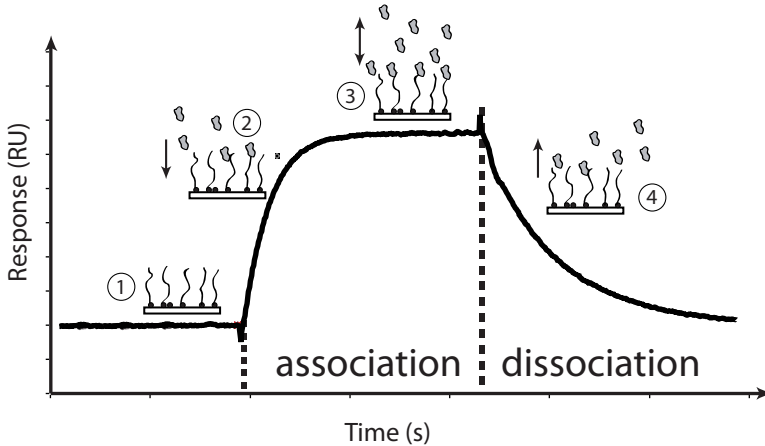
Figure 1.4. – Principle of an SPR measurement. For explanation see text

1.4.4. Setting up an assay

For a reliable determination of binding affinities, K_D, and kinetic rate constants, k_a and k_d, there are several important points to consider [166,167]:

1. The density of the ligand of the chip surface should be kept as low as possible to avoid mass transport limitation. Myszka suggests values of RU_{max} of $\leq 50\,RU$ [167] although there are different opinions [168].

2. The measurement data should be double-referenced to a sensor spot in a reference cell as well as to injections of blank buffer.

3. As a rule of thumb, for a steady-state analysis, the range of injections should cover analyte concentrations of $0.1 \cdot K_D \leq K_D \leq 10 \cdot K_D$ (and sufficient time has to be allowed to reach the steady-state).

4. Sensorgrams should exhibit sufficient curvature. Especially, k_d cannot be determined reliably, if there is no significant loss of analyte during the dissociation time chosen.

5. At least two concentrations should be measured in duplicates to show reproducibility and completeness of regeneration (cf. section 2.1.3, p. 35).

1.4.5. Fitting of the data

The shape of the binding curves determines the kinetic parameters. A fitting algorithm which is provided with the control software of todays SPR machines, determines the kinetic

rate constants, k_a and k_d, and/or the equilibrium dissociation constant, K_D, by fitting the experimental curves to a given binding model. There are several binding models available [156]: a 1:1 binding model which assumes one binding site of the chip-bound ligand per analyte. It is the most commonly used binding model and should be applied whenever possible. It is calculated with the following formulas:

$$\frac{dAB}{dt} = k_a \cdot (RU_{max} - AB) - k_d AB \tag{1.1}$$

$$Response = AB + R_0 \tag{1.2}$$

The second most binding model is the "heterogeneous Ligand" or "surface heterogeneity" binding model which assumes one analyte to bind to two binding sites of the ligand. It is calculated with the formulas:

$$\frac{dAB_1}{dt} = Ak_{a1} \cdot (RU_{max,1} - AB_1) - k_{d1} AB_1 \tag{1.3}$$

$$\frac{dAB_2}{dt} = Ak_{a2} \cdot (RU_{max,2} - AB_2) - k_{d2} AB_2 \tag{1.4}$$

$$Response = AB_1 + AB_2 + R_0 \tag{1.5}$$

where for both:

A_x	is the free concentration of analyte x
B_x	is the bound concentration of ligand x
$A_x B_x$	is the bound concentration of complex A_x with $B_x$ligand x
RU_{max}	is the surface concentration of ligand binding site x
K_D	is the equilibrium dissociation constant (unit: M)
k_a	is the association rate constant (unit: $M^{-1}s^{-1}$)
k_d	is the dissociation rate constant (unit: s^{-1})

Further binding models are: a "heterogeneous analyte" binding model which assumes two different analytes in the analyte solution (this should be avoidable by reliable purification of the analyte solution); a "bivalent analyte" binding model which assumes two binding sites of one analyte for the ligand (e.g. antibodies) and a "conformational change" binding model which assumes a change in conformation of the ligand upon binding of the analyte. These models are less often used and should be avoided, if the nature of the binding is unknown [167].

All binding models can be combined with an account for Mass transport limitation. Mass transport limitation (MTL) is the result of a slow rate of delivery of the analyte from the bulk solution onto the chip surface. This is the case for high immobilization levels of the ligand and/or low flow rates of the buffer/analyte solution. Although most algorithms take MTL into account the experimentalist should try to avoid this by a proper setup of the experiment [167].

1.4.6. K_D vs. k_d: The importance of kinetic parameter determination

Contemporary lead discovery employs affinity-based high-troughput screening (HTS) methods [169] as the overall binding affinity is regarded to be paramount for the activity of a pharmacon [170]. These screening methods do not account for different binding kinetics which may be a crucial factor of *in vivo* activity, e.g. regarding the drug-residence time [170]. Unless the function of a drug target is persistently influenced after the dissociation of the drug, the duration of the action of a drug is limited to the time in which the drug is bound to its target. This is especially true for ASOs which act in a sterical blocking mechanism as their pharmacological action is restricted to the time of target occupancy. Therefore the selection of ASOs with low dissociation rate constants, k_d, is ideally preferred [170, 171]. Equally high binding affinities, however, can be the deriving from completely different binding kinetics as shown in fig. 1.5: The three compounds have exactly the same overall binding affinity, K_D, but their kinetic profiles differ substantially. Whereas compound A has high association and dissociation rate constants, compound C has 2000 times lower k_a and k_d rate constants whilst having the same overall binding affinity.

compound	k_a / [M$^{-1} \cdot$s^{-1}]	k_d / [s^{-1}]	K_D / [nM]
A	$2 \cdot 10^6$	0.2	100
B	$1 \cdot 10^5$	0.01	100
C	$1 \cdot 10^3$	0.0001	100
	∗	∗∗	
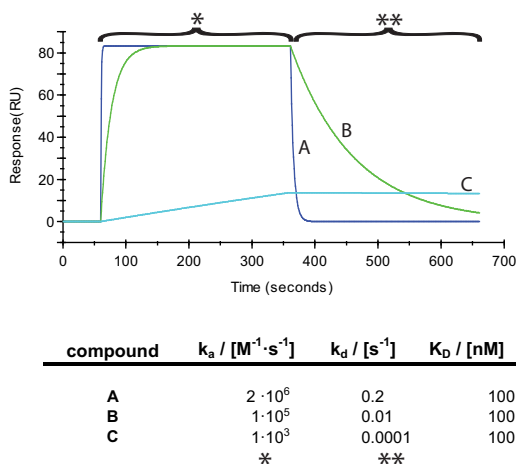
Figure 1.5. – Comparison of different kinetic profiles. These are simulated binding curves of three compounds with the same K_D (100 nM) but different rate constants, injected at the same concentrations (500 nM) for the same RU$_{max}$. Compound A has high association (*) and dissociation (**) rate constants, compound C has low rate constants, although the overall binding affinity is the same for all compounds.

This example demonstrates the importance of the determination of the kinetic rates. Additionally, it shows that an unimolar screen may mislead the experimentalist unless there are countermeasures done such as normalization for RU$_{max}$ (cf. section 2.2.3.1, p. 42).

1.5. Overview over the thesis—the strategy

The investigations made by Michlewski et al. [31] and Zhang and Zeng [108] indicated that the loop region of miRNA precursors may have an important role in the processing of pri-

/pre-miRNAs, either by directly inhibiting Drosha/Dicer or by the interfering with cofactors such as hnRNP A1.

Using the example of pre-miR-122 (cf. section 2.1.1.2, p. 33) we wished to develop modified oligoribonucleotides with enhanced binding affinity for preferred binding sites on the terminal loop of pre-miR-122. We anticipated that these would be potentially of value for inhibiting miR-122 biogenesis in a therapeutic setting. The strategy employed was divided into two phases:

In a first phase we identified preferred binding sites for short complementary 2'-OMe RNA oligoribonucleotides based on a "walkaround" (cf. section 2.1.1, p. 31) against three hairpin structured RNAs: h-ras (cf. section 2.3.1, p. 43), pre-miR-122 (cf. section 2.3.2, p. 51), and miR-18a (cf. section 2.3.3, p. 60). An in-depth investigation of the identified region for preferred binding (cf. section 2.3.2.2, p. 54) was intended to yield insights into the optimal length and position of loop-targeting ASOs.

A second phase investigated the affinity-enhancing properties of modifications of oligoribonucleotides (cf. chapter 4).

In collaborative work carried out under my supervision with Dr. F. Paun, we developed an RNase H assay for the determination and identification of RNase H cleavage products of pre-miR-122 derived RNAs (cf. chapter 5).

Finally, I developed a new assay for the SPR-based determination of extremely low dissociation rate constants, k_d, in the range of 10^{-6}–10^{-7} which we called INSTED. This method uses periodic injections of an indicator molecule that binds rapidly and reversibly to the analyte of interest. This allows measurements even in the presence of drifting base lines. The method successfully applied for the determination of the k_d of biotin-streptavidin (cf. chapter 6, published in ChemBioChem [172]).

1 INTRODUCTION

2. SPR-based evaluation of target site accessibility on pre-microRNAs: The "Walkarounds"

2.1. Introduction

As outlined in section 1.3.2 SPR is a valuable method for the detection and quantification of RNA/RNA interactions. With the intention to inhibit the biogenesis of mature miRNA and encouraged by the work of Wagner et al. [173] we initiated a program to test the binding affinity of fully complementary short 2'-OMe-RNA oligoribonucleotides against the hairpin precursors of miRNAs. The goal was to identify oligoribonucleotides with elevated affinity for their structurally preferred target sites.

In order to be able to design optimal (modified) AMO's based on target site accessibility we planned the affinity measurements of short 2'-OMe-oligoribonucleotides "walking" around a hairpin with sequences shifted by 1 nucleotide from each oligoribonucleotide to the next.

After a first feasibility study with the confirmed hairpin structure of ha-RAS we went on to the target structure of pre-miR-122. A third "walkaround" for pre-miR-18a was tested which confirmed in the main the findings of the previous assay. Finally, a set of short LooptomiRs (cf. section 1.3.1, p. 18) against the hairpin of pre-let-7a-2 was tested and the data obtained was compared to that of ELISA-based affinity measurements performed by Martina Roos.

2.1.1. Systematic screens against microRNA hairpins

I performed systematic screens of full sets of antisense oligoribonucleotides against different targets. The principle of these screens—called "walkarounds"—is the synthesis of all possible reverse complements of a given length against the linear sequence. This is achieved by systematically shifting the first oligonucleotide by 1 base until the end is reached. Fig. 2.1 shows an illustration of such a "walkaround" using the example of pre-miR-122.

2.1.1.1. H-RAS

As we want to investigate the impact of AMO's to RNA hairpin structures, we first searched for a reported measurement of antisense oligoribonucleotides against a confirmed hairpin structure. The aim was to find a hairpin which was previously investigated for an interaction with one or more antisense oligonucleotides as a proof-of-concept study for our following Biacore experiments.

Figure 2.1. – Schematic of a "walkaround". A) Sequence and structure of pre-miR-122. The first 7-mer oligoribonucleotide which binds to the very 5'-end is indicated with a red bar. B) By shifting the sequences by one base towards the 3'-end one obtains a complete set of all possible 7-mers against pre-miR-122.

We found such a hairpin in form of the transcript of the activated h-ras[i] gene, which was studied by Lima et al. ([109, 110], cf. section 1.3.2).

The proto-oncogene Ras (from Rat sarcoma) and the protein it codes for (also called Ras) plays an important role in cancer development [174, 175]. The Ras protein is a small G-protein (a GTPase) with an important role in signal transduction [176]. Certain mutations in Ras-gene can activate the Ras protein permanently which therefore leads to an incorrect propagation of intracellular signals causing tumor growth and metastasis. 20–25 % of all human tumors contain activated Ras-genes and in certain tumor types (lung cancer) this ratio reaches 90 % [177] (reviewed in [178]).

Lima et al. reported the preparation of a 47-nucleotide transcript of the activated h-ras gene as a stable hairpin containing an activating mutation. They designed 6 antisense decaribonucleotides, from which two were fully complementary to the stem region, one targeted the boundary stem/loop and three the loop region. Two of these oligonucleotides, that targeted the loop had nearly equal affinity for the transcript compared to an unstructured complement. The others bound approx. 10^5–10^6-fold less tightly to the transcript compared to the complement [109].

Allawi et al. performed similar experiments yielding a second data set for comparison with our data [179].

The hairpin of h-ras has a different overall-structure compared to the hairpins generated during miRNA biosynthesis: The stem of h-ras consists of 12 base pairing nucleotides, whereas the stem of a pre-miRNA consists of normally ~ 22 nt; the loop is quite large and consists of 19 single-stranded nucleotides. Only members of the let-7 family exhibit such exceptionally large loop regions.

Therefore we tested 37 decamers walking around the h-ras hairpin against the hairpin as well as two sequences which were tested by Lima et al..

---

[i] as well named HRas or ha-ras

2.1.1.2. pre-miR-122

MiR-122 is a highly abundant miRNA with a specific occurrence in liver cells and constitutes of up to 70 % of all microRNA in these cells. It plays an important role in fatty acid metabolism and cell differentiation [122, 180, 181]. As it is regulated by Rev-ErbA alpha, a nuclear receptor, which acts as a transcriptional repressor and which is known to participate in the circadian regulation of genes in the liver, mir-122 is thought to be a circadian metabolic regulator [182, 183]. It has been shown that targeting mir-122 with an antisense oligonucleotide led to lowered blood plasma cholesterol levels in mice [122].

Mir-122 enhances the replication of Hepatitis-C-virus (HCV) through a partially understood mechanism by interacting with binding sites in the 5' UTR of the viral genome [184–186]. Recently it was shown that miR-122 recruits AGO2 for the protection of the 5'-terminus of the viral RNA from cellular nucleases as it lacks the 5' capping of endogenous RNAs [187, 188]. Lanford et al. showed that the ASO SPC3649 (an oligoribonucleotide with alternating DNA/LNA nucleotides) antagonizes mir-122 and significantly suppresses viremia in chronically HCV-infected chimpanzees and patients [189]. Miravirsen (SPC3649), developed by Santaris Pharma A/S, is the first miRNA-targeted drug to enter human clinical trials and it's currently undergoing Phase II clinical studies [190].

Miravirsen targets the mature miRNA. By targeting the pre-miR-122 we hope to be able to block new synthesis of miR-122 as an alternative therapeutic strategy. This may be advantageous because the loop-region may offer key binding sites for short oligoribonucleotides due to structural preference.

Taken together, the targeting of pre-miR-122 is a potential therapeutic approach for the treatment of hepatitis C and possibly other diseases [191].

Finding binding sites for short (7–10 nt) modified oligonucleotides for the hairpin precursor pre-miR-122 as an example of structured noncoding RNA, was one of the major goals of this PhD-thesis. After the experience with h-ras we decided to employ *Surface Plasmon Resonance*-technology as technique to identify the best binders.

2.1.1.3. miR-18a

Many miRNAs are involved in the processes of tumorigenesis by targeting mRNAs, responsible for proliferation, differentiation or apoptosis [192]. The miR17-92 miRNA cluster which contains pri-miRNA-18a has been shown that an overexpression of this cluster leads to an accelerated tumor development in a mouse B cell lymphoma model [3].

Michlewski et al. have shown that hnRNP A1, an RNA binding protein (RBP) which is involved in many steps of RNA processing, regulates the processing of pri-miRNA-18a by the microprocessor. Upon binding to the terminal loop and internal bulges at the base of the stem it induces a relaxation of the stem, which leads to an enhanced processing by Drosha

via a more favored secondary structure for cleavage [193]. Additionally, they could reverse the processing enhancing activity of hnRNP A1 by blocking the accessibility of the terminal loop with a 2'-OMe RNA fully complementary to the loop region. These LooptomiRs were able to specifically block the Drosha mediated cleavage of pri-miRNAs to the pre-form [31] (cf. section 1.3.2, p. 19).

Encouraged by these findings we started an investigation of the accessibility of the loop region for short complementary 2'-OMe RNA oligoribonucleotides with the intention of reducing the length to an optimal blend of shortness, activity and selectivity (the LooptomiR used by Michlewski et al. was a 16-mer).

In section 2.3.3, p. 60 I describe the binding assay of 78 oligoribonucleotides ranging from 7 to 18 nucleotides in length. The results are discussed in section 7.1.1.3, p. 124.

2.1.1.4. pre-let-7a-2

After the discovery of the regulation of gene expression by miRNAs, the fine tuning of this regulation by auxiliary factors that influence miRNA processing has begun to emerge. The positive regulation of Drosha cleavage by hnRNP A1 (see previous section), is such a mechanism. Another example of such a positive regulation mechanism is the promotion of the Drosha-mediated processing of the oncogenic mir-21 by TGF-β/BMP signaling [194].

The RBP Lin28 and its homologous Lin28b is an example of a negative regulation: upon binding to the terminal loop region Lin28 inhibits the maturation of members of the let-7 family (for a review see [195]). Let-7 is a tumor suppressor responsible for suppressing genes involved in proliferation. Its expression is lost in many tumors [196, 197]. Some groups report a blocking of Drosha-mediated cleavage of pri-let-7 [198–200] others describe a dicer-dependent inhibition of pre-miRNA processing [201, 202]. However, the reduction of the negative suppression (by lin-28) of an oncogene regulator (let-7) by LooptomiRs may be a promising way to rescue the expression of let-7 in certain cancers.

We designed LooptomiRs for the specific antagonizing of Lin28 binding to pri-/pre-let-7. The results obtained by a newly developed RNA based competition ELISA assay in our lab are compared to the affinities obtained with SPR and presented in section 2.3.4, p. 63. These results are shortly discussed in section 7.1.1.4, p. 125.

A manuscript for publication is in preparation.

2.1.2. Strand invasion of Miravirsen into pre-miR-122

Besides the SPR binding assay we established in our group a variety of novel assays for the characterization of pre-miR-122/ ligand interactions. These assays include an in vitro Dicer assay and a cellular reporter assay for Microprocessor cleavage of pri-miRNAs.

In the course of this work, L. Gebert a co-worker in our group, discovered that the active compound of Miravirsen (cf. section 2.1.1.2), SPC3649, suppressed the biogenesis of pre-miR-122 at the pri- and pre-miRNA levels. This indicated that SPC3649 was capable of invading the stem of pre-miR-122. To support this data I employed SPR for the determination of binding affinity of SPC3649 for pre-miR-122.

The results are presented in section 2.3.5, p. 66 and discussed in section 7.1.1.4, p. 125.

These results are published by our group in *Nucleic Acids Research* [203].

2.1.3. Regeneration scouting

The most important parameter in SPR experiments is the complete regeneration of the sensor surface without any damage or alteration of the immobilized ligand molecules.

For the first experiments performed with the walkaround of the h-ras hairpin (with Dr. H. Towbin) we used a 1 mM HCl solution for the regeneration. In further studies with molecules binding in the pM range, regeneration was a problem for our SPR2 system: although the hairpins on the chip surface were perfectly regenerated with a 1 mM HCl solution on Biacore SA chips. I assign this phenomenon to the different chip architecture. With the Biacore system I used two chips: a ready-to-use streptavidin chip and a CM5 chip which had to be immobilized with streptavidin first. Both chips have a 100 nm dextran-matrix, whereas our SPR2 amine chips were based on a C1-type coating without such a dextran matrix.

This example shows the importance of evaluating the regeneration procedure empirically.

I optimized the method of Andersson et al. [204] for my experiments. The basis of this approach is 6 different multicomponent cocktails of stock regeneration solutions which are combined to yield 18 final regeneration solutions. These 18 regeneration solutions are then tested, ranked, and—if necessary—further optimized (cf. section 2.2.2.4, p. 39).

2.2. Materials and Methods

2.2.1. Materials

2.2.1.1. Equipment

The total equipment for all experiments of this chapter is listed in table 2.1.

2.2.1.2. Reagents

The reagents used for the experiments are listed in table 2.2.

2.2.1.3. Software

The Software used for the experiments are listed in table 2.3.

Table 2.1. – Equipment for oligonucleotide synthesis and SPR measurements.

Type	Producer	Identifier	Volume	Dimensions	Remarks
Vial	Greiner Bio-One GmbH	Cryo.S	1.5 ml		
	Molecular BioProducts		1.5 ml		Microcentrifuge tube
96-well plate	Orochem	Standard 96-well filter plate	0.7 ml/well		plates used for synthesis of oligoribonucleotides
	Costar	Assay block 96-well	2 ml		plates used for reactions and purification
	Bio-Rad	Hard-Shell PCR Plates 96-well WHT/CLR	200 µl		plates used for analysis in LC/MS
	Eppendorf	Deepwellplate 96/500 sterile	500 µl		plates used for storage and SPR-measurements
	Costar	UV Plate, 96-well, no lid with UV transp. flat bottom			plates used for UV-measurements in plate-reader
	Millipore	Multiscreen Column Loader	80 µl		Loading tool for Polypak resin
Pipettes	Mettler Toledo	VoluMate Liquisystems	2.5–1000 µl		
Filter tips	Star Lab		10–1000 µl		
Centrifuge	Eppendorf	5415C			
Lyophilizer	Thermo Electronic	Savant SPD 2010 SpeedVac			
	GeneVac	miVac duo concentrator			DNA Concentrator
HPLC column	Waters	XBridge OST C18		2.1 x 50 mm	analytical
				4.6 x 50 mm	semi-preparative
SPR-system	GE-Healthcare	Biacore 3000			property of IPW, established in lab. of Prof. D. Neri
		Biacore T-100			property of fgcz
	SierraSensors GmbH	SPR 2			property of group Prof. J. Hall
SPR Sensor chip	GE-Healthcare	CM5			
		SA			
	SierraSensors	Amine			
pH-Meter	MettlerToledo	seveneasy			Inlab 413 Open Junction Combination pH-Electrode
					Calibration solutions with pH 4.01, 7.00, and 9.21
DNA/RNA-Synthesizer	BioAutomation Inc.	MerMade 12			For 12 separate columns, 50 nmole scale
		MerMade 192			For one/two 96-well plate(s)
HPLC-system	Agilent	1200 series			Pump: G1312B Binary Pump, G1365C MWD, G1367C HiP-ALS
MS-system	Agilent	6130			quadrupole ESI-MS
Mixer	Eppendorf	Thermomixer Comfort			
UV/VIS-spectrometer	Thermo Fisher	NanoDrop 2000			
	Molecular Devices	SpectraMax Plus384			Property of Institute of Microbiology
Filterunit	TPP	Filter-Top with PES-membrane	500 ml		

Table 2.2. – Reagents used for oligonucleotide synthesis and SPR measurements.

Name	Abbreviation	Quality	Producer	Remarks
3'-Biotin-TEG-CPG			Glen Research	
5-(Benzylthio)-1H-Tetrazole Acetic acid		puriss. p.a. $\geq$ 99.8 %	Biosolve BV	
Acetonitrile	ACN	LC-MS Chromasolv $\geq$ 99.9 %	Fluka Analytical	
Ammonium hydroxide		puriss. p.a.; Reag. Ph. Eur.	Sigma-Aldrich	
Bond-Breaker® TCEP solution			Thermo Scientific	neutral pH, 5 ml of a 0.5 M solution
Calcium chloride standard solution			Fluka Analytical	1 M
CAP A (with Lutidine)			Biosolve BV	10 % Lutidine, 80 % THF, 10 % Acetic anhydride, water $\geq$ 0.01 %
CAP B 16 %			Biosolve BV	16 % N-Methylimidazole
CHAPS			ABCR GmbH & Co. KG	
Dimethyl sulfoxide	DMSO	puriss. p.a., dried, $\geq$ 99.9 %	Sigma-Aldrich	
di-Sodium hydrogen phosphate dihydrate		MicroSelect; $\geq$ 99.0 % (T)	Fluka BioChemika	
DL-Dithiothreitol	DTT		Sigma-Aldrich	1 M aqueous solution
Ethanol absolute		multisolvent HPLC grade	Scharlau	
HEPES buffer solution			Sigma	1 M
Hexadecyltrimethylammonium bromide	CTAB	MicroSelect; > 99 % (AT)	Fluka BioChemika	
Hexafluoroisopropanol	HFIP	97 %	ABCR GmbH & Co. KG	
L(+)-Ascorbic acid sodium salt		$\geq$ 99 % (NT)	Fluka BioChemika	
Magnesium chloride solution			Fluka Analytical	1 M
Malonic acid		> 99.0 %	TCI	
Methanol	MeOH	Chromasolv, gradient grade, for HPLC, $\geq$ 99.9 %	Sigma-Aldrich	
Methylamine, 40 wt% solution in water			Acros organics	
MOPS sodium salt		98 %	ABCR GmbH & Co. KG	
N-Methyl-2-pyrrolidone	NMP	99.5 % extra dry, over molecular sieves	Acros Organics	
Oxalic acid		puriss. p.a., anhydrous, > 99.0 % (RT)	Sigma-Aldrich	
Oxidizer 0.02 M for ABI			Biosolve BV	20 % Pyridine, 70 % THF, 0.5 % Iodine (I$_2$)
Poly-Pak resin			Glen Research	Resin for purification of oligoribonucleotides
Potassium chloride		puriss. p.a.; > 99 % (AT)	Fluka Chemika	
Potassium dihydrogen phosphate		puriss. p.a. ACS; $\geq$ 99.5 % (T)	Fluka Chemika	
Potassium phosphate monobasic		puriss. p.a. ACS; $\geq$ 99.0 % (T)	Fluka Chemika	
RNase Exitus Plus®			Applichem	removes RNases on washable surfaces
Sodium acetate trihydrate		purum p.a. $\geq$ 99.0 % (NT)	Fluka Chemika	
Sodium chloride		AnalaR Normapur	VWR	
Sodium dihydrogen phosphate dihydrate		purum p.a.; crystallized; $\geq$ 99.0 % (T)	Fluka Chemika	
Sodium dodecyl sulfate		purum; $\geq$ 96.0 % (GC)	Fluka Chemika	
Sodium phosphate dibasic anhydrous		puriss. p.a. ACS; $\geq$ 99.0 % (T)	Fluka	
Sodium phosphate		96 %	Aldrich Chemistry	= Trisodium phosphate
Sulfobetaine SB 12			Applichem	
Triethylamine	TEA	99.7 % extra pure	Acros Organics	
Triethylamine-hydrofluoric acid	TEA-3HF	98 %	Aldrich Chemistry	
Trifluoroacetic acid	TFA	purum; $\geq$ 98.0 %	Fluka	
Trimethylethoxysilane		> 98.0 %	TCI	
Triton X-100		Electrophoresis Grade	Fisher Scientific	
Trizma® hydrochloride buffer solution		BioUltra, for molecular biology	Fluka Analytical	1 M, pH 7.4
Tween 20		Molecular Biology grade	Applichem	
Tween 80		BioChemica	Applichem	
Universal UnyLinker Support	CPG		ChemGenes	500 Å, 1'000 Å
Ureum crist		PhEur	Hänseler AG	

Table 2.3. – Software used for calculations / fittings.

Purpose	Name of Software	Producer	Version number	Remarks
Design of oligos	Excel	Microsoft	2003	Using Excel-Makro "Oligo_scoop" made by me
Purification of oligos	Chemstation	Agilent	Revision - B.03.03 [341] January 17, 2008	
Characterization of oligos	Chemstation	Agilent	Revision - B.03.03 [341] January 17, 2008	
Normalization	Excel	Microsoft	2003	Using Excel-Makro "Oligo_scoop" made by me
	Hamilton-software for Starlet robot	Hamilton	4.2.1.6670	Sequences were loaded with Excel-sheet made with "Oligo_scoop"
SPR-experiments	Control-software for Biacore 3000	GE-Healthcare	v. 3.2	
	Control-software for Biacore T-100	GE-Healthcare	???	
	Control-software for SPR2	Sierra-Sensors	SPR-K2 1.0.4524.24848	
Data evaluation	BiaEval	GE-Healthcare		
	Analyzer	SierraSensors	miscellaneous	As this program was stil in developoment we got continuous updates from SierraSensors
	Scrubber	Biologic Software	2.0a	
	Clamp XP	Biologic Software	v. 3.70	
	Evilfit	Peter Schuck	v.3	https://sedfitsedphat.nibib.nih.gov
RNA structure modeling	RNAstructure	Mathews Lab, Rochester	5.03	Possibility of "walkaround" simulation

2.2.2. Methods

2.2.2.1. Design of "walkaround"-oligoribonucleotides

The oligoribonucleotides were defined using the Excel-macro "Oligo_scoop" as described in section 3.2, p. 70.

2.2.2.2. Synthesis of oligoribonucleotides

All oligoribonucleotides were synthesized "DMT-on" according to a standard MerMade12 RNA protocol using $\approx$1.5–4 mg of CPG. For the synthesis in 96-well-plates I used a custom "CPG-loading-tool" made from teflon. This tool was used to load the wells of the 96-well plates with CPG and yielded very reproducible amounts of $\approx$2–3 mg of CPG / well in a very short time. A certain amount of CPG was lost due to the high electrostatic properties of teflon.

Cleavage and Deprotection CPG-cleavage and deprotection of oligoribonucleotides in single columns was performed according to manufacturers recommendations in AMA (40 % methylamine, ammoniumhydroxide solution; 1:1) for 10–30 min at 65 °C. Oligoribonucleotides were isolated by centrifugation of cleaved CPG (10'000 rpm, 3–5 min, 5 °C). The CPG was washed twice with aqueous ethanol (200 μl, ethanol:water 1:1) and once with 100 μl water. The supernatant and the washing solutions were removed in a SpeedVac apparatus (45 °C, quantum satis) to yield crude oligoribonucleotides.

CPG-cleavage and deprotection of oligoribonucleotides in 96-well plates was performed according to manufacturers recommendations in gaseous methylamine for 150 min at 70 °C. Oligoribonucleotides were directly washed from the support in a plate twice with aqueous ethanol (200 μl, ethanol:water 1:1) and once with 100 μl water using vacuum. The supernatant and the washing solutions were removed in a speed vac apparatus (45 °C, quantum satis) to yield crude oligoribonucleotides.

RNA (containing) oligoribonucleotides require further deprotection of the 2'-O-TBDMS protecting group.

DNA and 2'-OMe-RNA molecules were directly purified by HPLC.

Desilylation of 2'-O-TBDMS protected RNA   Desilylation was effected with fluoride (60 µl NMP, 30 µl TEA, 40 µl TEA·3HF; 65 °C, 2.5 h). After addition of trimethylethoxysilane (160 µl) the solution was vortexed for 10 min to yield one phase and a precipitate. Diethyl ether was added (1 ml). The mixture was vortexed and then centrifuged (4 000 rpm, 5 min, 5 °C). The pellet was washed twice with diethyl ether, dried and dissolved in water (300 µl).

Purification and characterization   The crude DMT-on oligoribonucleotides were purified by reversed-phase HPLC in (mostly) 2–3 batches on the Agilent HPLC semi-preparative apparatus using a 0.1 M TEAA-solution (A) with an appropriate gradient for separation (usually 20–70 % methanol (B)) over 8–15 min. After pooling and lyophilization of product-containing fractions, the product was detritylated with 40 % aqueous AcOH (45 min, rt). The solution was again lyophilized, redissolved in water and desalted via HPLC using an appropriate gradient depending on length and chemistry of oligonucleotides. A last lyophilization processus for the removal of methanol (from the desalting step) and dissolving in 150–400 µl of water finished the synthesis.

Purity and identity of the products were further supported by analytical LC/MS analysis using a 0.4 M HFIP / 8.6 mM TEAA solution as solvent A and 100 % MeOH as solvent B (0.2 ml/min.; 60 °C).

Purification and detritylation of a plate using Sephadex resin   The 78 ASOs for the pre-miR-18a screen (cf. 2.3.3, p. 60) were purified using bulk polypak/sephadex resin with a modified protocol. The purification comprised the following steps:

1. Loading of the polypak resin onto the 96-well synthesis frit-plate using the *MultiScreen Column Loader* and scraper (Millipore).

2. Equilibration of the resin with ACN (3 x 300 µl) and TEAA (0.5 M, 1 x 450 µl).

3. Loading of the crude oligonucleotides after cleavage/deprotection (300 µl).

4. Removal of failure sequences with ammonium hydroxide (1:20 dil., 200 µl).

5. Washing with water (400 µl).

6. On-column detritylation with TFA (2 %, 400 µl, 5 min.).

7. Washing with water (400 µl).

8. Elution of purified oligoribonucleotides with ACN (30 % in H_2O, 400 µl).

Purity and identity of oligonucleotides were confirmed using LC/MS.

2.2.2.3. Quantification and normalization of oligoribonucleotides

For the UV-based quantification of a series of oligoribonucleotides the excel-based macro "Oligo_scoop" was used as described in section 3.4, p. 71. The absorptions of a relatively small number of oligoribonucleotides were measured using the NanoDrop machine. For large amounts of analytes, aliquots (5 µl) were transferred into the appropriate UV-permeable 96-well plates, diluted to ≈ 150 µl with water and measured using the SpectraMax Plus apparatus.

The concentration/dilution values calculated by "Oligo_scoop" were then either pipetted manually or by using our Hamilton StarLet pipetting robot. For a more precise concentration and ease of process the volumes were dried to completeness and filled up with the desired/calculated volumes of water.

2.2.2.4. Regeneration scouting

As already mentioned (cf. 2.1.3, p. 35), I used a variation of the regeneration scouting of Andersson et al. [204].

The basis of this approach is a set of 6 multicomponent stock regeneration solutions (cf. table2.4) which are combined to 18 possible regeneration solutions and systematically tested for surface regeneration.

I made the 18 regeneration solutions (cf. table 2.5, p. 40) and injected them all separated by fresh injections of analyte. As some of the regeneration solutions altered the chip surface, the quality of the regeneration was judged from the end-of-injection level of the subsequent analyte: the more analyte bound the better was the previous regeneration. However, I was able to select the optimal regeneration solution for even the highest binder, see section 2.3.5.2, p. 67 for an example.

Table 2.4. – Stock solutions used for the regeneration scouting. The ionic solution was aliquotted and stored at -80 °C in order to minimize the separation of urea. From these stock solutions the final regeneration solutions as listed in table 2.5 were made. As opposed to the literature [204] I adjusted the pH of the acidic solution to pH 3.0 (instead of pH 5.0)

Abbr.	Principle of solution	Chemical	Concentration	Volume
A	Acidic, pH 3.0	Oxalic acid	0.15 M	10 ml
		Phosphoric acid	0.15 M	10 ml
		Formic acid	0.15 M	10 ml
		Malonic acid	0.15 M	10 ml
B	Basic, pH 9.0	Ethanolamine	0.2 M	10 ml
		Sodium phosphate	0.2 M	10 ml
		Piperazine hexahydrate	0.2 M	10 ml
		Glycine	0.2 M	10 ml
I	Ionic	Potassium thiocyanate	0.46 M	ad 50 ml
		Magnesium chloride hexahydrate	1.83 M	
		Urea	0.92	
		Guanidine hydrochloride	1.83	
U	Non Polar	Dimethylsulfoxide, DMSO		10 ml
		Formamide		10 ml
		Ethanol		10 ml
		Acetonitril, ACN		10 ml
		1-Butanol		10 ml
D	Detergents	CHAPS	0.3 % (w/w)	
		Zwittergent 3-12	0.3 % (v/v)	
		TWEEN-20	0.3 % (v/v)	
		TWEEN-80	0.3 % (v/v)	
		Triton-X100	0.3 % (v/v)	
C	Chelating	EDTA (Na)	0.02 M	

Table 2.5. – 18 Regeneration solutions used for the regeneration scouting. The capitals refer to the abbreviations as listed in table 2.4, "w" indicates water. The solutions were mixed to equal parts. The final regeneration solution I used for my SPR experiments with the high binders was AIw (one part Acidic solution, one part Ionic solution, and one part water).

Mix	Mix	Mix
Aww	BAw	ACw
Bww	BDw	IDw
Iww	BCw	ICw
Uww	AIw	DUw
Dww	AUw	DCw
Cww	ADw	UCw

2.2.2.5. SPR experiments

For my SPR experiments with the Biacore machines I used either pre-immobilized SPR chips (T-100: Series S Sensorchip SA; Biacore 3000: Sensorchip SA) or a CM5-chip which was loaded with streptavidin as described below. The experiments performed with the SPR2 machine were carried out with amine chips that were first immobilized with streptavidin prior to the binding of biotinylated ligands.

General preparations A cleaning procedure was performed regularly in order to remove possible contaminations with proteins/ribonucleic acids from earlier experiments.

The system was sequentially primed with two solutions (0.5 % SDS; 50 mM aq. glycine (pH 9)) which were primed through and left in the fluidic system for a few minutes. The flow system was then flushed twice with water. After priming of a 1–2 % aq. solution of sodium hypochlorite the system was flushed with water twice. For extensive experiments, I primed the system with a 1:1 dilution of RNase Exitus Plus in order to remove RNases. The teflon tubings reaching into the buffer reservoir flask were also wiped with RNase Exitus Plus-containing tissues and were not touched further.

Immobilization of streptavidin For the immobilization running buffer was replaced by PBS/DPBS to avoid that the amine group of the TRIS buffer substance binds to the chip surface as well. The immobilization of streptavidin on SPR2 amine chips was done in three steps:

1. Activation of the chip surface with a 1:1 mixture of aqueous solutions of EDC (400 mM) and NHS (100 mM, 6–8 min.). The solutions were stored at -80 °C in order to prevent hydrolysis of EDC. After thawing, the solutions were thoroughly degassed in the empty GeneVac concentrator (4 min., RT)

2. After activation, an buffered solution of streptavidin (100 µg/ml, 10 mM acetate) was used for the immobilization at an optimized pH of 5.5.

3. Finally, the chip surface was neutralized by blocking the unreacted activated carboxylic groups with ethanolamine (1 M, pH 8, 6 min.)

A typical example of a sensorgram is shown in fig. 2.2.
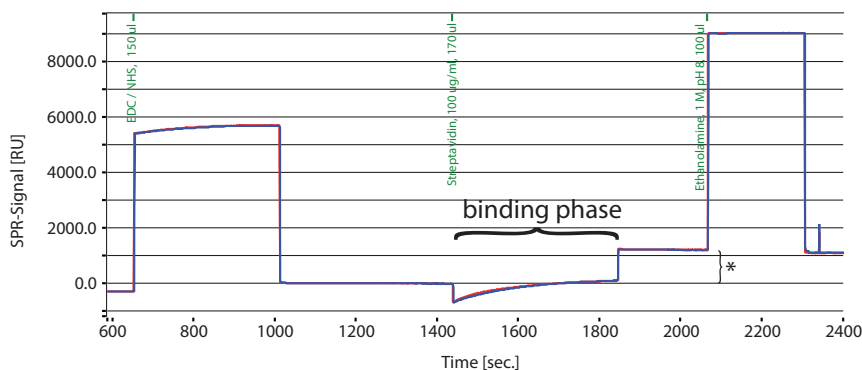
Figure 2.2. – Immobilization of streptavidin on a SPR2 amine chip. In this example ≈ 1'200 RU of streptavidin were immobilized on the chip during the binding phase. The asterisk marks the difference of signal before and after the binding

The immobilization procedure was performed at 25 °C or 37 °C. In general, the immobilization values at 37 °C were about 1.5 times higher (≈ 1'500–1'800 RU) than the values after immobilization at 25 °C (≈ 1'000–1'200 RU).

After the immobilization procedure the system was twice primed with the final running buffer and left for equilibration for a few hours.

Capture of biotinylated ligands Biotinylated ligands were prepared in TRIS solutions (30–60 nM, pH 7) containing at least 50 mM of salt. The injection times for the immobilization of the ligand were 20–150 seconds. Detailed information about the immobilization of nucleic acids with biotin-streptavidin can be found in [205].

SPR binding assays Except for the H-ras study, all binding assays were performed with "double referencing": Sensor spot # 1 was used as a reference spot. Repeated injections of buffer referenced for bulk-shifts due to small changes in refractive index of the analyte solutions or drift of the signal (see difference in signals "Referenced" and "Blanked" of fig. 2.3, p. 44).

The final running buffer was chosen to be a TRIS-buffer as listed in table 2.6. The final pH-value was always around 7.45. Compared to the 10-fold PBS buffer solution of Biacore, this buffer contains 10 times more surfactant (0.05 %) which corresponds to the current standard. TRIS, $MgCl_2 \cdot 6 H_2O$, and $CaCl_2 \cdot 6 H_2O$ were taken from standard solutions (cf. table 2.2, p. 36), for KCl, NaCl, and TWEEN I made 1 M, 5 M and 10 % stock solutions. The composition was suggested by SierraSensors.

2.2.3. Analysis of the data

For the analysis of the sensorgrams I used 5 different software programs: BiaEvaluation, SierraSenors Analyzer, Scrubber, Clamp XP, and Evilfit (cf. table 2.3, p. 37). Most of the

Table 2.6. – Composition of the TRIS running buffer for the further experiments with (modified) loop-binders.

Substance	Formula / Abbr.	concentration
Trishydroxymethylaminomethane	TRIS	20 mM
Magnesiumchloride hexahydrate	$MgCl_2 \cdot 6\,H_2O$	5 mM
Calciumchloride hexahydrate	$CaCl_2 \cdot 6\,H_2O$	2 mM
Potassium chloride	KCl	2 mM
Sodiumchloride	NaCl	140 mM
Polyoxyethylen(20)-sorbitan-monolaurate	TWEEN®20	0.05 %

sensorgrams were analyzed using BiaEvaluation and Scrubber because of their ease of use and the ability of processing batches of sensorgrams (see below).

2.2.3.1. The importance of a uniform RU_{max}.

A quality fitting of sensorgram data for single analytes binding a surface, needs a double-referenced broad-spectrum assay containing duplicates over the whole affinity range (cf. section 1.4.5, p. 26).

For large screens a proper optimization of the conditions for all analytes is practically impossible. Additionally, the reproducibility of an assay against a biotinylated ligand which is captured on the chip surface via streptavidin is not a given (especially at elevated temperatures, cf. chapter 6)).

For our screens I made an estimation of RU_{max}. This estimated RU_{max} value was subsequently set as a fixed parameter for all analytes. When the binding affinity of an analyte with a K_D value much higher than the highest measured concentration is determined, the uncertainty of the value increases dramatically. This method is only valid when performing a fitting with a 1:1 binding model. Additionally, the value of this procedure is first and foremost for the removal of artifacts with low-affinity analytes.

The normalization was performed by first determining a most probable RU_{max} value for all analytes except outliers. Then this "general RU_{max} value" is inserted for all analytes and a second fit with the constraint of this fixed RU_{max} value is performed. Analytes which overshoot this value indicate probably a second binding site.

2.2.3.2. Analysis with BiaEvaluation

The analysis of the data with BiaEvaluation can be performed for steady-state and kinetic analyses. For the referencing one can choose different blank injections and they are averaged and subtracted from each analyte injection. For the refractive index change I used a fixed value of 0 as the double referencing could remove bulk-shifts in practically every sensorgram.

2.2.3.3. Analysis with Scrubber

The analysis performed with Scrubber2.0 was done for large numbers of analytes with no major problems due to high mass transport limitation or bad referencing. One can choose between a "closest blank" subtraction which takes for every analyte injection the signal of the closest blank injection or an "average blank" option which average the blank signals and subtracts one and the same value from all analyte injections. If the blank injections were very uniform (as e.g. in fig. 2.3) I chose the "average blank" option. In the case of varying signals of blank injections I chose the "closest blank" option. Single outliers were removed.

Fig. 2.3 shows a general procedure of the data processing with Scrubber as an example. The sensorgrams can be saved in a format which can be read by ClampXP for further detailed kinetic analysis with different models or a "Monte Carlo"-analysis of the data fitting.

2.2.3.4. Analysis with EVILFIT

EVILFIT is a non-commercial program based on the matlab runtime environment. It was developed by P. Schuck [168] and uses a so-called Thikonov-regularization for the analysis of the dataset. With evilfit it is possible to identify mass transport limitations as well as multiple binding sites. For best analyses the data should be well determined (long association and dissociation times, signal noise ratio of $\geq 100\,\mathrm{RU}$).

The analysis of the data with EVILFIT was performed as described.

The description for the data handling was downloaded from the homepage of the National Institutes of Health, USA (https://sedfitsedphat.nibib.nih.gov).

## 2.3. Results

2.3.1. H-Ras "walkaround"

After a general introduction into the setup of the experiments I will present the results gained from the affinity experiments against the two single-stranded linear complements and their impact on further SPR-measurements as an example in a more detailed way. Finally, the results for the walkaround are given together with a comparison of the results obtained by Lima et al. [109, 110]. The results are discussed in section 7.1.1.1, p. 123

All K_D values given in this section are estimates as the experiments were performed with a unimolar screen and not with a concentration series.

2.3.1.1. General setup of experiments

The oligonucleotides for the walkaround of ha-Ras were designed by Dr. H. Towbin and synthesized by M. Zimmermann.

After preconditioning of the chip (3 x 50 mM NaOH and 1 M NaCl, 1 min., 20 µl·min^{-1}) the sensorchip was immobilized with the ligands (10 nM, 10 min. each).
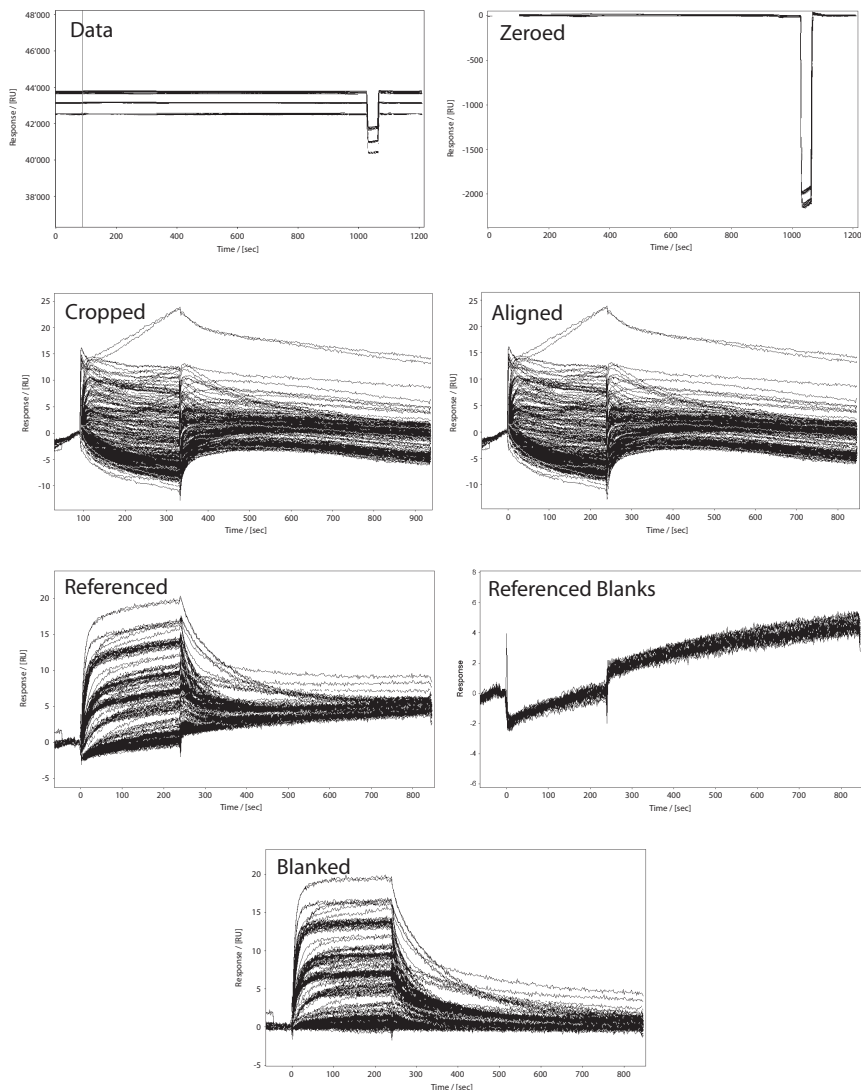
Figure 2.3. – Workflow of the data processing with Scrubber2.0a. The imported raw data (top left) is zeroed shortly before the injection time (top right). After cutting of the regeneration solution signals ("Cropped"), the data is aligned for a uniform injection time ("Aligned"). Then the signal of the reference cell/spot is subtracted from the measuring cell/spot ("Referenced"). In good assays this data already looks like the final sensorgrams. In this example the measurements were influenced by a constant drift which is seen in the baseline of the referenced blanks. Fortunately, the drift was quite uniform for all injections and could be removed by the referenced blank injections ("Referenced Blanks") to yield the final sensorgrams ("Blanked") in an overlay.
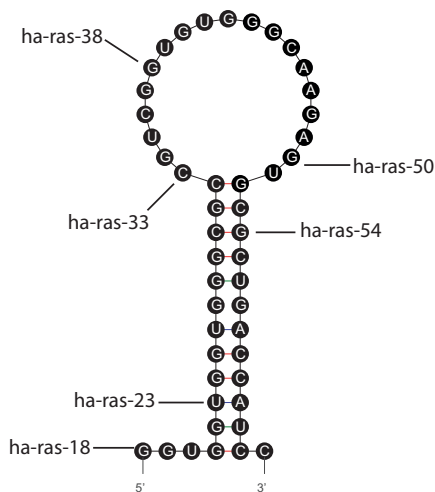
Figure 2.4. – Scheme of the h-ras hairpin with starting points of selected decamers. The molecule was biotinylated at the 3'-end with a dT$_6$-linker (not shown).

We used for the immobilization 4 different oligonucleotides: a random 21-mer as control (fc 1), the h-ras hairpin (fc 2, cf. fig. 2.4), the linear "33-complement" (fc3), and the linear"38-complement" (fc 4). The latter two were used as well by Lima et al. and are linear representatives of two segments of the hairpin within the stem and the loop. Table A.1, p. 133 lists these biotinylated ligands and their immobilization levels.

The final screen was performed with 37 decamers (cf. table A.3, p. 134) which were tested against these 3 targets twice in unimolar concentrations of either 500 nM or 2000 nM (data not shown). The experiment was performed with the conditions listed in table A.2, p. 133. Running buffer was composed of 10 mM HEPES, 0.5 M NaCl, 3 mM EDTA, and 0.005 % TWEEN 20.

The data was processed with Excel2003 and Scrubber (cf. section 2.2.3.3).

2.3.1.2. Data analysis of the linear "33-complement"

Fig. 2.5 shows the determination of the K_D values of the 37 decamers (where possible to determine) against the linear "33-complement". Part A shows the values directly fitted after the processing by Scrubber as described in section 2.2.3.3, p. 43. After equalizing the parameter for RU$_{max}$ to 646 RU for all oligoribonucleotides a second fitting process revealed almost the same K_D values yet a bit smaller (Part B). Part C shows the determined RU$_{max}$ values of the first fitting. The structure of the h-ras hairpin an the location of the 33-complement which is a part of this stem-loop structure is shown in fig. 2.5/D.

The fitting process for this ligand was quite straight forward and yielded the expected result: ha_ras_33 binds to this linear complement with the highest affinity weakened by each nucleotide shifted away from the fully complementary sequence. The binding affinity of
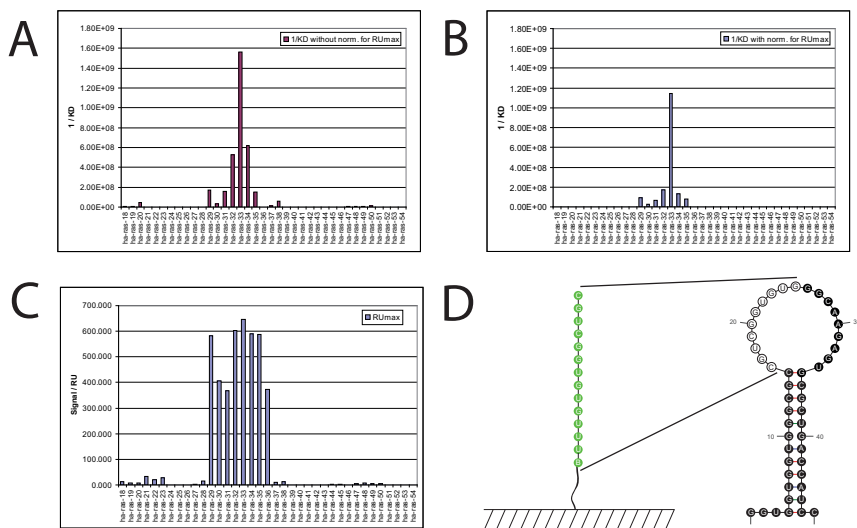
Figure 2.5. – A) Determination of estimated K_D values in a first fitting process. C) plot of the RU_{max} values determined with these fittings. B) Corrected fitting with normalization for a uniform RU_{max} value. D) Structure of h-ras as determined by Lima et al. and location of the 33-complement as a part of the hairpin (green symbols).

ha_ras_33 for its complement was determined to be in the subnanomolar range (around 0.9 nM, cf. table A.3, p. 134).

2.3.1.3. Data analysis of the linear "38-complement"

The same procedure as for the linear 33-complement was done for the 38-complement.

Fig. 2.6 shows the same analysis as for the previous ligand: The unmodified dataset, a set which was normalized for a uniform RU_{max} of 112.5 RU the determined RU_{max} values and the localisation of the linear target in the whole hairpin structure.

With the exception of ha_ras_22 the fingerprint of the best binding oligoribonucleotides is similar in the normalized and the not normalized profiles.

2.3.1.4. Analysis of the h-ras hairpin

Figure B.1, p. 144 shows the sensorgrams of all 37 decamers walking around the hairpin. When analyzing the data of the walkaround against the full length hairpin of h-ras one can draw the following conclusions:

1. ha_ras_36 is binding best to the hairpin in both, normalized and unnormalized data sets.

2. after normalization, the binding fingerprint seems to be much more distinct although the main affinities do not really change. Besides the 4 oligoribonucleotides ha_ras_51–

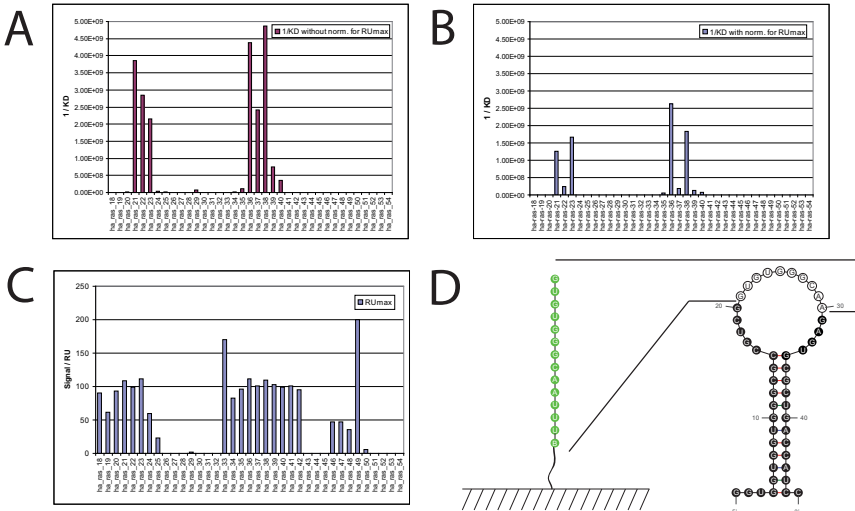**Figure 2.6.** – Same determination of K_D values for the decamers against the linear 38-complement as in the previous fig. A) K_D values as determined without modification. C) RU_{max} values determined with these fittings. B) Corrected K_D values and D) Localization of the 38-complement in the hairpin.
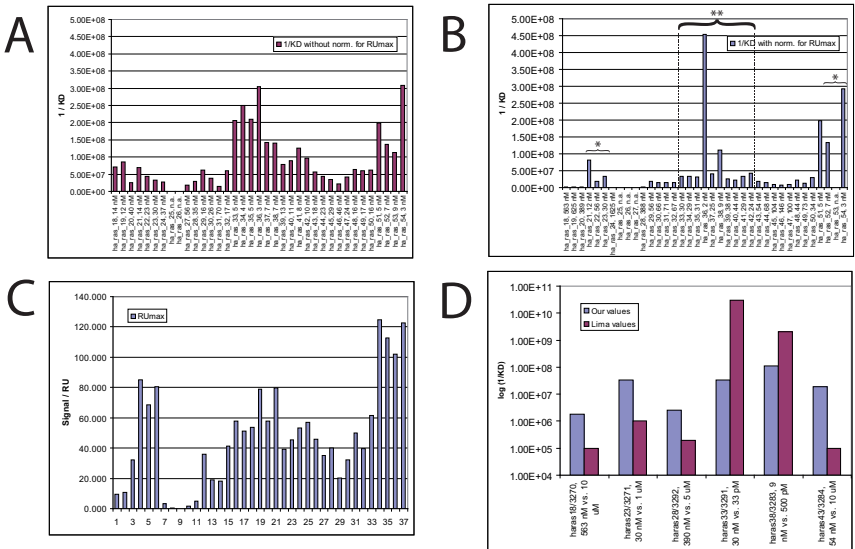

Figure 2.7. – Determination of K_D values for the decamers against the h-ras hairpin. A) K_D values as determined without modification. C) RU_{max} values determined with these fittings. For the normalization a value of 80 RU was taken B) Corrected K_D values. These values now exhibit a rather different finger printing than the unnormalized ones. Although ha_ras_36 binds in both cases best, this effect is much more prone after normalization. * marks the 3 oligoribonucleotides which are fully complementary to the stem on the 5'-/3'- site. ** marks the 10 oligoribonucleotides which are complementary to only single-stranded sequences in the loop.D) Comparison of the K_D values determined with Biacore and by Lima et al. (see text).

54 (which had to fitted differently due to their extraordinary high RU_{max} value and most probably > 1 binding site) there are only 3 oligoribonucleotides with "outstanding" binding affinities: ha_ras_21, ha_ras_36, and ha_ras_38.

3. as shown in the experiment against the linear complement ha_ras_38, ha_ras_21/22/23 are binding strongly to the sequence homologue region within the loop. Therefore, the binding of these 3 oligoribonucleotides is most probably not happening to the complementary regions of the stem. Of note, the complementary regions for ha_ras_21–23 are the only ones which lie completely within the stem (cf. asterisks in fig. 2.7, p. 47/B) —where they were designed to bind at—but in the loop-region.

4. Taking this as a given, the first substantial binding of oligoribonucleotides to the hairpin begins with ha_ras_28/29 (cf. fig. 2.4, p. 45). These oligoribonucleotides have already $\geq 50\%$ of the sequence that bind to the loop-region (cf. fig. 2.6, p. 47). This would mean that the 5'-part of the stem is not amenable for binding of antisense decamers (at least in reasonable concentrations at 25 °C) whereas the 3'-part is. The same observation was made with the hairpin of pre-miR-122 (cf. section 2.3.2.1, p. 51).

2.3.1.5. Comparison with published values

Our test series of 37 RNA decamers around the hairpin showed that the oligoribonucleotide with the highest affinity was lying approximately in the middle of the loop-region with an affinity of $\approx 2\,nM$ (cf. table A.3, p. 134). The 5'-site of the hairpin stem was not amenable for binding.

Lima et al. showed that their highest binding oligoribonucleotide was lying in the loop-region, too, with an affinity of $\leq 33\,pM$. They showed that the two best binders (3291, 3283, cf. table 2.7) were binding with almost equal affinity to the hairpin loop as compared to the single-stranded complements (50/50 pM vs. 33/500 pM). We observed a similar ratio for ha_ras_38 (540 pM vs. 9 nM) but a completely different result for ha_ras_33/3291: whereas the affinity of 3291 against the hairpin was higher than for the complement, our determined value for the same molecule was ≈ 35-fold lower (870 pM vs. 30 nM).

Table 2.7 lists all entries for the comparable values, fig. 2.7/D shows a graphical comparison of these values.

Although Lima et al. point out the 10^6-fold difference in affinity for their 6 decamers ($\leq 33\,pM$ for 3291 vs. $> 10\,\mu M$ for 3284), we could not observe such a strong difference. With our assay the maximum difference for the same analytes was about 60-fold (9 nM vs. 560 nM) or about 800-fold for the highest overall difference (2 nM vs. 1625 nM).

When introducing their new method (RT–ROL[ii]) for the determination of accessible sites within structured RNA, Allawi et al. [179] performed the same gel shift assay as Lima, but with a larger number of 26 decamers. Their results are close to our SPR data as shown in fig. 2.8 and table 2.8. Not only exactly the same decamer with the highest affinity was identified but as well a similar ranking and close K_D values were found.

Finally, the set ups of the two (three) assays is rather limited:

[ii]RT–ROL: reverse transcription with random oligonucleotide libraries

Table 2.7. – Comparison of the determined binding affinities for the 6 decamers chosen by Lima with our values. I give the values as given in [109] calculated as K_D (together with the originally published K_A values).

Our name	Lima name	location	h-ras hairpin		complement	
			Our K_D value	Lima K_D value (+ orig. K_A val.)	Our K_D value / [M]	Lima K_D value / [M]
haras_18	3270		563 nM	10 μM ($1\cdot10^5$ M^{-1})	n.a.	33 pM
haras_23	3271		30 nM	1 μM ($1\cdot10^6$ M^{-1})	n.a.	10 pM
haras_28	3292		390 nM	5 μM ($2\cdot10^5$ M^{-1})	n.a.	20 pM
haras_33	3291		30 nM	$\leq$ 33 pM ($\geq 3\cdot10^{10}$ M^{-1})	870 pM	50 pM
haras_38	3283		9.0 nM	500 pM ($2\cdot10^9$ M^{-1})	540 pM	50 pM
haras_43	3284		54 nM	$>$ 10 μM ($< 1\cdot10^5$ M^{-1})	n.a.	50 pM

1. Lima et al. used a gel-shift assay for the determination of K_A (10 mM PO$_4$, 100 mM Na$^+$). After mixing of the antisense oligoribonucleotides with the target, they incubated the probes at 37 °C for 20 hours with a subsequent loading of the 12 % polyacrylamid gel at 10 °C.

2. Allawi et al. performed the same assay, but with TRIS instead of phosphate and 5 mM Mg^{2+}. Additionally, they performed an annealing procedure (75 °C for 3 min.) prior to incubation for 4 h at 37 °C.

3. We used our oligonucleotides without pre-annealing directly at 25 °C with similar salt concentrations (10 mM HEPES, 100 mM Na$^+$) but no Mg^{2+}.

Table 2.8. – Comparison of the determined binding affinities for the 8 highest K_D values as determined by Allawi et al. with gel shift. The values correlate well and show not only the same preferred binding site (ha_ras_36 / 19–28) but as well the same fingerprint. Values were taken from [179] and estimated from the figure (no numbers given).

		Affinity against h-ras hairpin	
Our name	Allawi name	Our K_D value / [M]	Allawi K_D value / [M]
ha_ras_23	6-15	30 nM	22 nM
ha_ras_35	18-27	31 nM	29 nM
ha_ras_36	19-28	2 nM	7 nM
ha_ras_37	20-29	25 nM	13 nM
ha_ras_38	21-30	9 nM	12 nM
ha_ras_39	22-31	38 nM	22 nM
ha_ras_41	24-33	29 nM	20 nM
ha_ras_51	34-43	5 nM	40 nM
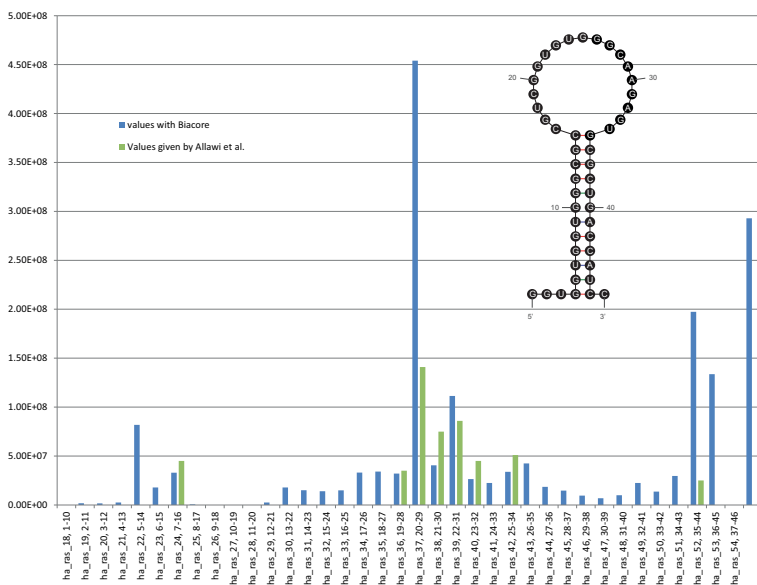
Figure 2.8. – Comparison of the own determined K_D values for the decamers against the full length h-ras hairpin (cf. inset) with the values published by Allawi et al. [179]. The same preferred binding site with the same best binder was determined and validates the 2 approaches. The values are very similar to our values as shown in table 2.8.

2.3.2. pre-miR-122 "walkaround"

This subsection is divided into the following 3 parts:

Preliminary "walkaround" experiments which Biacore T-100 was done with a set of 52 oligoribonucleotides against the full length hairpin of pre-miR-122 (p. 51).

Finding the optimal loop-binder In this experiment I investigated the optimal length and position of a LooptomiRs (p. 54).

Structured vs. unstructured RNA In a series of experiments the binding affinities and kinetic rate constants of RNA, DNA, and 2'-OMe RNA LooptomiRs have been determined against structured (hairpin) and unstructured (linear complement) RNA (p. 58).

A discussion of the results with conclusions for the design of optimal LooptomiRs is given in section 7.1.1.2, p. 123.

2.3.2.1. Preliminary "walkaround" experiments

On a Biacore T-100 machine with the conditions listed in table A.2, p. 133 (pre-miR-122 I) the binding assay was performed with a set of 52 2'-OMe-heptaribonucleotides around pre-miR-122. The oligoribonucleotides were synthesized, purified twice, and analysed as described in section 2.2.2.2, p. 37. The normalization was done with UV-based measurements by NanoDrop. At this stage I used a weighted sum method for the calculation of ε-values as used by Kibbe et al. [206][iii]. Table A.4, p. 135 lists the sequences used in this assay.

As ligands for the Series S Sensorchip SA the following oligonucleotides were prepared (cf. table A.1, p. 133):

1. The hairpin of pre-miR-122 in fc 2

2. A short 7-mer with a sequence identical to a part of the stem-region ("control_1_8_14") in fc3 and

3. A 7-mer identical to a part of the loop region ("control_2_26_32") in fc4.

All three ligands were provided with a linker composed of 6 thymidine nucleotides and were biotinylated at the 3'-end. They were synthesized with a 3'-Biotin-TEG-CPG.

Fig. 2.9 shows a scheme of the hairpin structure of pre-miR-122 with the two isolated randomly selected sequences highlighted in green.

Based on preliminary experiments (data not shown) we decided to assay at 25 °C with a content of 10 mM Mg^{2+} in running buffer (HBS-P+-buffer)[iv]. This experiment was performed with a 2-fold dilution series made with a concentration range from 5000 down to 156.25 nM and a blank buffer injection for each concentration series. The resulting 364 oligoribonucleotide solutions ($= 52 \cdot 7$) were divided in 5 different 96-well plates. Every 6th injection an injection of a control oligo (oligo_26 which is completely complementary to the control2 in fc4) was made for monitoring of surface stability.

[iii]$\varepsilon = (\#\,A \cdot 15'400 + \#\,C \cdot 9'000 + \#\,G \cdot 13'700 + \#\,U \cdot 10'000)\,l \cdot mol^{-1} \cdot cm^{-1}$

[iv]a 10-fold stock solution from Biacore containing: 0.1 M HEPES, 1.5 M NaCl and 0.5 % v/v Surfactant P20, Prod.code BR-1008-27, provided by the fgcz.
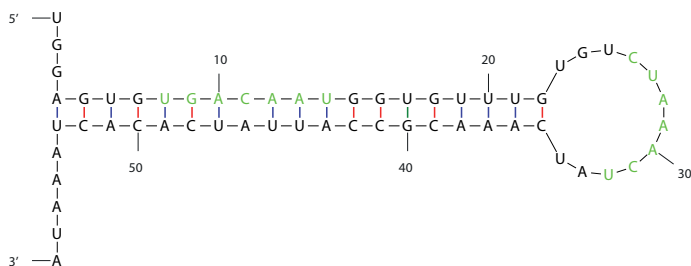
Figure 2.9. – Schematic of the structure of pre-miR-122 (without linker / biotin) and the separate two control sequences (highlighted in green): one is lying in the stem-region, one in the loop-region.

The analysis of the binding affinities against the controls in fc 3 and 4 is straight forward: mir-122-aso-8 which is complementary to the control oligo bound to the surface of fc 3 had a calculated affinity of 550 nM. Neighbouring sequences showed a distribution around this value similar to the result yielded for ha_ras_33 to 33-complement (cf. fig. 2.5, p. 46, data not shown). mir-122-aso-26 (which is complementary to the ligand in fc4) and mir-122-aso-25 had an affinity of both around 1 µM (data not shown).

The analysis of the hairpin was not completely fittable for all heptanucleotides using a 1:1 model. The determination of K_D with steady-state analysis worked well with the method of uniform RU_{max} values as developed with h-ras.

The figs. B.2, p. 145 and B.3, p. 146 show all resulting sensorgrams which yielded an acceptable response.

Fig. 2.10 shows a bar graph plot of the binding response level[v] for all concentrations. At a first glance one can already see the oligonucleotides binding to the loop-region. As the fitting to a kinetic model failed and as all oligoribonucleotides were reaching steady-state values I analyzed the sensorgrams only by steady-state analysis.

Prior to the steady state analysis by Scrubber I normalized all values for their molecular weight. After that the analysis was performed as described in section 2.3.1.2, p. 45.

Due to the big differences in RU_{max} values (cf. fig.2.11/C) sensorgrams with the lowest response levels have the highest affinity (cf. fig.2.11/A and B) simulating a preferred binding site in the 3'-part of the stem. After normalization of all sensorgrams to RU_{max} = 55 RU the calculated K_D values reveal a highest affinity binding site only in the central part of the loop region (cf. fig.2.11/D).

From this assay one can draw the following conclusions:

1. As with the decamers of the h-ras assay the preferred bindings sites of the heptamers against pre-miR-122 lie within the loop-region.

2. The 3'-part of the stem seems to be much more amenable for oligonucleotide binding then the 5'-part (also observed for the h-ras "walkaround").

3. The best two binders were starting at the 5'-end of the loop shifted by 3/4 nucleotides towards the 3'-end. This was also observed for the h-ras assay.

---

[v] report point 5 sec. before end-of-injection
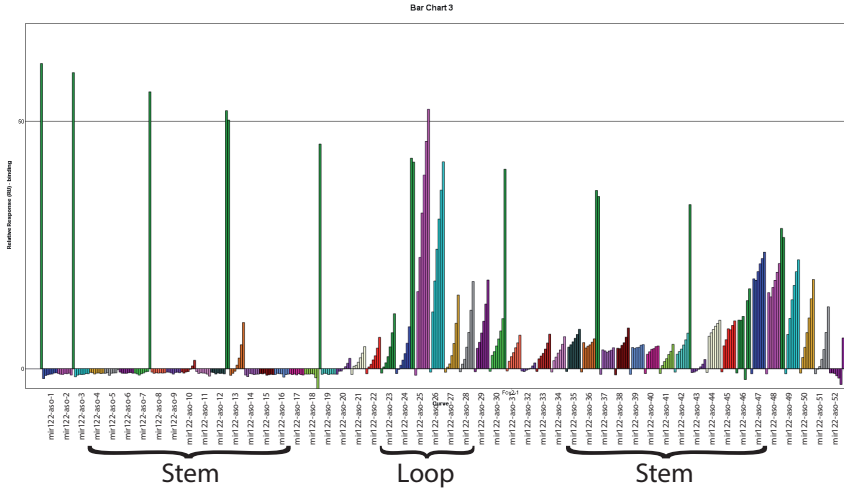
Figure 2.10. – Comparison of the end-of-injection levels of all sensorgrams. The green intermediate bars indicate the injection of the control oligonucleotide oligo 26. The oligonucleotides which are complementary against only double-stranded regions are marked with "Stem", the oligonucleotides which are complementary to only single-stranded regions are marked with "Loop".
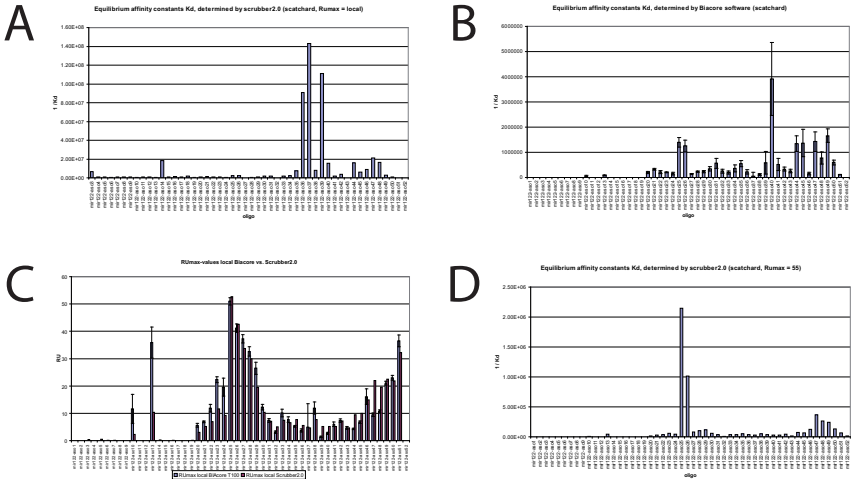
Figure 2.11. – Determination of the K_D values for the "walkaround" of pre-miR-122. A) Determination by steady-state analysis with Scrubber and floating RU_{max} values. B) Determination by steady-state analysis with BiaEvaluation (only floating RU_{max} values possible). The analyses A) and B) exhibit preferred binding sites in the 3'-part of the stem. C) Determined RU_{max} values by Scrubber. The RU_{max} values correlate with the accessible sites. D) Corrected K_D values determined by steady-state analysis with fixed RU_{max} values (at 55 RU).

Additionally, there were some phenomena which interfered with the assay. There was a loss of surface binding of the control oligonucleotide by as much as 77 % over the whole assay (cf. green bars in fig. 2.10). This was due to a dissociation of the biotin-streptavidin interaction (cf. chapter 6). Although the binding of biotinylated oligoribonucleotides to streptavidin is extraordinary high ($\approx 1 \cdot 10^{-13}$ M) this interaction is not high enough for a very long assay (the assay lasted for ≈ 96 hours).

Secondly, the fitting to a kinetic model could not be performed well. I assign this to three reasons:

1. The immobilization levels were quite high ($\approx 1'000$ RU for the hairpin and ≈ 170 RU for the controls) and the flow rate was set to a rather low value (10 µl·min^{-1}). These two facts facilitate / raise the influence of mass transport limitation (MTL)/rebinding and aggravate a proper binding mechanism [168].

2. At least in some cases there was most probably more than one binding site for the corresponding oligoribonucleotide (e.g. ASOs 46–48).

3. During purification of these oligonucleotides I observed for some sequences multiple and broadened peaks in the LCMS-chromatograms (even at 60 °C). Analysis with ESI-MS revealed a uniform mass. As these peaks could be converted into sharp single peaks after a heat treatment with 8 M Urea, I assign this to secondary structure formation of these short heptamers. The same phenomenon could occur in the solutions used for the SPR experiments yielding a heterogeneous distribution of analytes and changing the concentration of free analyte in solution.

Further partial repetitions of this assay[vi] confirmed these findings. Additional experiments[vii] with modified hairpins showed further that the affinity of these loop-binding oligoribonucleotides is strongly sequence dependent (data not shown).

2.3.2.2. Finding the optimal loop-binders

In the previous SPR-experiments I showed, that the optimal position for antisense oligoribonucleotides with a length of 7 nucleotides is within the loop region and that there are only two molecules with a considerable binding-affinity in the sub-µM range (cf. table A.4, p. 135).

The goal of this experiment was to evaluate the affinity of oligonucleotides with different length and positions for the understanding of the influence of these factors to find optimal inhibitors of pre-miR-122-processing. The question we asked was if there is a cutoff in length, above which there is no improvement in binding affinity (or even worsening) and if there is a common start- or end-point of these oligoribonucleotides. Of the best binders, also kinetic properties (k_a, k_d) would be determined.

For this purpose I designed a set of 60 oligonucleotides starting with a length of 7 nucleotides at position 22 (last base of the stem) using "oligo_scoop". The length of the oligonucleotides was increased to 14.The sequences of the designed oligonucleotides are listed in table A.5, p. 136. This set of oligonucleotides has been synthesized, purified and analyzed as described in section 2.2.2.2, p. 37.

[vi]with an SPR2 machine at SierraSensors at Hamburg

[vii]performed with Biacore T-100

For normalization I employed our Hamilton Starlet pipetting robot. A sophisticated normalization procedure comprising two pre-normalization steps yielded the final normalized 1 µM solutions as shown in fig. 2.12. These normalized solutions were lyophilized and dissolved in running buffer (20 mM HEPES, 150 mM NaCl, 10 mM MgCl$_2$, and 0.005 % TWEEN). The experiments were performed with conditions listed in table A.2, p. 133 (pre-miR-122 II).
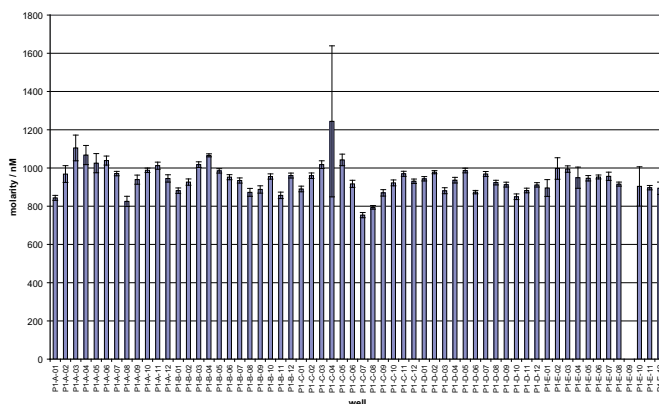

Figure 2.12. – Comparison of the measured concentrations of the 60 analytes for the screen of the LooptomiRs after normalization by the robot. The oligoribonucleotides were normalized for 1 µM solutions and showed an error range of $\pm 10\%$ (with outliers)

When analyzing the sensorgrams of the normalized[viii] analytes one can see that the differences in binding response are considerable (cf. figs. B.4, p. 147 / B.5, p. 148). For some of the sensorgrams (especially for the longer ones) the binding behaviour does not fit into a 1:1 binding model. This can have multiple reasons:

1. The samples were not pure to 100 % and contained contaminants with a n-1 oligonucleotide. Of course this can affect the binding, especially if the two oligoribonucleotides contained in the sample have a strongly differing binding affinity.

2. The influence of MTL can not be determined without a concentration series in the appropriate concentration range around K_D. Especially for analytes with higher affinity (i.e. longer ASOs) the effect of MTL is higher than for shorter ones.

3. If there are two (or even more) binding sites within the target RNA only a high concentration series covering both K_D values will reveal the nature and affinity of/for the heterogeneous ligand.

However, I performed a calculation of the affinity values with and without (data not shown) normalization for RU$_{max}$ to see whether there is an observable trend for this screen or not. Fig. 2.13 shows a plot of the estimated K_D values for the screen. Fig. 2.14 shows a comparison of the stability values taken as an average of the signals between 380 and 400 seconds.

[viii]the sensorgrams were divided by the molecular weight of the analyte and multiplied with 3000
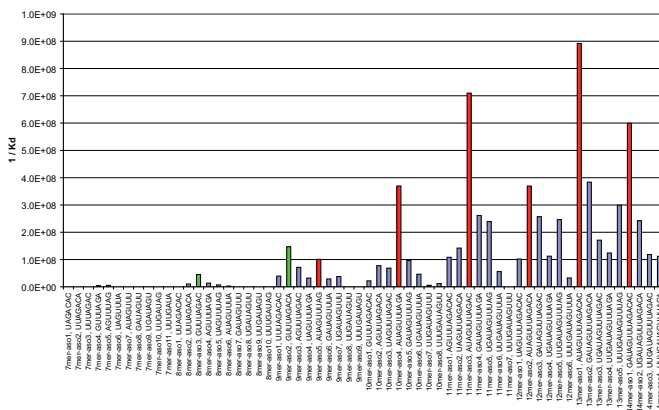
Figure 2.13. – Estimated K_D values for the screen of loop-binders against pre-miR-122 without normalization for RU_{max}. As one can see there is a preference for one oligonucleotide in each length series (7-mers, 8-mers, . . .). For the 9–13 mers these binders have all one binding motif in common. For the explanation of the colored bars see text.
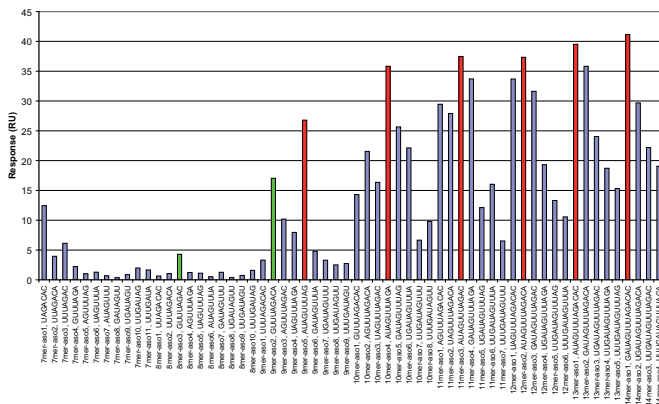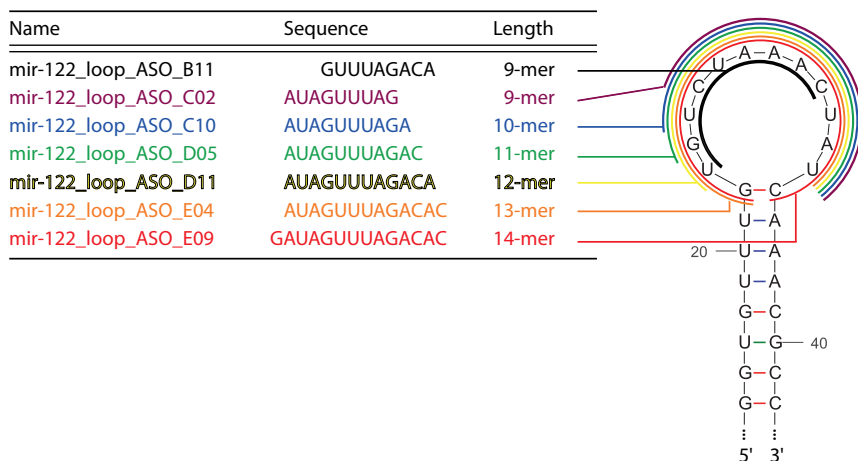

Figure 2.14. – Stability values for the screen of loop-binders against pre-miR-122 (Average from 380-400 sec.). The same distribution as observed in fig. 2.13 can be observed. This is a good hint for the validity of the result and indicates that the raised affinity for the analytes with higher affinity is most probably due to a lowered dissociation rate constant, k_d.

As one can see there is a rather clear trend for the binding affinity/behaviour of the loop-binding oligoribonucleotides. From the comparison of the "K_D" values and the stability levels the following conclusions can be drawn:

1. The difference in binding affinity amongst oligoribonucleotides of the same length is at least of factor 4 (e.g. for the 12-mers) and there is one clearly favourized binder in each series from the 10-mers on and longer (cf. red bars in fig. 2.13).

2. These highest binders within the series of 10-, 11-, 12-, and 13-mers share a common binding motif beginning with the sequence 5'-AUAGUUU.... Within the 14-mers the sequence begins with 5'-GAUAGUUU.... This observation is made for the normalized and unnormalized "K_D" values as well as for the stability levels at end-of-dissociation (cf. red bars in fig. 2.14). The corresponding binding region within the hairpin of pre-miR-122 lies exactly at the 3'-end of the loop (...AAACUAU-3', cf. fig 2.15).

3. The two best binders of the initial "walkaround" were confirmed. For these 7-mers and the 8-mers the preferred binding site of ASOs lies within the middle of the loop (green bars in fig. 2.13) beginning with the sequence 5'-GUUUAG....

4. The preferred binding site for the 9-mers is at the boundary middle-of-loop / end-of-loop. Depending on the kind of analysis there are contradictory results for the highest affinity and the preferred binding site is not clearly defined as with the longer oligoribonucleotides.

Fig. 2.15 shows a scheme of the best 7 loop-binders against pre-miR-122 with length and position around the loop-region.

Name	Sequence	Length
mir-122_loop_ASO_B11	GUUUAGACA	9-mer
mir-122_loop_ASO_C02	AUAGUUUAG	9-mer
mir-122_loop_ASO_C10	AUAGUUUAGA	10-mer
mir-122_loop_ASO_D05	AUAGUUUAGAC	11-mer
mir-122_loop_ASO_D11	AUAGUUUAGACA	12-mer
mir-122_loop_ASO_E04	AUAGUUUAGACAC	13-mer
mir-122_loop_ASO_E09	GAUAGUUUAGACAC	14-mer

Figure 2.15. – Scheme of the 7 best loop binder as described in text. For the 9-mers there are two: one beginning at the 5'-end of the loop ("B11"), and one ending at the 3'-part of the loop ("C2"). The 10-, 11-, 12-, and 13-mers are all ending at the 3'-part of the loop. The 14-mer covers the whole loop and the last two bases of the stem.

When comparing the ratios of the highest and the lowest k_a value for each length series as shown in fig. 2.16 one can see a very clear trend for reduced influence of the association

rate with longer oligoribonucleotides. Although a proper determination of the kinetic rate constants was not doable, this clear trend indicates that the raised affinity of longer oligo-ribonucleotides to the loop-region is more and more due to the dissociation rate[ix].
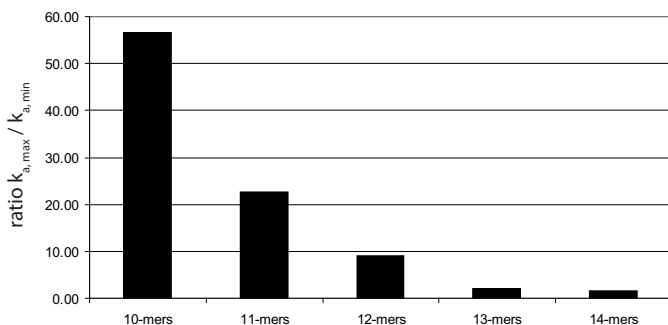
Figure 2.16. – Comparison of the ratios of the highest and lowest k_a value of each length series. Whereas the factor in k_a values is > 50-fold for the 10-mers, the factor in k_a values is only ≈ 1.5-fold for the 14-mers

The affinities and kinetic properties of these highest binders were then further analyzed (cf. next section). At this stage I analyzed the binding affinity of the loop-binders with different buffers (data not shown). Finally I decided to take a TRIS-buffer with Ca^{2+} and Mg^{2+} as suggested by SierraSensors (cf. table 2.6).

2.3.2.3. Structured vs. unstructured RNA

After the determination of the preferred binding site for the LooptomiRs at the 3'-end of the pre-miR-122-loop I went on for the investigation of the binding affinities, K_D, and the kinetic rate constants, k_a and k_d. The final determination of these parameters presented herein was performed with the Biacore T-100 under the conditions listed in table A.2, p. 133 (pre-miR-122 III). For better comparability of the results I finally took one biotinylated ligand (loop-region) which contained all sequences and immobilized this ligand together with the hairpin of pre-miR-122 on two different flow cells of the same Series S sensor chip SA[x]. The runs were performed with a freshly made TRIS-buffer (cf. table 2.6, p. 42) at 25 °C. To reduce MTL I raised the flow-rate to $50\,\mu\text{l}\cdot\text{min}^{-1}$ for all experiments.

I made the concentration series in 2-fold dilutions with duplicates of the three highest concentrations. In order to be in the right concentration range for the concentration series I adjusted the stock solutions from which the dilution series was made to the binding affinity. Table A.6, p. 137 lists all dilutions of the analytes.

On pages 149–151 in the appendix all sensorgrams are shown for the RNA (fig. B.6), 2'-OMe RNA (fig. B.7), and DNA (fig. B.8) analytes.

[ix]This analysis was done for the k_d values as well. Although a similar trend was resulting, the trend was not that clear due to the bad fittings for the longer oligoribonucleotides

[x]so the same solution is used for the determination of the affinities against both, hairpin and linear complement (loop-region).

The analysis of the binders, which was performed with BiaEvaluation, could be done—with only two exceptions—to a 1:1 binding model. As seen in figures B.6 and B.7, the sensorgrams of the RNA and 2'-OMe RNA analytes against the linear complement are showing practically no dissociation due to the high binding affinity[xi]. Therefore these values have to be regarded with suspicion.

Fig. 2.17 shows a comparison of the determined K_D values of the high-affinity loop-binder with RNA chemistry against the hairpin of pre-miR-122 and the linear loop-region. Fig. 2.18 the same for the analytes with 2'-OMe chemistry.
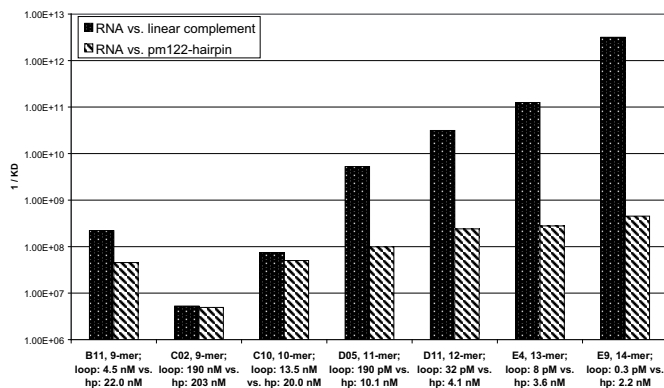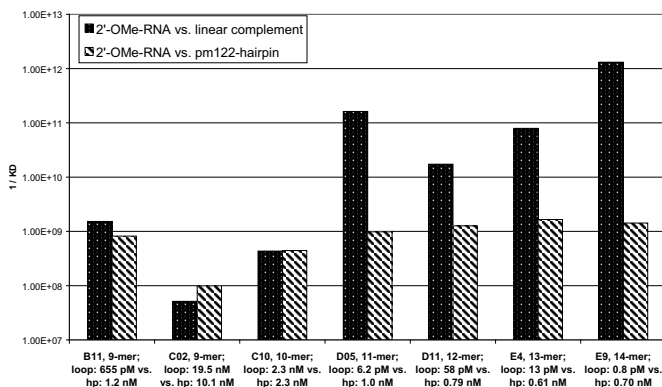

Figure 2.17. – Comparison of the affinities of the selected loop-binders with RNA chemistry against structured and unstructured target RNA. Whereas the affinity against the unstructured loop-region raises with each additional nucleotide there is only a small increase in affinity against the structured hairpin above a length of 11 nucleotides.

In the appendix there are additional figures comparing the affinity of the three differently modified loop-binders against the hairpin (cf. fig. B.9, p. 152) and the unstructured linear loop-region (cf. fig. B.10, p. 153) as well as a table with all determined affinity and rate constants (cf. table A.7, p. 138)

The raised affinity of the 2'-OMe RNA 9-mer ending at the loop, mir122_loop_ASO_C02 (cf. fig. 2.15, p. 57), may derive from a structurally favoured pre-structure of the hairpin of pre-miR-122. This sequence, which we termed later 26-9 (for the position and length of the ASO, was successfully tested in an *in vitro* assay for its ability of inhibiting miRNA maturation by Dicer. Therefore we tested in later experiments the possibility of even raising this affinity for a more potent and selective inhibition of pre-miRNA processing.

Of note, oligoribonucleotides of length $\geq$ n (n = size of loop) are as well binding to the hairpin.

[xi]for a proper determination one would have to make one strongly elongated dissociation for the determination of k_d and insert that as a fixed value into the parameters for the fitting. This is not doable with biotinylated ligands as the binding affinity of biotin-streptavidin lies in the same magnitude as the binding affinity of the analytes (cf. chapter 6).

Figure 2.18. – Comparison of the affinities of the selected loop-binders with 2'-OMe RNA chemistry against structured and unstructured target RNA. The 9-mer ending at the 3'-end of the loop region—mir122_loop_ASO_C02—has as only analyte a higher affinity towards the hairpin than to the loop-region. As with the RNA analytes a length of 11 nucleotides sets the benchmark for the maximum affinity.

2.3.3. pre-miR-18a loop-screen

For the loop-screening of pre-miR-18a I synthesized 78 2'-OMe RNA ASOs with lengths from 7-mers to 18-mers (cf. table A.8, p. 139). The oligonucleotides were designed with "Oligo_scoop". The start position was chosen to be complementary to base 23 of pre-miR-18a, the end position was base 40 which is complementary to base 23 (according to mir-base). This region includes a 1 nt-bulge at position 39. The synthesis was performed using the MM192 apparatus. Purification was done using Sephadex resin as described (cf. section 2.2.2.2, p. 38).

Fig. 2.19 shows the secondary structure of pre-miR-18a as given by mirbase.
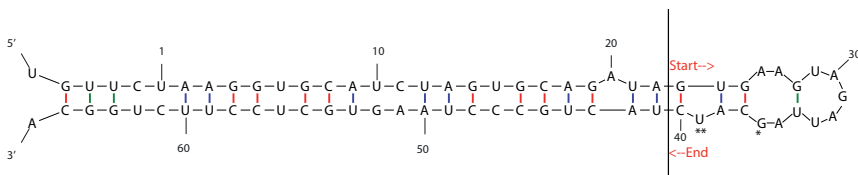
Figure 2.19. – Structure of pre-miR-18a as given by mirbase. "Start" end "End" mark the region over which the ASOs were synthesized. */** indicate the 5'-ends of the best sequences as described in text.

The pre-miR-18a was synthesized using a 3'-Biotin-TEG-CPG with the full sequence given by mirbase cf. table A.1, p. 133).

The "walkaround" assay was performed three times: once with SPR2, twice with Biacore. Here I present the data of the first SPR2 and the last Biacore screen[xii].

[xii]The second Biacore screen could not be used for reasons of MTL.

The conditions of the experiments are listed in table A.2, p. 133. Both screens were performed using 1 µM concentrations. The regeneration solution for this screen (10 mM EDTA) was chosen after a series of experiments as I was faced with regeneration problems of very high affinity analytes.

2.3.3.1. SPR2 screen

The data was processed with Scrubber as described (cf. section 2.2.3.3, p. 43). The fittings could be performed with a 1:1 binding model. With this screen I was faced with a not fully regenerated ligand. As the analytes of a length of 13 nucleotides and longer started to exhibit not quantitative regenerations, I used only the sensorgrams of 57 analytes with a length $\leq$ 12 nucleotides. The sensorgrams for the 7–12 mers are shown in figs. B.11–B.13 (pp. 154–156).

The sensorgrams were normalized to molecular weight and fitted to the 1:1 model. Whereas the normalization for a RU_{max} value as described (cf. sections 2.3.1 and 2.3.2.1) could be well performed for shorter oligonucleotides of 7/8-mer in length, this procedure failed for analytes longer than 10 nucleotides for unknown reasons.

Fig. 2.20 shows the estimated K_D values for the 7–12 mers (A: in total. B: only 7-8 mers with normalization for RU_{max})

There is a high occurrence of the same 5'-starting point within the oligoribonucleotides of the highest affinity in each group from 8–11-mers: 5'-CUAAUCU.... The corresponding target sequence of pre-miR-18a for oligoribonucleotides with this 5'-sequence is again exactly at the 3'-end of the loop region, disregarding the G—U wobble (between bases 28–34, cf. star (*) in fig. 2.19). The 7-mers have a second high binder at the very 5'-end of the series. Within the 12-mers this expected sequence (cf. green bar in fig. 2.20, part A) is overhauled by the sequence which is shifted 3 bases towards the 3'-end of the hairpin. This sequence corresponds to the U at position 39 which is forming a bulge (** in fig. 2.19).

2.3.3.2. Biacore screen

The analysis of the Biacore screen was done with BiaEvaluation. The regeneration solution has fully regenerated the surface for all oligonucleotides, but for comparability I used only the same 57 sequences as in the SPR2 screen, additionally, the oligoribonucleotides of a length of $\geq$ 14 nt the dissociation rate constants are to small for a reliable differentiation of the affinity values (within the chosen dissociation time of 600 sec.). The sensorgrams were analyzed (after double referencing) without possibility of normalization for molecular weight. This normalizing procedure is only important for normalization for RU_{max} and therefore this does not have any influence without normalization for RU_{max}.

Fig. 2.21 shows the estimated K_D values of this screen.

For the 7-, 8-, and 9-mers there is the same preferred binding site as with the SPR2 assay.

Although a determination of K_D values was not possible, a rough estimation of the binding affinities based on dissociation rate constants (determined in the very last dissociation phase) can be done. If doing so, one can see that the LooptomiR chosen by Michlewski
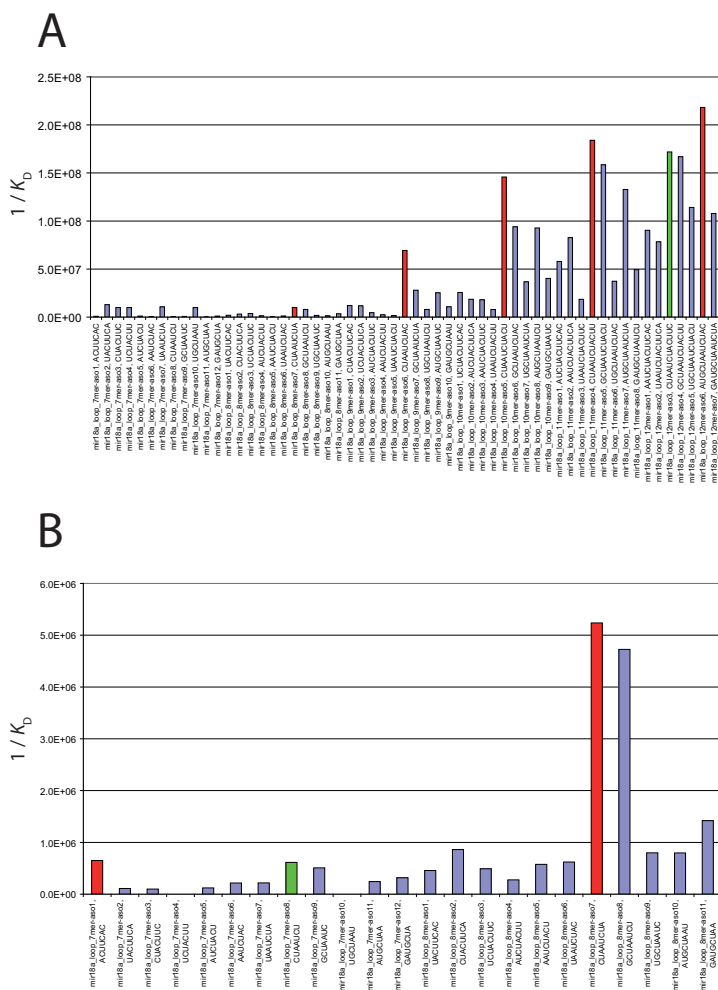
Figure 2.20. – Estimated K_D values for affinity ranking of loop-binder against pre-miR-18a as determined with SPR2 A) Comparison of all values with normalization for molecular weight, but without normalization for uniform RU_{max}. The red bars indicate the analyte with highest affinity of a length-series. B) Comparison of values of 7- and 8-mer with normalization for molecular weight and RU_{max}. Red bars indicate analytes with highest affinity of a group.
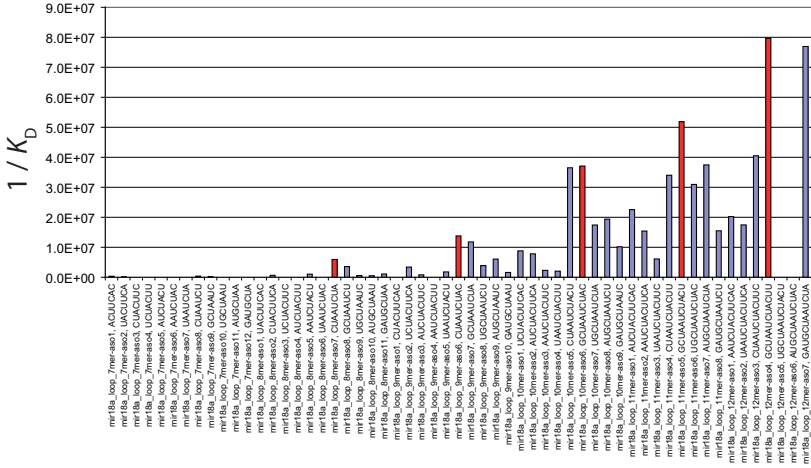
Figure 2.21. – Estimated K_{D} values for affinity ranking of loop-binder against pre-miR-18a as determined with Biacore. The red bars indicate the highest affinity within a length series.

et al. against pre-miR-18a had a 2-fold higher dissociation rate than the two neighbouring ASOs (cf. fig. 2.22).

2.3.4. pre-let-7a-2 loop-screen

As mentioned in section 2.1.1.4, p. 34 our lab designed, synthesized and tested 2'-OMe RNA antisense oligonucleotides (ASO) to specifically antagonize Lin28 from binding to the terminal loop region of pre-let-7a-2, in order to increase processing by Dicer and Drosha to recover mature let-7 levels. These ASOs were tested by a newly developed RNA based competition ELISA as previously described in [207] and compared to the K_{D} values as determined by SPR.

The LooptomiR oligoribonucleotides tested for the affinity against pre-let-7a-2 were designed and synthesized by Martina Roos (cf. table A.9, p. 140). They were tested with the Biacore T-100 according with the conditions listed in table A.2, p. 133.

The assay of the LooptomiRs was done against pre-let-7a-2, the linear loop region and pre-miR-122. pre-let-7a-2 was obtained from Philipp Wenter (Department of Oligonucleotide Manufacturing, Eurofins MWG Operon, Huntsville, AL 35805-3848, USA). The linear loop region was synthesized, purified and quantified as described (cf. section 2.2.2.2, p. 37). The hairpin of pre-miR-122 was obtained from Dr. A. Brunschweiger. The specifications of the ligands are listed in table A.1, p. 133, the sensorgrams of the assay are shown in fig. B.14, p. 157.

As the affinities of the analytes are in the sub-nM range, they were analyzed with EVILFIT using a bayesian prior [168,208,209]. This prior assumes a uniform (homogeneous) ligand distribution on the chip surface. For this analysis, two constraints were made:
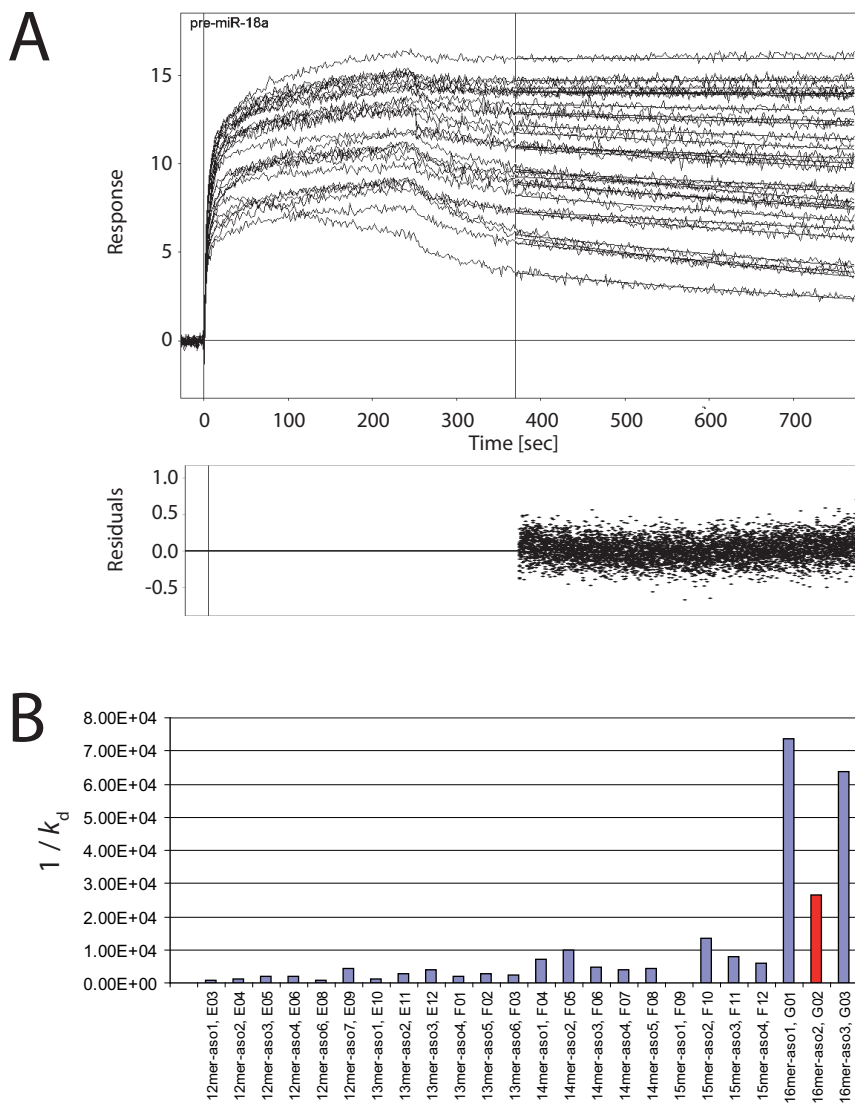
Figure 2.22. – Comparison of dissociation rate constants of long LooptomiRs. A) Overlaid sensorgrams of 12–16 mers with corresponding residuals of the fits for the end-of-dissociation. B) Plot of these k_d values. The red bar indicates the LooptomiR against pre-miR-18a as used by Michlewski et al. [31].

1. The hairpin on the chip surface is uniform due to only one possible site of attachment (the biotin) and due to its rather rigid structure. The structure calculations given by MFold with a 50 % deviation gives 4 structures. The first structure is very similar to the structure as given by mirbase (-22 kcal/mol). The second stable structure is more than 20 % less stable (-17 kcal/mol) and has additionally the same loop region. All other calculated structures are $\geq$ 50 % less stable (cf.fig. B.15, p. 158/A).

2. The calculated K_D values for the discrete prior are equally distributed around an average value. The shape of the distribution and experiments performed with simulated, badly-defined data give a hint for this, but to prove this constraint further experiments would have to be performed.

Fig. B.15, p. 158/B) shows the initial plot with discrete prior for an example case. The limits for the fitting are set to a very large range in order to cover a wide range of possible distributions. Due to the very low dissociation rate, the data is broadly distributed. After integration of the of the area at about half peak height the data is fitted again and yields the plot as shown in C). D) corresponding sensorgram with residuals.

In the ELISA assay, ASOs were pre-incubated with a known Lin28 binder pre-let-7a-2 which was coated on wells. HEK 293 T cell lysate containing Myc-tagged Lin28 was added to well and finally the fraction of bound Lin28 was determined by immunostaining of its myc-tag (cf. fig.2.23/A). Binding affinities K_D were calculated from the IC_{50} values of the inhibition curves (cf. fig.2.23/B). ASO 29-13 appeared to be the strongest binder whereas the negative control did not show any binding affinity.
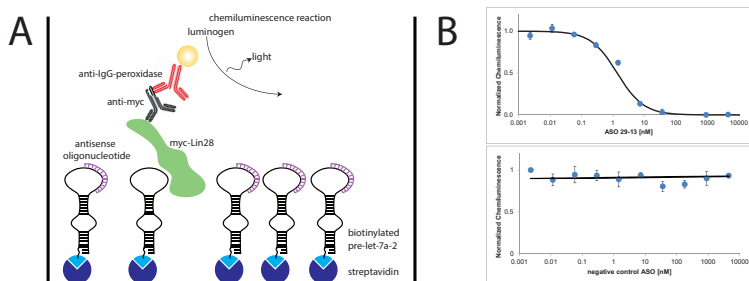
Figure 2.23. – RNA-based ELISA competition assay. A) principle of detection B) Inhibition curves for the best binder (ASO 29-13, upper curve) and the negative control (lower curve) (figs. were kindly provided by M. Roos).

The comparison of affinity rankings reveals a rather good correlation between the two assays although they differ substantially in procedure and even though the SPR data was poorly defined. Fig. 2.24 show the K_D values of both assays. The binding affinity as determined with ELISA is about 1'000-fold lower compared to the SPR-based affinity values but the ranking of the best (red bar in fig. 2.24), the second best (green bar) and the worst (value most right, no bar visible) is identical. Fig. 2.25 shows the binding sites of the two best binders in the loop region of the putative secondary structure.
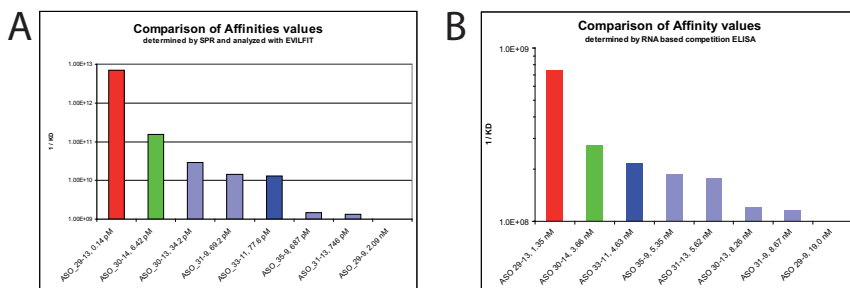
Figure 2.24. – Comparison of the affinities as determined by ELISA and SPR. The best (red bar), second best (green bar) and worst (rightmost value) are identical.
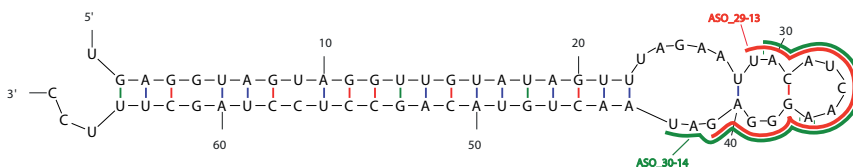
Figure 2.25. – Scheme of pre-let-7a-2 (based on the structure given by mirbase/MFold with the two best ASOs: ASO 29-13 (red) and ASO 30-14 (green).

2.3.5. Strand invasion of Miravirsen into pre-miR-122

2.3.5.1. Introduction

In the course of biochemical assays to characterize ligands that are modulating the Dicer processing of pre-miRNAs (cf. section 2.1.2, p. 34) L. Gebert discovered that SPC3649, the active compound of Miravirsen, was capable of inhibiting the processing of pre-miR-122 at the pri- and pre-miRNA levels.

The effect of antimiRs on the processing of pre-miR-122 by Dicer was investigated by incubation of Dicer with pre-miR-122 in presence or absence of antimiRs. The reaction was monitored by HPLC.

L. Gebert tested four antimiRs for their capability of inhibition of pri-/pre-miR-122 processing:

1. SPC3649 (Miravirsen), a 15-nt LNA/DNA phosphorothioate sequence complementary to nt 2–16 of miR-122 5p [210],

2. SPCcon, identical in sequence to SPC3649 except for 2 mismatched nt,

3. AMO-122, partially-phosphorothioated 2'-OMe RNA antimiR, fully complementary to miR-122 5p, which was previously described by Krützfeldt et al. [103] and

4. AMOcon, a scrambled sequence of AMO-122 bearing no significant complementarity to pre-miR-122.

The results of these experiments are published in Nucleic Acid Research [203].

2.3.5.2. Materials and methods

The oligonucleotides were obtained by L. Gebert. Table 2.9 lists the oligoribonucleotides used for the SPR assay.

Table 2.9. – Oligoribonucleotides used for the SPR assay. SPC3649 and SPCcon are sequences with LNA (in upper case) and DNA (in lower case) nucleotides. AMO-122 and AMOcon are fully 2'-OMe RNA oligonucleotides with intermediate PS linkages (indicated by *).

Name	Sequence
SPC3649	CcAttGTcaCaCtCC
SPCcon	CcAttCTcaCaCtGC
AMO-122	A*C*AAACACCAUUGUCACAC*U*C*C*A
AMOcon	C*C*A*CACUCUAACACAGUCA*C*U*A

The synthesis of the biotinylated pre-miR-122 for capturing with streptavidin was done as described in section 4.2.1, p. 77 with "click-chemistry" by Dr. A. Brunschweiger.

The amine chip was loaded with 1'850 RU of streptavidin and 165 RU of biotinylated pre-miR-122 as described in section 2.2.2.5, p. 40.

The binding experiments were performed at 25 °C and 37 °C with the molecules described in table 2.9. The fitting of the double referenced sensorgrams was performed with Scrubber2.0. As running buffer, the TRIS buffer as described in table 2.6, p. 42 was chosen.

The ligand surface was successfully regenerated with the Alw regeneration solution as described previously.

2.3.5.3. Results

HPLC-based inhibition experiments   The experiments were performed by L. Gebert.

The hairpin of pre-miR-122 was synthesized by L. Gebert as described in section 2.2.2.2, p. 37 (cf. fig. 2.26/a). Incubation of Dicer with pre-miR-122 resulted in the cleavage of the precursor hairpin into well-separated products (cf. fig. 2.26/b). These products were unambiguously identified (by ESI-MS) to be the miR-122 5p and phosphorylated miR-122 3p miRNAs (data not shown).

Incubation of pre-miR-122 with SPCcon (cf. fig. 2.26/c) or AMOcon (cf. fig. 2.26/d) did not affect significantly its processing by Dicer.

In contrast, SPC3649 (cf. fig. 2.26/e) slowed the reaction significantly resulting in barely detectable levels of miRNAs. Of note, AMO-122 also appeared to inhibit the processing. Surprisingly, the cleavage event was shifted into the loop region (cf. fig. 2.26/f).

The SPR-based binding assays of SPC3649 and AMO-122 binding to pre-miR-122 yielded very similar results. As seen in fig. 2.27 SPC3649 (A) and AMO-122 (C) were capable of invading the stem of pre-miR-122 (calculated K_D values at 25 °C 22 nM and 18 nM, respectively) whereas SPCcon (B) and AMOcon (D) were not.

Of note, the dissociation rate of SPC3649 was calculated to be $3.8 \cdot 10^{-4}\,\mathrm{s}^{-1}$. However, a binding assay of SPC3649 against the mature miR-122 sequence showed a very strong binding with no detectable dissociation (data not shown).
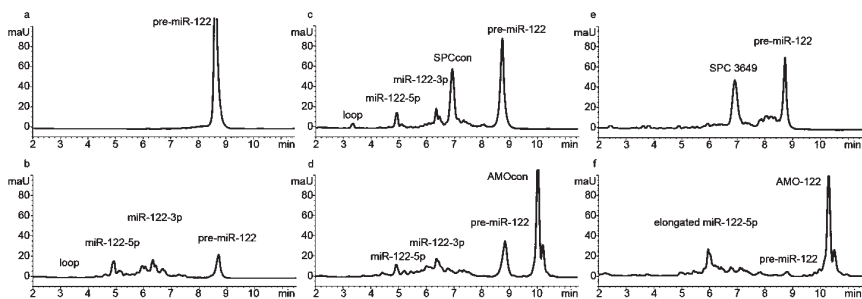
Figure 2.26. – HPLC traces of the inhibition assay as performed by L. Gebert. For explanation see text.
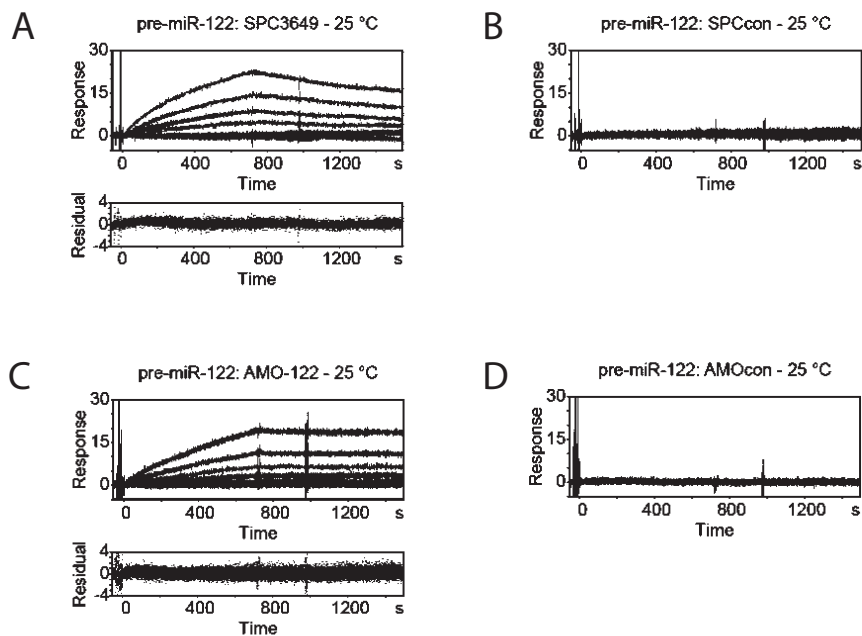
Figure 2.27. – Binding assay for the identification of strand-invasion of pre-miR-122 by SPC3649 and AMO-122 at 25 °C. A) Sensorgrams of SPC3649 against pre-miR-122. lower part shows residuals of the fit. B) Sensorgrams of SPCcon against pre-miR-122 which resulted in no detectable binding events. C) Sensorgrams of AMO-122 against pre-miR-122. D) Sensorgrams of AMOcon against pre-miR-122.

3. "Oligo_scoop": Design, Quantification, and Normalization of oligonucleotides

During the design of the ASOs against pre-miR-122 various problems concerning the design of a large set of antisense oligoribonucleotides of different lengths, the calculation of the masses thereof, as well as quantification and normalization based on UV measurements occurred.

There are several ways of converting the UV absorption values into concentrations which can lead to differences of up to 50 % [211]. Our lab performs chemical and biochemical experiments using interchanged solutions which makes it advantageous to calculate the concentrations of oligoribonucleotide solutions in a uniform way throughout the whole lab.

For circumventing these issues I developed an MS Excel-based macro with the following features:

1. input of single sequences or import of text-files with sequences (FASTA-format or plain text). The sequences can be composed of oligoribonucleotides bearing two different nucleic acid chemistries including RNA, DNA, 2'-OMe RNA and PS linkages at selected positions.

2. Calculation of molecular masses thereof.

3. Design of antisense oligoribonucleotide "walkarounds" against a given sequence with chosen length and start-/stop position.

4. Download of the current mirbase database for the search of particular sequence motivs or names.

5. Handling of HPLC report files with deconvoluted masses for the analysis of large sets of oligoribonucleotides.

6. Quantification and normalization calculations including four different calculation methods.

7. Calculation of cleavage products of enzymatic or hydrolysis cleavage assays.

Within this chapter I will shortly discuss the points 2, 3, and 7. The Quantification will be explained in detail.

3.1. Calculation of masses

The calculation of the masses is based on the exact masses without correction for isotope pattern (therefore there is a general difference of 1-2 Da to the masses given by electrospray ionization mass-spectrometry (ESI-MS)). The masses are calculated by multiplication of the

count of nucleotides of the same type (A, C, G, U, T) with the masses of the corresponding nucleotides and subtraction of 61.96 g/mol (= − 3'-PO$_2$ + 5'-H). Input sequences can be pure RNA, DNA or 2'-OMe RNA oligoribonucleotides and mixmers of RNA/DNA, RNA/2'-OMe RNA, and DNA/2'-OMe RNA. If necessary, the number of PS linkages was multiplied by 16.07 (difference MW S-O) and added. Table 3.1 lists the used masses. For the calculation of the mass of a biotinylated molecule synthesized with a Biotin-TEG-CPG, 569.6 g/mol were added.

Table 3.1. – Masses of the single nucleotides used in "Oligo_scoop"

Nucleotide	DNA	RNA	2'-OMe RNA
A	313.21 g/mol	329.21 g/mol	343.24 g/mol
C	289.18 g/mol	305.18 g/mol	319.21 g/mol
G	329.21 g/mol	345.21 g/mol	359.24 g/mol
U	—	306.17 g/mol	320.20 g/mol
T	304.20 g/mol	—	—

3.2. Design of "walkarounds"

The "walkarounds" were made by the truncation of the target sequence (RNA or DNA) to the desired length and position followed by the build of the reverse fully complement with desired chemistry (RNA, DNA, 2'-OMe RNA). The yielding sequences are listed in the format *praefix*-aso-A-B (with *praefix* being any name, A starting position of the ASO and B length of the ASO, e.g. mir-122-aso-26-9) and the masses corresponding to the chemistry of the ASO are calculated (*vide supra*).

For the synthesis these sequences were exported to a text file which can be read by our synthesizers after having given optional parameters for the synthesis (DMT-on/off, Standard/Universal-support).

3.3. Calculation of products from nuclease cleavage reactions

When we performed the RNase H assay (cf. chapter 5) we found a problem to identify the sequences of the 7 cleavage products although we could deconvolute their masses (cf. fig. 5.9, p. 101). As RNase H produces 3'–OH and 3'–O–PO$_3$ termini [95] which are different from the nucleotides yielded by the synthesizers, the hitherto used calculation of sequences can't be used. Additionally, there are different enzymatic cleavage mechanisms: The degradative enzymes of *E. coli* (such as RNase I, M or R) cleave the target oligonucleotide into 5'–OH and 3'–O–PO$_3$ fragments, whereas the processing endoribonucleases of *E. coli* (such as RNase E, H, P, and III (Dicer)) or snake venom phosphodiesterase (SVP) release 5'–O–PO$_3$ and 3'–OH oligonucleotides [212,213]. More complicated mechanisms such as the alkaline-catalyzed hydrolysis of RNA, which yields a mixture of 2'– and 3'–O–PO$_3$-groups and 5'$-OH$ termini [214].

Therefore I implemented an algorithm in "Oligo_scoop" for the calculation of possible cleavage products which was successfully tested in the RNase H assay as described in chapter 5.

As a target sequence, the same sequences as described in section 3.1 can be used with 3'-OH and 5'-OH/5'-phosphate/5'-triphosphate termini and a range of output fragment masses can be given. The output list comprises all possible fragments with corresponding masses enabling a rapid identification of the cleavage products. An example is see in fig 5.10, p. 102. The code is written as a sub within a userform and given in chapter C, p. 159 in the appendix.

3.4. Quantification and normalization of nucleotides

The most important function of "Oligo_scoop" is the possibility of calculating large amounts of concentrations (based on different calculating methods) for normalization of oligoribonucleotide solutions.

Although there are much more precise methods for the measurement of the concentration of an oligoribonucleotide solution, such as NMR [215] or a "general phosphate analysis" [216], these techniques are not used in the daily lab work as they are tedious

Therefore the commonly accepted method of choice for the determination of an oligoribonucleotide concentration is based on the determination of the UV absorption at 260 nm. For the conversion into the concentration there are three different methods (for an overview see [217]):

1. A "general OD assumption method". This method is not based on the law of Lambert-Beer and uses a fixed value for the conversion. In 2004, Cavaluzzi and Borer revised the values by new NMR-based values: 38 µg/ODU for ssDNA, and 39 µg/ODU for ssRNA. According to them, the error is within -2% to $+3\%$ [211].

2. A weighted sum method which accounts for the base composition: the number of each base is multiplied with the corresponding ε-values and summed up. This method is employed by the frequently used online calculator "OligoCalc" [206] and is sequence-unspecific.

3. A nearest neighbour method. This method takes into account that the absorptivity of a nucleotide which is incorporated into an oligoribonucleotide is influenced by the neighbouring nucleotides resulting in a reduced or raised extinction coefficient for the dimer in the sequence. This method is considered to yield the most accurate values and is according to Owcarzy et al. error-prone to 2–4 % [218]

The method as described by Cavaluzzi and Borer is only accurate, if the sequences are non-repetitive and contain a GC-content between 40–80 % [211]. As this is not a given for our sequences (cf. ASO sequences h-ras in table A.3, p. 134) I chose the nearest neighbour method for the calculation of ε.

The molar extinction coefficient, ε, is calculated by the sum of the extinction coefficients of the specific dimers, $f_{(i,i+1)}\varepsilon_{(i,i+1)}$ shifted by one nucleotide plus the extinction coefficients of the end-bases divided by two:

$$\varepsilon = \frac{\sum_{i=1}^{n-1} f_{(i,i+1)}\varepsilon_{(i,i+1)} + \varepsilon_i + \varepsilon_n}{2} \tag{3.1}$$

For example, the extinction coefficient of the linear oligoribonucleotide 5'-AUCGUU-3' is:

$$\varepsilon_{\text{AUCGUU}} = \frac{\varepsilon_{\text{AU}} + \varepsilon_{\text{UC}} + \varepsilon_{\text{CG}} + \varepsilon_{\text{GU}} + \varepsilon_{\text{UU}} + \varepsilon_{\text{A}} + \varepsilon_{\text{U}}}{2} \qquad (3.2)$$

Table A.10, p. 140 lists all ε values of the mono- and dimers.

Finally, The calculation of the concentration is made using the Lambert-Beer equation (3.3):

$$A = \varepsilon \cdot c \cdot d \qquad (3.3)$$

where
A is the Absorption at 260 nm
ε is the molar extinction coefficient [l·mol^{-1}·cm^{-1}]
c is the concentration [M] and
d is the path length through the solution (usually 1 cm for a standard cuvette)

The absorption values given by NanoDrop are normalized for 1 cm. Solving the equation 3.3 for c yields (d = 1 cm):

$$c = \frac{A}{\varepsilon} \qquad (3.4)$$

where
A is the Absorption measured with NanoDrop (260 nm) and
ε is the molar extinction coefficient determined with formula 3.1

As there are no published values for 2'-OMe RNA, the values are taken from RNA.

3.4.1. Comparison with published online calculators

There are—to my best knowledge—only two online calculators described in the literature. A third one which is often used in the lab is provided by the danish company Ribotask:

1. OligoCalc is an online tool for the calculation of masses, extinction coefficients and melting temperatures at different salt concentrations (Online-link, [206]). The extinction coefficients are calculated with the nearest neighbour method and the values as described in footnote *iii*, p. 51. It provides different 3'-/5'- modifications but no possibility for PS linkages. Whereas the calculation of a synthesized DNA oligoribonucleotide works well, the algorithm assumes a 5'-triphosphate and a 3'-monophosphate and one has to subtract 221 g/mol.

2. Tataurov et al. (Integrated DNA Technologies Inc.) published a method for the prediction of ultraviolet spectra of single- and double stranded DNA (Website IDT Biophysics, [218]). This tool calculates the molar extinction coefficient at 260 nm for unmodified RNA.

3. Ribotask is a danish company[i] specialised on RNA reagents. They provide an online calculator (Link) which calculates the masses for all possible combinations of oligo-ribonucleotides including RNA, DNA, 2'-OMe RNA, LNA, 2'-Fluoro-RNA, and many labels as well as PS linkers. Molar extinction coefficients are calculated for DNA and RNA. The sequence has to be given in a special format.

All products have in common that they are not able of handling large amounts of oligoribo-nucleotides at once.

The ε values and masses obtained by "Oligo_scoop" were compared to the values obtained by the three mentioned calculators. The accordance with the tool published by Tataurov et al. is 100 % as it uses the same algorithm. Fig. 3.1 shows a comparison for 10 random sequences from 5–50 deoxyribonucleotides (sequences of the deoxyribonucleotides are listed in table A.11, p. 141).
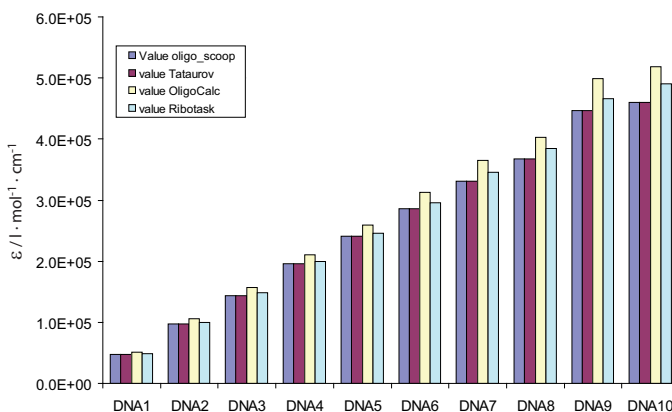
Figure 3.1. – Comparison of calculated ε values for the three online calculators with "Oligo_scoop". The values of "Oligo_scoop" and the IDT tool ([218]) are identical due to the same algorithm.

The values given by Oligocalc are by 6–8 percent higher than the values given by Tataurov et al.. This results in lower concentration values.

---

[i]co-founded by Jesper Wengel, co-inventor of LNA

4. Loop-binder 2.0: Enhancement of binding-affinity with modifications

4.1. Introduction

AFTER the successful identification of preferred binding sites of miRNA hairpin precursors for short complementary oligoribonucleotides we investigated the possibilities for increasing their binding affinity further by the attachment of small molecule moieties which are known to bind to nucleic acids. For the final screening of the modifications we used the 9-mer which ends at the 3'-site of the loop-region: mir-122-26-9, which was successfully tested in the biochemical assay performed by L. Gebert.

Strategies in our lab comprise the modification of nucleotides at the 2'-position of the sugar and at the 5'-position of the uracil of uridine. These modifications were made by two coworkers in our lab: Dr. A. Brunschweiger, who synthesized the 2'-modified nucleotides, and B. Wild, who synthesized the modified uridines. The modifications were attached to the nucleotides by "click-chemistry" (a copper-catalyzed alkyne-azide cycloaddition (CuAAC), in a similar approach as described previously [219]).

As outlined in section 1.1, p. 13 a few small molecules such as the aforementioned streptomycin [11] are known to interact directly with nucleic acids in general or miRNA in particular.

By screening libraries of small molecules in binding assays or biological assays, several groups identified some lead structures as inhibitors of miRNAs. Gummireddy et al. described a screen of > 1000 compounds in a luciferase assay which revealed diazobenzene as an initial hit which could further be optimized [220]. Melo et al. report an increased processing of three miRNAs (miR-124, miR-125, and miR-99) out of 157 by the small molecules enoxacin, ciprofloxacin, and norfloxacin analogues [221].

Dr. Brunschweiger shifted the data of these and other reports, including a virtual screen [222], and assembled a small library of 42 compounds which was used to modify the most promising LooptomiRs against pre-miR-122. Fig. 4.1 shows all compounds of the library.

Endogenous polyamines such as spermine, spermidine and putrescine are known to bind to RNA [223]. By attaching spermine to a nucleotide we hoped to raise the binding affinity for the target RNA. Spermine molecules were attached at the 2'-position of the ribose and at the 5'-position of the uracil.

The modifications which are attached to the 5'-position of the uracil are intended to bind in the major groove. The modifications attached to the 2'-position of the ribose are intended to bind to the minor groove.

In total several hundred modified LooptomiRs were synthesized and tested by SPR. It would go beyond the scope of this thesis to present all details. In the results section I therefore

No.	name	structure	No.	name	structure
1	1-chloromethylnaphthalene		22	4-(Bromomethyl)-2,1,3-benzoxadiazole	
2	3-phenoxybenzylchloride		24	p-Hydroxyphenethylbromide	
3	5-chloromethyluracil		26	4-(2-bromoethyl)-2,6-bis((dimethylamino)methyl)phenol AB-125	
4	6-chloromethyluracil		27	2-bromomethyl-1,4-benzodioxane	
5	2-chloromethylpyridine		28	4-(chloromethyl)-2-methyl-1,3-thiazole	
6	3-chloromethylpyridine		29	TMS-propargylbromide	
7	4-chloromethylpyridine		30	3-Bromomethyl-2(1H)-quinoxalinone	
8	9-chloromethylanthracene		31	2-(Bromomethyl)benzothiazole	
9	2-chloromethylbenzimidazole		32	2-Bromomethyl-3-hydroxypyridine hydrobromide	
10	2-chloromethylquinoline		33	2-(Chloromethyl)-6-methyl imidazo[1,2-a]pyridine hydrochloride	
12	4-(Bromomethyl)-2(1H)-quinolinone		34	2-(Chloromethyl)-1-methyl-1H-imidazole hydrochloride	
13	3-(Bromomethyl)-5-methylisoxazole		35	3-[3-(Chloromethyl)phenoxy]-N,N-dimethylpropylamine hydrochloride	
14	9-(2-Bromoethoxy)-7H-furo[3,2-g]chromen-7-one AB-6		36	3-(Chloromethyl)-1-methyl-1H-indazole	
15	4'-Chloromethyltrioxsalen AB-35		37	2-(Chloromethyl)-4-hydroxyquinazoline	
16	fmoc-bromoethylamine		38	2-(2-Chloroethyl)-3-hydroxy-3,4-dihydro-2H-1,3-benzoxazin-4-one	
17	fmoc-bromobutylamine		39	Bromomethylacridine	
18	4-fluorobenzylbromide		40	Spermine azide	
19	3-(2-Bromoethyl)indole		41	aminoglucopyranose	
20	8-(Bromomethyl)quinoline		42	Nalidixic acid amide	
21	7-(2-chloroethyl)theophylline				

Figure 4.1. – Modifications for LooptomiRs. The modifications were attached to the 2'-pentinyl / 2'-propargyl linker as described in section 4.2.1 by a Huisgen-reaction.

present a summary of the results obtained, including the K_D values for functional groups and positions of modification in the sequences.

4.2. Materials and methods

4.2.1. Synthesis of modified LooptomiRs

All syntheses described in this section were performed by Dr. A. Brunschweiger and B. Wild.

4.2.1.1. Synthesis of the modified ribose

In a first step the 2'-propargyl- or 2'-pentinyladenosine phosphoramidite building blocks were synthesized according to Egli et al. [224] (cf. fig 4.2/A). After thoroughly drying, the phosphoramidite building block was dissolved in acetonitrile and coupled in a synthesis cycle as a replacement for an unmodified adenosine at the selected position.

After conversion to the azide, the specified moieties were postsynthetically[i] linked to the alkyne (pentinyl- or propargyl) in a copper-catalyzed alkyne-azide Huisgen cycloaddition (CuAAC) (cf. fig 4.2/A).
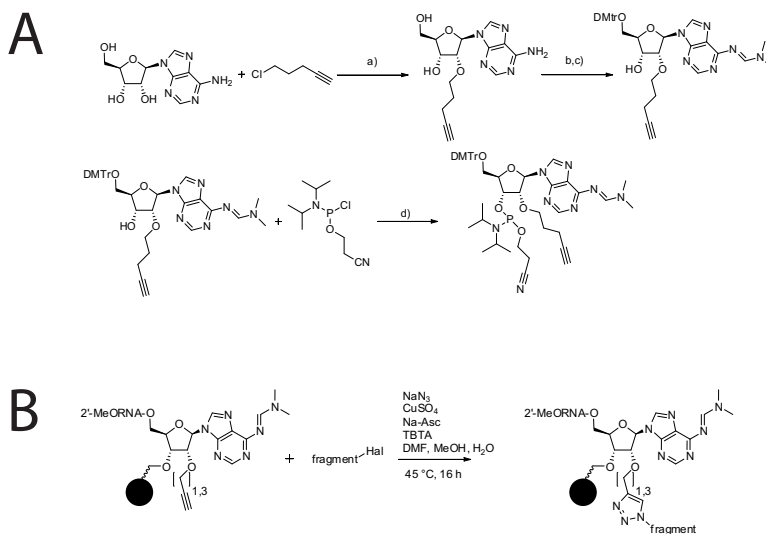
Figure 4.2. – Synthesis of the sugar-modified LooptomiRs as performed by Dr. Brunschweiger. A) Synthesis of the 2'-pentinyladenosine phosphoramidite. Reagents and conditions: a) NaH, dry DMF, TBAI, 65 °C, argon, 48 h; b) DMF-DMA, DMF, 50 °C, 1 h; c) DMTr-chloride, cat. DMAP, dry pyridine, 12 h, 0 °C to rt; d) dry CH_2Cl_2, DIPEA, rt, 30 min. B) Conjugation of small molecule fragments to short oligonucleotides by a copper-catalyzed alkyne-azide cycloaddition (CuAAC)

---

[i]after synthesis of the oligoribonucleotide, prior to cleavage from the support

4.2.1.2. Synthesis of the modified uracil

The synthesis of the 5-ethynyl-2'-O-methyluridine phosphoramidite building block starts with the conversion of commercially available uridine **1** into the 2,2'-anhydrouridine **2** and subsequent ring opening with in situ generated magnesium methoxide [225]. Iodination of 2'-O-methyluridine **3** according to [226] yielded 5-Iodo-2'-O-methyluridine **4**. Subsequent Sonogashira coupling yielded **5** [227], which afforded 5-ethynyl-2'-O-methyluridine **6** after TMS group removal. The final steps were the dimethoxytritylation to **7** and the phosphitylation to the phosphoramidite **8**. (cf. fig 4.3)

The 5-ethynyl uridine phosphoramidite building block was then incorporated into the oligonucleotide at the desired position. The CuAAC reaction was then performed as described for the oligonucleotides bearing the modified adenosine phoshoramidite (vide supra).
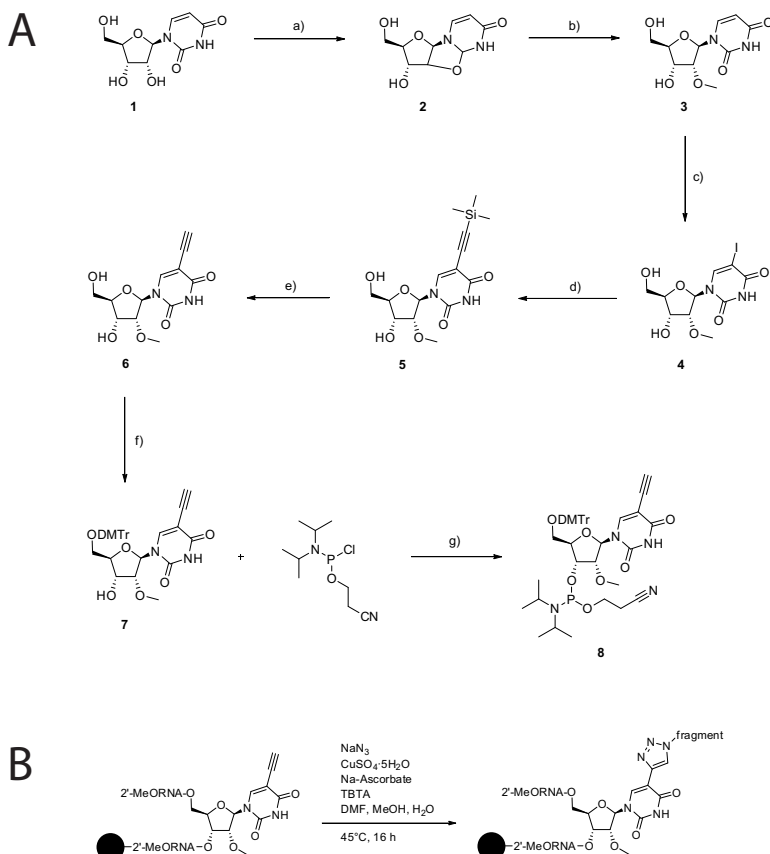
Figure 4.3. – Synthesis of the sugar-modified LooptomiRs as performed by B. Wild. Reagents and conditions: $(C_6H_5)_2CO$, $NaHCO_3$, DMF, 120 °C, 4 h, then rt, overnight; b) Mg, MeOH, 90 °C, 2 d; c) I_2, $(NH_4)_2Ce(NO_3)_6$, AcOH, 80 °C, 90 min; d) TMS-acetylene, $Pd(PPh_3)_2Cl_2$, CuI, Et_3N, DMF, 100 °C, 1 h; e) NH_4F, MeOH, 80 °C, 2 h; f) DMTrCl, DMAP, pyridine, Et_3N, rt, overnight; g) DIPEA, CH_2Cl_2/THF 1:1, 0 °C to rt, 2 h.

4.2.2. Determination of binding affinity of spermine for RNA

To measure the binding affinity of small molecule spermine against a structured RNA I employed our SPR2 machine. After the immobilization of streptavidin (pH 5.5, 1000 RU) the hairpin of pre-miR-122 was captured (TRIS-buffer, 570 RU). 6 Injections of DMSO around 3 % were made for normalization of refractive index change. Spermine in 3 % DMSO was injected in a concentration series of 3 mM, 2-fold. The analysis was done with Scrubber2.0a, accounting for refractive index change by normalization for DMSO injections.

4.2.3. Test of modified loop-binders with SPR

The modified LooptomiRs were tested with the Biacore T100 against the full length hairpin of pre-miR-122 and the linear loop region for the comparison of the influence of structure. They were all tested with the TRIS-buffer (cf. table) at 25 °C.

4.3. Results

4.3.1. Spermine binding to RNA

The analysis of the binding of spermine against pre-miR-122 revealed a good correlation for a 2-binding site model with steady-state analysis. Fig. 4.4 shows the sensorgrams and steady-state analysis. If a single-site binding model is applied, the residuals show a curved deviation of ± 0.6 RU, if a double-site binding model is applied, the residuals are randomly scattered with a deviation of ± 0.15 RU. This was confirmed in separate measurements (data not shown). The ratio was calculated to be $\approx 1{:}6\text{--}7$, which means that one hairpin can bind multiple spermines. A more precise ratio cannot be given with this dataset.

4.3.2. General observations for the modifications

The influence of the attachment of a modification (to either the uracil base of a uridine or the 2'-position of the ribose) depended clearly on the length of the linker. In most cases a modifications linked through the pentinyl linker yielded higher affinities than through the propargyl linker. From 42 modifications there were 6 preferred modifications which were capable of enhancing the affinity for either their linear complement (a fully complementary, single-stranded RNA) or the hairpin structure compared to the completely unmodified oligo-ribonucleotide: the alkyne-linker alone without modification, uracil (nr. 3), quinolinone (nr. 12), quinoline (nr. 20), acridine (nr. 39) and the spermine (nr. 40). The impact of these modifications was as well strongly dependent on the position within the sequence.

4.3.3. Base modifications

B. Wild attached different modifications to the 5'-position of the uracil. The unmodified parent compound (fully 2'-OMe mir122-ASO-26-9, cpd. H) has an affinity of ~ 10 nM vs. the hairpin
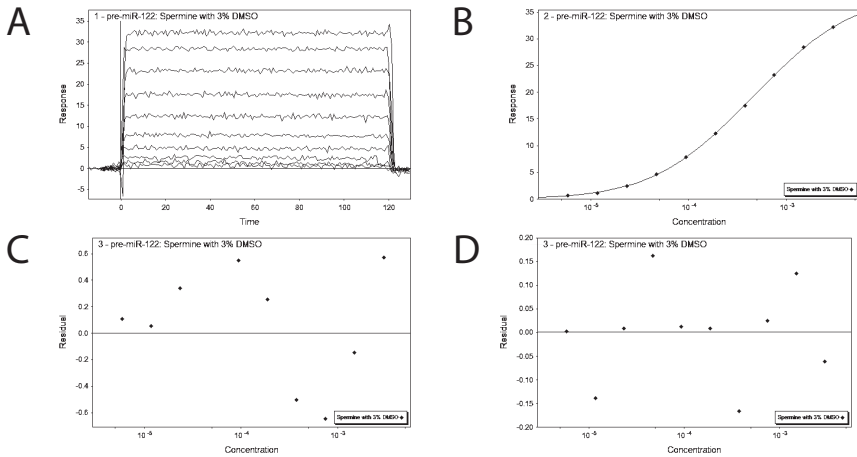
Figure 4.4. – Binding affinity of spermine against pre-miR-122. A) raw normalized sensorgrams B) steady-state analysis with a two-site binding model reveals affinities of 100–200 µM and 800–1'000 µM C) Residuals of a one-site binding model; the residuals show a curved deviation of ± 0.6 RU D) Residuals of a two-site binding model; the residuals are randomly scattered with a deviation of ± 0.15 RU

and ~ 17 nM vs. the single-stranded loop (cf. fig. 2.18, p. 60). Fig. 4.5 shows a comparison of the affinities of selected modified LooptomiRs with different modifications. Table 4.1 lists the compounds shown in fig. 4.5.
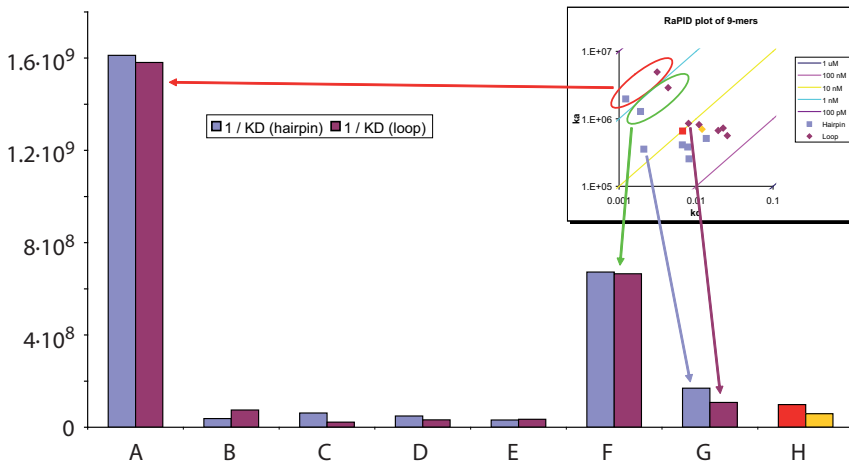
Figure 4.5. – Modified major groove binder. The spermine modified nucleotides have a binding affinity of up to ~ 30-fold higher than the unmodified parent compound (cf. table 4.1). Inset: this raised affinity is due to both, raised association and raised dissociation rate.

With the attachment of a single spermine to this position the affinity of the molecule was raised by a factor of ~ 27 in the case of the linear complement and by a factor of ~ 16

Table 4.1. – Comparison of binding affinities of base modified LooptomiRs. The "X" indicates the position of the modification in the sequence.

			Affinity to	
Lettercode	Sequence	Modification	Hairpin	Loop
A	AXAGUUUAG	Spermine	620 pM	630 pM
B	AXAGUUUAG	Aminoglucopyranose	27 nM	13 nM
C	AUAGXUUAG	Aminoglucopyranose	16 nM	45 nM
D	AXAGUUXAG	4-hydroxyquinazoline	20 nM	31 nM
E	AXAGUUXAG	Methylacridine	32 nM	29 nM
F	AXAGUUXAG	Spermine	1.5 nM	1.5 nM
G	AXAGUUXAG	Aminoglucopyranose	5.9 nM	9.3 nM
H	AUAGUUUAG	—	10 nM	17 nM

in the case of the hairpin. Of note, the same position with the same modification but a shorter linker (propargyl instead of pentinyl) completely abolished the affinity (at least in the measured concentration range, data not shown) indicating, that this is not an unspecific binding of the positively charged polyamine to the negatively charged surface of the SPR chip.

4.3.4. Ribose modifications

As mentioned in section 4.3.2 there was a general trend for a higher affinity with modifications attached via the pentinyl linker. In summary we tested 21 different modifications at three different positions against both, the hairpin and the linear complement (loop region). Additionally we tested some double and triply modified LooptomiRs. The highest increase in affinity was observed for a triply modified LooptomiR with two spermines (S) at positions 1 and 2 and a quinolinone (Q) at position 3 ($SUSGUUUQG$). The binding affinity could be raised to ~ 920 pM against the hairpin (~ 11-fold) and to ~ 2.4 nM against the linear loop region (~ 8-fold) compared to the parent sequence.

Table 4.2 lists the binding affinities of these 21 modifications (where measured).

Table 4.2. – Determined equilibrium dissociation constants for 21 different modifications at three different positions. 26/9 is the 9-mer which is ending at the 3'-end of the loop. A/B/C indicate the position of the modification in the sequence with A being the first A, B being the second A and C being the third A. Bold values in red/black indicate a significantly raised affinity (values below 10 nM)

compound, sequence		a (no)	b 1	c 2	d 3	e 9	f 12	g 18	h 19	l 20	j 21	k 27
AB-234, 26/9A XUAGUUUAG	hairpin	11.95	46.2	47.3	9.8	32.5	15.9	27.8	37.6	46.8	21.6	33.7
AB-234, 26/9A XUAGUUUAG	loop	13.52	**4.71**	7.39	5.4	10.6	**1.9**	10.8	10.2	5.0	5.0	7.8
AB-235, 26/9B AUXGUUUAG	hairpin	12.2	324	37.9	**4.7**	19	17.2	24.9	24.1	31	14	28.1
AB-235, 26/9B AUXGUUUAG	loop	13.1	n.a.	35.7	10.5	25.1	23.7	29	13.6	39	17	37.7
AB-236, 26/9C AUAGUUUXG	hairpin	7.4	14.7	27	nd	12.5	**4.0**	16.8	30.7	**9.7**	17.4	22.3
AB-236, 26/9C AUAGUUUXG	Loop	10.9	19.4	30.3	nd	15.9	**5.8**	24.5	35.9	17.6	25.8	24.5

compound, sequence		l 30	m 31	N 34	o 35	p 36	q 37	r 39	s 40	t 41	u 42
AB-234, 26/9A XUAGUUUAG	hairpin	59.2	45.8	12.2	21.9	36.6	41.8	17.5	dc	24.6	15.1
AB-234, 26/9A XUAGUUUAG	Loop	7.7	6.0	10.1	5.55	5.95	5.3	**2.0**	dc	13	**1.4**
AB-235, 26/9B AUXGUUUAG	hairpin	55.1	34.1	12.1	27.1	54	32.1	60.4	**4.6**	13.7	
AB-235, 26/9B AUXGUUUAG	Loop	77.7	19.9	11.4	25.6	76.5	43.5	108.9	**5.4**	25.8	
AB-236, 26/9C AUAGUUUXG	hairpin	14.1	27.8	10.8	21.6	34.1	15.4	14.0	11.4	14.8	14.4
AB-236, 26/9C AUAGUUUXG	Loop	21.1		18.1	21.1	29.5	27.4	19.5	13.1	25.6	20.6
AB-234AB, 26/9AB XUXGUUUAG	hairpin							56.9	**3.3**	48.6	35.1
AB-234AB, 26/9AB XUXGUUUAG	Loop							18.6	**2.6**	55.3	7.4
AB-234AC, 26/9AC XUAGUUUXG	hairpin	33.5					34.2		**1.6**	21.3	
AB-234AC, 26/9AC XUAGUUUXG	Loop	12.9					9.5		**1.2**	19.5	
AB-234BC, 26/9BC AUXGUUUXG	hairpin	94.7					74.1		**6.2**	38.6	27
AB-234BC, 26/9BC AUXGUUUXG	Loop	123.6					89.8		**4.5**	66.5	19.6

X: A^{pent}

5. Development of an RNase H assay for cleavage of RNA hairpins by DNA loop-binders

5.1. Introduction

As outlined in chapter 1, the general mechanism of action of antisense oligonucleotides (ASOs) in order to modulate the metabolism of mRNA can be divided in two principal pharmacological effects: simple occupancy or an occupancy-mediated destabilisation [84]. This destabilization is the result of an RNase-mediated degradation of the target RNA. In the case of RNA/RNA duplexes after binding of the antisense strand of a siRNA (in the RISC) this is by Argonaute 2. In the case of DNA-like ASOs, this is due to induction of RNase H.

Besides our lab's research for the inhibition of the maturation of pre-miRNA's with (modified) loop binding oligonucleotides (cf. chapters 2 and 4) we initiated an investigation of cleavage of miRNA precursors by RNase H-inducing antisense oligoribonucleotides. As in earlier experiments we took the hairpin structure of pre-miR-122 as a target system.

For practical reasons we wanted to circumvent the necessity of radioactive labeling and therefore established an RNase H assay based on gel electrophoresis and HPLC/MS. As target we used a short linear sequence (18-mer) as surrogate for the loop of pre-miR-122. For this sequence we could not only show cleavage, but as well a catalytic activity of the DNA antisense strand that is targeting it. Additionally, we could make a rough estimation of the binding affinity of the RNase H–DNA/RNA complex. In a second phase we explored the impact of our loop-binders on pre-miR-122 in the presence of RNase H. Although we successfully monitored the cleavage of this hairpin structure, we could not identify the identity of the cleavage products. In order to characterise the products we deployed an LC/MS-based enzymatic assay with a sophisticated method for normalisation. Although we successfully determined the identity of the products of the short sequences by ESI-MS, this attempt failed for the products of the hairpin (pre-miR-122) cleavage.

After an overview of the structure and function of human RNase H1, a brief outline of its roles in the effects of DNA containing ASOs is given. The deployment of our RNase H assay and the development of the LC/MS-based enzymatic assay are expanded. A discussion of the results with an outlook with recommendations for further experiments is given in section 7.1.3, p. 128 and section 7.2, p. 130.

The experiments presented in this chapter were performed by Dr. med. F. Paun, a master student in pharmaceutical sciences who worked under my supervision. The synthesis of the oligonucleotides and the establishment of the LC/MS-based enzymatic assay were prepared by me.

5.1.1. Ribonuclease H

5.1.1.1. General properties of the RNase H family

Enzymes of the RNase H (Ribonuclease H) family belong to a nucleotidyl-transferase superfamily (which contains inter alia the RISC nuclease Argonaute 2) and hydrolyze RNA molecules which are Watson-Crick base-paired to DNA [228]. Although the RNA in such an RNA/DNA complex is cleaved sequence unspecifically [229], and even though it can bind RNA/RNA duplexes in addition, RNase H recognizes specifically the A-form RNA and the B-form DNA strands [230]. After the cleavage of the 3'-O-P bond yielding 3'-hydroxyl and 5'- phosphate termini, the cleavage-inducing DNA strand is released unchanged, able to induce the cleavage of another RNA target.

It has been shown by different groups that the ribonuclease H motif belongs to the most ancient protein folds found [231, 232] and shares—although varying substantially in molecular weight—very similar properties amongst difference species such as no sequence selectivity, the requirement of divalent cations, and a uniform product formation [229].

5.1.1.2. Biodiversity of RNase H

Mammalian cells express two classes of RNase H, RNase H1/H2, which differ e.g. in activity under reducing conditions, and the need for specific cofactors (RNase H1 can be activated by Mg^{2+} or Mn^{2+} ions, RNase H2 is only active in presence of Mg^{2+} ions and is strongly inhibited by Mn^{2+} ions). Besides prokaryotes which express three classes of RNases H (H1, H2, and H3; [233]), even retroviruses express RNase H as a domain of the reverse transcriptase which acts as a crucial regulator of virus replication. As the viral RNase H differs sufficiently from mammalian RNase H [234, 235] there have been efforts to develop RNase H inhibitors as a novel class of anti-HIV drugs [236, 237]. Human cells express universally the two RNases H (H1 and H2). RNase H1 is a protein composed of 286 amino acids (aa) and a calculated mass of 32 kDa [238]. RNase H2 contains 299 amino acids, has a molecular weight of 33.4 kDa, and is ubiquitously expressed [239]. Whereas the function and properties of (human) RNase H1 are well known, RNase H2 is of less interest as it is inactive as a monomer and in gel renaturation assays [84]. Additionally, RNase H2 has been shown to be not involved in the biological inhibition of different targets by several DNA-like ASOs [240]. For these reasons I will focus only on human RNase H1 in this chapter.

5.1.1.3. Human RNases H1

Biochemical properties of RNase H1 RNase H 1, which is active as a single polypeptide chain, is a Mg^{2+}-dependent enzyme that shows optimal activity in 10–20 mM concentrations of NaCl/KCl. The Mg^{2+} concentration for optimal catalysis was determined to be 1 mM, but the range is quite narrow as the enzyme was already inhibited at concentrations of 5 mM Mg^{2+} [241]. The optimum proton concentration was determined to be between a pH of 7 and 8.
Concerning the influence of ions there is a little uncertainty: Wu et al. [241] report an inhibition of RNase H1 by Mn^{2+} in the presence of Mg^{2+}, whereas Bsen et al. [242] describe the activation of RNase H1 by Mn^{2+}. There are different reports about the optimal Mg^{2+}

concentration for RNase H activity [230, 241]. However, strong influence of ionic strength is a uniquely reported phenomenon. Although RNase H1 has no sequence specificity, it selectively binds to an A-form duplex of RNA/DNA and does not cleave RNA in RNA/RNA duplexes. It shows a defined positional preference for cleavage which is at positions from 7 to 12 nucleotides from the 5'-RNA/3'-DNA terminus of the heteroduplex [241]. Lima et al. showed that human RNase H1 exhibits its catalytic activity only under reduced conditions and that there is a disulfide bond formed between two vicinal cysteines (C147-C148) of the protein under oxidized conditions which removes the ability of catalysis, but not its substrate binding affinity [243].

Structural basis of enzymatic cleavage   Human RNase H1 consists of an RNA-binding and a catalytic domain which are linked together by a spacer region [244] as shown in fig. 5.1. The RNA-binding domain (RNA-BD)[i] consists of 73 amino acids and is conserved in other eukaryotic RNases H1 [245]. Several site-directed mutagenesis experiments performed by Lima et al. have shown that there are five important amino acid residues contributing to the binding affinity of the RNA binding domain: 2 lysines (K59, K,60), 1 tryptophan (W43), and 2 cysteines (C18, C46). These residues participate in both electrostatic interactions with the phosphate backbone (K59, K60) as well as stacking interactions/hydrogen bonds with the nucleobases (W43). The interaction of the RNase H1 binding domain with its substrate occurs at the very end of the duplex at its 5'-RNA/3'-DNA end and assures the proper natural biological function of the enzyme as it aligns the enzyme accurately with the heteroduplex [246]. Wu et al. showed that there is a strong predilection for the site of cleavage in human RNase H1: the RNA in the heteroduplex substrate has always been cleaved between 7 and 12 nucleotides away from its 5'-terminus [241].
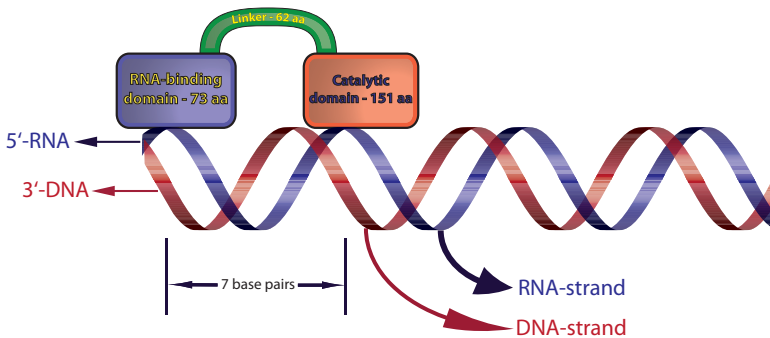
Figure 5.1. – Schematic of RNase H binding to a DNA/RNA heteroduplex. The RNA (hybrid) binding-domain positions the cleavage domain in such a manner that the preferred site of cleavage is about 7-12 nucleotides from the 5'-end of the heteroduplex. This corresponds to approximately 1 helical turn.

This positional preference was even more distinct when the experiments were performed under conditions with a single turnover where this cleavage frame was reduced by two nucleotides to the positions 7–10 [246]. Whereas the substitution of the terminal hydroxyl groups by a phosphate either at the DNA or RNA strand has no effect on cleavage rate or pattern, the replacement of the 2'-OH of the DNA by an alkoxy group (MOE) at the very 3'-end shifted the site of the first cleavage by one nucleotide. The same phenomenon was

---

[i]sometimes denoted as RNA/DNA hybrid-binding domain (RHBD)

observed by Lima et al. when they introduced a mismatched base pair at the same position. This constant positioning of the catalytic domain of RNase H1 7 base pairs away from the RNA binding domain corresponds to approximately 1 helical turn of the heteroduplex (cf. fig. 5.1). Interestingly, as Wu et al. showed, the cleavage rate of a mutant enzyme without the RNA binding domain was doubled compared to an unmodified wild-type enzyme, indicating that the RNA binding domain is responsible for the proper positioning of the substrate and increasing the affinity for the substrate with a concurrent sacrifice of cleavage efficiency [244]. Compared to other RNases H1, the catalytic domain of human RNase H1 is highly conserved [247, 248]. There are at least nine amino acid residues determined to play key roles in the catalytic domain/activity [244]. Several site-directed mutagenesis experiments performed by Lima et al. ruled out their function which led to the following conclusions [249, 250] for optimal properties of modified DNA-like antisense oligonucleotides:

1. A flexible ribose conformation with an eastern O4'-endo pucker as it was shown e.g. for the 2'-ara-fluoro modification [250, 251]

2. No modifications that lead to strong northern or southern conformations and no bulky moieties at the 2'-end [250].

3. A phosphate backbone with enough conformational rigidity (flexible hydrocarbon linkers abolished the catalytic activity). Base modifications that do not form hydrogen bonds to the opposite strand but exhibit π-stacking properties (e.g.2-fluoro-6-methyl-benzoimidazole, 4-methylbenzoimidazole, and 2,4-difluorotoluyl modifications) ensured enough conformational flexibility.

Nowotny et al. report the solution structure of RNase H bound to a 18-mer RNA/DNA heteroduplex [252]. They show the molecular basis for the cleavage and a detailed map of the interaction sites of the enzyme with the heteroduplex (cf. fig. 5.2). This analysis shows that the possible interaction range for modifications is rather limited and has to occur in the DNA at the very 5'-end of the target RNA.
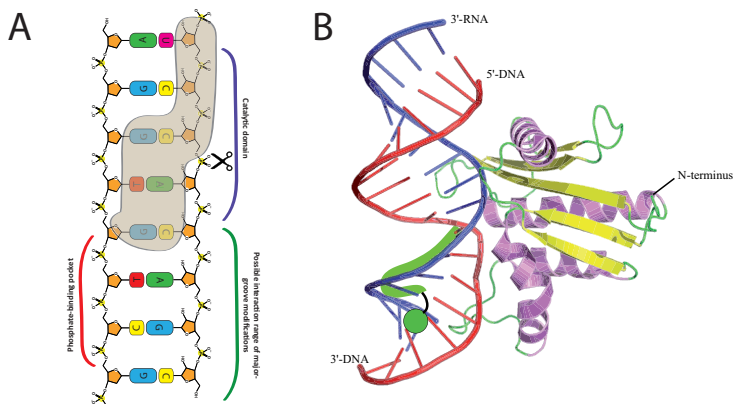
Figure 5.2. – Scheme and solution structure of the interaction of an 18-mer RNA/DNA heteroduplex with RNase H as reported by Nowotny et al. A) Scheme of the interacting parts of RNase H with the heteroduplex (modified from Novotny et al.) Possible interaction sites for base-modifications are indicated (cf. section 7.2). B) solution structure of a 18-mer RNA/DNA heteroduplex bound to RNase H. The picture was made with Pymol (DeLano, W.L. The PyMOL Molecular Graphics System (2002), DeLano Scientific, San Carlos, CA, USA) from the published structure (PDB ID: 2QKK).

The impact of modified gapmer ASOs on RNase H1 activity   Oligodeoxyribonucleotides are rapidly degraded in vivo. Consequently, in order to be used as therapeutics they have to be modified with a phosphorothioate-linked backbone and/or 2'-modifications such as 2'-O-Me or 2'-MOE in order to circumvent endonuclease cleavage. First-generation phosphorothioate DNA ASOs, which showed an increased nuclease stability, reduced target RNA in humans, but still had to be given intravenously every other day because of a reduced half life in vivo [84].Second-generation ASOs, which were composed of a DNA-like window with flanking 2'-MOE modified nucleotides, have been shown to exhibit a way higher potency. Lima et al. made an extensive investigation of the effects of MOE-containing oligonucleotides on the cleavage rate of human RNase H1 [253]. By successive substitution of the nucleotides at the 3'- terminus with MOE modified nucleotides they observed an displacement of the outermost cleavage site to the 5'-end with a concomitant shift of the cleavage position and a slower overall cleavage rate. Interestingly, they observed a general trend in reduction of the cleavage rate when introducing more than two MOE modifications. Their presentation of the data leads to the conclusion that there have to be at least nine unmodified DNA nucleotides in order for the enzyme to function. This impact of the MOE modifications on the activity/cleavage rate of human RNase H1 is consistent with the solution structure of a 2'-OMe-RNA/DNA gapmer described by Nishizaki et al. [254]. The conformation needed by RNase H1 in order to be able to cleave the target (eastern O4'-endo) is influenced by the flanking MOE-modified nucleotides which exhibit a northern conformation: DNA nucleotides next to the flanking region had the same northern conformation which was conveyed by the modified nucleotides [249,254]. This effect was enhanced with the strongly northern-biased LNA modified positioned at the junctions [253].

5.2. Materials and methods

5.2.1. Design and synthesis of oligonucleotides

In a first step we reproduced the RNase H assay as described by Galarneau et al. ([255], data not shown). After we successfully confirmed the activity of the enzyme we used for the upcoming experiments the 3 target RNAs as described in table 5.1: two short, linear 18-mers in RNA and DNA chemistry (DNA for negative control), and a full-length hairpin of pre-miR-122. As ASOs I chose to take 5 out of the best 7 loop-binders I identified (cf. section 2.3.2.2, p. 54 and fig. 2.15, p. 57) in fully DNA chemistry without any modifications (neither thioate-linkages nor 2'-OMe riboses at the ends). We used a negative control which was the 9-mer B11 in full RNA chemistry. Table 5.2 describes all used ASOs.

Table 5.1. – Selected targets for the RNase H assay. The two short 18-mers correspond to the loop-region of pre-miR-122 with 3 additional base pairs on each end.

Target name	Sequence	Length / chemistry	Mol. weight / [g/mol]
18_mer_RNA_target	5'-UUGUGUCUAAACUAUCAA-3'	18-mer / RNA	5662.5
18_mer_DNA_target	5'-TTGTGTCTAAACTATCAA-3'	18-mer / DNA	5472.7
Pre-miR-122	5'-UGGAGUGUGACAAUGGUGUUUGUGUCUA AACUAUCAAACGCCAUUAUCACACUAAAUA-3'	58-mer / RNA	18553.1

Table 5.2. – DNA and RNA ASOs for the RNase H assay. The DNA sequences equal to the best loop-binders identified in chapter ref, but with DNA chemistry. The RNA sequence was employed as negative control.

ASO name	Sequence	Length / chemistry	Mol. weight / [g/mol]
B11_pure_DNA	5'-GTTTAGACA-3'	9-mer / DNA	2737.9
B11_pure_RNA	5'-GUUUAGACA-3'	9-mer / RNA	2839.9
C2_pure_DNA	5'-ATAGTTTAG-3'	9-mer / DNA	2752.9
C10_pure_DNA	5'-ATAGTTTAGA-3'	10-mer / DNA	3066.1
D5_pure_DNA	5'-ATAGTTTAGAC-3'	11-mer / DNA	3355.2
E4_pure_DNA	5'-ATAGTTTAGACAC-3'	13-mer / DNA	3957.6

The synthesis of the oligonucleotides was performed as described in chapter 2. For the cleavage reactions we used only oligonucleotides with a purity of $\geq$95 % as confirmed by ESI-MS.

5.2.2. Quantification and normalization of the oligonucleotides

The determination of the concentrations of the oligoribonucleotides was performed using UV-absorbance at 260 nM and subsequent calculation with oligo_scoop (cf. chapter 3). Measurements of UV-absorbance of the oligonucleotide solutions were carried out using our NanoDrop 2000 machine (Thermo Scientific, Wohlen, CH) with previous water blanks. The UV-absorbance at 260 nM was then copied into oligo_scoop and calculated according the formula described in chapter3.

5.2.3. RNase H and reaction buffer

For our experiments we used an RNase H from *E. coli* from New England BioLabs (cat.-nr.: M0297L, size: 1250 units, concentration: 5000 U/ml). Corresponding to the information given by the manufacturer, this enzyme was extracted from an *E. coli* strain carrying the cloned RNase H gene from *E. coli*.

The units used with the delivered enzyme is defined as "the amount of RNase H that hydrolyzes 1 nmol of RNA in [3H]-labeled poly(rA)·poly(dT), to acid-soluble ribonucleotides in a total reaction volume of 50 µl in 20 minutes at 37 °C in the delivered 1-fold RNase H reaction buffer with 10 nmol [3H]-labelled poly(rA) and 12.5 µg poly(dT)".

The composition of the provided reaction buffer is listed in table 5.3.

Table 5.3. – Composition of the final 1-fold reaction buffer for the RNase H cleavage experiments. The pH value of the solution is given as 8.3 at 25 °C. The buffer was provided with the enzyme as a 10-fold stock solution.

Component	Concentration
TRIS-HCl	50 mM
KCl	75 mM
MgCl$_2$	3 mM
DTT	10 mM

The pH of the buffer solution was 8.3 @ 25 °C. The enzyme as well as the 10-fold reaction buffer stock solution were stored @ -20 °C. As the 10-fold reaction buffer stock solution tends to precipitate, the buffer was examined for visual precipitations after thawing and-if necessary-vortexed with the Eppendorf Thermomixer comfort @ 37 °C for 15 min. (1000-1400 rpm).

The recommended temperature for the cleavage reaction is @ 37 °C. Inactivation of the enzyme was described to be a heat-treatment at 65 °C for 20 minutes. As we wanted to avoid any risky contaminations of our LC/MS-system, we raised this temperature to 70 °C and leaned to longer times than 20 minutes.

5.2.4. RNase H-mediated reaction

General composition and treatment of the reaction mixture

The reaction mixtures were constituted in Eppendorf vials with the following composition:

1. Target RNA or negative control DNA
2. Fully complementary DNA-ASOs or negative control RNA-equivalents
3. RNase H
4. 10-fold reaction buffer stock solution
5. Millipore water

According to the different particular protocols (cf. section Results), variable amounts of the reagents were used. After pipetting of the two oligonucleotide solutions according to the different protocols into the Eppendorf vial, the mixture was vortexed and spun down. If necessary, as in the case of pre-miR-122, an annealing procedure was performed (see below). After that the 10-fold reaction buffer stock solution and water was added to yield a final 1-fold buffer concentration. In order to avoid deactivation of the enzyme by heat (annealing procedure) or inappropriate salt-concentrations (cf. section 1), the enzyme was added at last. Finally, the reaction mixture was vortexed and spun down again before incubation.

Annealing procedure for pre-miR-122

In the case of short complementary oligonucleotides the assay worked well without pre-treatment with heat. However, an annealing procedure was found to be necessary in the case of the mir-122 precursor. As shown in chapter 4, the affinity of a pure DNA oligonucleotide for the hairpin of pre-miR-122 is in the mid-µM range. In order to obtain optimal results without concern for affinity-related problems, we annealed the two complementary strands by heating them together to 80–90 °C for 5 minutes, followed by a very slow cooling process to RT over about 90 minutes by switching off the heating unit. This was necessary as we could not obtain an annealing when placing the solution on an ice-bath after heating (data not shown). As this procedure was performed prior to the addition of the buffer stock, this annealing was made in absence of (divalent) ions.

Incubation

The reported optimum temperature for cleavage is 37 °C. The temperature controlled incubation was performed in a Memmert incubator (model UFE500) without shaking/vortexing of the probes during the reaction time. The exact duration of reaction was varying between 1 and 48 hours as indicated in the Results part.

5.2.5. PAGE

Composition of denaturating PAGE-gels

Table 5.4. – Composition of 10 ml Urea-PAGE gel.

Component	Quantity	Operation	Identity
Urea	4.8 g	place in a 15 ml Falkon-tube	Acros 327380010
10-fold TBE	1 ml	add	Preparation as described in table 5.5
40 % Acrylamide / N,N'-methylene bis-acrylamide	5.0 ml	add	BioRad 161-0156
Distilled water	0.261 ml	add and dissolve shortly in MiWa	Millipore Ultrapure
TEMED	8 μl	add quickly	BioRad 161-0700
10 % APS	60 μl	add quickly	BioRad 161-0800 aliquot from freezer

Polyacrylamide gel electrophoresis (PAGE) was employed for the estimation of substrate hydrolysis and eventually identification of the cleavage products (cf. Results). In order to obtain product separation we used denaturating conditions with 48 % urea in the gels. For composition of the gel see table 5.4.

Immediately after the addition of TEMED/APS the gel was cast on 0.75 mm plates with a 10-well-comb (BioRad Mini-PROTEAN tetra cell system, cat.-nr.: 165-8000). Depending on the quality of the APS and room temperature the polymerization process was finished within 5 minutes to 2 hours.

The solution loaded on the gels was constituted of 10 μl reaction mixture and 10 μl of a 2-fold loading buffer which were vortexed and spun down as well.

Marker

As marker we used the microRNA Marker offered by NEB (New England BioLabs, cat.-nr.: N2102S). This marker contains 3 synthetic single-stranded RNA oligonucleotides with a length of 17, 21 and 25 nucleotides. The three marker oligoribonucleotides contain the same core sequence. Additionally, a biotinylated 21-mer DNA oligonucleotide which is complementary to the marker sequences is included. Therefore, this marker could theoretically be used also for a positive control reaction as it contains already a DNA/RNA duplex.

Electrophoresis

After loading of the samples the plate was placed in the according Mini-PROTEAN running module and filled with 1-fold TBE buffer. For the composition of the TBE-buffer see table 5.5.

The gel was left at a current of 150 V for 120–150 minutes (depending on the running velocity of the samples).

Table 5.5. – Composition of 1 lt of 1-fold TBE buffer.

Component	Quantity (1-fold)	Concentration
TRIS base	10.8 g	89 mM
Boric acid	5.5 g	89 mM
Disodium EDTA	0.7 g	2 mM

Staining

After the removal of the gel from the glass-plate, the gel was placed in a shaking rack for staining. As staining reagent we used SYBR GOLD (Invitrogen Inc., S11494, 10000-fold concentrate in DMSO). 50 ml of a gel staining solution were constituted by 5 µl SYBR GOLD in 50 ml Millipore water. The gel was bathed in this solution for approx. 5–7 minutes at a low pacing. After the staining the solution was removed (for a further use if used for the first time) and the gel was directly analyzed. The gel-staining is not visible under daylight and has to be analyzed with UV-light in a dark chamber shortly after the staining as it vanished over time.

Gel imaging

A BioRad gel imager (Universal Hood, S.N. 76S/04866) was used for the analysis of the gel in UV-light using the enclosed software ("Quantity One"). The quantification of the spots generated by the Gel imager was done using the open-source JAVA-based software ImageJ (NIH, http://rsbweb.nih.gov/ij/).

Analysis by LC/MS

For the unambiguous identification of the cleavage products we employed our Agilent 1200 LC/MS-system. Instead of casting a gel, we heat-inactivated the reaction mixture (see above) and filled the reaction mixture to 100 µl with Millipore water prior to the injection into the HPLC system. The separation of the substrate and products was performed with an Acquity UPLC OST C18 column (130 Å, 1.7 µm, 2.1 x 50 mm; Waters Inc., Prod.-Nr.: 186003949). Depending on the protocol we used different times with a running buffer A (0.4 M HFIP, 15 mM TEA, pH 8) and a gradient of 2 % to 23 % B (100 % MeOH) at 60 °C. The determination of the masses was performed with our Agilent 6130 Quadrupole ESI-MS. The analysis was done with the deconvolution tool implemented in the control and analysis software of the LC/MS-system.

5.3. Results

5.3.1. Denaturating Polyacrylamide Gel Electrophoresis PAGE

#### 5.3.1.1. Addressing the general potency of RNase H inducing DNA loop-binders

After having reproduced the results of an assay as described by Galarneau et al. (data not shown), we directly went to our model target system—pre-miR-122. We investigated, if our loop-binders generally can induce RNase H-mediated cleavage of fully complementary RNA sequences. For this purpose we chose the elongated version of the loop-region of pre-miR-122 containing the sequence of the loop (termed RNA_18_mer_target). We then prepared reaction mixtures with two of the loop-binders: the 9-mer beginning at the predicted loop (B11_pure_DNA) and the 9-mer ending at the loop (C2_pure_DNA). For control reasons we made them in duplicates: one containing RNase H and one lacking of RNase H. As an overall negative control we used the B11_pure_DNA against the sequence of the loop but with DNA chemistry (DNA_18_mer_target) and prepared as well a solution with and one without enzyme. As RNase H does not cleave/bind DNA/DNA complexes there should be no indication of cleavage. Finally, we added RNase H into a reaction mixture containing the microRNA marker purchased from NEB (see Materials and Methods). As this marker contains a biotinylated fully complementary 21-mer DNA, this should result also in a decomposition of the middle lane of the marker. The complete list is given in table 5.6.

Table 5.6. – Composition and reaction volumes of the first experiment. All volumes are given in µl. After addition of the loading buffer, the total volumes in the gel were 20 µl.

Substance / Lane	1	2	3	4	5	6	7	8
RNA_18_mer_target			4	4	4	4		
DNA_18_mer_target							4	4
B11_pure_DNA			4	4			4	4
C2_pure_DNA					4	4		
Marker	8	8						
Reaction buffer	1	1	1	1	1	1	1	1
RNase H		1		1		1		1
Water	1		1		1		1	
Total reaction volume	10	10	10	10	10	10	10	10

The oligonucleotide concentrations were 4 ng/ul for all probes. Although we assumed a catalytic reaction we initially used twice as much DNA than RNA (calculated molar ratio RNA:DNA $\approx$ 0.48) in the case of the RNA target. The reaction mixtures were incubated for 1 hour.

Figure 5.3 shows the gel of this experiment. From this experiment the following conclusions can be made: There is an obvious and strong cleavage induced by the 9-mer that begins at the loop (B11_pure_DNA) against the linear elongated loop-region (lane 4). As there is no cleavage in the absence of RNase H (lane 3) this indicates a strong evidence for an RNase H-mediated cleavage and the power of this DNA molecule to induce RNase H activity. The calculated extent of cleavage for this reaction is $\approx$ 70 % (as calculated with ImageJ) In the case of the ASO that ends at the loop (C2_pure_DNA, lanes 5 and 6) this effect is seen as well but to a much smaller extent (there is a calculated cleavage fraction
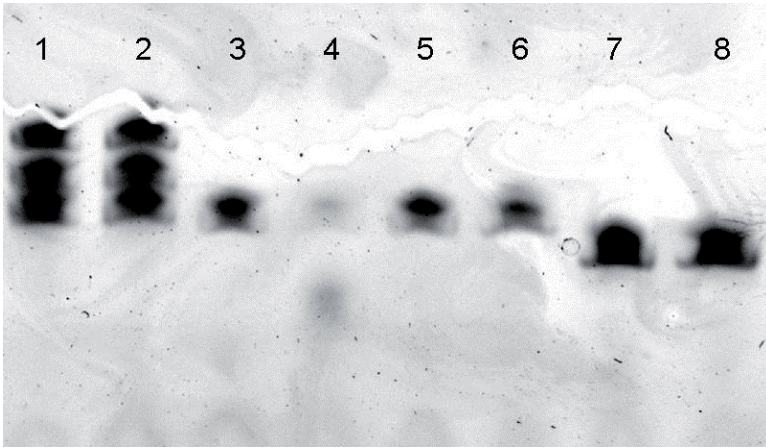
Figure 5.3. – First PAGE gel of the RNase H induced of the linear 18_mer_RNA_target by the two 9-mers that begin and end at the loop-region of pre-miR-122.

of ≈ 7 %). As our linear substrate lacks major secondary structure this must be a sequence specific effect: the sequence of B11 is containing 3 G-C-pairs whereas C2 only has 2 G-C-pairs. The DNA/DNA duplex is-as expected-not cleaved (cf. lanes 7 and 8). Although the marker contains a fully complementary sequence against the middle 21-mer, there is no cleavage observed with this duplex. There are several possible reasons for this, e.g.: it could be that there is not enough duplex formation. Finally, the DNA sequence is complementary to all three marker molecules (the 21-mer has the highest degree of complementarity). So it is possible, that there is a cleavage in the case of all three molecules, but we don't see it as there is still enough substrate material left and the reaction products are not seen in the gel due to their short lengths (The minimum length required for SYBR GOLD to stain it is estimated to be around 10–13 nucleotides). In lane 4 we see a faint spot under the original substrate spot. This is most probably representing a longer product that could be stained.

5.3.1.2. Do the loop-binders induce RNase H in a catalytic manner?

Having shown that the loop-binders principally can induce RNase H mediated cleavage, we wanted to address the catalytic properties of these molecules. RNase H cleaves only the RNA strand in a RNA/DNA duplex (cf. Introduction). After the cleavage process the complementary DNA strand is released unchanged and can induce cleavage in another molecules. Theoretically, a single molecule of DNA would be enough in an in vitro system without cellular cofactors and endonucleases to cleave all the RNA targets (in infinite time). To investigate this question we prepared the same reaction partners as in lanes 3 and 4 of fig. 5.3, but with differing molecular ratios of RNA/DNA. One probe was contained approximately the same amount of RNA and DNA, one probe had half as much DNA ASO, and one probe contained only a quarter as much (molecular ratios RNA/DNA: ≈ 1.2 : 1, 2.4 : 1, and 4.8 : 1). All probes were incubated again for 1 hour @ 37 °C. Table 5.7 shows the exact composition of the reaction mixtures. To exclude any unintended degradation processes we prepared the same solutions with and without enzyme as before. Additionally a negative

control (this time an RNA/RNA duplex) was prepared by the combination of the same RNA target with the original RNA 9-mer (B11).

Table 5.7. – Composition and reaction volumes of the second PAGE experiment. All volumes are given in µl.

Substance / Lane	1	2	3	4	5	6	7	8	9
RNA_18_mer_target		8	8	8	8	8	8	8	8
B11_pure_RNA		8	8						
B11_pure_DNA				8	8	4	4	2	2
Marker	8								
Reaction buffer	2	2	2	2	2	2	2	2	2
RNase H			1		1		1		1
Water	10	2	1	2	1	6	5	8	7
Total reaction volume	20	20	20	20	20	20	20	20	20
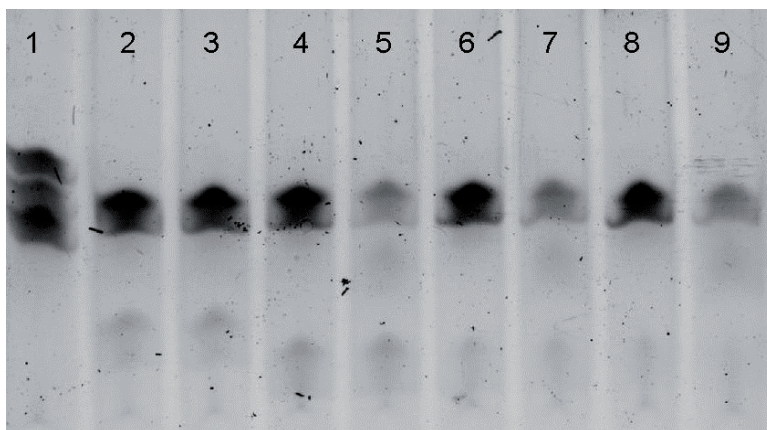
Figure 5.4. – PAGE gel of the second RNase H assay investigating the catalytic cleavage of the linear 18_mer_RNA_target. Although there is a 4-fold difference in ASO concentration between lanes 5 and 9 the extent of cleavage is the same.

Fig. 5.4 displays the stained gel as processed by the BioRad gel imager. From that we can make the following conclusions:

1. The RNase H induced cleavage of the linear target could be reproduced. This was the case not only in the reaction mixture containing equimolar amounts of DNA and RNA (cf. lane 5), but as well for the samples with 50 % (lane 7) and 25 % (lane 9) amounts of DNA. As the same reaction mixtures without enzyme do not exhibit any reduction in spot intensity (cf. lanes 4, 6, and 8), this indicates that a DNA ASO can act in a catalytic manner. Furthermore, all 3 RNase H containing mixtures show about the same extent of cleavage (lane 5: ≈60 %, lane 7: ≈55 %, lane 9: ≈60 %). So, at least in this configuration, the enzyme seems to be the rate limiting step and not the concentration of antisense DNA strand.

2. The RNA/RNA duplex is not cleaved by RNase H as one expects.

5.3.1.3. Second PAGE analysis of catalytic activity with a rough estimation of binding affinity

In order to further investigate the catalytic activity of the DNA loop-binders against the linear 18-mer we repeated the same experiment with progressively reduced amounts of DNA ASOs in a serial dilution. Starting with a concentration of 6.3 ng/ul (= 2.3 µM) of DNA we diluted the ASO 6 times (1:2) down to 0.09 ng/ul (= 36 nM). The concentration of the linear RNA_18_mer_target kept unchanged at 10 ng/µl (1.8 uM). The exact composition of the reaction mixtures is listed in table 5.8. All probes were incubated @ 37 °C for 70 minutes.

Table 5.8. – Composition and reaction volumes of the third PAGE experiment. All volumes are given in µl.

Substance / Lane	1	2	3	4	5	6	7	8	9
RNA_18_mer_target		9	9	9	9	9	9	9	9
B11_pure_DNA		8	8	8	8	8	8	8	8
Marker	4								
Reaction buffer	2	2	2	2	2	2	2	2	2
RNase H			1	1	1	1	1	1	1
Water	14								
Total reaction volume	20	20	20	20	20	20	20	20	20

Table 5.9. – Calculated molar ratios, concentrations and cleavage extents (as calculated with ImageJ).

Lane	2	3	4	5	6	7	8	9
Molar ratio RNA / DNA	0.86	0.86	1.72	3.45	6.90	13.81	27.63	55.26
Concentration (ng/µl)	6.3	6.3	3.15	1.57	0.78	0.39	0.19	0.09
Concentration (nM)	2300	2300	1150	575	288	144	72	36
Percentage of cleavage (%)	–	39.9	36.6	25.3	21.1	11.8	9.4	6.5
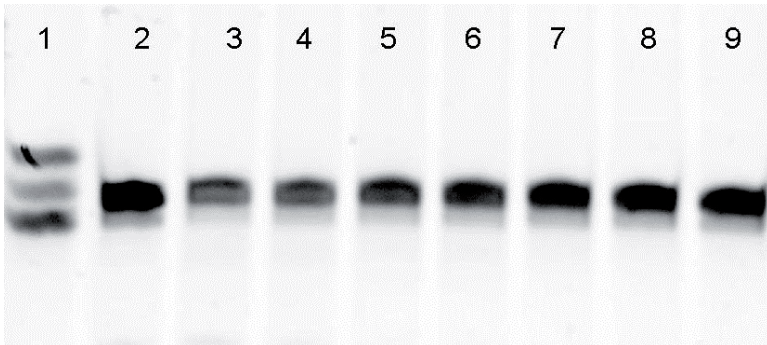
Figure 5.5. – Urea PAGE gel of RNase H reaction with serial dilution of the DNA ASO. The amount of cleaved substrate can be calculated with ImageJ (cf. table 5.9 and plottet against the concentrations to yield a rough estimation of binding affinity of the enzyme against the heteroduplex (cf. fig. 5.6).

At a first glance there seems to be not a big difference in the spots. However, a subsequent analysis of the spots on the gel with ImageJ shows a constant and uniform increase in intensity for each spot with decreasing concentration of ASO (cf. lanes 3 to 9). The reaction

mixture without RNase H shows no signs of degradation. Table 5.9 lists the molar ratios, the concentrations and the extent of cleavage as calculated with ImageJ.

When looking more closely at these values one can see a correlation between the extent of cleavage and the concentration of ASO. Fortunately we chose an optimal range for the dilution series. This method is not very robust and there are many uncertainties and possibilities for errors, e.g. very small pipetting volumes (volumes were all between 1–9µl), differences in gel loading, differences in washout from the gel during staining, etc.). Nevertheless the correlation of these values is excellent and one can make a rough estimation of binding affinity of the RNase H/substrate complex: assuming a strong correlation between the extent of cleavage and the amount of enzyme-substrate complex ([ES]), and between the maximum percentage of cleavage and the total enzyme concentration ([E_{tot}]). Then the amounts of cleavage plotted against the concentrations of DNA ASO can be fitted according to formula 5.4.

$$E + S \underset{k_d}{\overset{k_a}{\rightleftharpoons}} [ES] \tag{5.1}$$

$$K_D = \frac{k_d}{k_a} = \frac{E \cdot S}{[ES]} \tag{5.2}$$

$$[E_{tot}] = [E] + [ES] \tag{5.3}$$

$$[ES] = \frac{[E_{tot}] \cdot [S]}{K_D + [S]} \tag{5.4}$$

Fig. 5.6 shows a plot of the values for percentage of cleavage (cf. table 5.9) versus concentration. Assuming a correlation as given in formula 5.4, a nonlinear regression analysis performed with GraphPad Prism yields a KD value in the mid nM range (370 $\pm$ 170 nM). This is a quite surprising result as the gel electrophoresis seems not to be a suitable method for the determination of binding affinity.
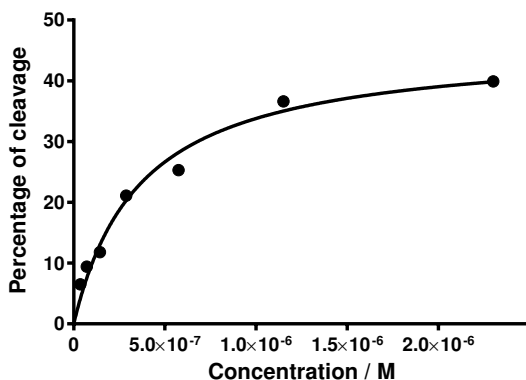

Figure 5.6. – Estimation of binding affinity of RNase H against the heteroduplex substrate. The plot of the calculated cleavage extents as listed in table 5.9 vs. the concentrations can be fitted with equation 5.4.

5.3.1.4. Cleavage of the hairpin structure of pre-miR-122

Having shown that the DNA loop-binders are capable of cleaving a linear 18-mer RNA oligoribonucleotides in a catalytic manner we went on to investigate the impact of these molecules on the RNase H mediated cleavage of pre-miR-122. In a first series we chose three of the loop-binders in a gel assay as described before: The DNA 9-mer beginning at the predicted loop (B11_pure_DNA), the DNA 9-mer ending at the loop (C2_pure_DNA), and the 10-mer ending at the loop (C10_pure_DNA). The chosen concentration for the ASOs was 4 ng/µl. After mixing them together they were incubated @ 37 °C for 1 hour. Table 5.10 lists the exact amounts of the reaction mixtures.

Table 5.10. – Composition and reaction volumes of the fourth PAGE experiment. All volumes are given in µl.

Substance / Lane	1	2	3	4	5	6	7	8
pre-miR-122			4	4	4	4	4	4
B11_pure_DNA			4	4				
C2_pure_DNA					4	4		
C10_pure_DNA							4	4
Marker	8	8						
Reaction buffer	1	1	1	1	1	1	1	1
RNase H		1		1		1		1
Water	1		1		1		1	
Total reaction volume	10	10	10	10	10	10	10	10
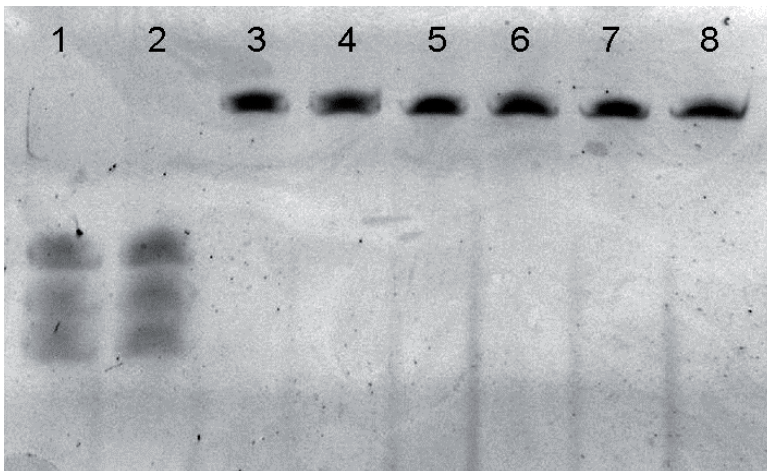
Figure 5.7. – Without prevenient annealing procedure there is practically no cleavage by RNase H

Fig. 5.7 shows the processed gel. The spots on lanes 4, 6, and 8 which containe RNase H, are very similar to the spot of the reaction mixtures without enzyme (3, 5, and 7). If one calculates the extent of cleavage the numbers are small compared to the previous experiments: 5.4 %, 0.8 %, and 11.6 % (for B11, C2, and C10). In his master-thesis, F. Paun stated that this could be even an error within pipetting inaccuracies (paun, master-thesis).

However, these numbers are in accordance to the previous experiments: B11 exhibits a greater supremacy over C2 and C10 is inducing cleavage to a greater extent as well (the only difference is an additional base pair in 5'-direction of the hairpin more towards the beginning of the loop).

It seemed possible that this could be due to the fact that the DNA ASOs could not disrupt the strong secondary structure of the hairpin of pre-miR-122.

Therefore we tried an annealing procedure. We addressed this by comparing the ability of inducing RNase H cleavage of the duplexes with and without previous annealing as described in materials and methods part (for this experiment we used only 1 oligonucleotide: B11_pure_DNA). For comparison reasons we simultaneously did the same for the linear target as used in the previous experiments.

Table 5.11. – Composition and reaction volumes of the last PAGE experiment. All volumes are given in µl.

Substance / Lane	1	2	3	4	5	6	7	8	9	10
pre-miR-122		8	8	8						
18_mer_RNA_target					8	8	8	8	8	8
B11_pure_DNA			8	8	8	8	8	4	4	4
Marker	4									
Reaction buffer	2	2	2	2	2	2	2	2	2	2
RNase H			1	1		1	1		1	1
Water	14	2	1	1	2	1	1	2	1	1
Annealing	no	no	no	yes	no	no	yes	no	no	yes
Total reaction volume	20	20	20	20	20	20	20	20	20	20
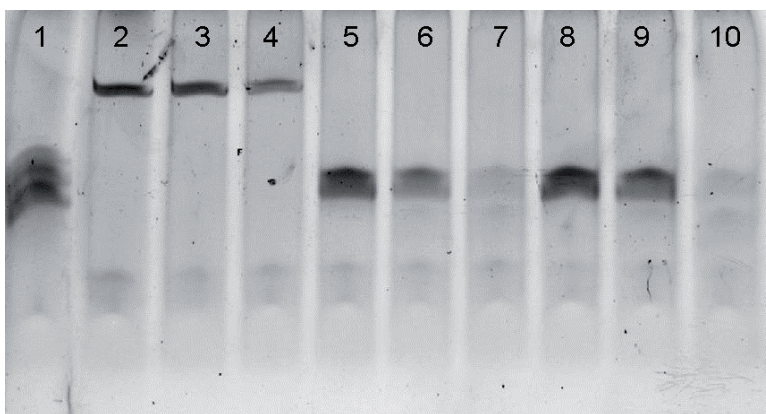
Figure 5.8. – When a preceding annealing procedure is performed, the cleavage extent is raised dramatically: lanes 6 and 9 lack of annealing, lanes 7 and 10 are composed identically but suffered a previous annealing procedure.

Mixtures of B11_pure_DNA with hairpin and the linear 18_mer_RNA_target were prepared in triplicates:

- without enzyme and annealing
- with enzyme and without annealing
- with enzyme and annealing

Except the 18_mer_RNA_target solution which was in a concentration of 10 ng/µl, all solutions were 4 ng/µl. The calculated molar ratios are: 0.1 for lanes 2-4 (this equals a 10-fold excess of DNA ASOs over hairpin), 1.2 for lanes 5-7, and 2.4 for lanes 8-10. Table 5.11 lists the complete compositions of the reaction mixtures. Fig. 5.8 shows the processed PAGE gel.

From this experiment the following conclusions can be drawn:

1. In the case of the pre-miR-122 hairpin, the annealing procedure significantly improved the RNase H cleavage (cf. lanes 3 and 4): A quantification of the extent of the cleavage as performed with ImageJ showed a roughly 4-fold higher cleavage rate for the complex with annealing procedure (11 % cleavage vs. 39 %).

2. In the case of the "linear" 18_mer_RNA_target (cf. lanes 5-10), the annealing procedure significantly improved the cleavage of the target RNA by RNase H by roughly 2-fold: 42 % vs. 73 % in the case of the low molecular ratio (cf. lanes 6 and 7), and 21 % vs. 71 % for the high molecular ratio (cf. lanes 9 and 10).

3. As the annealing process with the hairpin occurs in the loop region, the expected cleavage products in the case of the hairpin should have approximately the length of the stem of pre-miR-122 which is at least 22 nucleotides in length. As this length is in a very good range for staining (all oligonucleotides of about this length are stained perfectly) one would assume a new band/spot below the hairpin (at about the same height as the micro-RNA markers). As the hairpin with annealing of its complementary DNA ASO was cleaved by about 40 % one would expect a new band. If the cleaved hairpin would exhibit still an intact stem structure (even though there are strong denaturing conditions), it would very probably co-migrate with the intact hairpin and one would see no difference in spot intensity. This is not the case and the reason for this is unknown.

The difference between lanes 6 and 9 of 41 % vs. 21 % is as expected: lane 6 contained exactly the double amount of DNA ASO and exhibited as well a doubled cleavage rate. However, the explanation for the same mixtures after annealing is rather difficult: if the annealing would give such a strong difference, the spot in lane 10 would expected to be (much) darker as the release of the DNA ASO after cleavage of the opposite RNA strand by RNase H yield an unannealed strand which would require an afresh annealing process which did not occur. In a cellular environment one could propose a "hand-over" process as it is described for the Dicer-Ago2/RISC, but in such an artificial system without any cofactors this is not possible.

5.3.2. Getting to the bottom: identification of cleavage sites and extent of cleavage by LC/MS

After having shown that the DNA loop-binders were capable of inducing RNase H mediated cleavage of the target RNA 18-mer as well as the hairpin of pre-miR-122 in a catalytic manner (favorably after annealing) we wanted to be able to see or even identify the cleavage products. For practical reasons we wanted to avoid use of radioactive labeled oligonucleotides. Different attempts to identify the cleavage products with our BioRad Experion® Electrophoresis system failed due to too high noise levels (data not shown). Therefore we

decided to develop a HPLC-based method for the detection and identification of the cleavage products.

5.3.2.1. A first assay for the identification of cleavage products for the linear target

In a first LC/MS-based assay we focused on the identification of the cleavage products of the linear 18_mer_RNA_target induced by B11_pure_DNA. A so called single pot reaction method was used. This method depended upon aligning the amounts of substrate in the reaction and the control sample by making one reaction mixture from which an aliquot for the reaction and the control is taken. After having added the enzyme to one vial and an equal amount of water to the control, the mixtures are incubated and analyzed by HPLC. As the origin of both samples is the same, one can normalize the HPLC chromatograms to the peak of the ASO which is not altered thus removing the influence of different injection volumes. To be able to clearly identify the peaks of the ASO and the target RNA as well as impurities in these oligonucleotide solutions we also injected samples with only the ASO and only the target RNA. As the detection by LC/MS is less sensitive than the PAGE, we directly raised the oligonucleotide concentrations to 8 µM.

Table 5.12. – Composition and reaction volumes of the first HPLC-based assay against the linear target.

Substance / Sample	1	2	3	4
18_mer_RNA_target	13	13	13	
B11_pure_DNA	13	13		13
Reaction buffer	3	3	3	3
RNase H	1			
Water			1	14	14

Table 5.12 shows the composition of the reaction mixtures for the LC/MS assay. As the focus of the experiment depended upon on the identification of the cleavage products we annealed the reaction mixtures (80 °C, 5 minutes) and incubated them for a much longer time (37 °C, overnight ($\approx$21 hours)). In order to inactivate the enzyme, the reaction mixtures were treated with heat (cf. Materials and methods). The volumes of the samples were filled to 100 µl prior to injection into the LC/MS system. The single chromatograms were opened in the analysis software of the Agilent system and overlaid. By overlaying them one can directly identify 7 cleavage products as seen in fig. 5.9.

There are multiple sites for RNase H cleavage and these products differ in masses from synthesized analogues (RNase H produces products with 3'-OH and 5'-OPO$_3$ termini). For this reason I developed a tool for oligo_scoop (cf. chapter 3) which calculates all possible RNase H cleavage products of a given sequence with the possibility of narrowing the limits of the found masses (either in % or Dalton). With the help of oligo_scoop the identity of these 7 products was quickly elucidated. Fig. 5.10 shows the sequences and calculated masses of all possible fragments that can be produced by RNase H cleavage of the target. The fragments are calculated to have a 3'-OH and 5'-O$_3$PO terminus.

Table 5.13 lists the masses and identity of the found products. The found masses differ from the calculated masses by no more than 1 Dalton!
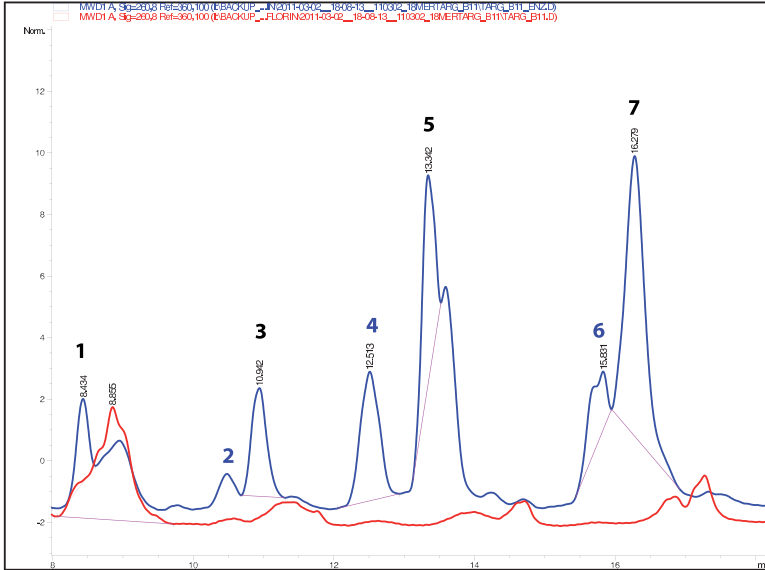
Figure 5.9. – Chromatogram of the RNase H cleavage products against 18‑mer‑RNA‑target. This is an overlay of the chromatograms of the samples 1 and 2 in table 5.12. Blue line: response of sample with enzyme, red line: response of sample without enzyme. The deconvoluted masses of the peaks are listed in table 5.13. Black numbers indicate 3'-OH cleavage products, blue numbers indicate the 5'-O$_3$PO cleavage products.

Table 5.13. – Identification of the cleavage products of the linear 18-mer target by HPLC. The numbers of the products refer to the numbering in fig. 5.9. A cross indicates an expected product peak that could not have been identified.

| Product peak	Ret. time (min.)	Deconv. mass	Calc. mass	Cleavage product
Target sequence				5'-UUGUGUCUAAAAUAUCAA-3'
1	8.42–8.62	2463.2	2464.5	5'-UUGUGUCU -3'
X			3216.0	5'-O$_3$PO-AAACUAUCAA-3'
3	10.91–11.13	2793.1	2793.7	5'-UUGUGUCUA -3'
X			2886.8	5'-O$_3$PO- AACUAUCAA-3'
5	13.34–13.74	3122.3	3122.9	5'-UUGUGUCUAA -3'
6	15.68–16.00	2556.9	2556.6	5'-O$_3$PO- ACUAUCAA-3'
7	16.23–16.43	3451.5	3452.1	5'-UUGUGUCUAAA -3'
4	12.36–12.66	2227.8	2227.4	5'-O$_3$PO- CUAUCAA-3'
X			3757.3	5'-UUGUGUCUAAAC-3'
2	10.43–10.63	1922.6	1923.2	5'-O$_3$PO- UAUCAA-3'

Fragmentation of target sequence

clear whole worksheet

Fragments	location in target sequence	length (w/o spacer/B)	mass calc.
Target-sequence	UUGUGUCUAAACUAUCAA	18-mer	5'662.5 g/mol
fragment 1 (Position 1-1)	UUGUGUCUAAACUAUCAA	1-mer	244.2 g/mol
fragment 2 (Position 1-2)	UUGUGUCUAAACUAUCAA	2-mer	550.4 g/mol
fragment 3 (Position 1-3)	UUGUGUCUAAACUAUCAA	3-mer	895.6 g/mol
fragment 4 (Position 1-4)	UUGUGUCUAAACUAUCAA	4-mer	1'201.8 g/mol
fragment 5 (Position 1-5)	UUGUGUCUAAACUAUCAA	5-mer	1'547.0 g/mol
fragment 6 (Position 1-6)	UUGUGUCUAAACUAUCAA	6-mer	1'853.1 g/mol
fragment 7 (Position 1-7)	UUGUGUCUAAACUAUCAA	7-mer	2'158.3 g/mol
fragment 8 (Position 1-8)	UUGUGUCUAAACUAUCAA	**8-mer**	**2'464.5 g/mol**
fragment 9 (Position 1-9)	UUGUGUCUAAACUAUCAA	**9-mer**	**2'793.7 g/mol**
fragment 10 (Position 1-10)	UUGUGUCUAAACUAUCAA	**10-mer**	**3'122.9 g/mol**
fragment 11 (Position 1-11)	UUGUGUCUAAACUAUCAA	**11-mer**	**3'452.1 g/mol**
fragment 12 (Position 1-12)	UUGUGUCUAAACUAUCAA	**12-mer**	**3'757.3 g/mol**
fragment 13 (Position 1-13)	UUGUGUCUAAACUAUCAA	13-mer	4'063.5 g/mol
fragment 14 (Position 1-14)	UUGUGUCUAAACUAUCAA	14-mer	4'392.7 g/mol
fragment 15 (Position 1-15)	UUGUGUCUAAACUAUCAA	15-mer	4'698.9 g/mol
fragment 16 (Position 1-16)	UUGUGUCUAAACUAUCAA	16-mer	5'004.0 g/mol
fragment 17 (Position 1-17)	UUGUGUCUAAACUAUCAA	17-mer	5'333.2 g/mol
fragment 18 (Position 18-18)	UUGUGUCUAAACUAUCAA	1-mer	347.2 g/mol
fragment 19 (Position 17-18)	UUGUGUCUAAACUAUCAA	2-mer	676.4 g/mol
fragment 20 (Position 16-18)	UUGUGUCUAAACUAUCAA	3-mer	981.6 g/mol
fragment 21 (Position 15-18)	UUGUGUCUAAACUAUCAA	4-mer	1'287.8 g/mol
fragment 22 (Position 14-18)	UUGUGUCUAAACUAUCAA	5-mer	1'617.0 g/mol
fragment 23 (Position 13-18)	UUGUGUCUAAACUAUCAA	**6-mer**	**1'923.2 g/mol**
fragment 24 (Position 12-18)	UUGUGUCUAAACUAUCAA	**7-mer**	**2'228.4 g/mol**
fragment 25 (Position 11-18)	UUGUGUCUAAACUAUCAA	**8-mer**	**2'557.6 g/mol**
fragment 26 (Position 10-18)	UUGUGUCUAAACUAUCAA	**9-mer**	**2'886.8 g/mol**
fragment 27 (Position 9-18)	UUGUGUCUAAACUAUCAA	**10-mer**	**3'216.0 g/mol**
fragment 28 (Position 8-18)	UUGUGUCUAAACUAUCAA	11-mer	3'522.1 g/mol
fragment 29 (Position 7-18)	UUGUGUCUAAACUAUCAA	12-mer	3'827.3 g/mol
fragment 30 (Position 6-18)	UUGUGUCUAAACUAUCAA	13-mer	4'133.5 g/mol
fragment 31 (Position 5-18)	UUGUGUCUAAACUAUCAA	14-mer	4'478.7 g/mol
fragment 32 (Position 4-18)	UUGUGUCUAAACUAUCAA	15-mer	4'784.9 g/mol
fragment 33 (Position 3-18)	UUGUGUCUAAACUAUCAA	16-mer	5'130.1 g/mol
fragment 34 (Position 2-18)	UUGUGUCUAAACUAUCAA	17-mer	5'436.3 g/mol

Figure 5.10. – Sequences and calculated masses of all possible RNase H product fragments (in red) as calculated by oligo_scoop. Bold numbers indicate the fragments found/expected.

The identified cleavage products can now be assigned to the cleavage sites as indicated in fig. 5.11
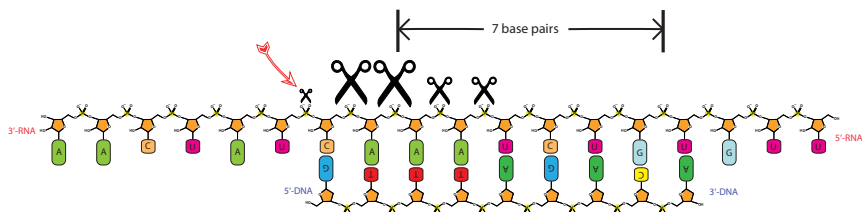
Figure 5.11. – Cleavage sites of RNase H for the linear target as determined by the HPLC-based enzymatic assay. The size of the scissors represent the amount of target cleavage at the specific positions.

By dividing the area under the curve of the peaks and multiplying them with the calculated molar absorption coefficients (for normalization in moles) one can make estimations for the amount of product per cleavage site. This procedure reveals that the most prominent site of cleavage is the 7th and 8th scissile phosphate group measured from the beginning of the heteroduplex at the 5'-end of the RNA. This is in good accordance with the results obtained by Lima et al.. Interestingly, the target RNA strand has also been cleaved after the last base pairing at the very end of the 5'-DNA (cf. red arrow in fig. 5.11). To my best knowledge, this site of cleavage has not been reported before.

This experiment showed that it is not only possible to reliably identify the cleavage products and therefore the different cleavage sites, but as well the extent of cleavage by LC/MS.

In a last step we wanted to repeat this experiment for the hairpin.

5.3.2.2. What are the cleavage products of the DNA ASOs with the hairpin?

In the last assay we addressed the RNase H inducing power of our DNA loop binders against the full length hairpin of pre-miR-122.

For this purpose we employed three loop-binding DNA ASOs: B11_pure_DNA (as before) and for reasons of increased binding affinity D5_pure_DNA (an 11-mer ending at the loop) and E4_pure_DNA (a 13-mer ending at the loop). The concentrations of these molecules were chosen to be 5 µM.

Although the injectors of todays HPLC systems yield reliable and reproducible results, there can still be some differences in injection volume. As we expect only small amounts of visible products we wanted to be sure to be able to correlate the peaks with and without enzyme to each other. For this purpose we made the reaction in a "single pot" way: instead of pipetting the reaction mixtures separately we prepared one single solution containing the DNA ASO, the RNA target (hairpin), and the reaction buffer. After mixing (vortex), spinning down of the solution, and annealing in the same way as described above we took twice the same amount out of the reaction vessel in two new eppendorf tubes. In one of them we pipetted the enzyme RNase H in the other we pipetted the same volume of water. By doing so, we could be sure, that the ratio of DNA ASO to the hairpin target is absolutely the same in both vials. Therefore, as the amount of DNA ASO remains unchanged, we could use the ASO peak as an internal standard for normalization of the two chromatograms. 24 µl of each solution (ASO/target) were used for the reaction. After annealing and separation, 3 µl RNase H or 3 µl water, respectively were added. The reaction was carried out at 37 °C for 24 hours. After incubation, the samples were heat inactivated (see above) and the volumes were filled up to 100 µl with water prior to injection onto the HPLC system. We used the following parameters: solvent A: 0.4 M HFIP, 8.6 mM TEA, pH 8; solvent B: 100 % MeOH; column temperature: 60 °C; gradient: 17.5–25 % B in 50 minutes; post time: 12 minutes.

Fig. 5.12 shows the overlaid chromatograms of B11_pure_DNA against the hairpin with enzyme (blue) and without enzyme (red)(A). At a first glance substrate peaks (ret. Time 28 min.) appear to be of the same height suggesting no reaction. A closer look at the enlarged region of the ASO peak at 10 min. shows that the signal of the ASO in the case of the reaction mixture with enzyme is significantly higher than in the mixture without enzyme. If one normalizes the two chromatograms to the peak height of the DNA ASO, one can see that the ratio of the two substrate peaks has changed: the peak of the substrate in the RNase H containing solution has decreased substantially. Besides that one can see some little peaks with retention times between 14 and 20 minutes (green ellipse). These are the peaks of the cleavage products. The peaks of the two other ASOs are similar.

Unfortunately, the absorption of these peaks is small (less than 10 mAU) and we could not perform a deconvolution for the identification of the products despite the long attempts of finding a suitable algorithm.

But as the aligning of the internal standard (the DNA ASOs) works perfectly, one can calculate the extent of cleavage by division of the areas under the curve (peak areas). The result of this analysis is given in table 5.14 and shows that roughly a quarter of the substrate was cleaved in all the cases.
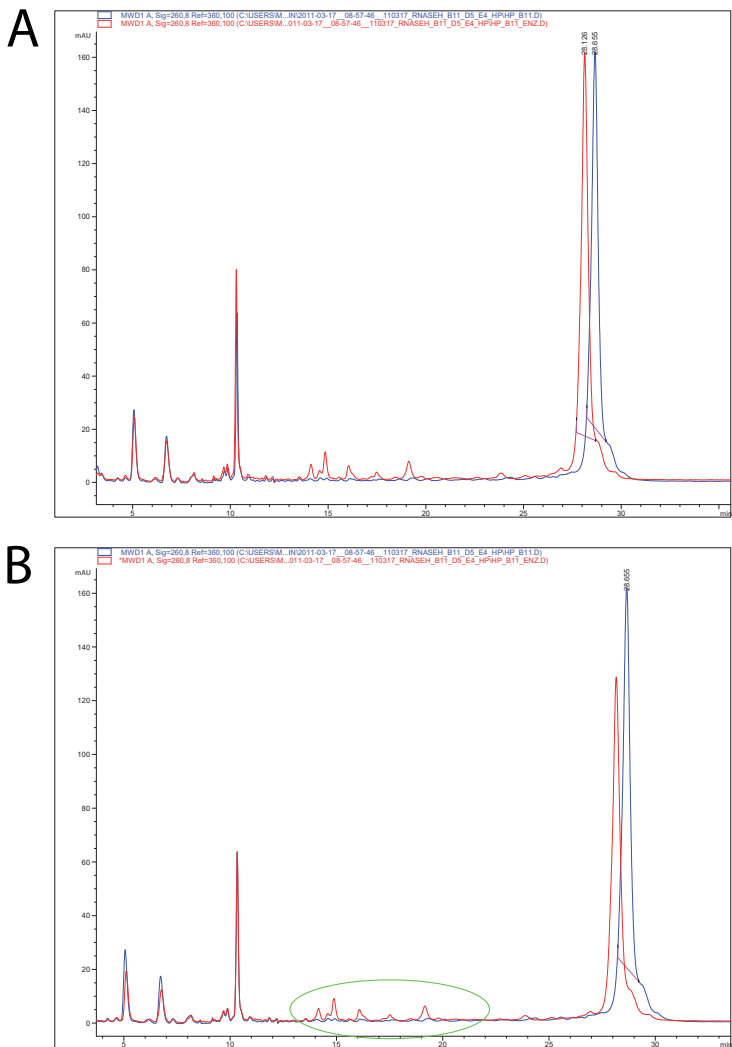
Figure 5.12. – Comparison of the chromatograms of the overlaid reaction mixtures with (red) and without (blue) enzyme. Part A shows the chromatograms before the normalization to the ASO-peak. The two substrate peaks are practically identical (in height). Part B shows the same chromatograms after normalization. The substrate peak of the reaction with enzyme has decreased significantly. The green ellipse indicates the putative cleavage products.

Table 5.14. – Calculated cleavage extents for the RNase H cleavage of the hairpin calculated for all three ASOs used.

ASO used for the reaction	Peak area w/ enzyme / (mAU·s)	Peak area w/o enzyme / (mAU·s)	Calc. cleavage extent (%)
B11_pure_DNA	5369.5	6946.3	22.6
D5_pure_DNA	5011.3	6662.5	24.7
E4_pure_DNA	5465.1	7213.8	24.2

6. How to deal with high-binders: Development of INSTED

6.1. Introduction

WHEN performing the SPR-experiments of the walkaround of pre-miR-122 I observed a strong loss of binding response for the control-oligonucleotides over the measuring time (cf. section 2.3 on page 43). As I found out later, this loss of surface activity is in fact related to a loss of biotinylated ligand (pre-miR-122). Although its extraordinary high equilibrium dissociation constant, K_D, of $\approx 10^{-15}$ [256, 257] there is a significant loss of biotinylated ligand, especially with very long assay times[i].

Due to the re-analysis of a previously purified sample of biotinylated pre-miR-122 I observed the complete aerial oxidation of this ligand to the biotin–sulfoxide during storage at -20 °C. When immobilizing such a fully oxidized hairpin on the chip surface of a gold-coated SPR chip and performing a normal binding assay against it, the sensorgrams showed such a strong drift due to the dissociation of the ligand that a fitting to a binding model was impossible.

Arguably, the most important interaction in analytical biochemistry is that of biotin–(strept)-avidin. Therefore I tried to directly determine the dissociation rate constant, k_d, for this complex which failed due to strong baseline drifts in the presence of even the smallest ambient temperature changes.

Therefore, I developed a new method which is completely independent of temperature-fluctuations for the measurement of extremely low dissociation rate constants: the method was called *Internal Referencing by Steady-State Analysis*—INSTED. With INSTED I revealed a difference in half-life that is ≈ 5 (25 °C) and ≈ 7 (37 °C) times lower for the oxidized biotin than for the unoxidized one. The determined dissociation rate constants are ranging from $1.52 \cdot 10^{-5}$ to $9.04 \cdot 10^{-7}$.

The results presented herein are published in ChemBioChem [172].

6.1.1. The Biotin–(Strept)avidin system and its use in SPR

Avidin, a 67-kDa glycoprotein found in egg white, has a very high binding affinity for biotin with a reported equilibrium dissociation constant of $1 \cdot 10^{-15}$ M [256, 257]. It consists of four identical subunits between which there are no interactions and therefore an equally high binding affinity for biotin independent of the amount of already bound biotin molecules [256–258]. Like avidin, streptavidin[ii] has a very high affinity towards biotin of about 10^{-13} M

---

[i]In the experiment described on page 43 the whole measuring time was about 96 hours
[ii]A protein deriving from the bacteria Streptomyces avidinii

[259]. This exceptionally high non-covalent binding affinity is reported to be due to 5 hydrogen bonds that cooperatively[iii] interact with the active site of streptavidin (three to the carbonyl oxygen and one for each -NH group of the ureido moiety) [260]. Although it has an about 100-fold lower affinity for biotin, streptavidin is more widely used in biochemistry than avidin as it does not contain any carbohydrates and has a substantially lower pI (about 5-6) which drastically reduces unspecific binding [261]. The preparation of the ligand surfaces can be done either with direct immobilization techniques or the usage of some capturing methods (cf. chapter 1 on page 13; for detailed immobilization protocols see Handbook of surface plasmon resonance 24). According to a statistical analysis performed by Rich and Myszka (in 2003, [262]) these two methods are used in approximately evenly cases (54 % and 46 %). In their analysis of 676 Biacore-based articles the overwhelming part (64 %) of the ligand capturing was performed using the biotin–streptavidin system. Because of the ease of synthesis/usage and the uniform attachment at well-defined positions I chose this system for the attachment of our (pre-)miRNAs on the SPR chip surface.

6.1.2. Ready oxidation of biotin during storage

When I was screening the walkaround against biotinylated pre-miR-122 with Biacore T100 I was evenly distributing some injections of control oligoribonucleotides for the monitoring of the activity of the chip surface (cf. section 2.3 on page 43). The comparison of these injections showed a constant decrease of surface activity over time resulting in decreased RU_{max} values.

As the biotin–streptavidin system belongs to the strongest non-covalent interactions known (cf. section 6.1.1) I did not assume such a strong decrease even when performing long-term experiments.

After having performed a control-analysis of a previously very pure sample of the biotinylated loop-region of pre-miR-122 I observed a closely running, but separable peak (cf. fig. 6.1) as it was observed as well during synthesis. This peak was corresponding to mass +16 as confirmed by ESI-MS (cf. inset in fig. 6.1). I assigned this to oxidation of the biotin sulphur as biotin is known to be oxidisable not only chemically [263] but as well during oligonucleotide synthesis [264] yielding two different types of sulfoxide due to the asymmetric sulfur of biotin. To our surprise, this oxidation occurred even during storage of aqueous solutions of purified oligonucleotides at -20 °C.

I found that repeated freeze/thawing cycles led even to complete oxidation after about one year (cf. fig. 6.2). By testing other RNA-biotin conjugates and also a small simple biotin molecule (tested in co-work with Dr. Andreas Brunschweiger) we checked if the oxidation was confined to a single rogue RNA sequence (data not shown). We found that these molecules were oxidized in the same manner which indicates that the influence of the attached macromolecule plays a tangential role. These findings imply that when working with biotin and macromolecular interactions it is likely that the biotin is oxidized. . . !

[iii]This cooperativity yields a stabilization energy higher than the expected sum of the individual energies of the single hydrogen-bonds.
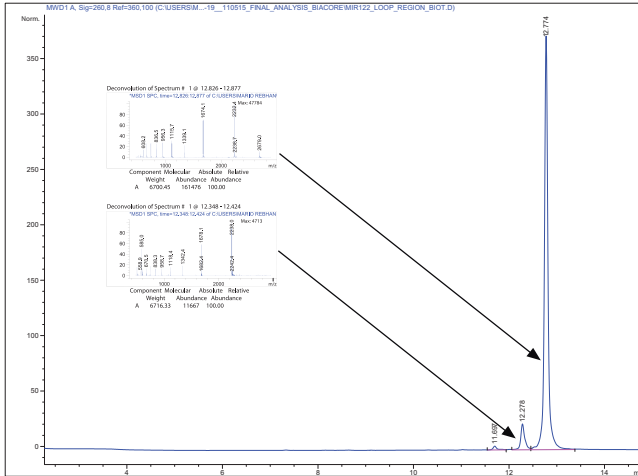
Figure 6.1. – Oxidation of the biotinylated loop-region of pre-miR-122 after short-term storage at -20 °C. The small peak with shorter retention time corresponds to target mass +16 as shown by ESI-MS (cf. inlet).
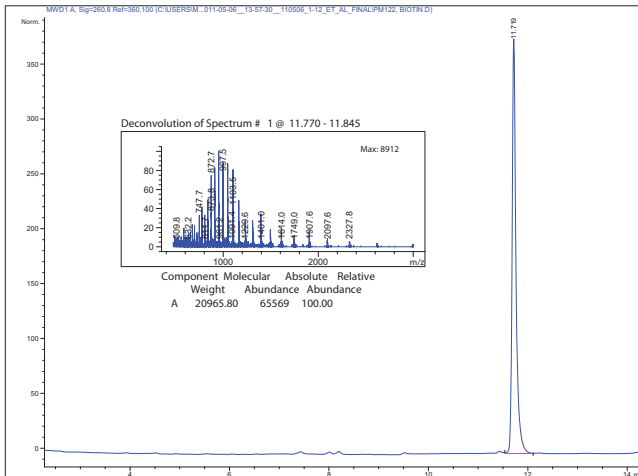

Figure 6.2. – Chromatogram of the fully oxidized hairpin of pre-miR-122. This oxidation was taking place during storage at -20 °C. The expected mass is 20'948 + 16 = 20'964 g/mol. The inset with the results of the deconvolution shows a mass of 20965.8 g/mol.

6.1.3. Impact of biotin-oxidation on binding affinity

When performing binding assays against such a completely oxidized biotinylated molecule, I observed such a strong loss of surface activity that an ordinary fitting of the resulting sensorgrams was practically impossible (cf. fig. 6.3).
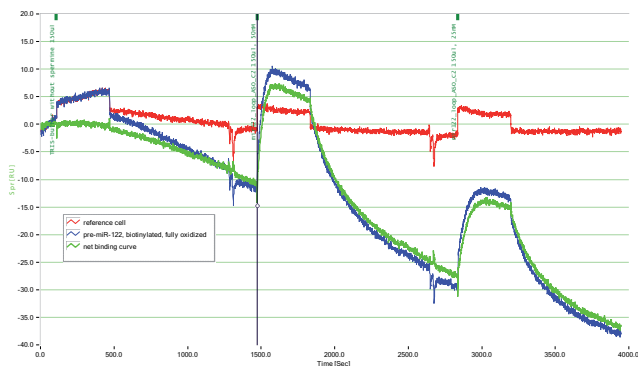
Figure 6.3. – Binding assay of a loop-to-mir against an immobilized fully oxidized hairpin of pre-miR-122. Marks at the top indicate the injection of buffer/analyte. As one can see there is a dramatic loss of surface activity due to relatively low binding affinity of oxidized biotin against streptavidin. This is even enhanced with the architecture of the C1-type gold-coated chips that lack of a dextran matrix which is favouring rebinding and MTL.

Garlick et al. measured the dissociation of a deliberately oxidized form of an iodo-biotin-derivative from avidin. They showed that the two formed isomers of that sulfoxide have substantially lower binding affinities to avidin than the unoxidized parent compound with great differences: 1.6-fold and 446-fold lower binding affinity ($t_{1/2}$ = 25 and 0.092 days vs. 41 days at 25 °C) [265]. They mention as well that their unmodified iodo-biotin-compound "required the presence of a thiol-stabilizer such as 2-mercaptoethanol to minimize its decomposition during storage to two more-polar products" [265]. As they identified these two products by tlc, it is not clear, whether these are oxidation products or not, but it is very likely. I tried four different known antioxidants for their ability of inhibiting this aerial oxidation (cf. section 6.3.2 on page 119). Amongst those I used as well β-mercaptoethanol (= 2-mercaptoethanol). Thereby I found out that β-mercaptoethanol completely destroyed our oligonucleotide which makes this substance useless for the oxidation-inhibition of biotinylated oligoribonucleotides.

6.1.4. Direct measurement of off-rates

The measurement of K_D values with SPR can mainly be achieved by steady-state or kinetic analysis [266]. However, all of these methods require either the achievement of steady-state or the robust determination of the dissociation rate constant (k_d), both of which is very difficult for high affinity analytes: the time for the ligand-analyte complex to reach equilibrium can be extremely long (up to several days!) and the reliable determination of the k_d s for such complexes can require time in the order of several hours or even days as they are usually extremely low ($< 1 \cdot 10^{-4}$). Although there are sophisticated methods for circumventing the problem of limited injection times like direct addition of the analyte into the running buffer [267] or affinity in solution measurements [268], they do not provide any kinetic constants.

In order to determine the half-life of these molecules I purified the oxidized and unoxidized biotinylated RNAs by HPLC and tried to directly measure the dissociation rate constants, k_d, for them over a few days.

Unfortunately, my attempts to directly measure k_d s in extended experiments failed due to strong baseline drifts, even under strictly controlled temperature conditions, which makes fitting to a (1:1) binding model impossible (data not shown). As SPR is a very temperature-sensitive method [269], this is not particularly astonishing. For the same reason I could not perform the equilibrium analysis described by Myszka et al. [267].

Additionally, with most SPR machines there is a limited time for the measurement of dissociation, e.g. the Biacore T-100 machine has a maximum dissociation time of 36'000 sec. (=10 h)[iv].

I therefore developed a new method which is completely independent of (moderate) temperature-fluctuations and can be applied for a very long time without supposable data-overflow: INSTED.

6.1.5. Development of INSTED

This new method which I termed INSTED (Indirect Steady-state Analysis) was tested with the dissociation of oxidized and unoxidized biotinylated oligonucleotides against streptavidin bound to a C1 type gold coated SPR chip.

Similar to the loss of surface activity that was observed for the mentioned control injections I used a comparable system for INSTED: the dissociation of biotinylated oligonucleotides bound to covalently immobilized (surface-bound) streptavidin is linked to the loss of surface activity. By indirectly monitoring this loss of surface activity with the repeated injection of a complementary indicator-molecule of low affinity over a sufficient amount of time (50 hours) the dissociation rate, k_d, can directly be measured if the values are plotted against the precise time of injection. A schematic of the principle of INSTED is shown in fig. 6.4.

For normalization/referencing two buffer injections were made prior to the injection of the indicator molecules.

This system is very robust for changes in ambient temperature and does not require a high data storage capacity, in fact, the injections of a whole 48-hour-run (including buffer) could have done within 1 file, although I separated them for performance reasons.

In principal I am determining the dissociation rate constant via the measurement of loss of surface activity. Now, there can be several reasons for such a loss of surface activity:

1. System-immanent reasons:

    - Aggregation/coagulation of the biotinylated molecules on the chip surface (e.g. due to partial self-complementarity) and therefore reduced RU_{max} values.

    - Aggregation of the indicator molecules in solution and therefore reduction of the analyte concentration.

2. Technical reasons:

[iv]source: Dr. St. Schauer, fgcz, pers. comm. on August, 21st, 2012
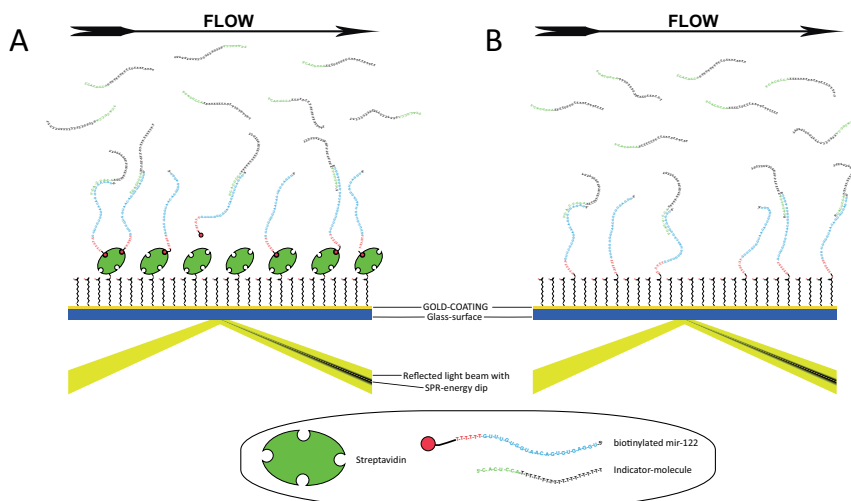
Figure 6.4. – Schematic representation of INSTED. A) Normal assay. The indicator molecules bind to the biotiny-lated mir-122 molecules bound via biotin to surface-immobilized streptavidin. As the biotin molecules dissociate away, the steady-state response of an indicator molecule at constant concentrations is reduced. B) The same experiment was repeated with a covalently attached mir-122 in order to exclude possible interferences

- Change of angle in opto-mechanical system due to vibrations.

- Disintegration of the gold-coating and loss of whole biotin/streptavidin complexes.

3. Biochemical reasons:

   - Contamination of buffers/flow system with RNases and therefore reduced surface activity due to degradation of ligand molecules.

   - Adsorption of the indicator molecules to the glass-/plastic vial and therefore reduction of the analyte concentration.

To exclude these possible reasons for the loss of surface activity I repeated the same assay but with a covalently bound mir-122 molecule as sketched in fig 6.4/B on page 112. The covalent micelle-mediated immobilization was performed as described in section 6.2.4 on page 114.

6.1.6. Inhibition of oxidation by addition of anti-oxidants

In order to prevent (aerial) oxidation, I tested 4 different known anti-oxidants used in biochemistry for their ability of inhibition of aerial biotin oxidation during storage: β-mercaptoethanol, DL-Dithiothreitol (DTT), Tris(2-carboxyethyl)phosphine hydrochloride (TCEP), and ascorbic acid.

6.2. Materials and Methods

6.2.1. Instrumentation

All surface plasmon resonance experiments were performed using our SierraSensors SPR2 machine (SierraSensors Inc., Hamburg, Germany). The synthesis, purification, characterization and normalization of the oligoribonucleotides was performed with the instrumentation as described in Section 2.2.2.2 on page 37. As mixer I used a Thermomixer comfort (Eppendorf, Prod. Nr. 5355 000.011) with an exchangeable thermoblock for 24 x 2.0 ml vials (Prod. Nr. 5362 000.019).

6.2.2. Reagents and Consumables

6.2.2.1. Oligonucleotide Synthesis

Universal UnyLinker CPG Support 500 Å was purchased from ChemGenes (Part No. N-4000-05). 3'-BiotinTEG-CPG was purchased from GlenResearch, Sterling, Virginia (Prod. Nr. 20-2955-01). Phosphoramidites were obtained from Thermo Fisher Scientific (see section 2.2.2.2 on page 37).

6.2.2.2. SPR-measurements

A 10-fold DPBS stock solution as running buffer was constituted as described in table 6.1.

Table 6.1. – Composition of 1 lt of 10-fold DPBS buffer.

Buffer substance	Quality	Mass	Origin
potassium chloride	puriss. p.a.	2.0 g/l	Fluka Chemika, Prod. Nr. 60130
potassium phosphate monobasic, anhydrous, KH_2PO_4	puriss. p.a.	2.0 g/l	Fluka Chemika, Prod. Nr. 60220
sodium chloride	EMSURE® ACS	80.0 g/l	Merck, Cat. No. 1.06404.1000
sodium phosphate dibasic, anhydrous, Na_2HPO_4	puriss. p.a.	11.5 g/l	Fluka, Prod. Nr. 71640

Streptavidin was purchased from Jackson ImmunoResearch (Prod. Nr. 016-000-114).

Hexadecyltrimethylammonium bromide (CTAB) was purchased from Fluka BioChemika (Prod. Nr. 52369).

1-ethyl-3-(3-dimethylaminopropyl)carbodiimide (EDC), N-hydroxysuccinimide (NHS), acetate buffer pH 5.5, 1 M ethanolamine solution, and standard C1 type gold-coated amine SPR chips were obtained from SierraSensors Inc., Hamburg, Germany.

The water used for dilution of oligonucleotides and constitution of buffers and reagent solutions was made by our in-lab Millipore Synergy Water Purification System (SYNS000WW) with a BioPak Point-of-use Ultrafilter for final purification (CDUFBI001). For long-term storage at -20 °C I used 1 ml Cryo.s™ pp vials (Greiner bio-one, Cat.-No. 123263-923).

6.2.2.3. Oxidation-Inhibition Experiments

DL-Dithiothreitol was purchased from Sigma-Aldrich as 1 M aqueous solutions (Prod. Nr. 646563). β-mercaptoethanol was purchased from Sigma (BioUltra, for molecular biology, $\geq$99 %, Prod. Nr. 63689), Sodium ascorbate was purchased from Fluka BioChemika (Prod. Nr. 11140), TCEP was purchased from Thermo Scientific as a 0.5 M buffered solution (Bond Breaker™, Prod. Nr. 77720).

6.2.3. Synthesis of oligoribonucleotides

The synthesis, purification, characterization and normalization of the oligoribonucleotides were performed as described in section 2.2.2.2 on page 37. The characteristics of the molecules used in this chapter are listed in table 6.2.

The long biotinylated oligoribonucleotide pre-let-7a-2 and the amine-coupled mir-122 were provided by Dr. A. Brunschweiger.

Table 6.2. – All oligoribonucleotides used for INSTED. The lengths are given without linker / biotin. pm122 is the abbreviation for pre-miR-122. The loop-region of pre-miR-122 was the sequence by which the oxidation of biotin was discovered (cf. fig. 6.1 on page 109). The biotinylated pre-let-7a-2 / pm122 loop-region, and amine-coupled mir-122 were synthesized using click-chemistry by Dr. A. Brunschweiger. (indicated by an asterisk)

Name	Sequence	Length / type	Purpose	Oxid.-state	Mass / [g/mol] calculated	found
pre-miR-122	5'-UGGAGUGUGACAAUGGUGUUUGUGUCUA- AACUAUCAAACGCCAUUAUCACACUAAAAUATTTTTT-B-3'	58-mer / RNA	Ligand	unox.:	20'948	20'949
				ox.:	20'964	20'965
pre-let-7a-2-loop region	5'-UAGAAUUACAUCAAGGGAGAUTTTTTT-B-3'	21-mer / RNA	Ox-inhib. test	unox.:	9'163	9'162
				ox.:	9'179	9'178
pm122, loop-region*	5'-GUGUCUAAACUAUCTTTTT-UB-3'	14-mer / RNA	Ligand	unox.:	6'701	6'700
				ox.:	6'717	6'716
mir-122	5'-UGGAGUGUGACAAUGGUGUUUGTTTTT-B-3'	22-mer / RNA	Ligand	unox.:	9'511	9'510
				ox.:	9'527	9'526
mir-122*	5'-UGGAGUGUGACAAUGGUGUUUGUGUCUA-Amine-3'	28-mer / RNA	Ligand	—	9'495	9'496
mir-122_ASO_1-7_T20	5'-CACUCCATTTTTTTTTTTTTTTTTTTTT-3'	7-mer / 2'-OMe	Indicator	—	8'306	8'304
mir-122_ASO_1-8_T20	5'-ACACUCCATTTTTTTTTTTTTTTTTTTTT-3'	7-mer / 2'-OMe	Indicator	—	8'649	8'647

6.2.4. SPR2 measurements

Standard EDC/NHS coupling was used to covalently immobilize streptavidin at 37 °C (cf. section 2.2.2.5, p. 40).

The biotinylated un-/oxidized mir-122 was injected in a 15 nM solution in DPBS-buffer with a flow-rate of 25 µl/min over spot 2 to yield between 20 and 30 RU of immobilization level. Spot 1 was left empty and acted as a reference spot.

The covalent micelle-mediated immobilization was adopted from the protocol as described by Seidel et al. [270]. After the activation of the chip surface, 40 µl of the immobilization solution (cf. table 6.3) were circulated over the chip surface at a low flow rate of 10 µl/min. (total 4 minutes). Alternatively one could use as well thiolated probes as described by Mannelli et al. [271].

Table 6.3. – Composition of the immobilization solution for the covalent immobilization of amine coupled mir-122.

Compound	Volume / [µl]	Remarks
Water	95	Millipore
DPBS	12	10-fold stock sol. w/o TWEEN, comp. see table 6.1
CTAB	12	6 mM (10-fold stock solution)
Amine coupled mir-122	1	≈ 1–$2\,\mu M$

After the immobilization, the flow rate was raised to 80 µl/min in order to minimize MTL. The binding experiments were performed at 25 °C and at 37 °C for each the unoxidized and the oxidized biotinylated mir-122 molecules.

6.2.5. Data analysis

The data was opened, examined and exported to Scrubber2.0 text-format with SierraSensors Analyzer (Version 1.0.4519.28690). Then the data was opened in Scrubber 2.0a, zeroed, cropped, referenced, and blanked (cf. fig. 6.7 (A) on page 117). For the double referencing two separate values were taken: with option "closest blank" and with "average blank". The average values of the steady-state responses were taken from 20–57 seconds for both differently blanked (cf. fig. 6.7, (B)) and transferred to Excel 2003 for merging together with the exact time-points of injection. Then the average of the two averages was determined. This complicated method was chosen as it gave the most accurate values. For final data analysis and fitting to a single exponential decay, the averaged data was imported into GraphPad Prism 6 (Version 6.01).

6.3. Results

6.3.1. Determination of binding affinity Biotin–Streptavidin with INSTED

After activation the ligand (streptavidin) was immobilized by amine-coupling (cf. section 6.2.4, p. 114) to sensor spot # 2 of a C1 type Amine chip. The first sensor spot acted as a reference spot (compensating refractive index changes and unspecific binding).

In order to minimize mass transport limitations (MTL) I immobilized only between 300–600 RU of streptavidin. This procedure was done 4 times with 4 different chips as the interaction of biotin/streptavidin is not regenerative and it would have taken too long to wait for complete dissociation (at least with the unoxidized one).

As indicator molecules I synthesized a few molecules and tested them for their applicability for the system in a short binding assay (cf. fig. 6.5). I decided to take a 7-mer at $2\,\mu M$ concentrations as indicator-molecule. The attached dT_{20}-linker has no influence on the binding affinity, but accounts for signal enhancement due to its high mass.

Every 90 min. three injections were made: two blank injections of DPBS buffer from two different vials and the indicator molecule at the previously determined $2\,\mu M$ concentration from a third vial. Each of these injections was done with 80 µl at the same flow rate of
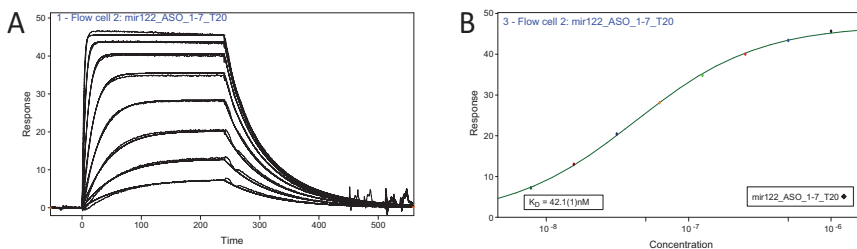
Figure 6.5. – Evaluation of binding affinity of mir-122_ASO_1-7_T20 for determination of optimal concentration of indicator molecule. A) Complete sensorgrams of concentrations from 1 µM down to 7.8 nM, B) steady-state analysis of the data shown in A). The highest concentration is already reaching RU_{max}.

80 µl/min (injection time = 60 sec.). Thereby the steady-state is reached for at least 30 seconds thus enhancing the sensitivity (cf. fig. 6.7 on page 117) The first buffer injection was done for reasons of temperature equilibration (this first injection after 1½ hours disturbs the signal due to temperature fluctuations). The second buffer injection served as reference for the double referencing.

Then the indicator molecule is repeatedly injected over the chip surface in intervals of 1–2 hours.

As the indicator molecule was designed to have a mid-nM affinity ($\approx$100-200 nM), the dissociation rate constant was such that there was no need of regeneration. After several hours, the data was saved and cleared (to prevent data overload). The total amount of injections was therefore divided into 4–5 separate files, although—as mentioned in section 6.1.5—the whole procedure could have recorded within one file.

Fig. 6.6 shows the concatenated files for such a run (in this example the unoxidized biotinylated mir-122 @ 25 °C; blue = reference spot, red = measuring spot with biotinylated mir-122, green = referenced net binding curve).
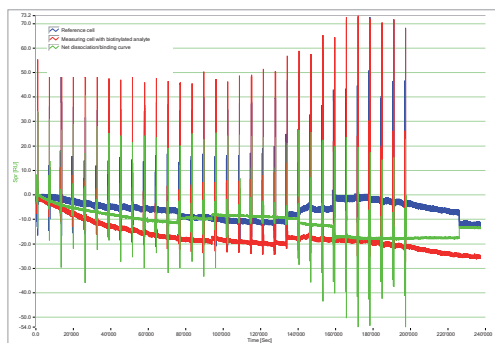
Figure 6.6. – Concatenated indicator molecule injections after processing by SierraSensors Analyzer. As one can see, the net binding curve (green) does (even without saltations) not fit to a 1:1 binding model.

The visual inspection of these concatenated injections of the indicator molecule shows already the disturbances deriving from changes in ambient temperature.

The data was processed as described in section 6.2.5 on page 115. Fig. 6.7 shows the different steps in data processing (above, A) and the resulting overlay of the single time-dependent sensorgrams (left, B). As one can see, the steady-state values are equally dropping from injection to injection (right, C) from 24.5 RU down to 20.5 RU.
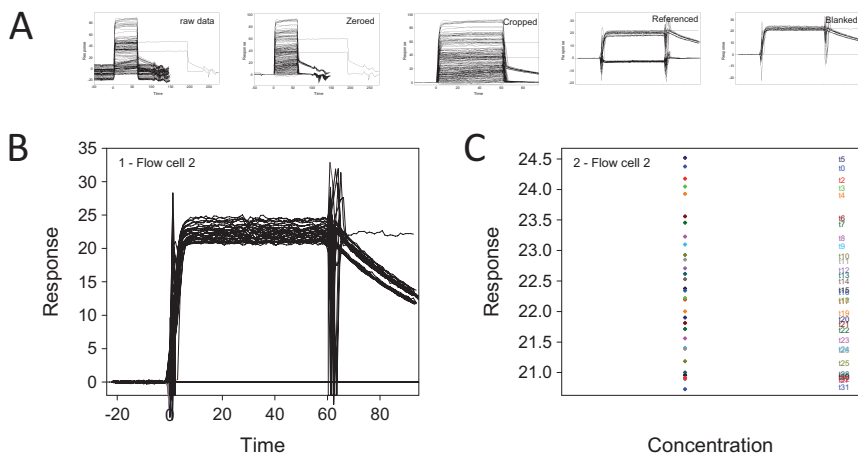

Figure 6.7. – Preparation of the INSTED data. The sensorgrams of the indicator molecule injections are normally processed by Scrubber2.0 (A). The final data for the Analysis (B) shows a constant decrease in steady-state values (C) and can directly be analyzed with GraphPad Prism.

After the importing of the data into GraphPad an exponential one phase decay fit was performed using the constraint that the plateau equals zero. When the data points are plotted against time one can directly see big differences in binding affinity of the oxidized and unoxidized molecules and the big influence of temperature on the half-life of the complexes (cf. fig. 6.8). Table 6.4 lists the values determined by INSTED with analysis by GraphPad. This analysis reveals that the oxidation of biotin reduced the half-life by a factor of roughly 5 at 25 °C and a factor of roughly 7 at 37 °C. As the R^2 values given by GraphPad Prism are very close to zero (values are ranging from 0.9857 to 0.9977) these data fits are of high significance.

Garlick et al. measured their components against avidin at 20 °C. As the affinity of streptavidin is about 100 times weaker and as our measuring temperature was 5 °C higher, the aerial oxidation might therefore probably lead to the α-form, but to be sure further experiments e.g. with NMR have to be performed.

Table 6.4. – Dissociation rate constants, k_d, and half-lives of biotinylated mir-122 against streptavidin as determined by INSTED (values are given with 95 % CI). k_d / [s^{-1}] are calculated as (k_d / [h^{-1}]) / 3600

Compound	Temp. / [°C]	$t_{1/2}$ / [h]	k_d / [h^{-1}]	k_d / [s^{-1}]	R^2 of the fit
mir-122, biot, unoxidized	25	212.9 ± 10.2	3.26 ± 0.15·10^{-3}	9.04 ± 0.41·10^{-7}	0.9857
mir-122, biot, oxidized	25	44.7 ± 0.9	1.55 ± 0.03·10^{-2}	4.31 ± 0.09·10^{-6}	0.9975
mir-122, biot, unoxidized	37	85.4 ± 2.4	8.11 ± 0.22·10^{-3}	2.25 ± 0.06·10^{-6}	0.9977
mir-122, biot, oxidized	37	12.7 ± 0.4	5.47 ± 0.18·10^{-2}	1.52 ± 0.05·10^{-5}	0.9953
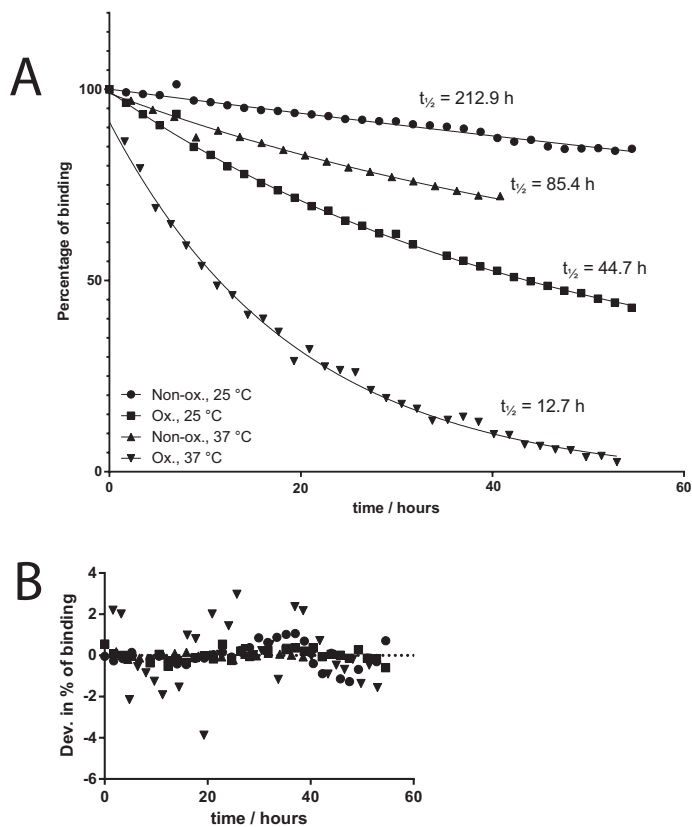
Figure 6.8. – Final plot of the data as given by GraphPad Prism. A) shows the steady-state values against the time and the calculated half-lives / k_d-values. As one can see the oxidized biotinylated mir-122 is almost completely dissociated after 2 days (at 37 °C) B) Residual plot with the same symbols as in A).

6.3.2. Oxidation-inhibition with Anti-oxidants

In order to minimize or even prevent the aerial oxidation of the biotinylated molecules during storage and their concomitant loss of binding affinity, I tested four different antioxidants known in biochemistry for their ability of stabilizing the parent compound. To do so, 5 separate vials containing an aqueous 500 nM solution of a biotinylated loop of the miRNA precursor[v] were prepared. Except one, which acted as a negative control, every vial was provided with one anti-oxidant to yield the following concentrations: 2 mM DTT, 2 mM sodium ascorbate, 1 mM TCEP, and 2 mM β-mercaptoethanol. Immediately after the addition of the anti-oxidants a HPLC analysis was performed (cf. fig. 6.9) and the probes were frozen at -20 ℃. The initial analysis showed an average purity of ≈95 %[vi].

After that, the probes have been thawed in the mixer at RT, vortexed, spun down, and opened for a few seconds as if one would have taken out a sample. This procedure has been performed 12 times on a daily basis over two weeks. After this period a new HPLC analysis of each solution has been performed. Although this was a rather short time, one can already see significant differences as fig. 6.10 shows: during this time, the parent compound and the sodium ascorbate containing solution have been oxidized by about 20 % (cf. fig. 6.11). The chromatograms of the two solutions containing DTT and TCEP were more or less unchanged. The solution containing β-mercaptoethanol showed multiple peaks with a not clearly assignable mass even in the main peak. At this point in time the solutions containing DTT or TCEP were inhibiting the oxidation process by about 80 %.

As further analyses revealed (data not shown), this trend remained over the following months in which the vials were opened on an unregularly basis: The solution containing β-mercaptoethanol was unambiguously completely destroyed. The solution containing sodium ascorbate had no influence on stability. The solution containing DTT was oxidized by about 8 %, the solution with TCEP was oxidized by about 10 %.

For further storage, I recommend the addition of 1 mM TCEP as it is not influencing the immobilization to surface-bound streptavidin (data not shown) and as it is not absorbing at 260 nm and thus not influencing the quantification by UV/VIS measurements.

---

[v]pre-let-7a-2 see table 6.2 on page 114

[vi]This is already oxidation due to lyophilization of the probe and small remaining amounts of oxidized product in the needle-loop of the fraction collector.
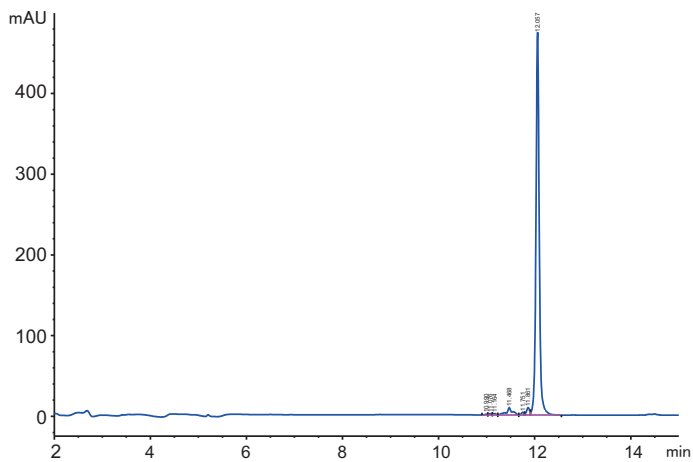
Figure 6.9. – Immediate analysis after addition of the antioxidant. The chromatogram (in this case β-mercaptoethanol) shows only a little fraction of oxidized product (see text).
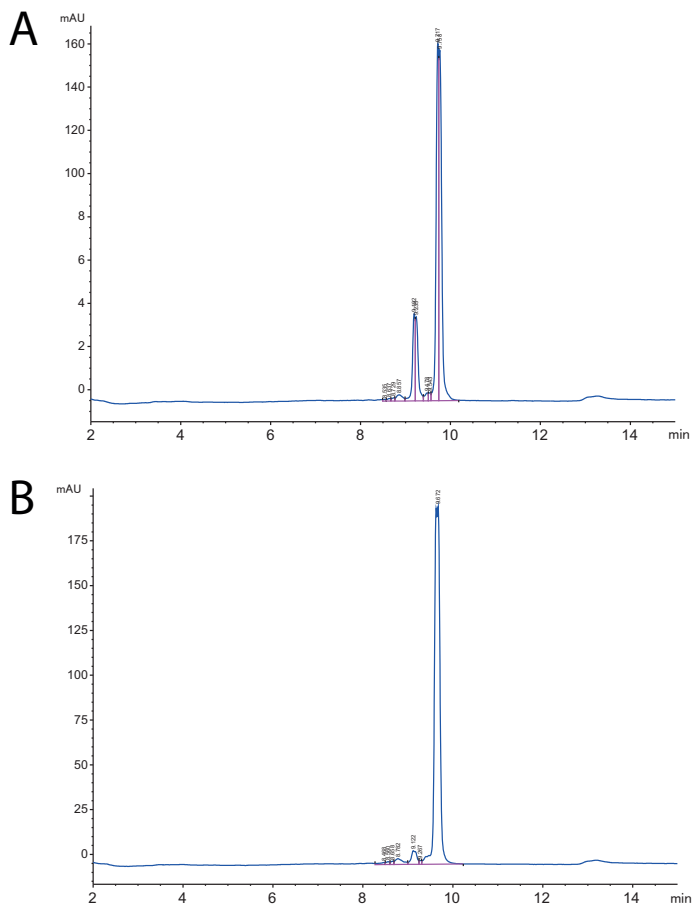
Figure 6.10. – After two weeks of daily thawing/freezing the compounds were substantially oxidized. A) Control solution without addition of an antioxidant. The compound is oxidized to $\approx$ 24 %. B) same solution but with addition of 2 mM DTT. The compound did not further oxidize and shows about 4 % of oxidation as in the beginning (cf. fig. 6.11).
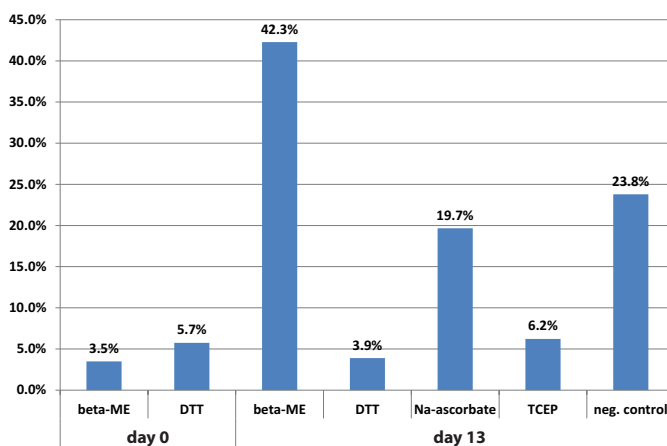
Figure 6.11. – Comparison of oxidation states after two weeks. The solutions containing DTT and TCEP showed no further oxidation. The solution containing β-mercaptoethanol (beta-ME) was already partially decomposed. The solutions containing Na-ascorbate or no antioxidant (neg. control) were oxidized by about 20 %.

7. Discussion and Outlook

7.1. Discussion

7.1.1. Chapter 2: Target Site Accessibility

7.1.1.1. H-Ras "walkaround"

The systematic screen of the decamers against the H-Ras hairpin was meant to be a feasibility study. The binding of different sets of decamers against this hairpin has been performed with gel-shift assays by two independent groups (Lima et al. [109, 110] and Allawi et al. [179]). We tested a set of 37 decamers (including the previously tested oligonucleotides) against this hairpin with SPR in an unimolar screen.

Although the validity of K_D values determined with an unimolar screen may be questionable, there is a clear trend that shows that only the loop-region is amenable for binding of unmodified fully complementary pure RNA decamers at the tested parameters as expected (cf. fig. 2.7, p. 47).

The binding assay against the linear 38-complement revealed the binding of ha_ras_21/22/23 to the loop region of the h-ras hairpin (cf. fig. 2.6, p. 47). Allawi et al. found that the same oligonucleotide binds with a raised affinity by gel shift assay.

In Summary, we obtained similar results as Allawi et al. [179] and to the same extent also Lima et al. [109, 110], although employing a completely different assay. Especially the calculated binding affinities of our best binders are very close to those given by Allawi (cf. table 2.8, p. 49). This indicates that the affinity measurements by SPR are a valuable method for the determination of accessible sites within structured RNA.

Finally, the distribution of 37 decamers over the whole hairpin without the necessity of a ^{32}P-labeling procedure makes the SPR measurements certainly superior to the gel shift assay, especially if the kinetic rate constants, k_a and k_d, can be determined.

7.1.1.2. pre-miR-122 "walkaround"

This is the main part of the investigation of the target site accessibility. A "walkaround" pre-miR-122 in general and an in-depth investigation of the amenability of the loop-region in particular was performed.

From the experiments described in sections 2.3.2.1, 2.3.2.2, and 2.3.2.3 (pp. 51–58) one can draw the following conclusions:

1. As for the hairpin of h-ras the preferred binding site of short complementary oligoribonucleotides lies within the loop region.

2. The 3'-part of the stem seems to be more amenable for binding of short complementary oligoribonucleotides than the 5'-part. This was shown for both, h-ras and pre-miR-122.

3. Depending on the length of the ASO, the preferred binding site is located either in the middle or at the very 3'-end of the loop region. Shorter oligoribonucleotides seem to prefer the middle of the loop region, whereas longer ones seem to bind stronger to the 3'-end of the loop region.

4. Although non of the evaluated ASOs lost its binding affinity, there is a cutoff, above which there is no increase in binding affinity. For pre-miR-122 this cutoff value was 2 nt shorter than the loop region.

5. With a 2'-OMe RNA modified ASO it was possible to raise the binding affinity of an ASO against the hairpin over the binding affinity against the linear complementary sequence.

Especially the fact that we found an oligoribonucleotide with enhanced affinity for the strucutred hairpin is promising as it may raise possibility for enhanced selectivity and potency of antisense-based nucleic acid drugs. Yet, if this is a general trend has to be ruled out with further experiments. The experiments including pre-miR-122 performed with different SPR platforms strongly indicate that pre-miR-122 builds only 1 secondary structure on the chip surface under the employed conditions.

7.1.1.3. Pre-miR-18a loop-screen

Although the screen was performed with only 1 concentration and could not be normalized to a uniform RU_{max} value for oligoribonucleotides longer than 8 nucleotides in length, the SPR2 screen yields a clear result as the same preferred binding site was identified for 4 (of 6) sets of oligoribonucleotides of the same length. Additionally, this preferred binding site seems to be shifted by 3 nt more and more towards the 3'-end the longer the complementary ASO is. Obviously the longer ASOs are able of opening the loop until the next stable stem structure at the position of the bulge whereas the shorter ones aren't. This result is consistent with the results of the screen against pre-miR-122.

The result obtained with Biacore differs for the preferred binding site of ASOs. Whereas for the 7-, 8-, and 9-mers the same preferred binding site was detected, oligoribonucleotides of ≥ 9 nt in length bind with higher affinity to a binding site shifted by 1 nt (this is as well a favourized site in the SPR2 assay) with the bulge at pos. 39 playing a minor role. The reason for this preferred binding site could be explained if one takes a different secondary structure of the hairpin into account. The two most stable secondary structures as given by the folding algorithms of MFold and RNAStructure5.03 are shown in fig. 7.1.

The binding site of pre-miR-18a for the ASOs beginning with 5'-GCUAA... would be complementary to the end of the small tetraloop of the structures 2 and 3 (cf. fig. 7.1, parts B/C) ending at position 37.
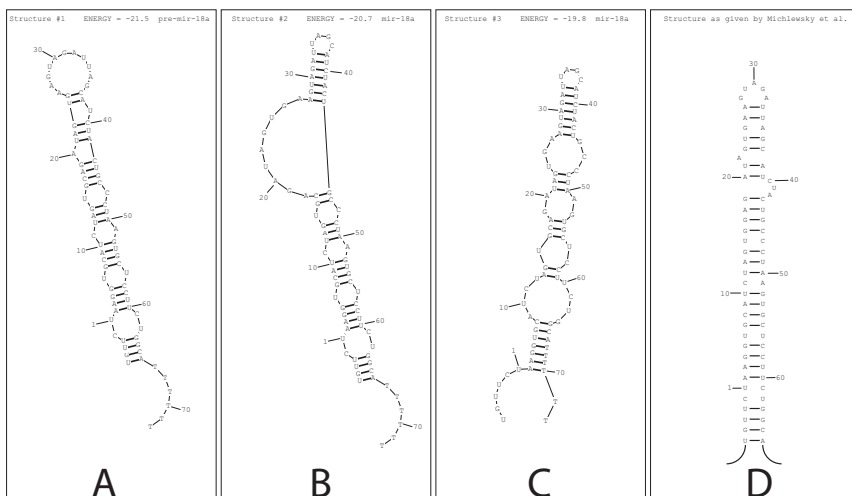
Figure 7.1. – Comparison of 4 different secondary structures of pre-miR-18a. A) most stable secondary structure as given by MFold and RNAStructure5.03. This is the same structure as given by mirbase without the G—U wobble in the loop. B) Second stable structure as given by MFold and RNAStructure5.03. C) Third stable structure as given by RNAStructure. This structure uses 4 of the 6 thymidine nucleotides of the linker for base pairing. D) Structure of pre-miR-18a as proposed by Michlewski et al. [31].

At least with these experiments, the structure of pre-miR-18a as proposed by Michlewski et al. [31] is less probable than the structure given by mirbase (which is in agreement with the calculated structures). The LooptomiR designed for the inhibition of pre-miR-18a processing by Drosha/DGCR8 was included in my screen (sequence 16_2). Based on the experiments and the fact that there are different calculated secondary structures with very close Δ G-values, pre-miR-18a builds most certainly more than one secondary structure on the chip surface as opposed to pre-miR-122 (cf. section 7.1.1.2). However, an in-depth analysis without reliable K_D values is impossible and the artificial system can dramatically change the hairpin on the chip surface (e.g. by interaction with the linker as seen in fig. 7.1, part C). Yet, a rough end-of-dissociation analysis could still be used for the lead identification as shown by fig. 2.22, p. 64).

7.1.1.4. Pre-let-7a-2 loop-screen

The determination of K_D values with the SPR-based affinity measurements is certainly not reliable. First of all the dissociation rate constants cannot be determined reliably within a reasonable time and secondly the dissociation rate lies probably within the same range as the dissociation of the biotin-streptavidin complex (cf. chapter 6). But for a lead-identification based on an affinity ranking this method could be well used as confirmed by ELISA.

The expected best binder ASO 30-14 which ends at the loop was at the second position in both assays. Possibly, this is due to the large size of the loop of pre-let-7a-2 (21 nt) and perhaps a less rigidly defined structure. For larger oligoribonucleotides of length ≥ 19 nt I would expect—based on the previous experiments—the very 3'-end to be the preferred position.

7.1.1.5. Strand-invasion of pre-miR-122 by Miravirsen

The invasion of structure RNAs by modified oligoribonucleotides which induces misfolding of the target RNA has been described. For example, the induced misfolding of group I introns from rRNA genes in pathogenic organisms by short LNA oligoribonucleotides [272] or the inhibition of the RNA component of telomerase by LNA [273].

Here we described the inhibition of Dicer processing by modified LNA/DNA oligoribonucleotides as measured by HPLC and the affinity of SPC3649 and AMO-122 for pre-miR-122 by SPR at 25 °C as example.

Both antimiRs slowed Dicer processing of pre-miR-122 significantly, whereas the non-complementary control sequenced did not. This is consistent with the observations made with SPR which showed an invasion of the stem of the hairpin of pre-miR-122.

SPC3649 is complementary to the bases 2–16 of (pri/pre-)miR-122 which results in a not detectable dissociation of the mature miR-122 (data not shown). Interestingly, the significantly higher dissociation rate against the hairpin of pre-miR-122 is indicating that the remaining bases of the end of the stem (bases 17–2) are capable of slowly forming a hairpin upon switch to buffer at the end of injection. This is consistent with the lower dissociation rate of AMO-122 against pre-miR-122 resulting in a higher binding affinity (AMO-122 is complementary against the full length stem leaving no bases left for formation of internucleotide bonds).

7.1.1.6. Conclusions and summary of chapter 2

With the experiments described in chapter 2 I have shown that the preferred binding sites for complementary oligonucleotides lie within the single-stranded loop region which is consistent with previous findings [109, 179]. Although a preference for the 5'- or 3'-strand would not have been expected, there is strong evidence for a preference for the 3'-strand of the pre-miR-hairpin.

The loop-region, which has been extensively investigated, exhibits different binding sites depending on the ratio between the length of the ASO and the loop-size: short ASOs with a length of at least 4 nt shorter than the length of the single stranded nucleotides of the loop seem to bind best right in the middle region of the loop, whereas longer ASOs with a length of $\geq$ n-3 (with n = loopsize) tend to bind with higher affinity to bases at the very end of the loop in my assays. For this region the following three cases can be stated for the pre-miR-122 assay:

1. For an optimal selectivity the length of the ASO was n-3 (in the case of pre-miR-122 the 9-mer 26-9). For 2'-OMe RNA the affinity was even higher for the hairpin than for the linear complement. This effect was seen a few times which confirm this finding (data not shown). The 9-mer beginning at the 5'-site of the loop had always higher binding affinities, but as this was as well the case for the linear complement this is most certainly a sequence-specific effect.

2. The optimal blend of binding affinity and selectivity was given for the ASO with length n-2. These ASOs had the highest identical binding affinity towards the hairpin and the loop.

3. The highest reasonable binding affinity was achieved with the ASOs of length n-1. For both, RNA and 2'-OMe RNA the affinity was doubled compared to the ASO bearing one nucleotide less (20 nM vs. 10 nM for RNA and 2.3 nM vs. 1 nM for 2'-OMe RNA). For this doubled affinity the selectivity has to be sacrificed: the affinity against the linear target was at least 50-fold higher (10.1 nM vs. 0.19 nM). All oligoribonucleotides above this length had no significant increase in binding affinity compared to the linear target.

This rule was true for both, RNA and 2'-OMe RNA. The fact that ASOs of a length $\geq$ n-1 were all binding within approximately the same range of binding affinity, indicates that for each ASO about the same number of nucleotides was involved in binding (with the constraint of same binding mechanism): against the linear loop-region there was a constant increase in binding affinity with each added nucleotide (except for the 2'-OMe 11-mer which could well be in the range of measurement uncertainty, cf. fig 2.18, p. 60).

Further, I showed that the increase in binding affinity with longer oligonucleotides is mostly due to a decrease of the dissociation rate (cf fig. 2.16, p. 58). Seeking for an optimal "drug residence time" [274] this is to our favour.

Finally, I showed that SPR-based affinity measurements can—even when not yielding precise K_D values—be used for target validation/lead discovery purposes as presented in section 2.3.4, p. 63.

7.1.2. Chapter 4: Enhancement of binding-affinity with modifications

In collaboration with two coworkers of our group I tested large series of modified LooptomiRs. The modifications which were selected from a published set of known RNA-binding small molecules, were attached at either the 5'-position of the uracil of a uridine or at the 2'-position of the ribose. The LooptomiR for the modification was based on a systematic screen of short 2'-OMe oligoribonucleotides around the loop region of pre-miR-122 and by *in vitro* assays performed by L. Gebert.

This investigation revealed that the binding affinity of a short complementary LooptomiR can be raised by a factor of up to $\sim$ 30-fold compared to the unmodified parent compound. This was achieved with the attachment of only 1 spermine molecule at the 5'-position of the uracil of uridine. A similar yet smaller raise in affinity was achieved by the attachment of three molecules to the LooptomiR: two spermines and one quinolinone which resulted in a sub-nM affinity. These molecules are currently tested in our lab for *in vitro* activity in cellular assays.

The attachment of a spermine to the 5'-position of the uracil resulted in a raised association rate and a decreased dissociation rate (cf. inset in fig. 4.5). Artifacts due to charge-charge interactions could be excluded (data not shown) as the length of the linker was deciding the fate of the binding affinity.

These findings may establish a good starting-point for the development of highly selective antisense-based nucleic acid drugs. Despite the vast amount of tested oligonucleotides it is difficult to give general rules for the optimal chemistry/position of the modifications.

7.1.3. Chapter 5: RNase H assay

7.1.3.1. RNase H - human vs. E. coli

For our experiments we used a commercially available enzyme expressed from *E. coli*. To our best knowledge there was no human RNase available on the market at the time of execution of the experiments. Research groups reporting experiments with human RNase H were extracting the enzyme themselves, e.g. Nowotny et al. who expressed the enzyme in *E. coli* from pET15-based vector [252]. Lima et al. report an up to 40-fold higher affinity of human RNase H1 for the heteroduplex than for the RNase H from *E. coli* [95] which could yield even better results than we observed with our oligonucleotides. On the other hand, we used DNA ASOs and the expected cleavage extent for modified gapmers is expected to be half as much as compared with the unmodified DNA ASOs (cf. section 5.1.1.3 on page 87). Finally, the human RNase H1 was reported to cleave further from the RNA-5'-end than the RNase H from *E. coli*. As the loop of pre-miR-122 is only 12 Nucleotides in length (cf. fig. 7.2), this could eventually ruin the possibility of RNase H-induction of our loop-binders. Certainly, more experiments have to be performed in order to evaluate the impact on modified DNA-gap-mers on the induction of RNase H mediated cleavage of structured microRNA precursors.

7.1.3.2. The necessity of annealing in our experiments

As shown in chapter 2 the affinity of pure DNA oligonucleotides for the hairpin of pre-miR-122 is rather low. From this perspective it is rather astonishing that they were at all able to induce RNase H mediated cleavage in the hairpin. The fact that we had to perform an annealing procedure for them to work indicates that they bind stably enough after disruption of the secondary structure of the hairpin. The fact that this temperature-based annealing is not available in a cellular environment, raises certainly the question of the efficacy of our oligonucleotides *in vivo*. However, the fact that a single annealing procedure was enough for the same amount of cleavage with 2.4-fold lower concentration of the DNA ASO and 1.2-fold lower concentrations remains unclear. As a cellular environment contains in any case a vast amount of proteins and other interacting ribonucleic acids that possibly interfere with this interaction (such as e.g. RNA chaperons, RNA annealers, RNA helicases, etc.), further cell-based experiments have to be performed.

7.1.3.3. PAGE experiments

The attraction of a PAGE-based enzymatic assay is its easy of use, costs, and sensitivity. Furthermore the need for small amounts of analytes makes this a method-of-choice for feasibility studies. Although we could not identify the cleavage fragments this method was suitable for a quantification of the cleavage. As the staining of very short fragments fails one would have switch to other methods such as e.g. radioactivity-based gel experiments or—as we did—HPLC-based methods.

With our PAGE-experiments we could reproduce known properties of the enzyme (no cleavage of RNA/RNA or DNA/DNA duplexes) and the ability of our DNA ASOs to induce RNase H mediated cleavage in a catalytic manner.

Additionally could make a rough estimation of the binding affinity for the RNase H / hetero-duplex complex (cf. fig. 5.6 on page 96).

However, the impact of these ASOs remains unclear in the case of the hairpin (cf. previous paragraph)

7.1.3.4. LC/MS experiments

This method was perfectly suitable not only for the detection and identification of even small cleavage products, but as well for the identification of cleavage sites and extent of cleavage. A disadvantage was certainly the need of higher amounts of analytes: whereas the amounts of analytes in the PAGE experiments were between 16–40 ng, we used between 260–1100 ng for the HPLC assay. As the deconvolution of molecules with higher molecular weights needs even higher amounts, this prevented the identification of cleavage products in the case of the hairpin.

7.1.4. Chapter 6: INSTED

Although there are plenty of paper describing the interaction of (strept)avidin and biotin (some of them are described in the paper of Piramowicz [275] or Wong [276] et al.), most of them are using AFM methodologies yielding only thermodynamic parameters. However, there are only a few papers which report k_d values for this interaction and none of them is providing any information about the oxidation-state of the biotin (moiety). The values given for the dissociation rate are contradictory: Piran and Riordan [277] give a value of $2.4 \cdot 10^{-6} \, \text{s}^{-1}$. Chilkoti and Stayton [278] give a value of $5.4 \cdot 10^{-6} \, \text{s}^{-1}$. Qureshi et al. do not provide a value for k_d, but they give a value for ka ($5.13 \cdot 10^{6} \, \text{M}^{-1}\text{s}^{-1}$). Assuming a K_D of $4 \cdot 10^{-14} \, \text{M}$ as reported by Broder et al. [279] this would give an estimation for a k_d value of $\approx 2 \cdot 10^{-7} \, \text{s}^{-1}$. Our determined value for the unoxidized form at 25 °C lies between these values.

Although the concentration of the indicator molecule should not necessarily yield surface saturation (RU_{max}) this is desired as it reduces the influence of concentration changes.

Although there are examples that a lower dissociation rate constant does not provide more bioactivity [280, 281], it is generally regarded to be optimal when selecting not only the drugs with the highest affinity, but preferentially those with the lowest dissociation rate constant for optimal drug-target residence time thus reducing off-target toxicity while enhancing biological activity [274, 282]. However, the kinetic properties of the drug-target interaction certainly play a crucial role in drug development not only for protein-protein interactions [283], but as well for protein-RNA/DNA and RNA/DNA-RNA/DNA interactions.

For the optimal design, improvement and development of antagomirs/loop-to-mirs for modulation/inhibition of miRNA biosynthesis an in-depth characterization of kinetic binding constants is often required as one might want to choose not only the ones with the highest binding affinities but maybe the ones with the lowest off-rates.

With INSTED I provide a robust and reliable method for the determination of extremely low dissociation rate constants, k_d, in the range of 10^{-6} / 10^{-7} which is completely independent of ambient temperature and other measurement related fluctuations.

Additionally, when measuring the K_D (thus k_d) values of high-affinity molecules against a biotinylated ligand on the chip surface, my experiments showed that it is very likely to be highly influenced by the dissociation of biotin–streptavidin. In extreme cases one measures more probably this interaction than the target interaction. Especially when performing a large kinetic screen over a longer period of time like I did (cf. section 2.3 on page 43) with analytes of highly different equilibrium dissociation constants, a uniform RU_{max} value is very important. This is not given for the conventional biotin–streptavidin system.

I showed the applicability of INSTED for the biotin–streptavidin system. A similar assay for the investigation of other interactions like e.g. for the interaction of an antibody with an antigen could be very possible. In such an assay (with the antigen covalently immobilized on the chip surface) one could try an (unspecific) low-affinity binder against the Fc region as indicator molecule for the antibody (in solution).

Most probably this method is not applicable for large screens of high-affinity molecular interactions. On the other hand it could be conceivable that a specially designed assay is able of measuring *multiple* dissociation rate constants on *one* spot: if the specificities of the indicator molecules are high enough and if they are not disturbing the binding / dissociation of the other molecules there are theoretically no limits....

7.2. Outlook: Implication for optimal design of further DNA-like antisense oligonucleotides

The primary sequence of a target RNA is normally well-known and therefore one can easily design an ASO perfectly complementary to this RNA. However, the secondary structure of the target RNA can strongly change the predicted binding affinity of such a designed ASO. We therefore determined the equilibrium dissociation constants of a series of ASOs to its structured RNA target in order to embrace the diminished/raised binding affinities due to structure (cf. chapter 2). These systematic screens revealed in all probability preferred binding sites at the very 3'-end of the single-stranded loop region of a microRNA hairpin precursor, even though the "final" binding affinity in a cellular environment might be different.

In chapter 4 I showed (in collaboration with other group members) that it was possible to raise the binding affinity of such a LooptomiR for its (linear) target by a factor of ∼30 by the attachment of a spermin moiety.

As shown by many groups, a central window (gap) of unmodified DNA nucleotides in gap-mers with an O4'-endo confirmation is needed by RNase H1 as alkoxy-modified sugars as well as substitutions of the phosphodiester linkage of the phosphate backbone blocked the enzymatic activity.

As a consensus in the found literature, this window should comprise at least 7 DNA nucleotides.

As we showed that spermine-modified oligonucleotides were greatly enhancing the binding affinities of Watson-Crick base-paired antisense-oligonucleotides this could be a possible way of enhancing as well the potency of RNase H-inducing DNA-like gapmers. Nowotny et al. showed that the majority of the binding interaction happens along the minor groove of the hybrid [230]. The base modifications developed in our lab which point towards the major groove could therefore be in general a good way of enhancing the binding affinity whilst
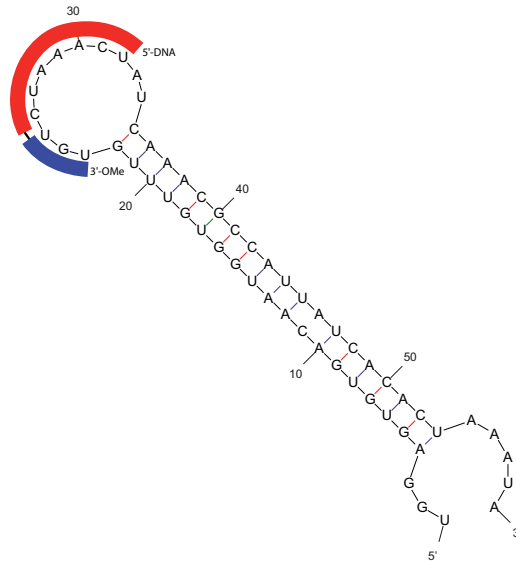
Figure 7.2. – Scheme of the hairpin of pre-miR-122 with a suggested ASO-design for the induction of RNase H mediated cleavage. Putative structure was calculated by MFold and is in accordance to the structure reported by Mirbase.

still enabling this interaction. But as outlined in fig. 5.2 (part A), p. 86 the possibilities for attachment of such modifications are rare. Fig. 7.3 shows an enlarged stereo-view of this region at the 5'-RNA/3'-DNA terminus.

As we showed, the 9-mer DNA which was beginning at the predicted loop of pre-miR-122 was exhibiting much greater RNase H-induction in the linear complement. Therefore, for further investigations of the potency of DNA-like gapmers against pre-miR-122, I would suggest to use a 10-mer nucleotide as shown in fig. 7.2 with 3 2'-OMe-modified RNA moieties (blue), 7 DNA nucleotides at positions 4-10 (red) and a spermine modification at positions 2 or 3.
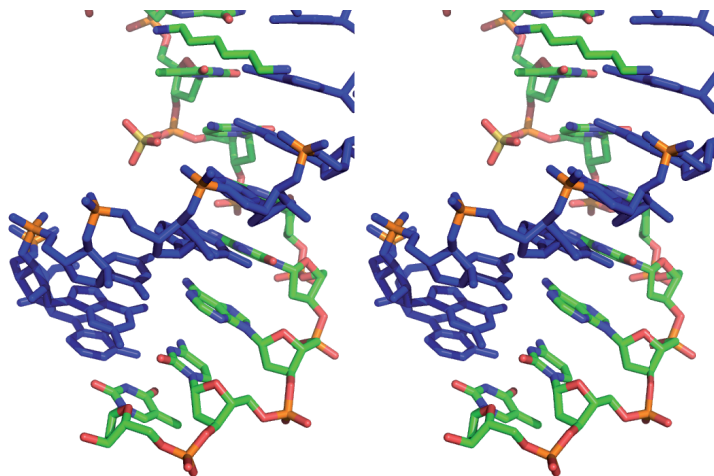
Figure 7.3. – Stereo view of the enlarged RNA-5'-/DNA-3'-end of the duplex shown in fig. 5.2 (without enzyme). The target RNA strand is shown in blue with brown phosphorus atoms of the backbone. Figure was mady with Pymol from the published structure.

A. Supplementary tables

Assay	Name	Sequence	Mass	Immobilization level
H-ras	C21 (control)	5'-ACAGAUAAUUGAUUUAGAUUU-B-3'	7'237.7 g/mol	1467 RU
	h-ras	5'-GGUGGUGGUGGGCGCCGUCGUGUGG- -GCAAGAGUGCGCUGACCAUCCTTTTTT-B-3'	17'686.0 g/mol	1251 RU
	33-complement	5'-CGUCGGUGUGUUU-B-3'	4'681.1 g/mol	971 RU
	38-complement	5'-GUGUGGGCAAUUU-B-3'	4'728.1 g/mol	1029 RU
pre-miR-122 I	pre_mir_122	5'-UGGAGUGUGACAAUGGUGUUUGUGUCUAAA- -CUAUCAAACGCCAUUAUCACACUAAAAUATTTTTT-B-3'	20'948 g/mol	993.7 RU
	control1_8_14	5'-UGACAAUTTTTTT-B-3'	4'583.2 g/mol	171.3 RU
	control2_26_32	5'-CUAAACUTTTTTT-B-3'	4'543.17 g/mol	168.4 RU
pre-miR-18a I	pre-miR-18a	5'-UGUUCUAAGGUGCAUCUAGUGCAGAUAGUGAAGUAGAUUA- -GCAUCUACUGCCCUAAGUGCUCCUUCUGGCA-TTTTTT-B-3'	25'111.4 g/mol	150 RU
pre-miR-18a II				175 RU
pre-let-7a-2	pre-let-7a-2	5'-UGAGGUAGUAGGUUGUAUAGUUUAGAAUUA- -CAUCAAGGGAGAUAACUGUACAGCCUCCUAGCUUUCC-B-3'	22'072.5 g/mol	158 RU
	pre-let-7a-2, loop region	5'-UAGAAUUACAUCAAGGGAGAU-TTTTTT-B-3'	9'163 g/mol	60 RU
	pre-miR-122	5'-UGGAGUGUGACAAUGGUGUUUGUGUCUAAA- -CUAUCAAACGCCAUUAUCACACUAAAAUATTTTTT-UB-3'	21'166 g/mol	207 RU

Table A.1. – Ligands used for the screens

Assay	Maschine	Chip	Temperature	Flow rate	Buffer	Reg. sol.	Control
H-ras	Biacore 3000	SA	25 ℃	20 µl·min^{-1}	HEPES	1 mM HCl, 30 sec.	—
pre-miR-122 I	Biacore T-100	Series S SA	25 ℃	10 µl·min^{-1}	HBS–P+	1 mM HCl, 30 sec.	oligo_26
pre-miR-122 II	Biacore 3000	SA	25 ℃	30 µl·min^{-1}	HEPES	1 mM HCl, 30 sec.	—
pre-miR-122 III	Biacore T-100	Series S SA	25 ℃	50 µl·min^{-1}	TRIS	1/2 mM HCl, 30 sec.	—
pre-miR-18a I	SPR2	Amine	25 ℃	25 µl·min^{-1}	TRIS	10 mM EDTA, 108 sec.	—
pre-miR-18a II	SPR2	CM5	25 ℃	30 µl·min^{-1}	TRIS	5 mM EDTA, 3 mM HCl, 15 sec.	—
pre-let-7a-2	Biacore T-100	Series S SA	25 ℃	50 µl·min^{-1}	TRIS	2 mM HCl, 20 sec., 20 µl·min^{-1}	—

Table A.2. – Conditions used for the screens

Name	Sequence	Mass	Affinity against		
			h-ras hairpin	33-complement	38-complement
ha_ras_18	CACCACCACC	3061.93 g/mol	563 nM	23636 nM	1000 nM
ha_ras_19	CCACCACCAC	3061.93 g/mol	625 nM	36796 nM	847 nM
ha_ras_20	CCCACCACCA	3061.93 g/mol	389 nM	40145 nM	118 nM
ha_ras_21	GCCCACCACC	3077.93 g/mol	12 nM	9120 nM	0.80 nM
ha_ras_22	CGCCCACCAC	3077.93 g/mol	56 nM	14288 nM	4 nM
ha_ras_23	GCGCCCACCA	3117.96 g/mol	30 nM	11129 nM	0.60 nM
ha_ras_24	GGCGCCCACC	3133.96 g/mol	1625 nM		113 nM
ha_ras_25	CGGCGCCCAC	3133.96 g/mol	n.a.		844 nM
ha_ras_26	ACGGCGCCCA	3157.99 g/mol	n.a.		
ha_ras_27	GACGGCGCCC	3173.99 g/mol	n.a.		
ha_ras_28	CGACGGCGCC	3173.99 g/mol	388 nM	20204 nM	
ha_ras_29	CCGACGGCGC	3173.99 g/mol	56 nM	11 nM	5477 nM
ha_ras_30	ACCGACGGCG	3198.02 g/mol	66 nM	42 nM	
ha_ras_31	CACCGACGGC	3157.99 g/mol	71 nM	15 nM	
ha_ras_32	ACACCGACGG	3182.02 g/mol	67 nM	5.7 nM	
ha_ras_33	**CACACCGACG**	3141.99 g/mol	30 nM	**0.87 nM**	2556 nM
ha_ras_34	CCACACCGAC	3101.96 g/mol	29 nM	7.4 nM	225 nM
ha_ras_35	CCCACACCGA	3101.96 g/mol	31 nM	13 nM	21 nM
ha_ras_36	GCCCACACCG	3117.96 g/mol	2 nM	363 nM	0.38 nM
ha_ras_37	UGCCCACACC	3078.92 g/mol	25 nM	32469 nM	5 nM
ha_ras_38	**UUGCCCACAC**	3079.91 g/mol	9 nM	27372 nM	**0.54 nM**
ha_ras_39	CUUGCCCACA	3079.91 g/mol	38 nM		7 nM
ha_ras_40	UCUUGCCCAC	3056.87 g/mol	44 nM		12 nM
ha_ras_41	CUCUUGCCCA	3056.87 g/mol	29 nM		158 nM
ha_ras_42	ACUCUUGCCC	3056.87 g/mol	24 nM		1014 nM
ha_ras_43	CACUCUUGCC	3056.87 g/mol	54 nM		
ha_ras_44	GCACUCUUGC	3096.9 g/mol	68 nM		
ha_ras_45	CGCACUCUUG	3096.9 g/mol	104 nM		
ha_ras_46	GCGCACUCUU	3096.9 g/mol	146 nM		1996 nM
ha_ras_47	AGCGCACUCU	3119.94 g/mol	100 nM	73945 nM	1753 nM
ha_ras_48	CAGCGCACUC	3118.95 g/mol	44 nM	59298 nM	3950 nM
ha_ras_49	UCAGCGCACU	3119.94 g/mol	73 nM	96206 nM	10976 nM
ha_ras_50	GUCAGCGCAC	3158.98 g/mol	34 nM	86013 nM	15794 nM
ha_ras_51	GGUCAGCGCA	3199.01 g/mol	5 nM		
ha_ras_52	UGGUCAGCGC	3175.97 g/mol	7 nM		
ha_ras_53	AUGGUCAGCG	3200 g/mol	n.a.		
ha_ras_54	GAUGGUCAGC	3200 g/mol	3 nM		

Table A.3. – The 37 analyte RNA-oligos used for the binding assay against ha-Ras. The oligos were provided by M. Zimmermann.

Name	Sequence	Calc. ε / [l·mol^{-1}·cm^{-1}]	Mass / [g/mol]	Affinity / [µM]
mir122-aso-1	CACUCCA	76800	2221.5	
mir122-aso-2	ACACUCC	76800	2221.5	
mir122-aso-3	CACACUC	76800	2221.5	
mir122-aso-4	UCACACU	77800	2222.5	
mir122-aso-5	GUCACAC	81500	2261.6	500
mir122-aso-6	UGUCACA	82500	2262.6	
mir122-aso-7	UUGUCAC	77100	2239.5	
mir122-aso-8	AUUGUCA	83500	2263.5	
mir122-aso-9	CAUUGUC	77100	2239.5	
mir122-aso-10	CCAUUGU	77100	2239.5	118
mir122-aso-11	ACCAUUG	82500	2262.6	
mir122-aso-12	CACCAUU	77800	2222.5	
mir122-aso-13	ACACCAU	83200	2245.6	21
mir122-aso-14	AACACCA	88600	2268.6	
mir122-aso-15	AAACACC	88600	2268.6	
mir122-aso-16	CAAACAC	88600	2268.6	
mir122-aso-17	ACAAACA	95000	2292.6	
mir122-aso-18	CACAAAC	88600	2268.6	
mir122-aso-19	ACACAAA	95000	2292.6	
mir122-aso-20	GACACAA	93300	2308.6	75
mir122-aso-21	AGACACA	93300	2308.6	38.1
mir122-aso-22	UAGACAC	87900	2285.6	29.1
mir122-aso-23	UUAGACA	88900	2286.6	16.38
mir122-aso-24	UUUAGAC	83500	2263.5	22.3
mir122-aso-25	**GUUUAGA**	**88200**	**2303.6**	**0.466**
mir122-aso-26	**AGUUUAG**	**88200**	**2303.6**	**0.986**
mir122-aso-27	UAGUUUA	84500	2264.5	12.5
mir122-aso-28	AUAGUUU	84500	2264.5	9.4
mir122-aso-29	GAUAGUU	88200	2303.6	8.26
mir122-aso-30	UGAUAGU	88200	2303.6	17.1
mir122-aso-31	UUGAUAG	88200	2303.6	26.8
mir122-aso-32	UUUGAUA	84500	2264.5	150
mir122-aso-33	GUUUGAU	82800	2280.5	25.2
mir122-aso-34	CGUUUGA	81800	2279.5	27.5
mir122-aso-35	GCGUUUG	80100	2295.5	19.3
mir122-aso-36	GGCGUUU	80100	2295.5	25.6
mir122-aso-37	UGGCGUU	80100	2295.5	32
mir122-aso-38	AUGGCGU	85500	2318.6	18.8
mir122-aso-39	AAUGGCG	90900	2341.6	29
mir122-aso-40	UAAUGGC	87200	2302.6	31
mir122-aso-41	AUAAUGG	93600	2326.6	37
mir122-aso-42	GAUAAUG	93600	2326.6	22.7
mir122-aso-43	UGAUAAU	89900	2287.6	90
mir122-aso-44	GUGAUAA	93600	2326.6	14.2
mir122-aso-45	UGUGAUA	88200	2303.6	14.4
mir122-aso-46	GUGUGAU	86500	2319.6	8.2
mir122-aso-47	AGUGUGA	91900	2342.6	2.72
mir122-aso-48	UAGUGUG	86500	2319.6	3.8
mir122-aso-49	UUAGUGU	82800	2280.5	4.13
mir122-aso-50	UUUAGUG	82800	2280.5	7.5
mir122-aso-51	AUUUAGU	84500	2264.5	15.4
mir122-aso-52	UAUUUAG	84500	2264.5	66

Table A.4. – The 52 analytes used in the binding assay against pre-miR-122. The molar extinction coefficient were calculated as described. The two best binders targeting the loop region are highlighted in bold. The K_D values were calculated with a uniform RU$_{max}$ value as described in section 2.3.2.1, p. 51

Name	Sequence	Mass / [g/mol]
mir122_loop_7mer-aso1	UAGACAC	2285.6
mir122_loop_7mer-aso2	UUAGACA	2286.59
mir122_loop_7mer-aso3	UUUAGAC	2263.55
mir122_loop_7mer-aso4	GUUUAGA	2303.58
mir122_loop_7mer-aso5	AGUUUAG	2303.58
mir122_loop_7mer-aso6	UAGUUUA	2264.54
mir122_loop_7mer-aso7	AUAGUUU	2264.54
mir122_loop_7mer-aso8	GAUAGUU	2303.58
mir122_loop_7mer-aso9	UGAUAGU	2303.58
mir122_loop_7mer-aso10	UUGAUAG	2303.58
mir122_loop_7mer-aso11	UUUGAUA	2264.54
mir122_loop_8mer-aso1	UUAGACAC	2605.79
mir122_loop_8mer-aso2	UUUAGACA	2606.78
mir122_loop_8mer-aso3	GUUUAGAC	2622.78
mir122_loop_8mer-aso4	AGUUUAGA	2646.81
mir122_loop_8mer-aso5	UAGUUUAG	2623.77
mir122_loop_8mer-aso6	AUAGUUUA	2607.77
mir122_loop_8mer-aso7	GAUAGUUU	2623.77
mir122_loop_8mer-aso8	UGAUAGUU	2623.77
mir122_loop_8mer-aso9	UUGAUAGU	2623.77
mir122_loop_8mer-aso10	UUUGAUAG	2623.77
mir122_loop_9mer-aso1	UUUAGACAC	2925.99
mir122_loop_9mer-aso2	GUUUAGACA	2966.02
mir122_loop_9mer-aso3	AGUUUAGAC	2966.02
mir122_loop_9mer-aso4	UAGUUUAGA	2967.01
mir122_loop_9mer-aso5	AUAGUUUAG	2967.01
mir122_loop_9mer-aso6	GAUAGUUUA	2967.01
mir122_loop_9mer-aso7	UGAUAGUUU	2943.97
mir122_loop_9mer-aso8	UUGAUAGUU	2943.97
mir122_loop_9mer-aso9	UUUGAUAGU	2943.97
mir122_loop_10mer-aso1	GUUUAGACAC	3285.23
mir122_loop_10mer-aso2	AGUUUAGACA	3309.26
mir122_loop_10mer-aso3	UAGUUUAGAC	3286.22
mir122_loop_10mer-aso4	AUAGUUUAGA	3310.25
mir122_loop_10mer-aso5	GAUAGUUUAG	3326.25
mir122_loop_10mer-aso6	UGAUAGUUUA	3287.21
mir122_loop_10mer-aso7	UUGAUAGUUU	3264.17
mir122_loop_10mer-aso8	UUUGAUAGUU	3264.17
mir122_loop_11mer-aso1	AGUUUAGACAC	3628.46
mir122_loop_11mer-aso2	UAGUUUAGACA	3629.45
mir122_loop_11mer-aso3	AUAGUUUAGAC	3629.45
mir122_loop_11mer-aso4	GAUAGUUUAGA	3669.48
mir122_loop_11mer-aso5	UGAUAGUUUAG	3646.44
mir122_loop_11mer-aso6	UUGAUAGUUUA	3607.4
mir122_loop_11mer-aso7	UUUGAUAGUUU	3584.36
mir122_loop_12mer-aso1	UAGUUUAGACAC	3948.66
mir122_loop_12mer-aso2	AUAGUUUAGACA	3972.69
mir122_loop_12mer-aso3	GAUAGUUUAGAC	3988.69
mir122_loop_12mer-aso4	UGAUAGUUUAGA	3989.68
mir122_loop_12mer-aso5	UUGAUAGUUUAG	3966.64
mir122_loop_12mer-aso6	UUUGAUAGUUUA	3927.6
mir122_loop_13mer-aso1	AUAGUUUAGACAC	4291.9
mir122_loop_13mer-aso2	GAUAGUUUAGACA	4331.93
mir122_loop_13mer-aso3	UGAUAGUUUAGAC	4308.89
mir122_loop_13mer-aso4	UUGAUAGUUUAGA	4309.88
mir122_loop_13mer-aso5	UUUGAUAGUUUAG	4286.84
mir122_loop_14mer-aso1	GAUAGUUUAGACAC	4651.13
mir122_loop_14mer-aso2	UGAUAGUUUAGACA	4652.12

Table A.5.

Analyte	2'-chemistry		
	RNA	OMe	DNA
mir122_loop_ASO_B11	100 nM	10 nM	20 µM
mir122_loop_ASO_C02	2 µM	10 nM	20 µM
mir122_loop_ASO_C10	100 nM	10 nM	20 µM
mir122_loop_ASO_D05	100 nM	10 nM	2 µM
mir122_loop_ASO_D11	20 nM	10 nM	1 µM
mir122_loop_ASO_E04	20 nM	10 nM	1 µM
mir122_loop_ASO_E09	20 nM	10 nM	1 µM

Table A.6. – Start concentrations of the loop-binders for the 2-fold dilution series for the determination of affinity. The concentrations were adjusted to the affinities based on preliminary experiments.

A

DNA vs. linear complement, 25 °C, TRIS   e.m. = error margin

	k_d	e.m. of k_d	k_a	e.m. of k_a	K_D	e.m. of K_D	error in %
B11					1.22 uM		
C02					12.9 uM		
C10					5.79 uM		
D05	5.49E-02	6.20E-05	2.96E+05	3.90E+02	185 nM ± 0.45 nM		0.2%
D11	2.00E-02	4.50E-05	3.76E+05	9.20E+02	53.2 nM ± 0.25 nM		0.5%
E4	5.93E-04		3.53E+05		1.68 nM		
E9	8.74E-06		3.12E+05		28 pM		

RNA vs. linear complement, 25 °C, TRIS

	k_d	e.m. of k_d	k_a	e.m. of k_a	K_D	error in %
B11, 9-mer	4.67E-03	6.30E-06	1.03E+06	1.60E+03	4.5 nM ± 0.01 nM	0.3%
C02, 9-mer	9.60E-02	2.20E-04	5.05E+05	1.40E+03	190 nM ± 1 nM	0.5%
C10, 10-mer	1.18E-02	1.40E-05	8.73E+05	1.20E+03	13.5 nM ± 0.03 nM	0.3%
D05, 11-mer	2.94E-04	6.40E-07	1.54E+06	4.00E+03	191 pM ± 0.9 pM	0.5%
D11, 12-mer	4.32E-05	8.30E-07	1.36E+06	4.00E+03	31.8 pM ± 0.7 pM	2.2%
E4, 13-mer	1.17E-05	1.00E-07	1.46E+06	5.10E+03	8.0 pM ± 0.1 pM	1.2%
E9, 14-mer	4.39E-07	2.50E-07	1.39E+06	5.40E+03	315 fM ± 180 fM	57.3%

2'-OMe-RNA vs. linear complement, 25 °C, TRIS

	k_d	e.m. of k_d	k_a	e.m. of k_a	K_D	error in %
B11	6.11E-04	2.00E-06	9.33E+05	4.90E+03	655 pM ± 6 pM	0.9%
C02	1.05E-02	5.80E-05	5.36E+05	2.00E+04	19.5 nM ± 0.8 nM	4.3%
C10	1.31E-03	2.30E-06	5.70E+05	1.90E+03	2.3 nM ± 0.01 nM	0.5%
D05	1.02E-05	4.20E-06	1.66E+06	4.80E+04	6.2 pM ± 2.7 pM	43.9%
D11	6.77E-05	3.70E-06	1.17E+06	4.60E+03	58 pM ± 3 pM	5.9%
E4	1.76E-05	1.50E-06	1.40E+06	1.10E+03	13 pM ± 1 pM	8.6%
E9	9.35E-07	1.50E-06	1.23E+06	1.90E+03	0.8 pM ± 1.2 pM	160.5%

B

DNA vs. pm122-hairpin

	k_d	e.m. of k_d	k_a	e.m. of k_a	K_D	e.m. of K_D	error in %
B11					n.a.		
C02					22.8 uM		
C10					19.1 uM		
D05					n.a.		
D11					n.a.		
E4					n.a.		
E9					n.a.		

RNA vs. pm122-hairpin

	k_d	e.m. of k_d	k_a	e.m. of k_a	K_D	error in %
B11	4.71E-03	1.30E-05	2.15E+05	1.30E+03	22 nM ± 0.2 nM	0.9%
C02	4.78E-02	7.10E-05	2.36E+05	4.80E+02	203 nM ± 0.7 nM	0.4%
C10	2.70E-02	3.60E-04	1.36E+06	1.80E+04	19.9 nM ± 0.5 nM	2.7%
D05	7.27E-03	1.50E-04	7.21E+05	1.50E+04	10.1 nM ± 0.4 nM	4.1%
D11	7.36E-03	8.30E-05	1.78E+06	2.10E+04	4.1 nM ± 0.1 nM	2.3%
E4	3.76E-03	2.60E-05	1.05E+06	8.20E+03	3.6 nM ± 0.05 nM	1.5%
E9	2.26E-03	1.30E-05	1.02E+06	7.30E+03	2.2 nM ± 0.03 nM	1.3%

2'-OMe-RNA vs. pm122-hairpin

	k_d	e.m. of k_d	k_a	e.m. of k_a	K_D	error in %
B11	2.77E-03	2.60E-05	2.26E+06	2.60E+04	1.2 nM ± 0.03 nM	2.1%
C02	6.10E-03	6.20E-05	6.06E+05	8.70E+03	10.1 nM ± 0.2 nM	2.5%
C10	1.46E-03	3.00E-05	6.48E+05	2.10E+04	2.3 nM ± 0.2 nM	5.3%
D05	7.81E-04	1.80E-06	7.67E+05	2.60E+03	1.0 nM ± 0.006 nM	0.6%
D11	5.46E-04	3.70E-06	6.90E+05	3.70E+03	792 pM ± 10 pM	1.2%
E4	5.26E-04	2.10E-06	8.68E+05	5.40E+03	606 pM ± 6 pM	1.0%
E9	4.44E-04	3.60E-06	6.33E+05	3.80E+03	701 pM ± 10 pM	1.4%

A.7. – Determined affinity and rate constants for all analytes against the linear complement (A) and the full length hairpin of pre-miR-122 (B).

Name	Sequence	Length	Mass / [g/mol]
mir18a_loop_7mer-aso1	ACUUCAC	7-mer	2222.5
mir18a_loop_7mer-aso2	UACUUCA	7-mer	2223.5
mir18a_loop_7mer-aso3	CUACUUC	7-mer	2199.5
mir18a_loop_7mer-aso4	UCUACUU	7-mer	2200.5
mir18a_loop_7mer-aso5	AUCUACU	7-mer	2223.5
mir18a_loop_7mer-aso6	AAUCUAC	7-mer	2246.6
mir18a_loop_7mer-aso7	UAAUCUA	7-mer	2247.5
mir18a_loop_7mer-aso8	CUAAUCU	7-mer	2223.5
mir18a_loop_7mer-aso9	GCUAAUC	7-mer	2262.6
mir18a_loop_7mer-aso10	UGCUAAU	7-mer	2263.5
mir18a_loop_7mer-aso11	AUGCUAA	7-mer	2286.6
mir18a_loop_7mer-aso12	GAUGCUA	7-mer	2302.6
mir18a_loop_8mer-aso1	UACUUCAC	8-mer	2542.7
mir18a_loop_8mer-aso2	CUACUUCA	8-mer	2542.7
mir18a_loop_8mer-aso3	UCUACUUC	8-mer	2519.7
mir18a_loop_8mer-aso4	AUCUACUU	8-mer	2543.7
mir18a_loop_8mer-aso5	AAUCUACU	8-mer	2566.8
mir18a_loop_8mer-aso6	UAAUCUAC	8-mer	2566.8
mir18a_loop_8mer-aso7	CUAAUCUA	8-mer	2566.8
mir18a_loop_8mer-aso8	GCUAAUCU	8-mer	2582.8
mir18a_loop_8mer-aso9	UGCUAAUC	8-mer	2582.8
mir18a_loop_8mer-aso10	AUGCUAAU	8-mer	2606.8
mir18a_loop_8mer-aso11	GAUGCUAA	8-mer	2645.8
mir18a_loop_9mer-aso1	CUACUUCAC	9-mer	2861.9
mir18a_loop_9mer-aso2	UCUACUUCA	9-mer	2862.9
mir18a_loop_9mer-aso3	AUCUACUUC	9-mer	2862.9
mir18a_loop_9mer-aso4	AAUCUACUU	9-mer	2886.9
mir18a_loop_9mer-aso5	UAAUCUACU	9-mer	2886.9
mir18a_loop_9mer-aso6	CUAAUCUAC	9-mer	2886.0
mir18a_loop_9mer-aso7	GCUAAUCUA	9-mer	2926.0
mir18a_loop_9mer-aso8	UGCUAAUCU	9-mer	2902.9
mir18a_loop_9mer-aso9	AUGCUAAUC	9-mer	2926.0
mir18a_loop_9mer-aso10	GAUGCUAAU	9-mer	2966.0
mir18a_loop_10mer-aso1	UCUACUUCAC	10-mer	3182.1
mir18a_loop_10mer-aso2	AUCUACUUCA	10-mer	3206.2
mir18a_loop_10mer-aso3	AAUCUACUUC	10-mer	3206.2
mir18a_loop_10mer-aso4	UAAUCUACUU	10-mer	3207.1
mir18a_loop_10mer-aso5	CUAAUCUACU	10-mer	3206.2
mir18a_loop_10mer-aso6	GCUAAUCUAC	10-mer	3245.2
mir18a_loop_10mer-aso7	UGCUAAUCUA	10-mer	3246.2
mir18a_loop_10mer-aso8	AUGCUAAUCU	10-mer	3246.2
mir18a_loop_10mer-aso9	GAUGCUAAUC	10-mer	3285.2
mir18a_loop_11mer-aso1	AUCUACUUCAC	11-mer	3525.4
mir18a_loop_11mer-aso2	AAUCUACUUCA	11-mer	3549.4
mir18a_loop_11mer-aso3	UAAUCUACUUC	11-mer	3526.4
mir18a_loop_11mer-aso4	CUAAUCUACUU	11-mer	3526.4
mir18a_loop_11mer-aso5	GCUAAUCUACU	11-mer	3565.4
mir18a_loop_11mer-aso6	UGCUAAUCUAC	11-mer	3565.4
mir18a_loop_11mer-aso7	AUGCUAAUCUA	11-mer	3589.4
mir18a_loop_11mer-aso8	GAUGCUAAUCU	11-mer	3605.4
mir18a_loop_12mer-aso1	AAUCUACUUCAC	12-mer	3868.6
mir18a_loop_12mer-aso2	UAAUCUACUUCA	12-mer	3869.6
mir18a_loop_12mer-aso3	CUAAUCUACUUC	12-mer	3845.6
mir18a_loop_12mer-aso4	GCUAAUCUACUU	12-mer	3885.6
mir18a_loop_12mer-aso5	UGCUAAUCUACU	12-mer	3885.6
mir18a_loop_12mer-aso6	AUGCUAAUCUAC	12-mer	3908.6
mir18a_loop_12mer-aso7	GAUGCUAAUCUA	12-mer	3948.7
mir18a_loop_13mer-aso1	UAAUCUACUUCAC	13-mer	4188.8
mir18a_loop_13mer-aso2	CUAAUCUACUUCA	13-mer	4188.8
mir18a_loop_13mer-aso3	GCUAAUCUACUUC	13-mer	4204.8
mir18a_loop_13mer-aso4	UGCUAAUCUACUU	13-mer	4205.8
mir18a_loop_13mer-aso5	AUGCUAAUCUACU	13-mer	4228.8
mir18a_loop_13mer-aso6	GAUGCUAAUCUAC	13-mer	4267.9
mir18a_loop_14mer-aso1	CUAAUCUACUUCAC	14-mer	4508.0
mir18a_loop_14mer-aso2	GCUAAUCUACUUCA	14-mer	4548.0
mir18a_loop_14mer-aso3	UGCUAAUCUACUUC	14-mer	4525.0
mir18a_loop_14mer-aso4	AUGCUAAUCUACUU	14-mer	4549.0
mir18a_loop_14mer-aso5	GAUGCUAAUCUACU	14-mer	4588.1
mir18a_loop_15mer-aso1	GCUAAUCUACUUCAC	15-mer	4867.2
mir18a_loop_15mer-aso2	UGCUAAUCUACUUCA	15-mer	4868.2
mir18a_loop_15mer-aso3	AUGCUAAUCUACUUC	15-mer	4868.2
mir18a_loop_15mer-aso4	GAUGCUAAUCUACUU	15-mer	4908.3
mir18a_loop_16mer-aso1	UGCUAAUCUACUUCAC	16-mer	5187.4
mir18a_loop_16mer-aso2	AUGCUAAUCUACUUCA	16-mer	5211.5
mir18a_loop_16mer-aso3	GAUGCUAAUCUACUUC	16-mer	5227.5
mir18a_loop_17mer-aso1	AUGCUAAUCUACUUCAC	17-mer	5530.7
mir18a_loop_17mer-aso2	GAUGCUAAUCUACUUCA	17-mer	5570.7
mir18a_loop_18mer-aso1	GAUGCUAAUCUACUUCAC	18-mer	5889.9

Table A.8.

Name	Sequence	Length	Mass
ASO 29-13	CUCCCUUGAUGUA	13-mer	4220.8 g/mol
ASO 30-14	AUCUCCCUUGAUGU	14-mer	4541 g/mol
ASON 29-13	AUGUAGUUCCCUC	13-mer	4220.8 g/mol
ASO 29-9	CUUGAUGUA	9-mer	2943 g/mol
ASO 30-13	UCUCCCUUGAUGU	13-mer	4197.8 g/mol
ASO 31-9	CCCUUGAUG	9-mer	2918 g/mol
ASO 31-13	AUCUCCCUUGAUG	13-mer	4220.8 g/mol
ASO 33-11	AUCUCCCUUGA	11-mer	3541.4 g/mol
ASO 33-13	UUAUCUCCCUUGA	13-mer	4181.8 g/mol
ASO 34-13	GUUAUCUCCCUUG	13-mer	4197.8 g/mol
ASO 35-9	AUCUCCCUU	9-mer	2838.9 g/mol
ASO 36-8	AUCUCCCU	8-mer	2518.7 g/mol

Table A.9. – LooptomiRs for the assay against pre-let-7a-2. All oligoribonucleotides were fully 2'-OMe RNA

DNA		RNA	
Stack or monomer	Molar ext. coeff. / [l·mol^{-1}·cm^{-1}]	Stack or monomer	Molar ext. coeff. / [l·mol^{-1}·cm^{-1}]
pdA	15400	pA	15400
pdC	7400	pC	7200
pdG	11500	pG	11500
pdT	8700	pU	9900
dApdA	27400	ApA	27400
dApdC	21200	AdC	21000
dApdG	25000	ApG	25000
dApdT	22800	ApU	24000
dCpdA	21200	CpA	21000
dCpdC	14600	CpC	14200
dCpdG	18000	CpG	17800
dCpdT	15200	CpU	16200
dGpdA	25200	GpA	25200
dGpdC	17600	GpC	17400
dGpdG	21600	GpG	21600
dGpdT	20000	GpU	21200
dTpdA	23400	UpA	24600
dTpdC	16200	UpC	17200
dTpdG	19000	UpG	20000
dTpdT	16800	UpU	19600
		ApdT	22'800
		CpdT	15'200
		GpdT	20'000
		TpdT	16'800

Table A.10. – Molar extinction coefficients used for the nearest neighbour method for calculation of oligoribonucleotide concentrations. For RNA/2'-OMe RNA sequences containing a poly-T linker the last 4 values were added for the border RNA/DNA

Name	Sequence	Length	Mass
DNA1	ACTTG	5	1478 g/mol
DNA2	ATCGTTGAGC	10	3043 g/mol
DNA3	ATTCGTTAGCGATGC	15	4583 g/mol
DNA4	ATACGTCTTCGTAGACTGAT	20	6107 g/mol
DNA5	ATCTCTCGATAGATAGATCGCCGTC	25	7617 g/mol
DNA6	ACTCGCTAGATCGCTCGCTAGATAGCTCGA	30	9167 g/mol
DNA7	ATATATCGCGCTACGATGCTCGATGCTGCATAGCT	35	10722 g/mol
DNA8	ATCGCGCTATAATCGCGCGCGCATAATATGCTCTTTTCGC	40	12198 g/mol
DNA9	ACTCGATAAGAGAGAACGGCGGCTATCTCGCGATATCGCGGGCATA	45	13904 g/mol
DNA10	ACTGCTGCTCGAATGATCGCCGCGCCAAAATCGTGCTGCTGCTGCTGAGA	50	15363 g/mol

Table A.11. – Random DNA test ASOs for comparison of ε calculation as described in section 3.4.1, p. 72

A SUPPLEMENTARY TABLES

B. Supplementary figures
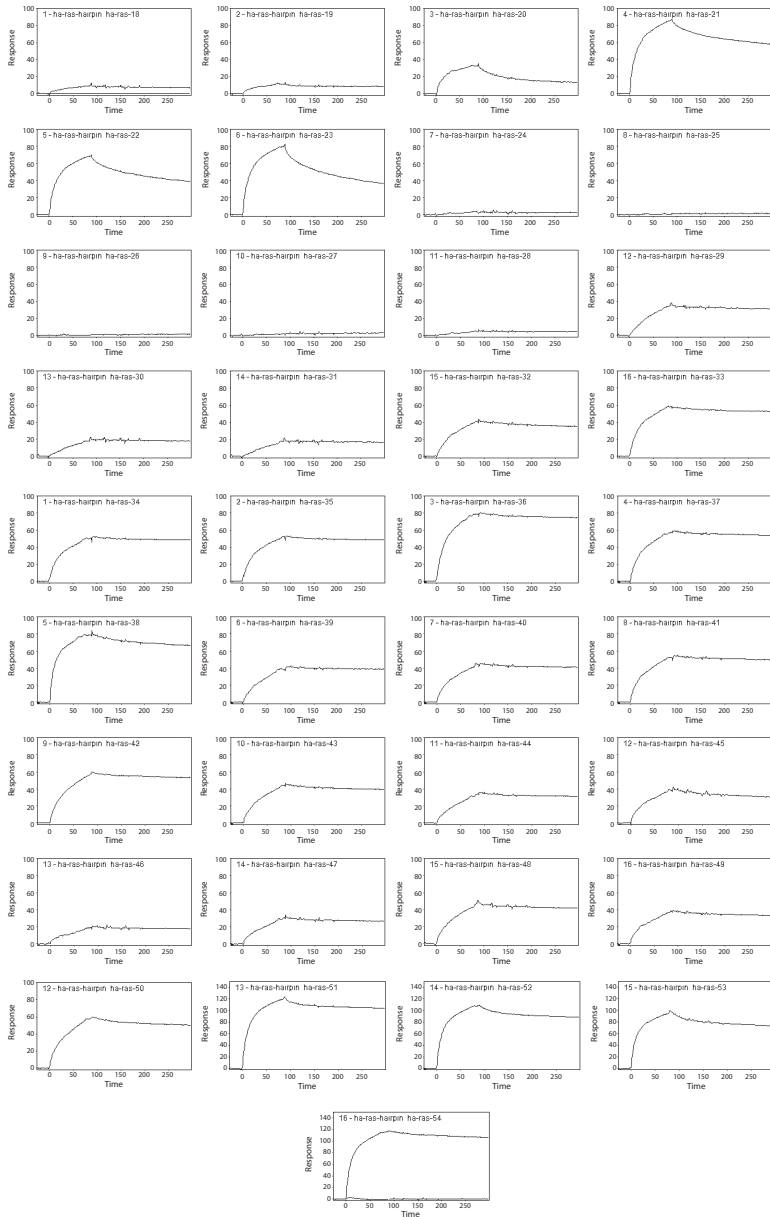
Figure B.1. – Sensorgrams of the 37 decamers "walking" around the hairpin of h-ras as described in section 2.1.1.1, p. 31 and in section 2.3.1, p. 43.
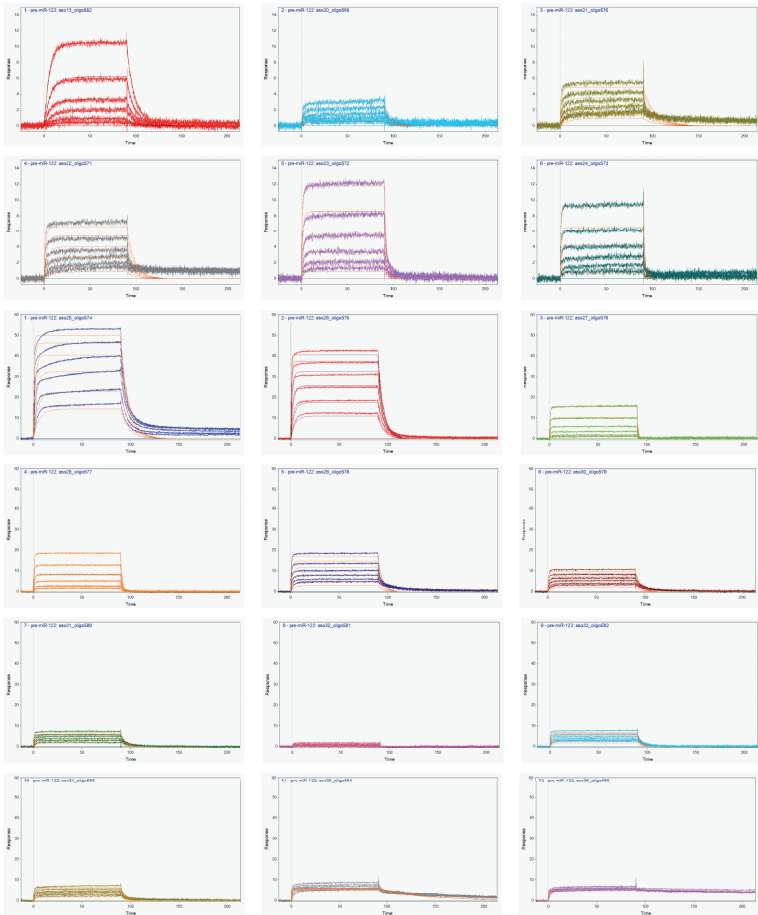
Figure B.2. – The first 18 (of 52) sensorgrams of the decamers "walking" around the hairpin of pre-miR-122 showing a reasonable response. The ordinates are all in the same scale (0-60 RU)
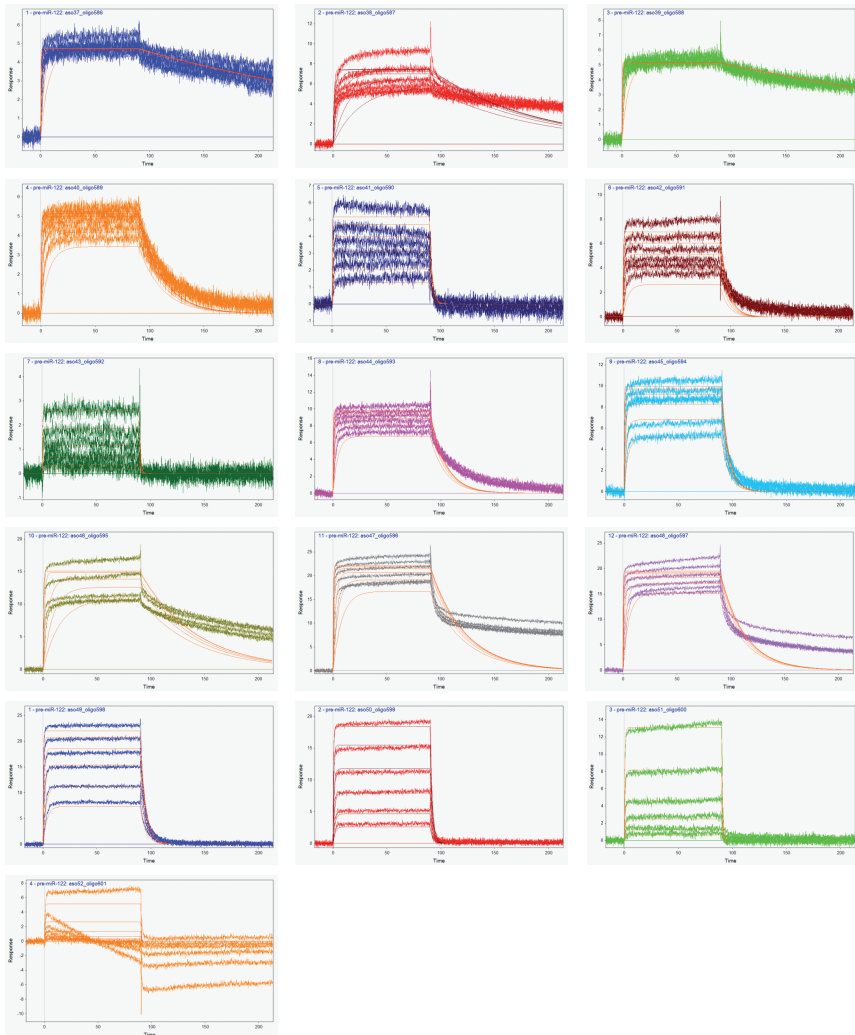
Figure B.3. – The remaining 16 (of 52) sensorgrams of the decamers "walking" around the hairpin of pre-miR-122 showing a reasonable response. The ordinates are all individually scaled.
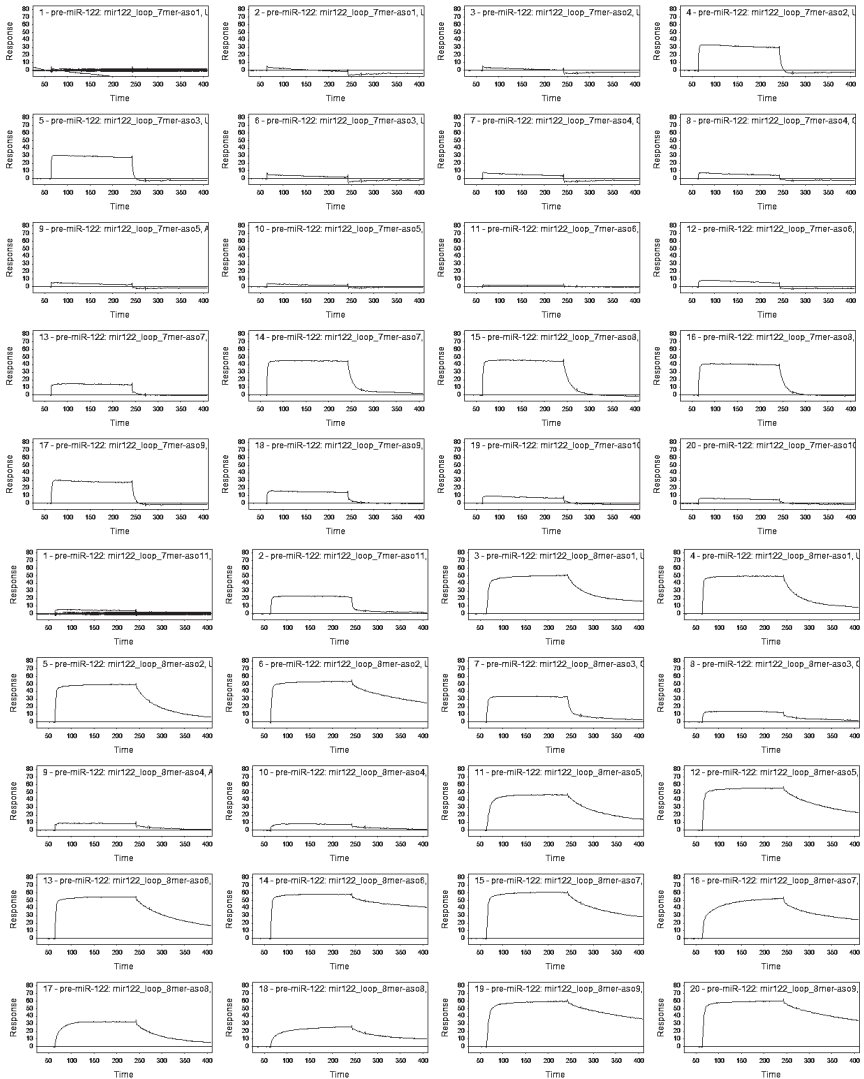
Figure B.4. – The first 40 (of 60) sensorgrams of the loop-binding oligonucleotides against the hairpin of pre-miR-122. The ordinates are in the same scale.
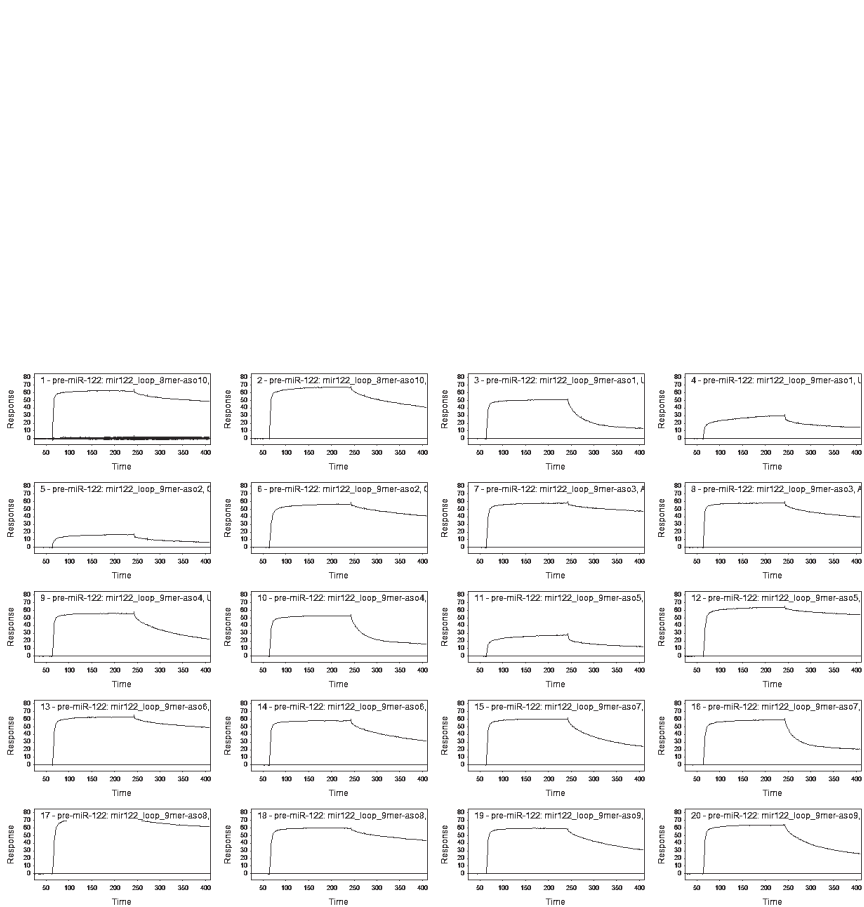
Figure B.5. – The last 20 sensorgrams of the loop-binding oligonucleotides against the hairpin of pre-miR-122. The ordinates are in the same scale.
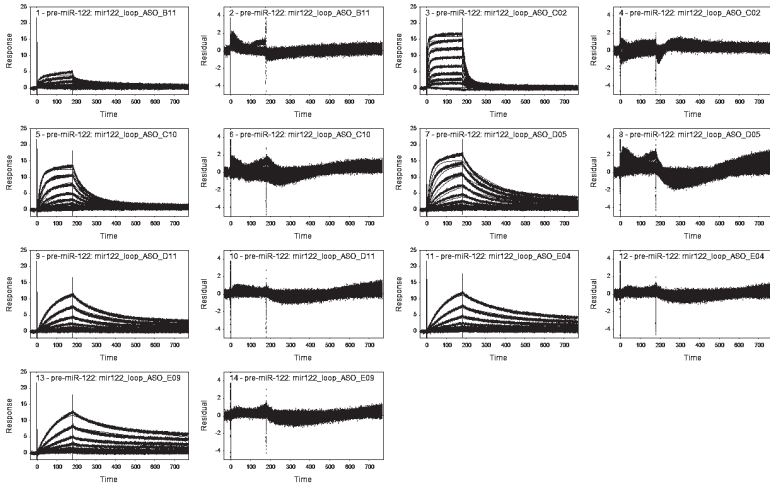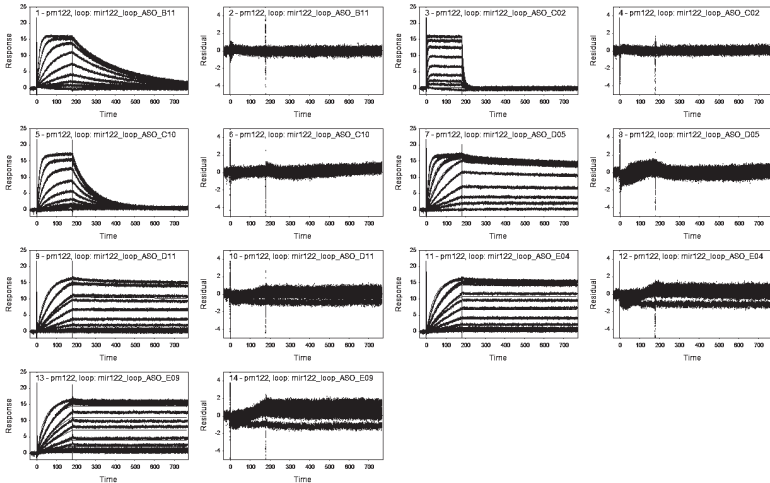
Figure B.6. – Sensorgrams with corresponding residuals for the affinity determination of the 7 best loop binders with RNA chemistry. A) Binding against pre-miR-122 hairpin. B) Binding against unstructured linear complement (isolated loop-region). The sensorgrams are made with Scrubber2.0a and scaled to the same ordinate for all analytes.
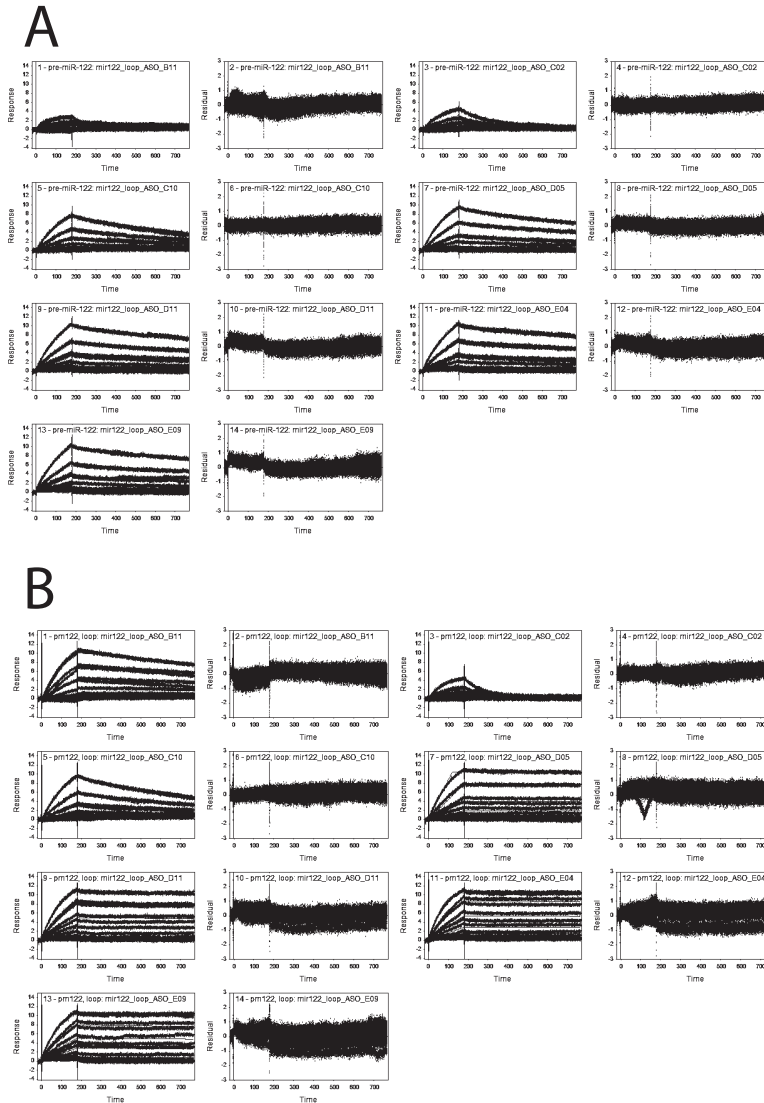
Figure B.7. – Sensorgrams with corresponding residuals for the affinity determination of the 7 best loop binders with 2'-OMe RNA chemistry. A) Binding against pre-miR-122 hairpin. B) Binding against unstructured linear complement (isolated loop-region). The sensorgrams are made with Scrubber2.0a and scaled to the same ordinate for all analytes.
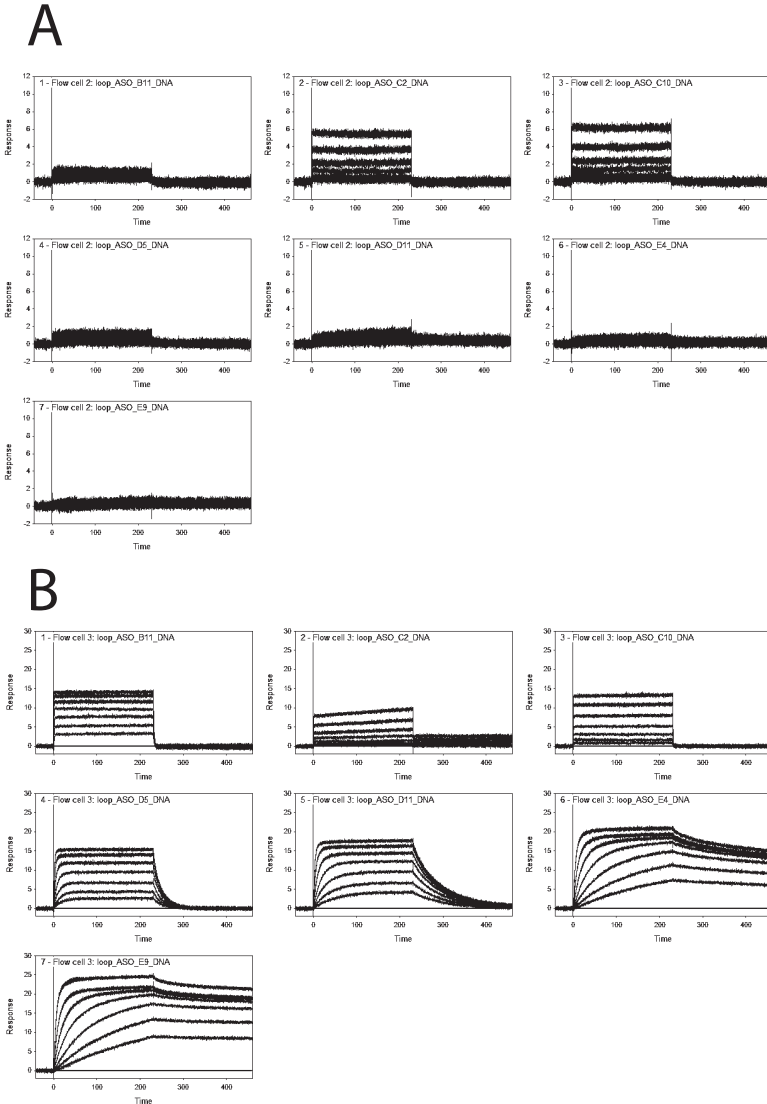
Figure B.8. – Sensorgrams with corresponding residuals for the affinity determination of the 7 best loop binders with DNA chemistry. A) Binding against pre-miR-122 hairpin. B) Binding against unstructured linear complement (isolated loop-region). The sensorgrams are made with Scrubber2.0a and scaled to the same ordinate for all analytes.
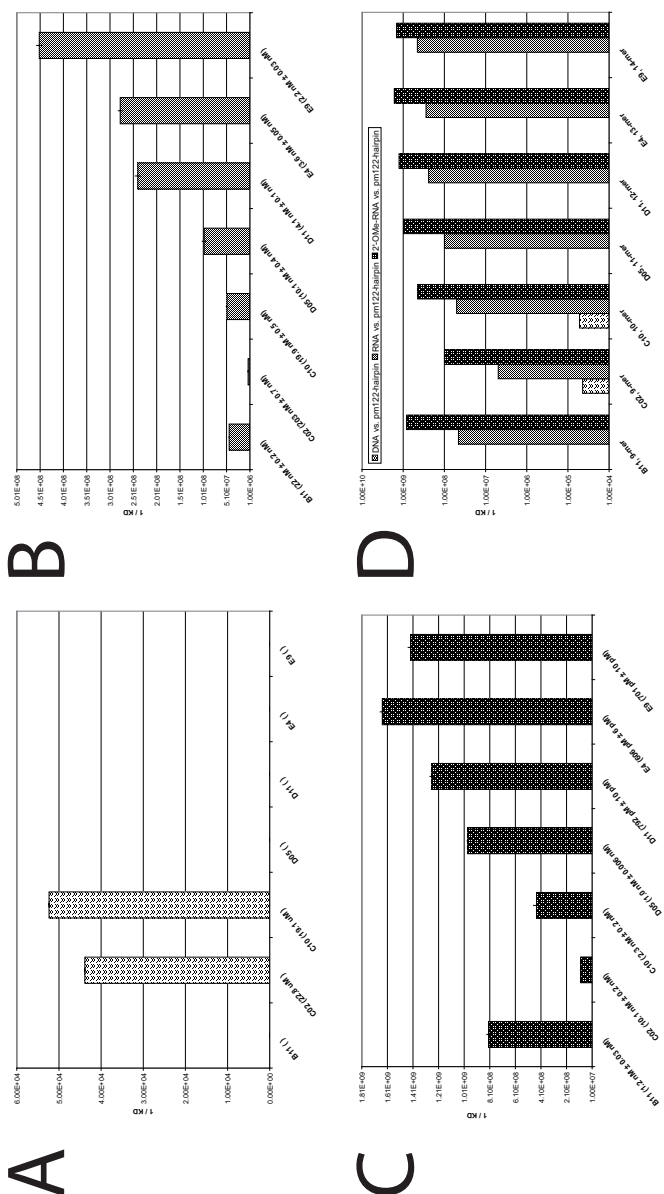
Figure B.9. – Comparison of binding affinities of RNA, 2'-OMe RNA, and DNA analytes against the structured hairpin of pre-miR-122. A) loop-binders with DNA, exhibiting only a very reduced binding affinity. Only one value could be determined (cf. sensorgrams in fig. B.8). B) unmodified RNA loop-binders against the hairpin. C) 2'-OMe RNA modified loop-binders against the hairpin. D) Comparison of binding affinities of all three types of analytes against the hairpin. The 10-mer with 2'-OMe RNA chemistry has a 10'000-fold higher affinity for the hairpin than the DNA oligoribonucleotide of same length and sequence.
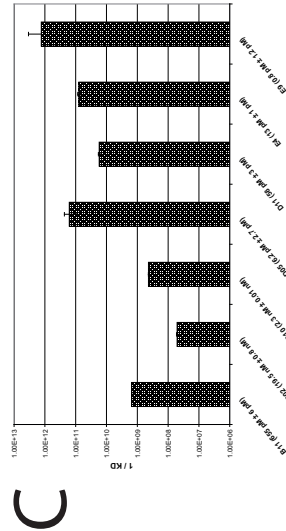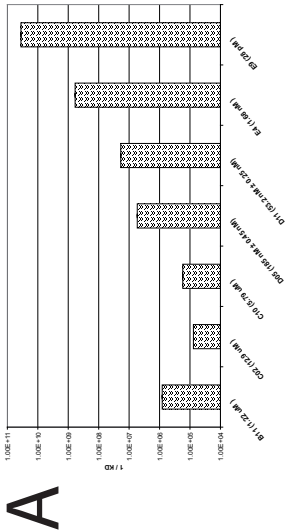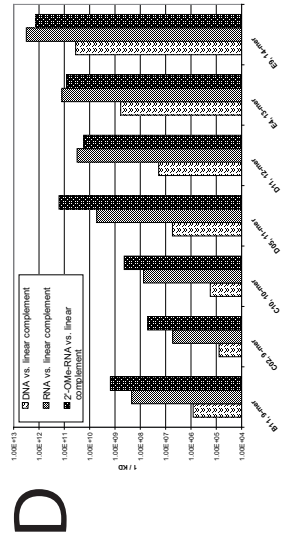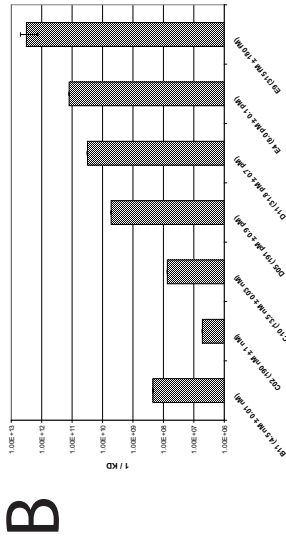
Figure B.10. – Comparison of binding affinities of RNA, 2'-OMe RNA, and DNA analytes against the unstructured linear complement (isolated loop-region). The affinities are proportional to the length of the oligonucleotides A) loop-binders with DNA, B) loop-binders with RNA, and C) loop-binders with 2'-OMe RNA modifications. D) Comparison of binding affinities of all three types of analytes against the loop.
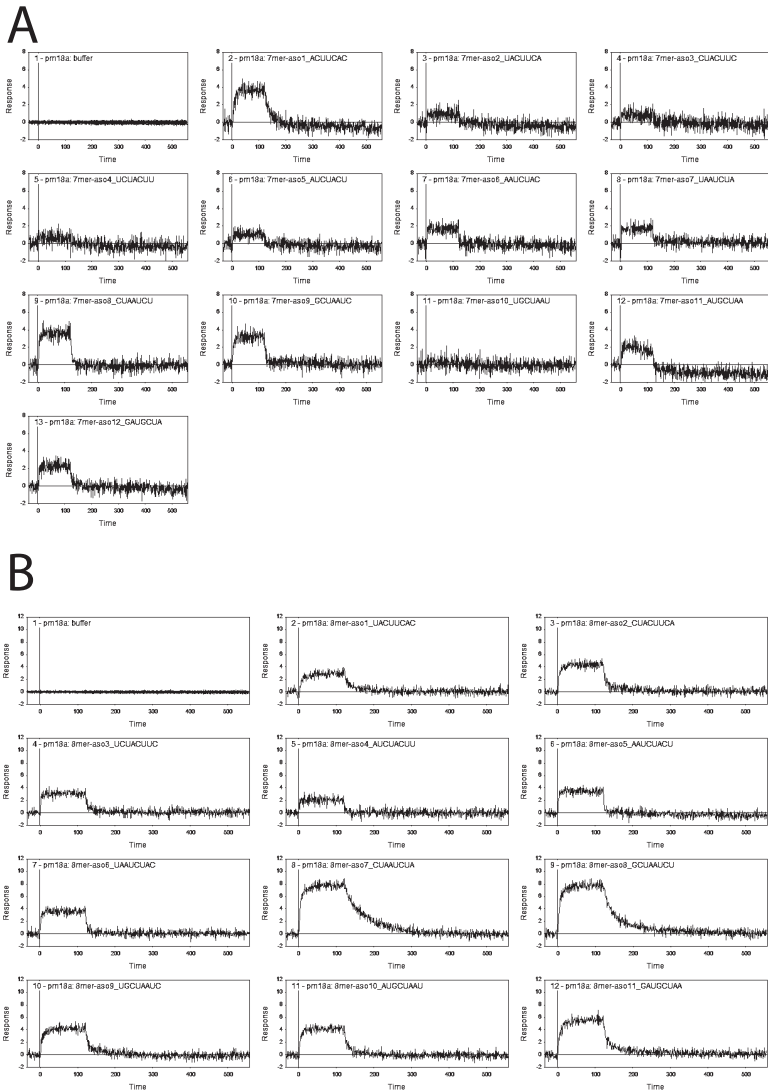
Figure B.11. – Sensorgrams for the 7-mer and 8-mer loop-binder against pre-miR-18a.
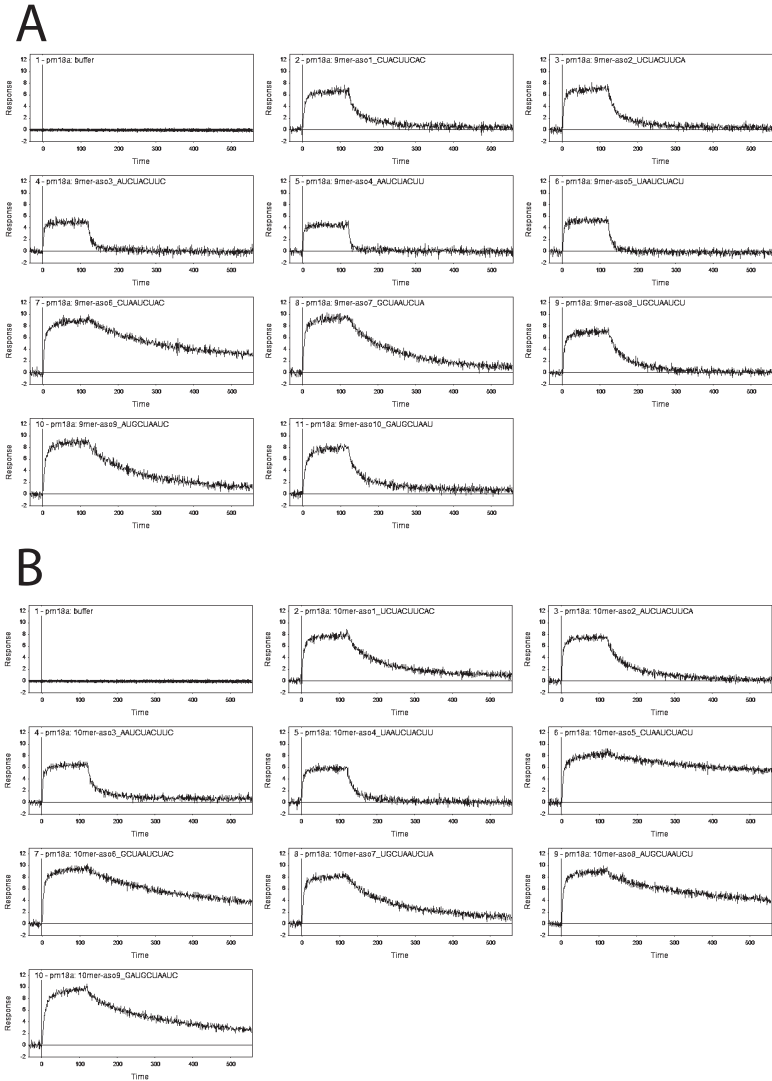
Figure B.12. – Sensorgrams for the 9-mer and 10-mer loop-binder against pre-miR-18a.

A
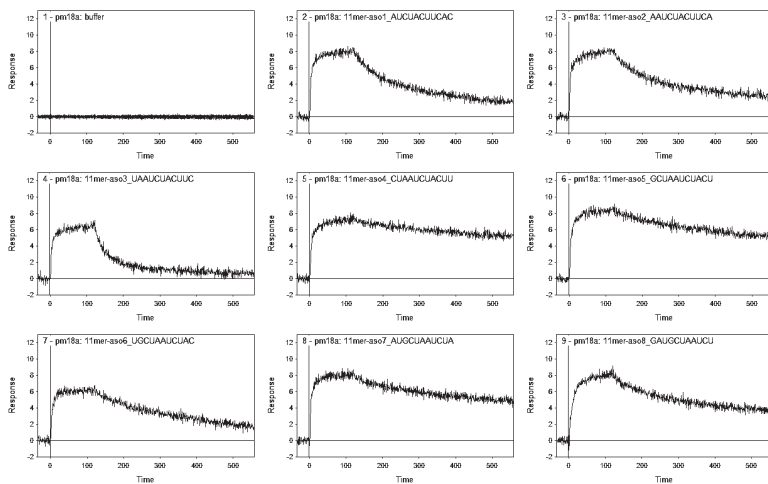
B
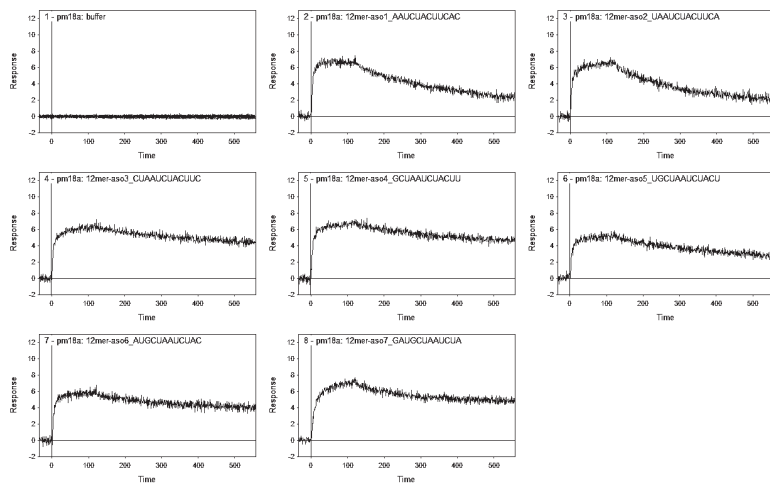
Figure B.13. – Sensorgrams for the 11-mer and 12-mer loop-binder against pre-miR-18a.

A

B
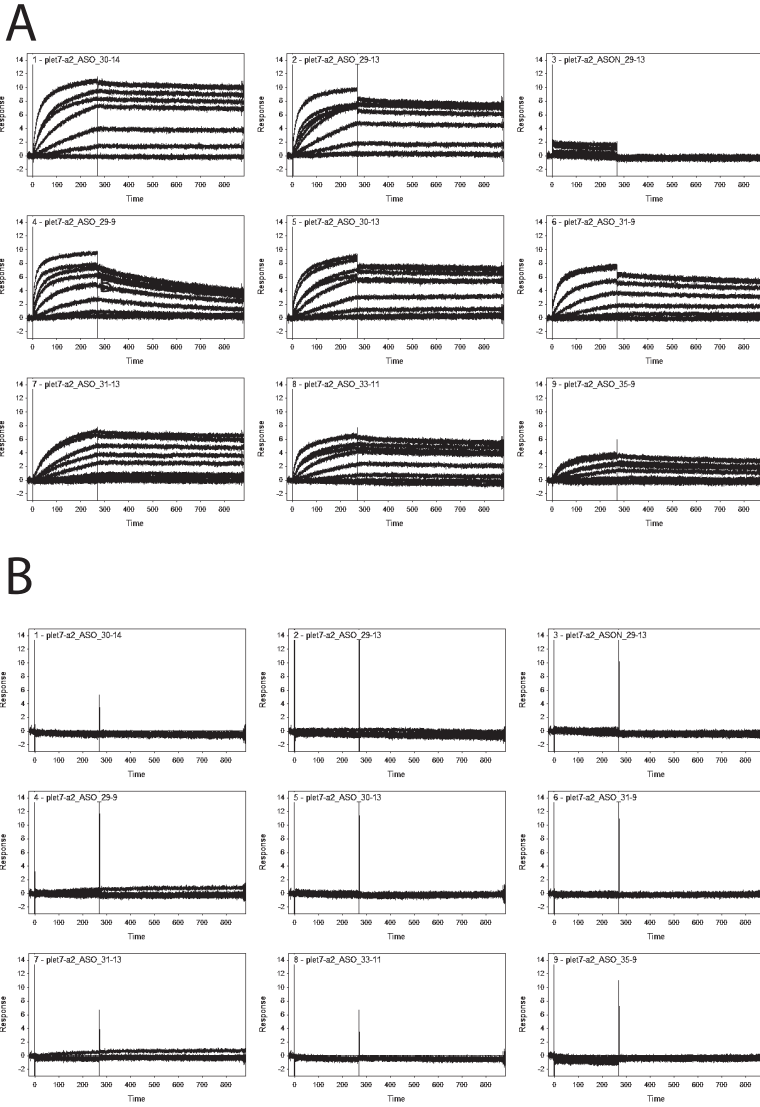
Figure B.14. – Sensorgrams of the LooptomiRs tested against A) pre-let-7a-2 and B) pre-miR-122.

A

Structure 1 Folding bases 1 to 67 of pre-let-7a-2
Initial ΔG = -22.00

```
           10        20        30
U--| G   U           UAGAAUUAC  AA
   GAG UAG AGGUUGUAUAGUU           AUC  G
   UUC AUC UCCGACAUGUCAA           UAG  G
CCU^  G   C          ---------     AG
      60        50                 40
```

Structure 2 Folding bases 1 to 67 of pre-let-7a-2
Initial ΔG = -17.00

```
           10        20        30
UGA  U-|  ----              UAGAAUUAC   AA
   GG AGU  AGGUUGUAUAGUU            AUC  G
   CC  UCG  UCCGACAUGUCAA           UAG  G
--- UU^  AUCC              ---------    AG
       60        50                 40
```

Structure 3 Folding bases 1 to 67 of pre-let-7a-2
Initial ΔG = -12.40

```
            10          20
U---------   A|  -   AUAG  A  AU
         GAGGU GUA GGUUGU   UUU GA  U
         CUCCG CAU UCAAUA   GAA CU  A
CCUUUCGAUC     A^  G     GAGG   -  AC
       60        50        40       30
```

Structure 4 Folding bases 1 to 67 of pre-let-7a-2
Initial ΔG = -11.30

```
           10        20        30
U--  G   U   AUAGUUUAGAAUU|  ----  AA
   GAG UAG AGGUUGU          ACA    UC  G
   UUC AUC UCCGACA          UGU    AG  G
CCU   G   C    -------------^  CAAU AG
       60        50                40
```

B

C

Figure B.15. – A) The four most stable secondary structures as calculated by MFold. B) above: plot of continuous prior fitting from EVILFIT, below: plot of bayesian 1-site fitting. C) Comparison of fittings with BiaEvaluation (left) and EVILFIT (right).

C. Code

C.0.1. Code for fragment calculation

```
Private Sub fragmentcalc()

Dim eingabezeile As Long
Dim RowNdx As Integer
Dim i As Integer
Dim j As Integer
Dim k As Integer
Dim ende As Integer
Dim oligotype As String
Dim fragment As String
Dim fragmentmass As Single
Dim namefragment As String
Dim zaehler As Integer
Dim minmass As Boolean
Dim maxmass As Boolean
Dim massunder As Single
Dim massupper As Single
Dim foundmass As Single
Dim monophos As Single
Dim hydrogen As Single
Dim triphos As Single
Dim antwort As VbMsgBoxResult

If foundmass_txt <> "" Then foundmass = foundmass_txt.Value
Application.ScreenUpdating = False
zaehler = 1
ende = Len(oligoeingabe_txt)

monophos = 79.97994
triphos = 239.94

If minmass_txt <> "" Then minmass = True
If maxmass_txt <> "" Then maxmass = True
Worksheets("Fragmentor").Visible = True
Worksheets("Fragmentor").Select

oligoeingabe_txt = Trim(oligoeingabe_txt)
eingabezeile = Worksheets("Fragmentor").Cells(65536, 1).End(xlUp).Row + 1
RowNdx = eingabezeile
oligotype = cbooligotype
Set rcell = Cells.Find(What:="Target-sequence", After:=Range("A1"), \_
LookIn:=xlFormulas,LookAt:=xlWhole, SearchOrder:=xlByRows, \_
SearchDirection:=xlNext, MatchCase:=False)
If rcell Is Nothing Then
Cells(RowNdx, 1).Value = "Target-sequence, " & oligoeingabe_txt
Cells(RowNdx, 1).Value = "Target-sequence"
```

```
Cells(RowNdx, 2).Value = oligoeingabe_txt
Cells(RowNdx, 3).Value = Len(oligoeingabe_txt)

If OptionButton4 = True Then
    Cells(RowNdx, 4).Value = masscalc(oligoeingabe_txt, cbooligotype) + triphos
ElseIf OptionButton5 = True Then
    Cells(RowNdx, 4).Value = masscalc(oligoeingabe_txt, cbooligotype) + monophos
ElseIf OptionButton6 = True Then
    Cells(RowNdx, 4).Value = masscalc(oligoeingabe_txt, cbooligotype)
End If
RowNdx = RowNdx + 1
End If


'----------------complete fragmentation:------------------------
If OptionButton7 = True Then
For i = 1 To ende
    For j = 1 To ende - i + 1
    fragment = Mid(oligoeingabe_txt, i, j)
    namefragment = "fragment " & zaehler & " (Position " & i & "-" & i + j - 1 & ")"
    If i = 1 Then
        If OptionButton4 = True Then
            fragmentmass = masscalc(fragment, oligotype) + triphos
        ElseIf OptionButton5 = True Then
            fragmentmass = masscalc(fragment, oligotype) + monophos
        Else
            fragmentmass = masscalc(fragment, oligotype)
        End If
    Else
        If OptionButton16 = True Then
            fragmentmass = masscalc(fragment, oligotype)
        ElseIf OptionButton17 = True Then
            fragmentmass = masscalc(fragment, oligotype) + monophos
        End If
    End If
    If OptionButton14 = True Then
        If minmass = True And maxmass = True Then
            If fragmentmass < minmass_txt.Value Or fragmentmass > maxmass_txt.Value\_
Then GoTo weiter:
        ElseIf minmass = True And maxmass = False Then
            If fragmentmass < minmass_txt.Value Then GoTo weiter:
        ElseIf minmass = False And maxmass = True Then
            If fragmentmass > maxmass_txt.Value Then GoTo weiter:
        End If
    ElseIf OptionButton15 = True Then
        If OptionButton13 = True Then
            massunder = foundmass - (foundmass * massrel_txt.Value / 100)
            massupper = foundmass + (foundmass * massrel_txt.Value / 100)
            If fragmentmass < massunder Or fragmentmass > massupper Then GoTo weiter:
        ElseIf OptionButton12 = True Then
            massunder = foundmass - massabs_txt.Value
            massupper = foundmass + massabs_txt.Value
            If fragmentmass < massunder Or fragmentmass > massupper Then GoTo weiter:
        End If
    End If
    Cells(RowNdx, 1).Value = namefragment
    Cells(RowNdx, 2).Value = oligoeingabe_txt
    Cells(RowNdx, 2).Characters(Start:=0, Length:=i - 1).Font.name = "Courier"
    Cells(RowNdx, 2).Characters(Start:=0, Length:=i - 1).Font.FontStyle = "Normal"
```

```
    Cells(RowNdx, 2).Characters(Start:=0, Length:=i - 1).Font.Size = 12
    Cells(RowNdx, 2).Characters(Start:=i, Length:=j).Font.name = "Courier"
    Cells(RowNdx, 2).Characters(Start:=i, Length:=j).Font.ColorIndex = 3
    Cells(RowNdx, 2).Characters(Start:=i, Length:=j).Font.Size = 12
    Cells(RowNdx, 2).Characters(Start:=j + 1, Length:=ende).Font.name = "Courier"
    Cells(RowNdx, 2).Characters(Start:=j + 1, Length:=ende).Font.FontStyle = "Normal"
    Cells(RowNdx, 2).Characters(Start:=j + 1, Length:=ende).Font.Size = 12
    Cells(RowNdx, 3).Value = Len(fragment)
    Cells(RowNdx, 4).Value = fragmentmass
    zaehler = zaehler + 1
    RowNdx = RowNdx + 1
weiter:
    Next j
Next i


'---------------------------RNase H fragmentation  ------------------------
ElseIf OptionButton8 = True Then

'---------------------------Calculation RNase H from the 5'-end --------------------
For i = 1 To ende - 1
    fragment = Mid(oligoeingabe_txt, 1, i)
    namefragment = "fragment " & zaehler & " (Position 1-" & i & ")"
        If OptionButton4 = True Then
            fragmentmass = masscalc(fragment, oligotype) + triphos
        ElseIf OptionButton5 = True Then
            fragmentmass = masscalc(fragment, oligotype) + monophos
        ElseIf OptionButton6 = True Then
            fragmentmass = masscalc(fragment, oligotype)
        End If
    If OptionButton14 = True Then
        If minmass = True And maxmass = True Then
            If fragmentmass < minmass_txt.Value Or fragmentmass > maxmass_txt.Value\_
Then GoTo weiter2:
        ElseIf minmass = True And maxmass = False Then
            If fragmentmass < minmass_txt.Value Then GoTo weiter2:
        ElseIf minmass = False And maxmass = True Then
            If fragmentmass > maxmass_txt.Value Then GoTo weiter2:
        End If
    ElseIf OptionButton15 = True Then
        If OptionButton13 = True Then
            massunder = foundmass - (foundmass * massrel_txt.Value / 100)
            massupper = foundmass + (foundmass * massrel_txt.Value / 100)
            If fragmentmass < massunder Or fragmentmass > massupper\_
Then GoTo weiter2:
        ElseIf OptionButton12 = True Then
            massunder = foundmass - massabs_txt.Value
            massupper = foundmass + massabs_txt.Value
            If fragmentmass < massunder Or fragmentmass > massupper\_
Then GoTo weiter2:
        End If
    End If
    Cells(RowNdx, 1).Value = namefragment
    Cells(RowNdx, 2).Value = oligoeingabe_txt
    Cells(RowNdx, 2).Characters(Start:=1, Length:=i).Font.name = "Courier"
    Cells(RowNdx, 2).Characters(Start:=1, Length:=i).Font.ColorIndex = 3
    Cells(RowNdx, 2).Characters(Start:=1, Length:=i).Font.Size = 12
    Cells(RowNdx, 2).Characters(Start:=i + 1, Length:=ende).Font.name = "Courier"
```

```
    Cells(RowNdx, 2).Characters(Start:=i + 1, Length:=ende).Font.ColorIndex = 0
    Cells(RowNdx, 2).Characters(Start:=i + 1, Length:=ende).Font.Size = 12
    Cells(RowNdx, 3).Value = Len(fragment)
    Cells(RowNdx, 4).Value = fragmentmass
    zaehler = zaehler + 1
    RowNdx = RowNdx + 1
weiter2:
Next i


'--------------------------Calculation RNase H from the 3'-end --------------------
For j = 1 To ende - 1
    fragment = Mid(oligoeingabe_txt, ende - j + 1, j)
    namefragment = "fragment " & zaehler & " (Position " & ende - j + 1 & "-" & ende & ")"
    fragmentmass = masscalc(fragment, oligotype) + monophos
    If OptionButton14 = True Then
        If minmass = True And maxmass = True Then
            If fragmentmass < minmass_txt.Value Or fragmentmass > maxmass_txt.Value\_
Then GoTo weiter3:
        ElseIf minmass = True And maxmass = False Then
            If fragmentmass < minmass_txt.Value Then GoTo weiter3:
        ElseIf minmass = False And maxmass = True Then
            If fragmentmass > maxmass_txt.Value Then GoTo weiter3:
        End If
    ElseIf OptionButton15 = True Then
        If OptionButton13 = True Then
            massunder = foundmass - (foundmass * massrel_txt.Value / 100)
            massupper = foundmass + (foundmass * massrel_txt.Value / 100)
            If fragmentmass < massunder Or fragmentmass > massupper\_
Then GoTo weiter3:
        ElseIf OptionButton12 = True Then
            massunder = foundmass - massabs_txt.Value
            massupper = foundmass + massabs_txt.Value
            If fragmentmass < massunder Or fragmentmass > massupper\_
Then GoTo weiter3:
        End If
    End If
    Cells(RowNdx, 1).Value = namefragment
    Cells(RowNdx, 2).Value = oligoeingabe_txt
    Cells(RowNdx, 2).Characters(Start:=ende - j, Length:=j).Font.name = "Courier"
    Cells(RowNdx, 2).Characters(Start:=ende - j, Length:=j).Font.ColorIndex = 0
    Cells(RowNdx, 2).Characters(Start:=ende - j, Length:=j).Font.Size = 12
    Cells(RowNdx, 2).Characters(Start:=ende - j + 1, Length:=j).Font.name = "Courier"
    Cells(RowNdx, 2).Characters(Start:=ende - j + 1, Length:=j).Font.ColorIndex = 3
    Cells(RowNdx, 2).Characters(Start:=ende - j + 1, Length:=j).Font.Size = 12
    Cells(RowNdx, 3).Value = Len(fragment)
    Cells(RowNdx, 4).Value = fragmentmass
    zaehler = zaehler + 1
    RowNdx = RowNdx + 1
weiter3:
Next j
End If

Range(Cells(4, 2), Cells(4, 2)).EntireColumn.AutoFit
Application.ScreenUpdating = True

End Sub
```

D. Nomenclature

ε	Molar extinction coefficient (unit: $l\cdot mol^{-1}\cdot cm^{-1}$)
2'-MOE	Ribonucleic acid with a methoxyethyl-group at the 2'-position
2'-OMe RNA	Ribonucleic acid with a methoxy-group at the 2'-position
K_A	Equilibrium association constant (unit: M^{-1})
k_a	Association rate constant (unit: $M^{-1}s^{-1}$)
K_D	Equilibrium dissociation constant (unit: M)
k_d	Dissociation rate constant (unit: s^{-1})
RU_{max}	Maximum binding response with respect to stoichiometric ratio.
AMO	Anti-microRNA oligonucleotide
ASO	Antisense oligonucleotide
AU	Absorbance units
bp	base pairs
Cap A/B	Capping solution used during oligonucleotide synthesis
CM5	Carboxy-methylated chip surface (100 nm)
CPG	Controlled pore glass (solid support for RNA/DNA synthesis)
Da	Dalton
DMSO	Dimethylsulfoxide
DNA	Desoxyribonucleic acid
DPBS	Dulbecco's phosphate buffered saline
DTT	Dithiothreitol
EDC	1-Ethyl-3-3(3-dimethylaminopropyl)-carbodiimide hydrochloride
EDC	1-ethyl-3-(3-dimethylaminopropyl)carbodiimide
ESI	Electrospray ionization
fc	flow cell
fig.	Figure
Hairpin	Secondary stem-loop structure of a long (non-coding) RNA.
HCV	Hepatitis C virus
HEPES	4-(2-hydroxyethyl)-1-piperazineethanesulfonic acid (a zwitterionic organic buffering agent)
HEPES	4-(2-hydroxyethyl)-1-piperazineethanesulfonic acid
HFIP	Hexafluoroisopropanol
HPLC	High performance liquid chromatography
HTS	High-throughput screening
IC_{50}	50 % inhibition constant
IFC	Integrated fluidic cartridge
Immob. lev.	Level of immobilization of a ligand
mAU	milli Absorption unit
miRNA	microRNA

D NOMENCLATURE

mRNA	messenger RNA
MS	Mass spectrometry
MTL	Mass transport limitation
MW	Molecular weight
MW	Molecular weight
ncRNA	noncoding RNA
NHS	N-Hydroxysuccinimide
nt	nucleotide(s)
Oligo	oligoribonucleotide
PAGE	Polyacrylamide gel electrophoresis
PBS	Phosphate buffered saline
PCR	Polymerase chain reaction
pm122	pre-miR-122
PMO	phosphorodiamidate morpholino oligonucleotides
PNA	Peptide nucleic acid
pre-miR	precursor microRNA
pri-miR	primary microRNA
PS	Phosphorothioate linkage of the backbone
PS	Phosphorothioate linkage of the nucleic acid backbone
R	Response
RBP	RNA binding protein
RNA	Ribonucleic acid
rt / RT	Room temperature
RU	Response unit (unitless)
RU	Response unit
SA	Streptavidin-coated Sensor chip for SPR measurements with Biacore instruments
SA	Streptavidin
shRNA	short hairpin RNA
siRNA	short interfering RNA
sol.	solution
SPR	Surface Plasmon Resonance
SPR	Surface plasmon resonance
TCEP	Tris(2-carboxyethyl)phosphine
TEA	Triethylamine
TEAA	Triethylammonium acetate
TFA	Trifluoro acetic acid
TFA	Trifluoroacetic acid
TRIS	Tris(hydroxymethyl)aminomethane (Tromethamine, Trometamol)

E. List of Tables and List of Figures

List of Tables

E | LIST OF TABLES

List of Figures

F. Index

F INDEX

G. Bibliography

[1] Philipp Kapranov, Jill Cheng, Sujit Dike, David A. Nix, Radharani Duttagupta, Aarron T. Willingham, Peter F. Stadler, Jana Hertel, Joerg Hackermueller, Ivo L. Hofacker, Ian Bell, Evelyn Cheung, Jorg Drenkow, Erica Dumais, Sandeep Patel, Gregg Helt, Madhavan Ganesh, Srinka Ghosh, Antonio Piccolboni, Victor Sementchenko, Hari Tammana, and Thomas R. Gingeras. RNA Maps Reveal New RNA Classes and a Possible Function for Pervasive Transcription. *Science (Washington, DC, United States)*, 316(5830):1484–1488, 2007.

[2] Yiping He, Bert Vogelstein, Victor E. Velculescu, Nickolas Papadopoulos, and Kenneth W. Kinzler. The Antisense Transcriptomes of Human Cells. *Science (Washington, DC, United States)*, 322 (5909):1855–1857, 2008.

[3] Lin He, J. Michael Thomson, Michael T. Hemann, Eva Hernando-Monge, David Mu, Summer Goodson, Scott Powers, Carlos Cordon-Cardo, Scott W. Lowe, Gregory J. Hannon, and Scott M. Hammond. A microRNA polycistron as a potential human oncogene. *Nature (London, United Kingdom)*, 435(7043):828–833, 2005.

[4] Thomas A. Cooper, Lili Wan, and Gideon Dreyfuss. RNA and disease. *Cell (Cambridge, MA, United States)*, 136(4):777–793, 2009.

[5] Jason R. O'Rourke and Maurice S. Swanson. Mechanisms of RNA-mediated Disease. *Journal of Biological Chemistry*, 284(12):7419–7423, 2009.

[6] Guido J.R. Zaman. Small Molecule Drug Targeting of RNA. *Frontiers in Drug Design & Discovery*, 1(1):17–28, 2005.

[7] Santiago Gomez-Ruiz, Danijela Maksimovic-Ivanic, Sanja Mijatovic, and Goran N. Kaluderovic. On the Discovery, Biological Effects, and Use of Cisplatin and Metallocenes in Anticancer Chemotherapy. *Bioinorganic Chemistry and Applications*, Article ID 140284:14 pp., 2012.

[8] R. Andrew Marshall and Joseph D. Puglisi. NMR structural studies of aminoglycoside:RNA interaction. In *Aminoglycoside Antibiot.*, pages 181–207. John Wiley & Sons, Inc., 2007.

[9] Ludmila Frolov, Andrew Dix, Yitzhak Tor, Alexander B. Tesler, Yulia Chaikin, Alexander Vaskevich, and Israel Rubinstein. Direct Observation of Aminoglycoside-RNA Binding by Localized Surface Plasmon Resonance Spectroscopy. *Analytical Chemistry (Washington, DC, United States)*, 85(4): 2200–2207, 2013.

[10] Herbert A. Kirst. Introduction to the macrolide antibiotics. In *Macrolide Antibiot.*, pages 1–13. Birkhaeuser Verlag, 2002.

[11] Debojit Bose, Gopal Jayaraj, Hemant Suryawanshi, Prachi Agarwala, Subrata Kumar Pore, Rajkumar Banerjee, and Souvik Maiti. The Tuberculosis Drug Streptomycin as a Potential Cancer Therapeutic: Inhibition of miR-21 Function by Directly Targeting Its Precursor. *Angewandte Chemie International Edition*, 51(4):1019–1023, 2012.

[12] P C Zamecnik and M L Stephenson. Inhibition of Rous sarcoma virus replication and cell transformation by a specific oligodeoxynucleotide. *Proceedings of the National Academy of Sciences*, 75 (1):280–284, 1978.

[13] Sanjay Bhanot. Developing Antisense Drugs for Metabolic Diseases. In *Antisense Drug Technology*, pages 641–663. CRC Press, July 2007.

[14] Martin Gleave and Boris Hadaschik. Antisense Oligonucleotides for the Treatment of Cancer. In *Antisense Drug Technology*, pages 699–720. CRC Press, July 2007.

[15] T Jesse Kwoh. An Overview of the Clinical Safety Experience of First- and Second-Generation Antisense Oligonucleotides. In *Antisense Drug Technology*, pages 365–399. CRC Press, July 2007.

[16] Mark Wedel, Rosanne Crooke, and Brenda Baker. Cardiovascular Therapeutic Applications. In *Antisense Drug Technology*, pages 601–639. CRC Press, July 2007.

[17] Yogesh S. Sanghvi. A Status Update of Modified Oligonucleotides for Chemotherapeutics Applications. In *Current Protocols in Nucleic Acid Chemistry*, pages 4.1.1–4.1.22. John Wiley & Sons, Inc., 2011.

[18] Laura. Bonetta. RNA-based therapeutics: ready for delivery? *Cell (Cambridge, MA, United States)*, 136(4):581–584, 2009.

[19] Marc Robert Fabian, Nahum Sonenberg, and Witold Filipowicz. Regulation of mRNA translation and stability by microRNAs. *Annual Review of Biochemistry*, 79:351–379, 2010.

[20] Lin He and Gregory J. Hannon. MicroRNAs: small RNAs with a big role in gene regulation. *Nature Reviews Genetics*, 5(7):522–531, 2004.

[21] Robin C Friedman, Kyle Kai-How Farh, Christopher B Burge, and David P Bartel. Most mammalian mRNAs are conserved targets of microRNAs. *Genome Research*, 19(1):92–105, January 2009.

[22] Anna M. Krichevsky and Galina Gabriely. MiR-21: a small multi-faceted RNA. *Journal of Cellular and Molecular Medicine*, 13(1):39–53, 2009.

[23] George A. Calin and Carlo M. Croce. MicroRNA signatures in human cancers. *Nature Reviews Cancer*, 6(11):857–866, 2006.

[24] Peter Olson, Jun Lu, Hao Zhang, Anny Shai, Matthew G. Chun, Yucheng Wang, Steven K. Libutti, Eric K. Nakakura, Todd R. Golub, and Douglas Hanahan. MicroRNA dynamics in the stages of tumorigenesis correlate with hallmark capabilities of cancer. *Genes & Development*, 23(18):2152–2165, 2009.

[25] Veerle Rottiers and Anders M. Naeaer. MicroRNAs in metabolism and metabolic disorders. *Nature Reviews Molecular Cell Biology*, 13(4):239–250, 2012.

[26] Thomas Hansen, Line Olsen, Morten Lindow, Klaus D. Jakobsen, Henrik Ullum, Erik Jonsson, Ole A. Andreassen, Srdjan Djurovic, Ingrid Melle, Ingrid Agartz, Håkan Hall, Sally Timm, August G. Wang, and Thomas Werge. Brain Expressed microRNAs Implicated in Schizophrenia Etiology. *PLoS ONE*, 2(9):e873, September 2007.

[27] Catherine L. Jopling. Liver-specific microRNA-122: Biogenesis and function. *RNA Biology*, 9(2): 137–142, 2012.

[28] Xing Chen, Ming-Xi Liu, and Gui-Ying Yan. RWRMDA: predicting novel human microRNA-disease associations. *Molecular BioSystems*, 8(10):2792–2798, 2012.

[29] Joshua T. Mendell and Eric N. Olson. MicroRNAs in Stress Signaling and Human Disease. *Cell (Cambridge, MA, United States)*, 148(6):1172–1187, 2012.

[30] Dong Wang, Juan Wang, Ming Lu, Fei Song, and Qing-hua Cui. Inferring the human microRNA functional similarity and functional network based on microRNA-associated diseases. *Bioinformatics*, 26(13):1644–1650, 2010.

[31] Gracjan Michlewski, Sonia Guil, Colin A. Semple, and Javier F. Caceres. Posttranscriptional regulation of miRNAs harboring conserved terminal loops. *Molecular Cell*, 32(3):383–393, 2008.

[32] R C Lee, R L Feinbaum, and V Ambros. The C. elegans heterochronic gene lin-4 encodes small RNAs with antisense complementarity to lin-14. *Cell*, 75(5):843–854, 1993.

[33] A E Pasquinelli, B J Reinhart, F Slack, M Q Martindale, M I Kuroda, B Maller, D C Hayward, E E Ball, B Degnan, P Müller, J Spring, A Srinivasan, M Fishman, J Finnerty, J Corbo, M Levine, P Leahy, E Davidson, and G Ruvkun. Conservation of the sequence and temporal expression of

let-7 heterochronic regulatory RNA. *Nature*, 408(6808):86–89, November 2000.

[34] B J Reinhart, F J Slack, M Basson, A E Pasquinelli, J C Bettinger, A E Rougvie, H R Horvitz, and G Ruvkun. The 21-nucleotide let-7 RNA regulates developmental timing in Caenorhabditis elegans. *Nature*, 403(6772):901–906, 2000.

[35] F J Slack, M Basson, Z Liu, V Ambros, H R Horvitz, and G Ruvkun. The lin-41 RBCC gene acts in the C. elegans heterochronic pathway between the let-7 regulatory RNA and the LIN-29 transcription factor. *Mol. Cell*, 5(4):659–669, 2000.

[36] M Lagos-Quintana, R Rauhut, W Lendeckel, and T Tuschl. Identification of novel genes coding for small expressed RNAs. *Science Signalling*, 294(5543):853, 2001.

[37] N C Lau, L P Lim, E G Weinstein, and D P Bartel. An abundant class of tiny RNAs with probable regulatory roles in Caenorhabditis elegans. *Science Signalling*, 294(5543):858–862, October 2001.

[38] R C Lee and V Ambros. An extensive class of small RNAs in Caenorhabditis elegans. *Science Signalling*, 294(5543):862, 2001.

[39] Marc R Fabian and Nahum Sonenberg. The mechanics of miRNA-mediated gene silencing: a look under the hood of miRISC. *Nature structural & molecular biology*, 19(6):586–593, June 2012.

[40] V Narry Kim, Jinju Han, and Mikiko C Siomi. Biogenesis of small RNAs in animals. *Nature Reviews Molecular Cell Biology*, 10(2):126–139, February 2009.

[41] Yoontae Lee, Minju Kim, Jinju Han, Kyu-Hyun Yeom, Sanghyuk Lee, Sung Hee Baek, and V Narry Kim. MicroRNA genes are transcribed by RNA polymerase II. *The EMBO journal*, 23(20):4051–4060, October 2004.

[42] George Adrian Calin, Calin Dan Dumitru, Masayoshi Shimizu, Roberta Bichi, Simona Zupo, Evan Noch, Hansjuerg Aldler, Sashi Rattan, Michael Keating, Kanti Rai, Laura Rassenti, Thomas Kipps, Massimo Negrini, Florencia Bullrich, and Carlo M Croce. Frequent deletions and down-regulation of micro- RNA genes miR15 and miR16 at 13q14 in chronic lymphocytic leukemia. *Proceedings of the National Academy of Sciences of the United States of America*, 99(24):15524–15529, November 2002.

[43] W. Tam. Identification and characterization of human BIC, a gene on chromosome 21 that encodes a noncoding RNA. *Gene*, 274(1-2):157–167, 2001.

[44] Chellappagounder Thangavel, Ettickan Boopathi, Adam Ertel, Meng Lim, Sankar Addya, Paolo Fortina, Agnieszka K. Witkiewicz, and Erik S. Knudsen. Regulation of miR106b cluster through the RB pathway: mechanism and functional targets. *Cell Cycle*, 12(1):98–111, 2013.

[45] Yoontae Lee, Kipyoung Jeon, Jun-Tae Lee, Sunyoung Kim, and V Narry Kim. MicroRNA maturation: stepwise processing and subcellular localization. *The EMBO journal*, 21(17):4663–4670, September 2002.

[46] Yael Altuvia, Pablo Landgraf, Gila Lithwick, Naama Elefant, Sébastien Pfeffer, Alexei Aravin, Michael J Brownstein, Thomas Tuschl, and Hanah Margalit. Clustering and conservation patterns of human microRNAs. *Nucleic acids research*, 33(8):2697–2706, 2005.

[47] Antony Rodriguez, Sam Griffiths-Jones, Jennifer L Ashurst, and Allan Bradley. Identification of mammalian microRNA host genes and transcription units. *Genome Research*, 14(10A):1902–1910, October 2004.

[48] F Ozsolak, L L Poling, Z Wang, H Liu, X S Liu, R G Roeder, X Zhang, J S Song, and D E Fisher. Chromatin structure analyses identify miRNA promoters. *Genes & Development*, 22(22):3172–3183, November 2008.

[49] Young-Kook Kim and V Narry Kim. Processing of intronic microRNAs. *The EMBO journal*, 26(3):775–783, February 2007.

[50] Xuezhong Cai, Curt H Hagedorn, and Bryan R Cullen. Human microRNAs are processed from capped, polyadenylated transcripts that can also function as mRNAs. *RNA*, 10(12):1957–1966, December 2004.

[51] Glen M Borchert, William Lanier, and Beverly L Davidson. RNA polymerase III transcribes human microRNAs. *Nature structural & molecular biology*, 13(12):1097–1101, November 2006.

[52] E Ladewig, K Okamura, A S Flynt, J O Westholm, and E C Lai. Discovery of hundreds of mirtrons in mouse and human small RNA data. *Genome Research*, 22(9):1634–1645, September 2012.

[53] Joshua E Babiarz, J Graham Ruby, Yangming Wang, David P Bartel, and Robert Blelloch. Mouse ES cells express endogenous shRNAs, siRNAs, and other Microprocessor-independent, Dicer-dependent small RNAs. *Genes & Development*, 22(20):2773–2785, October 2008.

[54] Christine Ender, Azra Krek, Marc R Friedländer, Michaela Beitzinger, Lasse Weinmann, Wei Chen, Sébastien Pfeffer, Nikolaus Rajewsky, and Gunter Meister. A Human snoRNA with MicroRNA-Like Functions. *Molecular Cell*, 32(4):519–528, November 2008.

[55] Yoontae Lee, Chiyoung Ahn, Jinju Han, Hyounjeong Choi, Jaekwang Kim, Jeongbin Yim, Junho Lee, Patrick Provost, Olof Rådmark, Sunyoung Kim, and V Narry Kim. The nuclear RNase III Drosha initiates microRNA processing. *Nature*, 425(6956):415–419, September 2003.

[56] Jinju Han, Yoontae Lee, Kyu-Hyun Yeom, Young-Kook Kim, Hua Jin, and V Narry Kim. The Drosha-DGCR8 complex in primary microRNA processing. *Genes & Development*, 18(24):3016–3027, December 2004.

[57] Richard I Gregory, Kai-ping Yan, Govindasamy Amuthan, Thimmaiah Chendrimada, Behzad Doratotaj, Neil Cooch, and Ramin Shiekhattar. The Microprocessor complex mediates the genesis of microRNAs. *Nature Publishing Group*, 432(7014):235–240, November 2004.

[58] Markus Landthaler, Abdullah Yalcin, and Thomas Tuschl. The Human DiGeorge Syndrome Critical Region Gene 8 and Its D. melanogaster Homolog Are Required for miRNA Biogenesis. *Current Biology*, 14(23):2162–2167, December 2004.

[59] Yan Zeng and Bryan R Cullen. Efficient processing of primary microRNA hairpins by Drosha requires flanking nonstructured RNA sequences. *The Journal of biological chemistry*, 280(30):27595–27603, July 2005.

[60] Jinju Han, Yoontae Lee, Kyu-Hyeon Yeom, Jin-Wu Nam, Inha Heo, Je-Keun Rhee, Sun Young Sohn, Yunje Cho, Byoung-Tak Zhang, and V Narry Kim. Molecular Basis for the Recognition of Primary microRNAs by the Drosha-DGCR8 Complex. *Cell*, 125(5):887–901, June 2006.

[61] Elsebet Lund, Stephan Güttinger, Angelo Calado, James E Dahlberg, and Ulrike Kutay. Nuclear export of microRNA precursors. *Science*, 303(5654):95–98, January 2004.

[62] Markus T Bohnsack, Kevin Czaplinski, and Dirk Gorlich. Exportin 5 is a RanGTP-dependent dsRNA-binding protein that mediates nuclear export of pre-miRNAs. *RNA*, 10(2):185–191, February 2004.

[63] Yan Zeng and Bryan R Cullen. Structural requirements for pre-microRNA binding and nuclear export by Exportin 5. *Nucleic acids research*, 32(16):4776–4785, 2004.

[64] Pick-Wei Lau, Keelan Z Guiley, Nabanita De, Clinton S Potter, Bridget Carragher, and Ian J MacRae. The molecular architecture of human Dicer. *Nature structural & molecular biology*, 19(4):436–440, March 2012.

[65] G Hutvagner, J McLachlan, A E Pasquinelli, E Bálint, T Tuschl, and P D Zamore. A cellular function for the RNA-interference enzyme Dicer in the maturation of the let-7 small temporal RNA. *Science*, 293(5531):834–838, August 2001.

[66] R F Ketting, S E Fischer, E Bernstein, T Sijen, G J Hannon, and R H Plasterk. Dicer functions in RNA interference and in synthesis of small RNA involved in developmental timing in C. elegans. *Genes & Development*, 15(20):2654–2659, October 2001.

[67] S W Knight and B L Bass. A role for the RNase III enzyme DCR-1 in RNA interference and germ line development in Caenorhabditis elegans. *Science*, 293(5538):2269–2271, September 2001.

[68] Astrid D Haase, Lukasz Jaskiewicz, Haidi Zhang, Sébastien Lainé, Ragna Sack, Anne Gatignol, and Witold Filipowicz. TRBP, a regulator of cellular PKR and HIV-1 virus expression, interacts with Dicer and functions in RNA silencing. *EMBO reports*, 6(10):961–967, October 2005.

[69] Yoontae Lee, Inha Hur, Seong-Yeon Park, Young-Kook Kim, Mi Ra Suh, and V Narry Kim. The role of PACT in the RNA silencing pathway. *The EMBO journal*, 25(3):522–532, February 2006.

[70] Yong Feng, Xiaoxiao Zhang, Paul Graves, and Yan Zeng. A comprehensive analysis of precursor microRNA cleavage by human Dicer. *RNA*, 18(11):2083–2092, October 2012.

[71] Thimmaiah P Chendrimada, Richard I Gregory, Easwari Kumaraswamy, Jessica Norman, Neil Cooch, Kazuko Nishikura, and Ramin Shiekhattar. TRBP recruits the Dicer complex to Ago2 for microRNA processing and gene silencing. *Nature Publishing Group*, 436(7051):740–744, June 2005.

[72] Elisavet Maniataki and Zissimos Mourelatos. A human, ATP-independent, RISC assembly machine fueled by pre-miRNA. *Genes & Development*, 19(24):2979–2990, December 2005.

[73] Ian J MacRae, Enbo Ma, Min Zhou, Carol V Robinson, and Jennifer A Doudna. In vitro reconstitution of the human RISC-loading complex. *Proceedings of the National Academy of Sciences of the United States of America*, 105(2):512–517, January 2008.

[74] Richard I Gregory, Thimmaiah P Chendrimada, Neil Cooch, and Ramin Shiekhattar. Human RISC Couples MicroRNA Biogenesis and Posttranscriptional Gene Silencing. *Cell*, 123(4):631–640, November 2005.

[75] Enbo Ma, Kaihong Zhou, Mary Anne Kidwell, and Jennifer A Doudna. Coordinated Activities of Human Dicer Domains in Regulatory RNA Processing. *Journal of Molecular Biology*, 422(4):466–476, September 2012.

[76] Jonathan B. Preall and Erik J. Sontheimer. RNAi: RISC Gets Loaded. *Cell*, 123(4):543–545, November 2005.

[77] Eric Huntzinger and Elisa Izaurralde. Gene silencing by microRNAs: contributions of translational repression and mRNA decay. *Nature reviews. Genetics*, 12(2):99–110, February 2011.

[78] Pieter Bas Kwak and Yukihide Tomari. The N domain of Argonaute drives duplex unwinding during RISC assembly. *Nature structural & molecular biology*, 19(2):145–151, January 2012.

[79] Dianne S Schwarz, György Hutvágner, Tingting Du, Zuoshang Xu, Neil Aronin, and Phillip D Zamore. Asymmetry in the assembly of the RNAi enzyme complex. *Cell*, 115(2):199–208, October 2003.

[80] Anastasia Khvorova, Angela Reynolds, and Sumedha D Jayasena. Functional siRNAs and miR-NAs exhibit strand bias. *Cell*, 115(2):209–216, October 2003.

[81] György Hutvágner and Martin J Simard. Argonaute proteins: key players in RNA silencing. *Nature Reviews Molecular Cell Biology*, 9(1):22–32, January 2008.

[82] E Huntzinger, D Kuzuoglu-Ozturk, J E Braun, A Eulalio, L Wohlbold, and E Izaurralde. The interactions of GW182 proteins with PABP and deadenylases are required for both translational repression and degradation of miRNA targets. *Nucleic acids research*, 41(2):978–994, November 2013.

[83] J. D. Watson and F. H. C. Crick. Molecular Structure of Nucleic Acids: A Structure for Deoxyribose Nucleic Acid. *Nature*, 171(4356):737–738, April 1953.

[84] Stanley Thomas Crooke, editor. *Antisense drug technology : principles, strategies, and applications.* Boca Raton, FL : CRC Press, Boca Raton, FL, 2008. – pp.

[85] C. Frank Bennett and Eric E. Swayze. RNA Targeting Therapeutics: Molecular Mechanisms of Antisense Oligonucleotides as a Therapeutic Platform. *Annu. Rev. Pharmacol. Toxicol.*, 50(1):

259–293, January 2010.

[86] C. Cazenave, C. A. Stein, N. Loreau, N. T. Thuong, L. M. Neckers, C. Subasinghe, C. Helene, J. S. Cohen, and J. J. Toulme. Comparative inhibition of rabbit globin mRNA translation by modified antisense oligodeoxynucleotides. *Nucleic Acids Research*, 17(11):4255–73, 1989.

[87] Brenda F. Baker, Sidney S. Lot, Thomas P. Condon, Shin Cheng-Flournoy, Elena A. Lesnik, Henri M. Sasmor, and C. Frank Bennett. 2'-O-(2-methoxy)ethyl-modified anti-intercellular adhesion molecule 1 (ICAM-1) oligonucleotides selectively increase the ICAM-1 mRNA level and inhibit formation of the ICAM-1 translation initiation complex in human umbilical vein endothelial cells. *Journal of Biological Chemistry*, 272(18):11994–12000, 1997.

[88] Zbigniew Dominski and Ryszard Kole. Restoration of correct splicing in thalassemic pre-mRNA by antisense oligonucleotides. *Proceedings of the National Academy of Sciences of the United States of America*, 90(18):8673–7, 1993.

[89] Yimin Hua, Timothy A. Vickers, Brenda F. Baker, C. Frank Bennett, and Adrian R. Krainer. Enhancement of SMN2 exon 7 inclusion by antisense oligonucleotides targeting the exon. *PLoS Biology*, 5(4):729–744, 2007.

[90] Peter Sazani, Maria Graziewicz, and Ryszard Kole. Splice Switching Oligonucleotides as Potential Therapeutics. In *Antisense Drug Technology*, pages 89–114. CRC Press, July 2007.

[91] Timothy A. Vickers, Jacqueline R. Wyatt, Todd Burckin, C. Frank Bennett, and Susan M. Freier. Fully modified 2' MOE oligonucleotides redirect polyadenylation. *Nucleic Acids Research*, 29(6): 1293–1299, 2001.

[92] Scott Davis, Stephanie Propp, Susan M. Freier, Laura E. Jones, Martin J. Serra, Garth Kinberger, Balkrishen Bhat, Eric E. Swayze, C. Frank Bennett, and Christine Esau. Potent inhibition of microRNA in vivo without degradation. *Nucleic Acids Research*, 37(1):70–77, 2009.

[93] Madhu S. Kumar, Stefan J. Erkeland, Ryan E. Pester, Cindy Y. Chen, Margaret S. Ebert, Phillip A. Sharp, and Tyler Jacks. Suppression of non-small cell lung tumor development by the let-7 microRNA family. *Proceedings of the National Academy of Sciences*, 105(10):3903–3908, 2008.

[94] John J. Turner, Andrey A. Arzumanov, and Michael J. Gait. Synthesis, cellular uptake and HIV-1 Tat-dependent trans-activation inhibition activity of oligonucleotide analogues disulphide-conjugated to cell-penetrating peptides. *Nucleic Acids Research*, 33(1):27–42, 2005.

[95] Hongjiang Wu, Stanley Crooke, and Walt Lima. The RNase H Mechanism. In *Antisense Drug Technology*, pages 47–74. CRC Press, July 2007.

[96] Hideo Inoue, Yoji Hayase, Shigenori Iwai, and Eiko Ohtsuka. Sequence-dependent hydrolysis of RNA using modified oligonucleotide splints and RNase H. *FEBS Letters*, 215(2):327–330, May 1987.

[97] B P Monia, E A Lesnik, C Gonzalez, W F Lima, D McGee, C J Guinosso, A M Kawasaki, P D Cook, and S M Freier. Evaluation of 2'-modified oligonucleotides containing 2'-deoxy gaps as antisense inhibitors of gene expression. *Journal of Biological Chemistry*, 268(19):14514–14522, 1993.

[98] Sayda M. Elbashir, Jens Harborth, Winfried Lendeckel, Abdullah Yalcin, Klaus Weber, and Thomas Tuschl. Duplexes of 21-nucleotide RNAs mediate RNA interference in cultured mammalian cells. *Nature*, 411(6836):494–498, May 2001.

[99] Jidong Liu, Michelle A. Carmell, Fabiola V. Rivas, Carolyn G. Marsden, J. Michael Thomson, Ji-Joon Song, Scott M. Hammond, Leemor Joshua-Tor, and Gregory J. Hannon. Argonaute2 Is the Catalytic Engine of Mammalian RNAi. *Science*, 305(5689):1437–1441, September 2004.

[100] Gunter Meister, Markus Landthaler, Agnieszka Patkaniowska, Yair Dorsett, Grace Teng, and Thomas Tuschl. Human Argonaute2 Mediates RNA Cleavage Targeted by miRNAs and siRNAs. *Molecular Cell*, 15(2):185–197, July 2004.

[101] K A Lennox and M A Behlke. Chemical modification and design of anti-miRNA oligonucleotides. *Gene Ther*, 18(12):1111–1120, December 2011.

[102] Scott Davis, Bridget Lollo, Susan Freier, and Christine Esau. Improved targeting of miRNA with antisense oligonucleotides. *Nucleic Acids Research*, 34(8):2294–2304, January 2006.

[103] Jan Kruetzfeldt, Nikolaus Rajewsky, Ravi Braich, Kallanthottathil G. Rajeev, Thomas Tuschl, Muthiah Manoharan, and Markus Stoffel. Silencing of microRNAs in vivo with 'antagomirs'. *Nature (London, United Kingdom)*, 438(7068):685–689, 2005.

[104] Thomas Thum, Carina Gross, Jan Fiedler, Thomas Fischer, Stephan Kissler, Markus Bussen, Paolo Galuppo, Steffen Just, Wolfgang Rottbauer, Stefan Frantz, Mirco Castoldi, Juergen Soutschek, Victor Koteliansky, Andreas Rosenwald, M. Albert Basson, Jonathan D. Licht, John T. R. Pena, Sara H. Rouhanifard, Martina U. Muckenthaler, Thomas Tuschl, Gail R. Martin, Johann Bauersachs, and Stefan Engelhardt. MicroRNA-21 contributes to myocardial disease by stimulating MAP kinase signalling in fibroblasts. *Nature (London, United Kingdom)*, 456(7224):980–984, 2008.

[105] Li Ma, Ferenc Reinhardt, Elizabeth Pan, Juergen Soutschek, Balkrishen Bhat, Eric G. Marcusson, Julie Teruya-Feldstein, George W. Bell, and Robert A. Weinberg. Therapeutic silencing of miR-10b inhibits metastasis in a mouse mammary tumor model. *Nature Biotechnology*, 28(4):341–347, 2010.

[106] Eugene Berezikov, Victor Guryev, Jose van, de Belt, Erno Wienholds, Ronald H. A. Plasterk, and Edwin Cuppen. Phylogenetic shadowing and computational identification of human microRNA genes. *Cell (Cambridge, MA, United States)*, 120(1):21–24, 2005.

[107] Christina E. Luense, Gracjan Michlewski, Christine S. Hopp, Andrea Rentmeister, Javier F. Caceres, Michael Famulok, and Guenter Mayer. An aptamer targeting the apical-loop domain modulates pri-miRNA processing. *Angewandte Chemie, International Edition*, 49(27):4674–4677, S4674/1–S4674/12–, 2010.

[108] Xiaoxiao Zhang and Yan Zeng. The terminal loop region controls microRNA processing by Drosha and Dicer. *Nucleic Acids Research*, 38(21):7689–7697, 2010.

[109] Walt F. Lima, Brett P. Monia, David J. Ecker, and Susan M. Freier. Implication of RNA structure on antisense oligonucleotide hybridization kinetics. *Biochemistry*, 31(48):12055–61, 1992.

[110] Thomas W. Bruice and Walt F. Lima. Control of Complexity Constraints on Combinatorial Screening for Preferred Oligonucleotide Hybridization Sites on Structured RNA. *Biochemistry*, 36(16):5004–5019, 1997.

[111] Elzbieta Kierzek. Binding of Short Oligonucleotides to RNA: Studies of the Binding of Common RNA Structural Motifs to Isoenergetic Microarrays. *Biochemistry*, 48(48):11344–11356, October 2009.

[112] Paul S. Eder, Rene J. Devine, John M. Dagle, and Joseph A. Walder. Substrate specificity and kinetics of degradation of antisense oligonucleotides by a 3' exonuclease in plasma. *Antisense Research and Development*, 1(2):141–51, 1991.

[113] Christine C. Esau and Brett P. Monia. Therapeutic potential for microRNAs. *Advanced Drug Delivery Reviews*, 59(2-3):101–114, 2007.

[114] Jan Stenvang, Andreas Petri, Morten Lindow, Susanna Obad, and Sakari Kauppinen. Inhibition of microRNA function by antimiR oligonucleotides. *Silence*, 3(1):1–17, 2012.

[115] Hideo Inoue, Yohji Hayase, Miyuki Asaka, Akihiro Imura, Shigenori Iwai, Kazunobu Miura, and Eiko Ohtsuka. Synthesis and properties of novel nucleic acid probes. *Nucleic Acids Symposium Series*, 16(Symp. Nucleic Acids Chem., 13th):165–8, 1985.

[116] Brian S. Sproat, Angus I. Lamond, Barbro Beijer, Philippe Neuner, and Ursula Ryder. Highly efficient chemical synthesis of 2'-O-methyloligoribonucleotides and tetrabiotinylated derivatives; novel probes that are resistant to degradation by RNA or DNA specific nucleases. *Nucleic Acids*

Research, 17(9):3373–86, 1989.

[117] Susan M. Freier and Karl-Heinz Altmann. The ups and downs of nucleic acid duplex stability: structure-stability studies on chemically-modified DNA:RNA duplexes. *Nucleic Acids Research*, 25 (22):4429–4443, 1997.

[118] Mark A. Behlke. Chemical Modification of siRNAs for In Vivo Use. *Oligonucleotides*, 18(4):305–320, 2008.

[119] Kim A. Lennox, Jaime L. Sabel, Maegan J. Johnson, Bernardo G. Moreira, Cherisa A. Fletcher, Scott D. Rose, Mark A. Behlke, Andrei L. Laikhter, Joseph A. Walder, and John M. Dagle. Characterization of Modified Antisense Oligonucleotides in Xenopus laevis Embryos. *Oligonucleotides*, 16(1):26–42, 2006.

[120] Kim A. Lennox and Mark A. Behlke. A direct comparison of anti-microRNA oligonucleotide potency. *Pharmaceutical Research*, 27(9):1788–1799, 2010.

[121] Christine Esau, Xiaolin Kang, Eigen Peralta, Elaine Hanson, Eric G. Marcusson, Lingamanaidu V. Ravichandran, Yingqing Sun, Seongjoon Koo, Ranjan J. Perera, Ravi Jain, Nicholas M. Dean, Susan M. Freier, C. Frank Bennett, Bridget Lollo, and Richard Griffey. MicroRNA-143 Regulates Adipocyte Differentiation. *Journal of Biological Chemistry*, 279(50):52361–52365, 2004.

[122] Christine Esau, Scott Davis, Susan F. Murray, Xing Xian Yu, Sanjay K. Pandey, Michael Pear, Lynnetta Watts, Sheri L. Booten, Mark Graham, Robert McKay, Amuthakannan Subramaniam, Stephanie Propp, Bridget A. Lollo, Susan Freier, C. Frank Bennett, Sanjay Bhanot, and Brett P. Monia. miR-122 regulation of lipid metabolism revealed by in vivo antisense targeting. *Cell Metabolism*, 3(2):87–98, 2006.

[123] Satoshi Obika, Daishu Nanbu, Yoshiyuki Hari, Ken-ichiro Morio, Yasuko In, Toshimasa Ishida, and Takeshi Imanishi. Synthesis of 2'-O,4'-C-methyleneuridine and -cytidine. Novel bicyclic nucleosides having a fixed C3, -endo sugar puckering. *Tetrahedron Letters*, 38(50):8735–8738, December 1997.

[124] Alexei A. Koshkin, Sanjay K. Singh, Poul Nielsen, Vivek K. Rajwanshi, Ravindra Kumar, Michael Meldgaard, Carl Erik Olsen, and Jesper Wengel. LNA (Locked Nucleic Acids): Synthesis of the adenine, cytosine, guanine, 5-methylcytosine, thymine and uracil bicyclonucleoside monomers, oligomerisation, and unprecedented nucleic acid recognition. *Tetrahedron*, 54(14):3607–3630, April 1998.

[125] Harleen Kaur, Amit Arora, Jesper Wengel, and Souvik Maiti. Thermodynamic, Counterion, and Hydration Effects for the Incorporation of Locked Nucleic Acid Nucleotides into DNA Duplexes. *Biochemistry*, 45(23):7347–7355, May 2006.

[126] Michael Petersen and Jesper Wengel. LNA: a versatile tool for therapeutics and genomics. *Trends in Biotechnology*, 21(2):74–81, 2003.

[127] Sheila J. Wood. DNA-DNA hybridization in real time using BIAcore. *Microchemical Journal*, 47(3): 330–7, 1993.

[128] Kristine Kilsaa Jensen, Henrik Oerum, Peter E. Nielsen, and Bengt Norden. Kinetics for Hybridization of Peptide Nucleic Acids (PNA) with DNA and RNA Studied with the BIAcore Technique. *Biochemistry*, 36(16):5072–5077, 1997.

[129] Frederic Duconge, Carmelo Di, Primo, and Jean-Jacques Toulme. Is a closing "GA pair" a rule for stable loop-loop RNA complexes? *Journal of Biological Chemistry*, 275(28):21287–21294, 2000.

[130] Jr. Gregorian, Razmic S. and Donald M. Crothers. Determinants of RNA hairpin loop-loop complex stability. *Journal of Molecular Biology*, 248(5):968–84, 1995.

[131] Kung-Yao Chang and Jr. Tinoco, Ignacio. The structure of an RNA "kissing" hairpin complex of the HIV TAR hairpin loop and its complement. *Journal of Molecular Biology*, 269(1):52–66, 1997.

[132] T. Murlidharan Nair, David G. Myszka, and Darrell R. Davis. Surface plasmon resonance kinetic studies of the HIV TAR RNA kissing hairpin complex and its stabilization by 2-thiouridine modification. *Nucleic Acids Research*, 28(9):1935–1940, 2000.

[133] R.K. Kumar and D.R. Davis. Synthesis and studies on the effect of 2-thiouridine and 4-thiouridine on sugar conformation and RNA duplex stability. *Nucleic acids research*, 25(6):1272–80, 1997.

[134] S. Yokoyama, Z. Yamaizumi, S. Nishimura, and T. Miyazawa. 1H NMR studies on the conformational characteristics of 2-thiopyrimidine nucleotides found in transfer RNAs. *Nucleic acids research*, 6(7):2611–26, 1979.

[135] Fabien Darfeuille, Christian Cazenave, Sergei Gryaznov, Frederic Duconge, Carmelo Di, Primo, and Jean-Jacques Toulme. RNA and N3' → P5' kissing aptamers targeted to the trans-activation responsive (TAR) RNA of the human immunodeficiency virus-1. *Nucleosides, Nucleotides & Nucleic Acids*, 20(4-7):441–449, 2001.

[136] Fabien Darfeuille, Andrey Arzumanov, Michael J. Gait, Carmelo Di, Primo, and Jean-Jacques Toulme. 2'-O-Methyl-RNA Hairpins Generate Loop-Loop Complexes and Selectively Inhibit HIV-1 Tat-Mediated Transcription. *Biochemistry*, 41(40):12186–12192, 2002.

[137] Fabien Darfeuille, Andrey Arzumanov, Sergei Gryaznov, Michael J. Gait, Carmelo Di Primo, and Jean-Jacques Toulm. Loop-loop interaction of HIV-1 TAR RNA with N3'→P5' deoxyphosphoramidate aptamers inhibits in vitro Tat-mediated transcription. *Proceedings of the National Academy of Sciences*, 99(15):9709–9714, 2002.

[138] Anna Astriab-Fisher, Dimitri Sergueev, Michael Fisher, Barbara Ramsay Shaw, and R. L. Juliano. Conjugates of Antisense Oligonucleotides with the Tat and Antennapedia Cell-Penetrating Peptides: Effects on Cellular Uptake, Binding to Target Sequences, and Biologic Actions. *Pharmaceutical Research*, 19(6):744–754, 2002.

[139] Fabien Darfeuille, Jens Bo Hansen, Henrik Orum, Carmelo Di, Primo, and Jean-Jacques Toulme. LNA/DNA chimeric oligomers mimic RNA aptamers targeted to the TAR RNA element of HIV-1. *Nucleic Acids Research*, 32(10):3101–3107, 2004.

[140] Steven H. L. Verhelst, Paul J. A. Michiels, Gijsbert A. Van, Der Marel, Constant A. A. Van, Boeckel, and Jacques H. Van, Boom. Surface plasmon resonance evaluation of various aminoglycoside-RNA hairpin interactions reveals low degree of selectivity. *ChemBioChem*, 5(7):937–942, 2004.

[141] David Boucard, Jean-Jacques Toulme, and Carmelo Di, Primo. Bimodal Loop-Loop Interactions Increase the Affinity of RNA Aptamers for HIV-1 RNA Structures. *Biochemistry*, 45(5):1518–1524, 2006.

[142] Yang Gao, Lauren K. Wolf, and Rosina M. Georgiadis. Secondary structure effects on DNA hybridization kinetics: a solution versus surface comparison. *Nucleic Acids Research*, 34(11):3370–3377, 2006.

[143] Alan Ironmonger, Benjamin Whittaker, Andrew J. Baron, Blandine Clique, Chris J. Adams, Alison E. Ashcroft, Peter G. Stockley, and Adam Nelson. Scanning conformational space with a library of stereo- and regiochemically diverse aminoglycoside derivatives: the discovery of new ligands for RNA hairpin sequences. *Organic & Biomolecular Chemistry*, 5(7):1081–1086, 2007.

[144] Carmelo Di Primo, Ivo Rudloff, Sandrine Reigadas, Andrey A. Arzumanov, Michael J. Gait, and Jean-Jacques Toulme. Systematic screening of LNA/2'-O-methyl chimeric derivatives of a TAR RNA aptamer. *FEBS Letters*, 581(4):771–774, 2007.

[145] Joshua B. Mandir, Matthew R. Lockett, Margaret F. Phillips, Hatim T. Allawi, Victor I. Lyamichev, and Lloyd M. Smith. Rapid determination of RNA accessible sites by surface plasmon resonance detection of hybridization to DNA arrays. *Analytical Chemistry (Washington, DC, United States)*, 81(21):8949–8956, 2009.

[146] R.W. Wood. XLII. On a remarkable case of uneven distribution of light in a diffraction grating spectrum. *Philosophical Magazine Series 6*, 4(21):396–402, September 1902.

[147] I. Pockrand, J. D. Swalen, II Gordon, J. G., and M. R. Philpott. Surface plasmon spectroscopy of organic monolayer assemblies. *Surface Science*, 74(1):237–44, 1978.

[148] Bo Liedberg, Claes Nylander, and Ingemar Lundstrm. Surface plasmon resonance for gas detection and biosensing. *Sensors and Actuators*, 4(0):299–304, 1983.

[149] M.T. Flanagan and R.H. Pantell. Surface plasmon resonance and immunosensors. *Electronics Letters*, 20(23):968–970, 1984.

[150] DC Cullen, RG Brown, and CR Lowe. Detection of immuno-complex formation via surface plasmon resonance on gold-coated diffraction gratings. *Biosensors*, 3(4):211–225–, 1987.

[151] C.S. Mayo and R.B. Hallock. Immunoassay based on surface plasmon oscillations. *Journal of Immunological Methods*, 120(1):105–114, June 1989.

[152] Lars G. Fägerstam, A Frostell, Robert Karlsson, Mari Kullman, Anita Larsson, Magnus Malmqvist, and Helena Butt. Detection of antigen–antibody interactions by surface plasmon resonance. Application to Epitope Mapping. *J. Mol. Recognit.*, 3(5-6):208–214, 1990.

[153] Rebecca L. Rich and David G. Myszka. Survey of the year 2005 commercial optical biosensor literature. *Journal of Molecular Recognition*, 19(6):478–534, 2006.

[154] Rebecca L. Rich and David G. Myszka. Survey of the year 2007 commercial optical biosensor literature. *Journal of Molecular Recognition*, 21(6):355–400, 2008.

[155] Rebecca L. Rich and David G. Myszka. Survey of the 2009 commercial optical biosensor literature. *Journal of Molecular Recognition*, 24(6):892–914, 2011.

[156] R. B. M. Schasfoort, Anna J. Tudos, and Editors., editors. *Handbook of Surface Plasmon Resonance.* Royal Society of Chemistry, 2008. 403 pp.– pp.

[157] Maria Minunni and Anna Rita Bilia. SPR in drug discovery: searching bioactive compounds in plant extracts. *Methods in Molecular Biology (Totowa, NJ, United States)*, 572(Ligand-Macromolecular Interactions in Drug Discovery):203–218, 2010.

[158] U. Helena Danielson. Integrating surface plasmon resonance biosensor-based interaction kinetic analyses into the lead discovery and optimization process. *Future Medicinal Chemistry*, 1(8): 1399–1414, 2009.

[159] Alan McWhirter and Lennart. Wahlstroem. The benefits and scope of surface plasmon resonance-based biosensors in food analysis. In *Handb. Surf. Plasmon Reson.*, pages 333–353. Royal Society of Chemistry, 2008.

[160] Patricia Schubert-Ullrich, Judith Rudol, Parisa Ansari, Brigitte Galler, Manuela Fuehrer, Alexandra Molinelli, and Sabine Baumgartner. Commercialized rapid immunoanalytical tests for determination of allergenic food proteins: an overview. *Analytical and Bioanalytical Chemistry*, 395(1):69–81, 2009.

[161] Fahriye Ceyda Dudak and Ismail Hakki Boyaci. Rapid and label-free bacteria detection by surface plasmon resonance (SPR) biosensors. *Biotechnology Journal*, 4(7):1003–1011, 2009.

[162] Jason E. Dover, Grace M. Hwang, Elaine H. Mullen, Barton C. Prorok, and Sang-Jin Suh. Recent advances in peptide probe-based biosensors for detection of infectious agents. *Journal of Microbiological Methods*, 78(1):10–19, 2009.

[163] Richa Garg, Vaishali Kapoor, Manasi Mittal, Manoj K. Singh, Nootan K. Shukla, and Satya N. Das. Abnormal expression of PI3K isoforms in patients with tobacco-related oral squamous cell carcinoma. *Clinica Chimica Acta*, 416:100–106, 2013.

[164] Oksana V. Gnedenko, Yury V. Mezentsev, Andrey A. Molnar, Andrey V. Lisitsa, Alexis S. Ivanov, and Alexander I. Archakov. Highly sensitive detection of human cardiac myoglobin using a reverse sandwich immunoassay with a gold nanoparticle-enhanced surface plasmon resonance biosensor. *Analytica Chimica Acta*, 759:105–109, 2013.

[165] Andreas Otto. Excitation of nonradiative surface plasma waves in silver by the method of frustrated total reflection. *Zeitschrift fr Physik*, 216(4):398–410, 1968.

[166] Iva Navratilova and David G. Myszka. Investigating biomolecular interactions and binding properties using SPR biosensors. *Springer Series on Chemical Sensors and Biosensors*, 4(Surface Plasmon Resonance Based Sensors):155–176, 2006.

[167] David G. Myszka. Improving biosensor analysis. *Journal of Molecular Recognition*, 12(5):279–284, 1999.

[168] Peter Schuck and Huaying Zhao. The role of mass transport limitation and surface heterogeneity in the biophysical characterization of macromolecular binding processes by SPR biosensing. *Methods in Molecular Biology (Totowa, NJ, United States)*, 627(Surface Plasmon Resonance):15–54, 2010.

[169] Kenneth M. Comess and Mark E. Schurdak. Affinity-based screening techniques for enhancing lead discovery. *Current opinion in drug discovery & development*, 7(4):411–6, 2004.

[170] Robert A. Copeland, David L. Pompliano, and Thomas D. Meek. Drug-target residence time and its implications for lead optimization. *Nature Reviews Drug Discovery*, 5(9):730–739, 2006.

[171] Robert A. Copeland. The dynamics of drug-target interactions: drug-target residence time and its impact on efficacy and safety. *Expert Opinion on Drug Discovery*, 5(4):305–310, 2010.

[172] Mario A. E. Rebhan, Andreas Brunschweiger, and Jonathan Hall. Measurement by SPR of Very Low Dissociation Rates: Oxidation-Mediated Loss of Biotin–Streptavidin Affinity. *ChemBioChem*, 14:2091–2094, 2013. doi:10.1002/cbic.201300468.

[173] Richard W. Wagner, Mark D. Matteucci, Deborah Grant, Teresa Huang, and Brian C. Froehler. Potent and selective inhibition of gene expression by an antisense heptanucleotide. *Nature Biotechnology*, 14(7):840–844, 1996.

[174] E. Premkumar Reddy, Roberta K. Reynolds, Eugenio Santos, and Mariano Barbacid. A point mutation is responsible for the acquisition of transforming properties by the T24 human bladder carcinoma oncogene. *Nature (London, United Kingdom)*, 300(5888):149–52, 1982.

[175] Clifford J. Tabin, M. Bradley, Scott, Cornelia I. Bargmann, Robert A. Weinberg, Alex G. Papageorge, Edward M. Scolnick, Ravi Dhar, Douglas R. Lowry, and Esther H. Chang. Mechanism of activation of a human oncogene. *Nature (London, United Kingdom)*, 300(5888):143–9, 1982.

[176] M. Barbacid. Ras oncogenes: their role in neoplasia. *European Journal of Clinical Investigation*, 20(3):225–35, 1990.

[177] C. Mascaux, N. Iannino, B. Martin, M. Paesmans, T. Berghmans, M. Dusart, A. Haller, P. Lothaire, A-P. Meert, S. Noel, J-J. Lafitte, and J-P. Sculier. The role of RAS oncogene in survival of patients with lung cancer: a systematic review of the literature with meta-analysis. *British Journal of Cancer*, 92(1):131–139, 2005.

[178] Marcos Malumbres and Mariano Barbacid. Time-line: RAS oncogenes: the first 30 years. *Nature Reviews Cancer*, 3(6):459–465, 2003.

[179] Hatim T. Allawi, Fang Dong, Hon S. Ip, Bruce P. Neri, and Victor I. Lyamichev. Mapping of RNA accessible sites by extension of random oligonucleotide libraries with reverse transcriptase. *RNA*, 7(2):314–327, 2001.

[180] Jinhong Chang, Emmanuelle Nicolas, Debora Marks, Chris Sander, Anthony Lerro, Marie Annick Buendia, Chunxiao Xu, William S. Mason, Thomas Moloshok, Roque Bort, Kenneth S. Zaret, and John M. Taylor. MiR-122, a mammalian liver-specific microRNA, is processed from hcr mRNA and may downregulate the high affinity cationic amino acid transporter CAT-1. *RNA Biology*, 1(2): 106–113, 2004.

[181] Mariana Lagos-Quintana, Reinhard Rauhut, Abdullah Yalcin, Jutta Meyer, Winfried Lendeckel, and Thomas Tuschl. Identification of Tissue-Specific MicroRNAs from Mouse. *Current Biology*, 12(9):

735–739, 2002.

[182] David Gatfield, Gwendal Le, Martelot, Charles E. Vejnar, Daniel Gerlach, Olivier Schaad, Fabienne Fleury-Olela, Anna-Liisa Ruskeepaa, Matej Oresic, Christine C. Esau, Evgeny M. Zdobnov, and Ueli Schibler. Integration of microRNA miR-122 in hepatic circadian gene expression. *Genes & Development*, 23(11):1313–1326, 2009.

[183] Nicolas Preitner, Francesca Damiola, Luis Lopez-Molina, Joszef Zakany, Denis Duboule, Urs Albrecht, and Ueli Schibler. The orphan nuclear receptor REV-ERBα controls circadian transcription within the positive limb of the mammalian circadian oscillator. *Cell (Cambridge, MA, United States)*, 110(2):251–260, 2002.

[184] Catherine L. Jopling, MinKyung Yi, Alissa M. Lancaster, Stanley M. Lemon, and Peter Sarnow. Modulation of Hepatitis C Virus RNA Abundance by a Liver-Specific MicroRNA. *Science (Washington, DC, United States)*, 309(5740):1577–1581, 2005.

[185] Catherine L. Jopling, Sylvia Schutz, and Peter Sarnow. Position-dependent function for a tandem microRNA miR-122-binding site located in the hepatitis C virus RNA genome. *Cell Host & Microbe*, 4(1):77–85, 2008.

[186] Catherine L. Jopling. Regulation of hepatitis C virus by microRNA-122. *Biochemical Society Transactions*, 36(6):1220–1223, 2008.

[187] Tetsuro Shimakami, Daisuke Yamane, Rohit K. Jangra, Brian J. Kempf, Carolyn Spaniel, David J. Barton, and Stanley M. Lemon. Stabilization of hepatitis C virus RNA by an Ago2-mir-122 complex. *Proceedings of the National Academy of Sciences of the United States of America*, 109(3):941–946, S941/1–S941/6–, 2012.

[188] Tetsuro Shimakami, Daisuke Yamane, Christoph Welsch, Lucinda Hensley, Rohit K. Jangra, and Stanley M. Lemon. Base Pairing between Hepatitis C Virus RNA and MicroRNA 122 3' of Its Seed Sequence is Essential for Genome Stabilization and Production of Infectious Virus. *Journal of Virology*, 86(13):7372–7383, 2012.

[189] Robert E. Lanford, Elisabeth S. Hildebrandt-Eriksen, Andreas Petri, Robert Persson, Morten Lindow, Martin E. Munk, Sakari Kauppinen, and Henrik Orum. Therapeutic Silencing of MicroRNA-122 in Primates with Chronic Hepatitis C Virus Infection. *Science (Washington, DC, United States)*, 327(5962):198–201, 2010.

[190] H.W. Reesink, H.L.A. Janssen, S. Zeuzem, E. Lawitz, M. Rodriguez-Torres, K. Patel, A. Chen, C. Davis, B. King, A. Levin, and M.R. Hodges. Randomized, double-blind, placebo-controlled safety, anti-viral proof-of-concept study fo miravirsen, an oligonucleotide targeting miR-122, in treatment-naive patients with genotype 1 chronic HCV. *Journal of Hepatology*, 56, Supplement 2(0):S26–, April 2012.

[191] Witold Filipowicz and Helge Grosshans. The liver-specific microRNA miR-122: biology and therapeutic potential. *Progress in Drug Research*, 67(Epigenetics and Disease):221–238, 2011.

[192] Madhu S. Kumar, Jun Lu, Kim L. Mercer, Todd R. Golub, and Tyler Jacks. Impaired microRNA processing enhances cellular transformation and tumorigenesis. *Nature Genetics*, 39(5):673–677, 2007.

[193] Sonia Guil and Javier F. Caceres. The multifunctional RNA-binding protein hnRNP A1 is required for processing of miR-18a. *Nature Structural & Molecular Biology*, 14(7):591–596, 2007.

[194] Brandi N. Davis, Aaron C. Hilyard, Giorgio Lagna, and Akiko Hata. SMAD proteins control DROSHA-mediated microRNA maturation. *Nature (London, United Kingdom)*, 454(7200):56–61, 2008.

[195] Srinivas R. Viswanathan and George Q. Daley. Lin28: a microRNA regulator with a macro role. *Cell (Cambridge, MA, United States)*, 140(4):445–449, 2010.

[196] Ingo Buessing, Frank J. Slack, and Helge Grosshans. Let-7 microRNAs in development, stem cells and cancer. *Trends in Molecular Medicine*, 14(9):400–409, 2008.

[197] Xavier C. Ding, Frank J. Slack, and Helge Grosshans. The let-7 microRNA interfaces extensively with the translation machinery to regulate cell differentiation. *Cell Cycle*, 7(19):3083–3090, 2008.

[198] Elena Piskounova, Srinivas R. Viswanathan, Maja Janas, Robert J. LaPierre, George Q. Daley, Piotr Sliz, and Richard I. Gregory. Determinants of microRNA processing inhibition by the developmentally regulated RNA-binding protein Lin28. *Journal of Biological Chemistry*, 283(31): 21310–21314, 2008.

[199] Srinivas R. Viswanathan, George Q. Daley, and Richard I. Gregory. Selective Blockade of MicroRNA Processing by Lin28. *Science (Washington, DC, United States)*, 320(5872):97–100, 2008.

[200] Martin A. Newman, J. Michael Thomson, and Scott M. Hammond. Lin-28 interaction with the Let-7 precursor loop mediates regulated microRNA processing. *RNA*, 14(8):1539–1549, 2008.

[201] Agnieszka Rybak, Heiko Fuchs, Lena Smirnova, Christine Brandt, Elena E. Pohl, Robert Nitsch, and F. Gregory Wulczyn. A feedback loop comprising lin-28 and let-7 controls pre-let-7 maturation during neural stem-cell commitment. *Nature Cell Biology*, 10(8):987–993, 2008.

[202] Inha Heo, Chirlmin Joo, Jun Cho, Minju Ha, Jinju Han, and V. Narry Kim. Lin28 mediates the terminal uridylation of let-7 precursor microRNA. *Molecular Cell*, 32(2):276–284, 2008.

[203] Luca F.R. Gebert, Mario A.E. Rebhan, Silvia E.M. Crivelli, Rmy Denzler, Markus Stoffel, and Jonathan Hall. Miravirsen (SPC3649) can inhibit the biogenesis of miR-122. *Nucleic acids research*, published online September, 24., 2013. doi:10.1093/nar/gkt852.

[204] Karl Andersson, Markku Haemaelaeinen, and Magnus Malmqvist. Identification and Optimization of Regeneration Conditions for Affinity-Based Biosensor Assays. A Multivariate Cocktail Approach. *Analytical Chemistry*, 71(13):2475–2481, 1999.

[205] Cassandra L. Smith, Jacqueline S. Milea, and Giang H. Nguyen. Immobilization of nucleic acids using biotin-strept(avidin) systems. *Topics in Current Chemistry*, 261(Immobilisation of DNA on Chips II):63–90, 2005.

[206] Warren A. Kibbe. OligoCalc: an online oligonucleotide properties calculator. *Nucleic Acids Research*, 35(suppl 2):W43–W46, July 2007.

[207] Harry Towbin, Philipp Wenter, Boris Guennewig, Jochen Imig, Julian A. Zagalak, Andre P. Gerber, and Jonathan Hall. Systematic screens of proteins binding to synthetic microRNA precursors. *Nucleic Acids Research*, 41(3):e47–, 2013.

[208] Juraj Svitel, Hacene Boukari, Donald Van, Ryk, Richard C. Willson, and Peter Schuck. Probing the functional heterogeneity of surface binding sites by analysis of experimental binding traces and the effect of mass transport limitation. *Biophysical Journal*, 92(5):1742–1758, 2007.

[209] Inna I. Gorshkova, Juraj Svitel, Faezeh Razjouyan, and Peter Schuck. Bayesian Analysis of Heterogeneity in the Distribution of Binding Properties of Immobilized Surface Sites. *Langmuir*, 24 (20):11577–11586, 2008.

[210] Joacim Elmén, Morten Lindow, Asli Silahtaroglu, Mads Bak, Mette Christensen, Allan Lind-Thomsen, Maj Hedtjärn, Jens Bo Hansen, Henrik Frydenlund Hansen, Ellen Marie Straarup, Keith McCullagh, Phil Kearney, and Sakari Kauppinen. Antagonism of microRNA-122 in mice by systemically administered LNA-antimiR leads to up-regulation of a large set of predicted target mRNAs in the liver. *Nucleic acids research*, 36(4):1153–1162, March 2008.

[211] Michael J. Cavaluzzi and Philip N. Borer. Revised UV extinction coefficients for nucleoside-5'-monophosphates and unpaired DNA and RNA. *Nucleic Acids Research*, 32(1):e13/1–e13/9, 2004.

[212] W.E. Razzell. [29] Phosphodiesterases. In *Methods in Enzymology*, volume Volume 6, pages 236–258. Academic Press, 1963.

[213] Vincent J. Cannistraro and David Kennell. The 5' ends of RNA oligonucleotides in Escherichia coli and mRNA degradation. *European Journal of Biochemistry*, 213(1):285–93, 1993.

[214] Tuomas Loennberg and Mikko Luomala. Intra-complex general acid/base catalyzed cleavage of RNA phosphodiester bonds: the leaving group effect. *Organic & Biomolecular Chemistry*, 10(33): 6785–6791, 2012.

[215] M. J. Cavaluzzi, D. J. Kerwood, and P. N. Borer. Accurate nucleic acid concentrations by nuclear magnetic resonance. *Analytical Biochemistry*, 308(2):373–380, 2002.

[216] James H. Murphy and Tina L. Trapane. Concentration and extinction coefficient determination for oligonucleotides and analogs using a general phosphate analysis. *Analytical Biochemistry*, 240 (2):273–282, 1996.

[217] S.R. Gallagher. Quantification of DNA and RNA with absorption and fluorescence spectroscopy. *Current protocols in cell biology / editorial board, Juan S. Bonifacino ... [et al.]*, Appendix 3: Appendix 3D–, 2001.

[218] Andrey V. Tataurov, Yong You, and Richard Owczarzy. Predicting ultraviolet spectrum of single stranded and double stranded deoxyribonucleic acids. *Biophysical Chemistry*, 133(1–3):66–70, march 2008.

[219] Takeshi Yamada, Chang Geng Peng, Shigeo Matsuda, Haripriya Addepalli, K. Narayanannair Jayaprakash, Md. Rowshon Alam, Kathy Mills, Martin A. Maier, Klaus Charisse, Mitsuo Sekine, Muthiah Manoharan, and Kallanthottathil G. Rajeev. Versatile Site-Specific Conjugation of Small Molecules to siRNA Using Click Chemistry. *Journal of Organic Chemistry*, 76(5):1198–1211, 2011.

[220] Kiranmai Gumireddy, Douglas D. Young, Xin Xiong, John B. Hogenesch, Qihong Huang, and Alexander Deiters. Small-molecule inhibitors of microRNA miR-21 function. *Angewandte Chemie, International Edition*, 47(39):7482–7484, 2008.

[221] Sonia Melo, Alberto Villaneuva, Catia Moutinho, Veronica Davalos, Riccardo Spizzo, Cristina Ivan, Simona Rossi, Fernando Setien, Oriol Casanovas, Laia Simo-Riudalbas, Javier Carmona, Jordi Carrere, August Vidal, Alvaro Aytes, Sara Puertas, Santiago Ropero, Raghu Kalluri, Carlo M. Croce, George A. Calin, and Manel Esteller. Small molecule enoxacin is a cancer-specific growth inhibitor that acts by enhancing TAR RNA-binding protein 2-mediated microRNA processing. *Proceedings of the National Academy of Sciences of the United States of America*, 108(11):4394–4399, S4394/1–S4394/10, 2011.

[222] Andrew C. Stelzer, Aaron T. Frank, Jeremy D. Kratz, Michael D. Swanson, Marta J. Gonzalez-Hernandez, Janghyun Lee, Ioan Andricioaei, David M. Markovitz, and Hashim M. Al-Hashimi. Discovery of selective bioactive small molecules by targeting an RNA dynamic ensemble. *Nature Chemical Biology*, 7(8):553–559, 2011.

[223] Kyohei Higashi, Yusuke Terui, Akiko Suganami, Yutaka Tamura, Kazuhiro Nishimura, Keiko Kashiwagi, and Kazuei Igarashi. Selective Structural Change by Spermidine in the Bulged-out Region of Double-stranded RNA and Its Effect on RNA Function. *Journal of Biological Chemistry*, 283(47): 32989–32994, 2008.

[224] Martin Egli, George Minasov, Valentina Tereshko, Pradeep S. Pallan, Marianna Teplova, Gopal B. Inamati, Elena A. Lesnik, Steve R. Owens, Bruce S. Ross, Thazha P. Prakash, and Muthiah Manoharan. Probing the Influence of Stereoelectronic Effects on the Biophysical Properties of Oligonucleotides: Comprehensive Analysis of the RNA Affinity, Nuclease Resistance, and Crystal Structure of Ten 2'-O-Ribonucleic Acid Modifications. *Biochemistry*, 44(25):9045–9057, 2005.

[225] Saroj K. Roy and Jin-yan Tang. Efficient Large Scale Synthesis of 2'-O-Alkyl Pyrimidine Ribonucleosides. *Organic Process Research & Development*, 4(3):170–171, 2000.

[226] Srinivasarao Meneni, Ingo Ott, Craig D. Sergeant, Adam Sniady, Ronald Gust, and Roman Dembinski. 5-Alkynyl-2'-deoxyuridines: Chromatography-free synthesis and cytotoxicity evaluation against human breast cancer cells. *Bioorganic & Medicinal Chemistry*, 15(8):3082–3088, 2007.

[227] Takanori Ito, Yoshihito Ueno, Yasuo Komatsu, and Akira Matsuda. Synthesis, thermal stability and resistance to enzymatic hydrolysis of the oligonucleotides containing 5-(N-aminohexyl)carbamoyl-2'-O-methyluridines. *Nucleic Acids Research*, 31(10):2514–2523, 2003.

[228] Hans Stein and Peter Hausen. Enzyme from calf thymus degrading the RNA moiety of DNA-RNA hybrids: effect on DNA-dependent RNA polymerase. *Science (Washington, DC, United States)*, 166(3903):393–5, 1969.

[229] Robert J. Crouch and Marie Luise Dirksen. Ribonucleases H. *Cold Spring Harbor Monograph Series*, 14(Nucleases):211–54, 1982.

[230] Marcin Nowotny, Sergei A. Gaidamakov, Robert J. Crouch, and Wei Yang. Crystal structures of RNase H bound to an RNA/DNA hybrid: Substrate specificity and metal-dependent catalysis. *Cell (Cambridge, MA, United States)*, 121(7):1005–1016, 2005.

[231] Minglei Wang, Simina Maria Boca, Rakhee Kalelkar, Jay E. Mittenthal, and Gustavo Caetano-Anolls. A phylogenomic reconstruction of the protein world based on a genomic census of protein fold architecture. *Complexity*, 12(1):27–40, September 2006.

[232] Bin-Guang Ma, Lei Chen, Hong-Fang Ji, Zhong-Hua Chen, Fu-Rong Yang, Ling Wang, Ge Qu, Ying-Ying Jiang, Cong Ji, and Hong-Yu Zhang. Characters of very ancient proteins. *Biochemical and Biophysical Research Communications*, 366(3):607–611, February 2008.

[233] Naoto Ohtani, Mitsuru Haruki, Masaaki Morikawa, Robert J. Crouch, Mitsuhiro Itaya, and Shigenori Kanaya. Identification of the genes encoding Mn^{2+}-dependent RNase HII and Mg^{2+}-dependent RNase HIII from Bacillus subtilis: Classification of RNases H into three families. *Biochemistry*, 38(2):605–618, 1999.

[234] Octavian Schatz, Frans V. Cromme, Thierry Naas, Dirk Lindemann, Jan Mous, and Stuart F. J. LeGrice. Inactivation of the RNaseH domain of HIV-1 reverse transcriptase blocks viral infectivity. *Advances in Applied Biotechnology Series*, 7(Gene Regul. AIDS):293–303, 1990.

[235] Marcin Nowotny, Susana M. Cerritelli, Rodolfo Ghirlando, Sergei A. Gaidamakov, Robert J. Crouch, and Wei Yang. Specific recognition of RNA/DNA hybrid and enhancement of human RNase H1 activity by HBD. *EMBO Journal*, 27(7):1172–1181, 2008.

[236] Karin Moelling. Targeting the retroviral ribonuclease H by rational drug design. *AIDS (London, United Kingdom)*, 26(16):1983–1993, 2012.

[237] E. Tramontano and R. Di, Santo. HIV-1 RT-associated RNase H function inhibitors: recent advances in drug development. *Current Medicinal Chemistry*, 17(26):2837–2853, 2010.

[238] Hongjiang Wu, Walt F. Lima, and Stanley T. Crooke. Molecular cloning and expression of cDNA for human RNase H. *Antisense & Nucleic Acid Drug Development*, 8(1):53–61, 1998.

[239] Peter Frank, Sylvie Albert, Christian Cazenave, and Jean-Jacques Toulme. Purification and characterization of human ribonuclease HII. *Nucleic Acids Research*, 22(24):5247–54, 1994.

[240] Hongjiang Wu, Walt F. Lima, Hong Zhang, Amy Fan, Hong Sun, and Stanley T. Crooke. Determination of the role of the human RNase H1 in the pharmacology of DNA-like antisense drugs. *Journal of Biological Chemistry*, 279(17):17181–17189, 2004.

[241] Hongjiang Wu, Walt F. Lima, and Stanley T. Crooke. Properties of cloned and expressed human RNase H1. *Journal of Biological Chemistry*, 274(40):28270–28278, 1999.

[242] Werner Buesen, J. Hinrich Peters, Peter Hausen, and Gabriele Crystalla. Ribonuclease H levels during the response of bovine lymphocytes to concanavalin A. *European Journal of Biochemistry*, 74(1):203–8, 1977.

[243] Walt F. Lima, Hongjiang Wu, Josh G. Nichols, Sherilynn M. Manalili, Jared J. Drader, Steven A. Hofstadler, and Stanley T. Crooke. Human RNase H1 Activity Is Regulated by a Unique Redox Switch Formed between Adjacent Cysteines. *Journal of Biological Chemistry*, 278(17):14906–14912, 2003.

[244] Hongjiang Wu, Walt F. Lima, and Stanley T. Crooke. Investigating the structure of human RNase H1 by site-directed mutagenesis. *Journal of Biological Chemistry*, 276(26):23547–23553, 2001.

[245] Sarah P. Evans and Mark Bycroft. NMR structure of the N-terminal domain of Saccharomyces cerevisiae RNase HI reveals a fold with a strong resemblance to the N-terminal domain of ribosomal protein L9. *Journal of Molecular Biology*, 291(3):661–669, 1999.

[246] Walt F. Lima, Hongjiang Wu, Josh G. Nichols, Thazha P. Prakash, Vasulinga Ravikumar, and Stanley T. Crooke. Human RNase H1 Uses One Tryptophan and Two Lysines to Position the Enzyme at the 3'-DNA/5'-RNA Terminus of the Heteroduplex Substrate. *Journal of Biological Chemistry*, 278(50):49860–49867, 2003.

[247] K. Katayanagi, M. Miyagawa, M. Matsushima, M. Ishikawa, S. Kanaya, M. Ikehara, T. Matsuzaki, and K. Morikawa. Three-dimensional structure of ribonuclease H from E. coli. *Nature (London, United Kingdom)*, 347(6290):306–9, 1990.

[248] Wei Yang, Wayne A. Hendrickson, Robert J. Crouch, and Yoshinori Satow. Structure of ribonuclease H phased at 2 Å resolution by MAD analysis of the selenomethionyl protein. *Science (Washington, DC, United States)*, 249(4975):1398–405, 1990.

[249] Walt Lima, Hongjiang Wu, and Stanley T. Crooke. The RNase H mechanism. In *Antisense Drug Technol. (2nd Ed.)*, pages 47–74. CRC Press LLC, 2008.

[250] Walt F. Lima, Josh G. Nichols, Hongjiang Wu, Thazha P. Prakash, Mike T. Migawa, Tadensz K. Wyrzykiewicz, Balkrishen Bhat, and Stanley T. Crooke. Structural Requirements at the Catalytic Site of the Heteroduplex Substrate for Human RNase H1 Catalysis. *Journal of Biological Chemistry*, 279(35):36317–36326, 2004.

[251] Alexei Yu. Denisov, Anne M. Noronha, Christopher J. Wilds, Jean-Francois Trempe, Richard T. Pon, Kalle Gehring, and Masad J. Damha. Solution structure of an arabinonucleic acid (ANA)/RNA duplex in a chimeric hairpin: comparison with 2'-fluoro-ANA/RNA and DNA/RNA hybrids. *Nucleic Acids Research*, 29(21):4284–4293, 2001.

[252] Marcin Nowotny, Sergei A. Gaidamakov, Rodolfo Ghirlando, Susana M. Cerritelli, Robert J. Crouch, and Wei Yang. Structure of human RNase H1 complexed with an RNA/DNA hybrid: insight into HIV reverse transcription. *Molecular Cell*, 28(2):264–276, 2007.

[253] Walt F. Lima, John B. Rose, Josh G. Nichols, Hongjiang Wu, Michael T. Migawa, Tadeusz K. Wyrzykiewicz, Guillermo Vasquez, Eric E. Swayze, and Stanley T. Crooke. The positional influence of the helical geometry of the heteroduplex substrate on human RNase H1 catalysis. *Molecular Pharmacology*, 71(1):73–82, 2007.

[254] Tomoko Nishizaki, Shigenori Iwai, Eiko Ohtsuka, and Haruki Nakamura. Solution Structure of an RNA·2'-*O*-Methylated RNA Hybrid Duplex Containing an RNA·DNA Hybrid Segment at the Center. *Biochemistry*, 36(9):2577–2585, 1997.

[255] Annie Galarneau, Kyung-Lyum Min, Maria M. Mangos, and Masad J. Damha. Assay for evaluating ribonuclease H-mediated degradation of RNA-antisense oligonucleotide duplexes. *Methods in Molecular Biology (Totowa, NJ, United States)*, 288(Oligonucleotide Synthesis):65–80, 2005.

[256] N. Michael Green. Avidin. In John T. Edsall C.B. Anfinsen and Frederic M. Richards, editors, *Advances in Protein Chemistry*, volume 29, pages 85–133. Academic Press, 1975.

[257] N. M. Green. Avidin. I. The use of [^{14}C]biotin for kinetic studies and for assay. *Biochemical Journal*, 89(3):585–91, 1963.

[258] N.M. Green and E.J. Toms. The properties of subunits of avidin coupled to sepharose. *The Biochemical journal*, 133(4):687–700, 1973.

[259] P. C. Weber, J. J. Wendoloski, M. W. Pantoliano, and F. R. Salemme. Crystallographic and thermodynamic comparison of natural and synthetic ligands bound to streptavidin. *J. Am. Chem. Soc.*, 114(9):3197–3200, April 1992.

[260] Jason DeChancie and K. N. Houk. The origins of femtomolar protein-ligand binding: hydrogen-bond cooperativity and desolvation energetics in the biotin-(strept)avidin binding site. *Journal of the American Chemical Society*, 129(17):5419–5429, 2007.

[261] Eleftherios P. Diamandis and Theodore K Christopoulos. The biotin-(strept)avidin system: princi-ples and applications in biotechnology. *Clinical Chemistry (Washington, DC, United States)*, 37(5): 625–36, 1991.

[262] Rebecca L. Rich and David G. Myszka. Survey of the year 2003 commercial optical biosensor literature. *Journal of Molecular Recognition*, 18(1):1–39, 2005.

[263] Donald B. Melville. Biotin sulfoxide. *Journal of Biological Chemistry*, 208:495–501, 1954.

[264] Krishna Upadhya, Iqbal K. Khattak, and Bashar Mullah. Oxidation of biotin during oligonucleotide synthesis. *Nucleosides, Nucleotides & Nucleic Acids*, 24(5-7):919–922, 2005.

[265] Russell K. Garlick and Roger W. Giese. Dissociative binding of α- and β-sulfoxides of biotinylamidoethyl-3-(4-hydroxy-3-[^{125}I]iodophenyl)propionamide to avidin. *Biochemical Journal*, 268(3):611–13, 1990.

[266] Yasmina S. N. Day, Cheryl L. Baird, Rebecca L. Rich, and David G. Myszka. Direct comparison of binding equilibrium, thermodynamic, and rate constants determined by surface- and solution-based biophysical methods. *Protein Science*, 11(5):1017–1025, 2002.

[267] David G. Myszka, Mathew D. Jonsen, and Barbara J. Graves. Equilibrium analysis of high affinity interactions using BIACORE. *Analytical Biochemistry*, 265(2):326–330, 1998.

[268] Laurence Heinrich, Nathalie Tissot, Daniel Jean Hartmann, and Richard Cohen. Comparison of the results obtained by ELISA and surface plasmon resonance for the determination of antibody affinity. *Journal of Immunological Methods*, 352(1-2):13–22, 2010.

[269] H. P. Chiang, C.-W. Chen, J. J. Wu, H. L. Li, T. Y. Lin, E. J. Sanchez, and P. T. Leung. Effects of temperature on the surface plasmon resonance at a metal-semiconductor interface. *Thin Solid Films*, 515(17):6953–6961, 2007.

[270] Gerald Seidel, Marco Diel, Norbert Fuchsbauer, and Wolfgang Hillen. Quantitative interdepen-dence of coeffectors, CcpA and *cre* in carbon catabolite regulation of *Bacillus subtilis*. *FEBS Journal*, 272(10):2566–2577, 2005.

[271] Ilaria Mannelli, Maria Minunni, Sara Tombelli, Ronghui Wang, Spiriti Maria Michela, and Marco Mascini. Direct immobilisation of DNA probes for the development of affinity biosensors. *Bioelec-trochemistry (Amsterdam, Netherlands)*, 66(1-2):129–38, 2005.

[272] Jessica L Childs, Matthew D Disney, and Douglas H Turner. Oligonucleotide directed misfolding of RNA inhibits Candida albicans group I intron splicing. *Proceedings of the National Academy of Sciences of the United States of America*, 99(17):11091–11096, August 2002.

[273] Anissa N Elayadi, Dwaine A Braasch, and David R Corey. Implications of High-Affinity Hybridization by Locked Nucleic Acid Oligomers for Inhibition of Human Telomerase. *Biochemistry*, 41(31):9973–9981, August 2002.

[274] Robert A. Copeland. Conformational adaptation in drug-target interactions and residence time. *Future Medicinal Chemistry*, 3(12):1491–1501, 2011.

[275] Odrowaz Piramowicz Marzena De, Pawel Czuba, Marta Targosz, Kvetoslava Burda, and Marek Szymonski. Dynamic force measurements of avidin-biotin and streptavdin-biotin interactions using AFM. *Acta biochimica Polonica*, 53(1):93–100, 2006.

[276] Joyce Wong, Ashutosh Chilkoti, and Vincent T. Moy. Direct force measurements of the streptavidin-biotin interaction. *Biomolecular Engineering*, 16(1-4):45–55, 1999.

[277] Uri Piran and William J. Riordan. Dissociation rate constant of the biotin-streptavidin complex. *Journal of Immunological Methods*, 133(1):141–3, 1990.

[278] Ashutosh Chilkoti and Patrick S. Stayton. Molecular Origins of the Slow Streptavidin-Biotin Disso-ciation Kinetics. *Journal of the American Chemical Society*, 117(43):10622–8, 1995.

G G. BIBLIOGRAPHY

[279] Graham R. Broder, Rohan T. Ranasinghe, Cameron Neylon, Hywel Morgan, and Peter L. Roach. Kinetics and Thermodynamics of Biotinylated Oligonucleotide Probe Binding to Particle-Immobilized Avidin and Implications for Multiplexing Applications. *Analytical Chemistry (Washington, DC, United States)*, 83(6):2005–2011, 2011.

[280] Yonghong Wang, Bo-Jiang Shen, and Walter Sebald. A mixed-charge pair in human interleukin 4 dominates high-affinity interaction with the receptor α-chain. *Proceedings of the National Academy of Sciences of the United States of America*, 94(5):1657–1662, 1997.

[281] Jr. Pearce, Kenneth H., Brian C. Cunningham, Germaine Fuh, Tuula Teeri, and James A. Wells. Growth Hormone Binding Affinity for Its Receptor Surpasses the Requirements for Cellular Activity. *Biochemistry*, 38(1):81–89, 1999.

[282] Rumin Zhang and Frederick Monsma. The importance of drug-target residence time. *Current Opinion in Drug Discovery & Development*, 12(4):488–496, 2009.

[283] Gideon Schreiber. Kinetic studies of protein-protein interactions. *Current Opinion in Structural Biology*, 12(1):41–47, 2002.

Acknowledgements

First and foremost, I wish to thank my two advisors:

Prof. Jonathan Hall, for offering me the opportunity to obtain my doctorate in your workgroup. Your critical but witty nature enriched working in our team immeasurably.

Prof. Gisbert Schneider, for your willingness to supervise my doctorate in word and deed. Your open and positive attitude helped me even in matters beyond my academic endeavors.

I also wish to thank Dr. Irmgard Werner and Prof. Bruno Gander, for your unwavering willingness to help and for the inspiring discussions.

Many LaTeX 2_ε-related problems where solved by Dr. Urs Hollenstein. Thank you very much for the help with the layout of this thesis and many fruitful coffee breaks.

Cordial and special thanks go to my co-workers Dr. Bettina Wild, Dr. Luca Gebert, Dr. Andreas Brunschweiger, and Dr. Florin Paun who greatly contributed to the work presented herein.

Special thanks go to my colleagues in Prof. Hall's workgroup: Hartmut Jahns, Moritz Stoltz, Dr. Afzal Doghar, Julian Zagalak, Martina Roos, Matje Lucic, Dr. Helen Lightfoot, Dr. Jochen Imig, Felicitas Floor and Dr. Boris Guennewig. The stimulating discussions and pleasant work environment you provided were essential to the success of my work. A great thank goes to Mauro Zimmermann who introduced me into the art of oligonucleotide synthesis and workup and Sylvia Peleg for her unflagging cooperativeness in all every-day matters.

Above all, I want to thank our senior scientist emeritus Dr. Harry Towbin. Your great willingness to help and your always unconventional and inventive ways were a constant enrichment. It was an honor to be able to work with you.

Many thanks go to Chris Whalen, Dr. Klaus Wiehler (SierraSensors inc., Hamburg, Germany) and your team for the very kind and constant support from the very first beginning on.

Finally, I wish to thank my family and friends for standing by my side throughout my doctorate and, in their own ways, for enabling this work to begin with.

Publications and posters

Publications

- Luca F. R. Gebert, Mario A. E. Rebhan, Silvia E. M. Crivelli, Rémy Denzler, Markus Stoffel, and Jonathan Hall. Miravirsen (SPC3649) can inhibit the biogenesis of miR-122 *Nucleic Acids Research*, 2013. doi:10.1093/nar/gkt852

- Mario A. E. Rebhan, Andreas Brunschweiger, and Jonathan Hall. Measurement by SPR of Very Low Dissociation Rates: Oxidation–Mediated Loss of Biotin–Streptavidin Affinity. *ChemBioChem*, 2013. doi:10.1002/cbic.201300468

Posters

- Mario A. Rebhan, Luca Gebert, Harry Towbin, Jonathan Hall; "Binding affinities of 2'-O-methyl oligoribonucleotides complementary to the loop of pre-miR-122: A Surface Plasmon Resonance Study. Swiss Chemical Society Meeting, September 16, 2010, Zurich, Switzerland

- L. Gebert, M. Rebhan , A. Brunschweiger, S. Crivelli, J. Hall; "Targeting MicroRNA Precursor", Cell Symposia: functional RNAs, December 2-4, 2012, Sitges, Spain